

Robert L. Bluntzen

Phase III

Final Report

Received 12/3/65

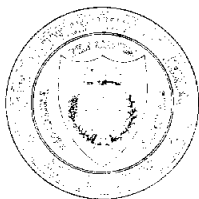
W. H. H.

BUREAU OF ECONOMIC GEOLOGY

THE UNIVERSITY OF TEXAS

AT AUSTIN

W. L. FISHER, DIRECTOR



PHASE III: EXAMINATION OF TEXAS SALT DOMES
AS POTENTIAL SITES FOR PERMANENT STORAGE
OF TOXIC CHEMICAL WASTE

Prepared by

S. J. Seni, E. W. Collins, H. S. Hamlin,
W. F. Mullican III, and D. A. Smith

Assisted by

L. Falconer and T. Walter

Report prepared for the Texas Water Commission
under Interagency Contract No. IAC(84-85)-2203

Bureau of Economic Geology
W. L. Fisher, Director
The University of Texas at Austin
University Station, Box X
Austin, Texas 78713

November 1985

CONTENTS

INTRODUCTION	1
RECOMMENDATIONS AND CONCLUSIONS, by S. J. Seni	1
REFERENCES	5
TOPICAL SUMMARIES OF RESEARCH REPORTS, by S. J. Seni	7
Subsidence and Collapse	7
Structural Patterns Around Texas Salt Domes	9
Cap Rock	10
Cap-Rock Hydrology	13
ACKNOWLEDGMENTS	15
RESEARCH REPORTS*	17
Subsidence over Texas Salt Domes, by W. F. Mullican III	18
Statistical Analysis of Structure in the Houston Diapir Province, by W. F. Mullican III	73
Petrography and Structure of Cap Rock with Emphasis on Core from Boling Salt Dome, Texas, by S. J. Seni	114
Geology and Hydrogeology, Barbers Hill Salt Dome, Texas, by H. S. Hamlin	181
Hydraulics of Cap Rock, Barbers Hill Salt Dome, Texas, by D. A. Smith	236
Review of the Geology and Plio-Pleistocene to Post-Pleistocene Deformation at Damon Mound Salt Dome, Texas, by E. C. Collins.	275
APPENDIX A. List of domes and codes	308

*All figures, tables, and references are listed within individual research reports.

INTRODUCTION

This report presents the results of final Phase III research in order to better quantify selected issues associated with permanent storage of toxic chemical wastes in solution-mined caverns in salt. Phase III research concentrated on understanding cap-rock genesis and hydrology at Boling, Barbers Hill, and Damon Mound Domes; subsidence and structure patterns around domes in the Houston diapir province; and near-dome structure, stratigraphy, and growth history of Boling, Barbers Hill, and Damon Mound Domes.

The report is divided into three main sections. The first section presents our recommendations and conclusions. The second includes topical summaries of each of the research reports. The final section includes individual research reports on (1) subsidence and collapse associated with salt domes; (2) statistical analysis of regional patterns of structure in the Houston diapir province; (3) petrography and structure of cap rock at Boling Dome; (4) stratigraphy, structure, and hydrology of Barbers Hill Dome; (5) cap-rock hydraulics of Barbers Hill Dome; and (6) stratigraphy and history of Late Pleistocene to recent structural deformation at Damon Mound Dome.

RECOMMENDATIONS AND CONCLUSIONS

by S. J. Seni

We conclude that domes may be suitable hosts for permanent isolation of some types of toxic chemical waste in solution-mined caverns in salt. Not all domes are appropriate sites for toxic waste disposal owing to uncertainties about dome size, shape, and depth, salt heterogeneities, cap-rock lost-circulation zones, hydrologic and structural stability, growth history, and the effects of resource exploration and development. Boling Dome is under consideration as a site for a toxic waste disposal facility. The intensive and extended history of sulfur production from the cap rock of Boling Dome continues to affect the

hydrologic and structural stability of the dome. These effects include broad surface subsidence, localized surface collapse, alterations to natural hydrologic regime, and uncertainties related to cap-rock and salt-stock heterogeneities. We are concerned that these instabilities could negatively affect the disposal of waste within the salt stock.

This document is Phase III of a two-year study commissioned by the Texas Department of Water Resources to evaluate the technical issues associated with the disposal of toxic chemical waste in solution-mined caverns in salt. Phase I characterized and cataloged (1) the geologic and hydrologic setting of the salt domes in Texas (Seni and others, 1984a, 1984b), (2) the safety and environmental problems that have already resulted from man's use of the domes (Seni and others, 1984b), and (3) the critical problems associated with the disposal of toxic chemical wastes in domes (Seni and others, 1984c). Phase II concentrated on defining the geometry, structure, and stratigraphy of certain domes and on investigating cavern stability and creep properties of salt (Seni and others, 1984d).

One finding of Phase III research is that history and type of resource recovery have a tremendous effect on the hydrologic and structural stability of a salt dome. Exploration, development, and production around and within salt domes cause tectonic and hydrologic instabilities that can extend beyond the immediate area and affect surface and subsurface structures and engineering works. Surface downwarping (subsidence) or collapse (rapid, localized subsidence) can result from extraction of subsurface fluids, gases, or solids. Changes in ground-water flow, water chemistry, pressure, and temperature arise from injection of large volumes of fluids at high rates. These surface and subsurface changes are especially pronounced at domes with a history of significant sulfur production.

Industry experience with temporary storage of liquid and gaseous petroleum products in more than 1,000 solution-mined caverns in salt is one indication that some form of waste isolation in salt caverns is feasible. However, we recommend that disposal of toxic liquid wastes in salt caverns be discouraged until further research on potential risks is completed.

The 1984 reauthorization of the Resource Conservation and Recovery Act temporarily prohibited disposal of liquids in salt domes in order to allow time for additional research into potential risks. Risks associated with disposal of liquids in solution-mined caverns include the potential for (1) waste migration through porous and permeable lost-circulation zones in the cap rock, (2) overpressurized liquids in sealed caverns, and (3) weakening of salt around the caverns (as evidenced by greater ease of salt deformation by fluid-film-assisted grain-boundary diffusion in salt exposed to brine as opposed to dry salt). Methods for slurry transport and disposal of solidified toxic waste in solution-mined caverns are needed. No specific studies of the waste disposal or in situ solidification within solution-mined caverns are available.

Boling Dome has both favorable and unfavorable aspects for the long-term isolation of waste in solution-mined caverns in the salt stock. Favorable aspects include (1) the large size of the salt stock at a depth neither too shallow nor too deep, (2) no evidence of positive topographic relief at the surface indicating recent rapid uplift, (3) no evidence of saline springs at the surface indicating rapid ongoing salt dissolution, (4) fine-grained clay-rich sediments over the cap rock that should act as an aquitard, and (5) the presence, at least locally, of a tight cap-rock - salt-stock interface that indicates local absence of active salt dissolution at the interface between anhydrite cap rock and salt.

Against these favorable aspects must be balanced a significant weight of unfavorable factors, including (1) more than 20,000 core holes penetrate the cap rock and possibly 100 penetrate to salt, allowing a possible pathway for meteoric (fresh) water to come in contact with and dissolve salt, (2) daily injection of 4 to 10 million gallons of water at temperatures of 315°F anomalously heats the shallow strata surrounding the cap rock, indicating the high probability of fluid migration from the cap rock into the surrounding strata, (3) areas of broad subsidence and collapse sinks occur at the surface over the salt dome as a result of natural collapse of subsurface voids and of cap-rock voids after removal of sulfur, and (4) incorporation of terrigenous elastics in cap-rock anhydrite indicates probable presence of exotic blocks of terrigenous elastics in salt.

Most negative aspects associated with Boling Dome are the result of man's activity. In addition to the drilling of a very large number of holes in the salt dome, the production of sulfur has caused the surface over the main sulfur area to subside at least 35 ft. A large system of levees must be maintained to prevent the sunken area from being flooded by the San Bernard River. The affected area covers approximately one-third of the surface of the dome. In 1983 a collapse sink rapidly formed over a small area of the dome. This sink developed over the site of a well that was drilled and abandoned in 1927. The well was abandoned owing to lost-circulation problems after a natural cavern with a vertical span exceeding 106 ft was intersected by the drill. The sink is interpreted to have formed because the cavern collapsed. The collapse of the cavern may have been natural or may have been aided by long-term dissolution as a result of improper or ineffective plugging of the old well.

We have found no characteristics applicable to domes in general that would disqualify all domes for toxic chemical waste disposal. However, we conclude that Boling Dome has significant unfavorable characteristics, including the large number of artificial penetrations, the heavy influence by man on the natural hydrologic system, the presence of natural(?) and man-induced subsidence and collapse, and the porous and permeable cap rock allowing free migration of fluids into and out of the cap rock. These characteristics are serious enough to discourage using Boling Dome as the first site for toxic chemical waste disposal. According to the proposed guidelines from the Nuclear Waste Policy Act of 1982, the presence of subsidence and collapse and the presence of a large number of drill-hole penetrations are disqualifying characteristics for nuclear waste isolation sites. It would be prudent to apply the same standards to toxic chemical waste isolation because of the permanent toxicity of the waste. If Boling Dome were used for toxic chemical waste disposal, then extraordinary engineering measures would be necessary to insure complete isolation of the cap rock from any waste, namely, mitigation and prevention of surface collapse through injection of supporting material, for instance cement, into subsurface

caverns, voids, and lost-circulation zones, and in situ solidification of waste to prevent waste migration.

We offer the following recommendations aimed at enhancing the stability of the natural system:

(1) All waste caverns are to be initiated with large diameter cores (approximately 6 inches) from the surface to 500 ft below the projected cavern depth to assure that adequate data are available to determine necessary geotechnical parameters. The core must be stored in perpetuity, preferably by the appropriate state or government agency.

(2) Extra casing strings are to be set through the surface strata and cap rock. If lost-circulation zones are encountered, then they must be filled with cement to prevent collapse and fluid migration. Cement shall be circulated until cement returns to the surface.

(3) If major discontinuities are encountered within the salt in the form of drill holes, faults, significant bodies of incorporated terrigenous clastics, or significant bodies of other non-salt material, then the position of the waste cavern shall be adjusted so that a minimum distance of 500 ft separates the anomalous zone from the nearest cavern wall.

(4) Waste material within the cavern must be solidified and have strength and density equivalent to or greater than salt.

REFERENCES

Seni, S. J., Mullican, W. F., III, and Ozment, R. W., 1984a, Computerized inventory of data on Texas salt domes: The University of Texas at Austin, Bureau of Economic Geology, report prepared for the Texas Department of Water Resources under inter-agency contract no. IAC(84-85)-1019, 34 p.

Seni, S. J., Mullican, W. F., III, and Hamlin, H. S., 1984b, Texas salt domes: natural resources, storage caverns, and extraction technology: The University of Texas at

Austin, Bureau of Economic Geology, report prepared for the Texas Department of Water Resources under interagency contract no. IAC(84-85)-1019, 161 p.

Seni, S. J., Hamlin, H. S., and Mullican, W. F., III, 1984c, Technical issues for chemical waste isolation in solution-mined caverns in salt domes: The University of Texas at Austin, Bureau of Economic Geology, report prepared for the Texas Department of Water Resources under interagency contract no. IAC(84-85)-1019, 8 p.

Seni, S. J., Mullican, W. F., III, and Hamlin, H. S., 1984d, Texas salt domes: aspects affecting disposal of toxic chemical waste in solution-mined caverns: The University of Texas at Austin, Bureau of Economic Geology, report prepared for the Texas Department of Water Resources under interagency contract no. IAC(84-85)-1019, 94 p.

TOPICAL SUMMARIES OF RESEARCH REPORTS

by S. J. Seni

Subsidence and Collapse

Salt domes provide a broad range of natural resources, including salt, brine, sulfur, oil, and natural gas, as well as space for product storage and disposal. Resource development and production can create tectonic and hydrologic instabilities around salt domes, affecting structures on the surface and engineering works in the subsurface. Subsidence is a major expression of these instabilities. Large volumes of subsurface material are removed during resource production and this creates voids (usually fluid filled). When a given volume of material is removed and nothing is inserted to replace it, the capability of the remaining rock to support the overburden load is weakened. Removal of subsurface solids generally has a greater surface effect than removal of liquids, because the solids support a greater percentage of the overburden load. All the strata above the zone of removal will subside or collapse if their strength is exceeded. As a result of man-directed resource removal in combination with natural processes of salt and cap-rock dissolution, those domes with a history of significant mass transfer of domal material have a history of surface subsidence and collapse.

Mining of sulfur by the Frasch method has caused the greatest and clearest expression of surface subsidence and collapse. The early, pre-1930's history of solution mining of brine also has had a clear record of collapse over the area of brine removal. Modern brine operations have been much more successful at preventing collapse at the surface. Although most subsidence occurs directly over the subsurface zone of removal, lateral offset of subsidence at the surface is documented at Orchard Dome. Similarly, although most subsidence occurs during production, surface subsidence and collapse have continued to occur over both Orchard and Palestine Domes 20 to 50 years after product withdrawal ceased.

Two end members of surface expression of subsurface collapse are distinct--subsidence and collapse. Subsidence is characterized by a shallow, saucer-shaped depression with large width-to-depth ratios. Subsidence is generally slower than collapse and usually expands by multiple, small, concentric fault planes. Although subsidence is a slow process and is generally thought to be a result of ductile deformation, it can continue for long periods of time and extend over broad areas. The long history of subsidence can create significant depressions. For example, the subsidence bowl over Boling Dome exceeds 35 ft in depth and covers 2.2 mi².

Collapse is characterized by steep-walled, flat-bottomed depressions with width-to-depth ratios much smaller than those that characterize subsidence bowls. Collapse usually occurs by subsurface caving, often with a single down-dropped fault block within a circular ring fault. Catastrophic collapse is usually presaged by saucer-shaped subsidence, though not all subsidence bowls collapse. A piping or stoping process initiates both subsidence and collapse, but the mechanism by which the void propagates to the surface is poorly understood. Gentle subsidence is probably dominated by ductile flow and microfaulting, whereas collapse occurs by steeply dipping normal faults, often with a master circular ring fault.

Various subsurface conditions influence the mechanism of upward void propagation and surface expression. Important considerations include the subsurface distribution of the product being removed and whether the product is liquid or solid. Subsidence is more common over areas of large-volume liquid production where the produced liquids occupy intergranular voids. Removal of the liquid lowers in situ pressure and causes compaction. The effect is eventually transmitted to the surface. Removal of a solid such as sulfur, on the other hand, is more localized and prone to a greater degree of subsidence or collapse because a greater percentage of the subsurface support is removed.

The cohesion and strength of the units overlying the zone of initial collapse and the structural attitude of subsurface anisotropies are major controls on surface expression of subsurface collapse. Dip of subsurface layers is one variable influencing surface expression

of subsidence. Where thin horizontal seams are removed, the surface effect will be gentle, broad subsidence. However, when a large volume of material is removed and the structural attitude is steeply dipping, subsidence is likely to evolve into catastrophic collapse. Sulfur production rigs have been swallowed by large sinkholes at Orchard Dome. Also, the steep dip of the productive cap rock at Orchard Dome caused the surface expression of the subsidence and collapse to migrate laterally up to 100 m.

Structural Patterns Around Texas Salt Domes

The suitability of salt domes as sites for waste disposal is affected by the distribution and genesis of near-dome structural patterns. Structural discontinuities, such as faults, lineaments, and collapse sinks, can influence the migration of ground water and contaminants. Accurate modeling of ground-water flow also requires an understanding of the distribution and nature of these structural features. Salt domes exert a variable influence on regional structural patterns depending on the timing and rate of dome growth.

The structural fabric of the Houston diapir province is dominated by strike-oriented, down-to-the-coast, normal growth faults. Regional growth faults and surface lineaments are aligned strongly parallel with the regional depositional strike, suggesting control of fault orientation by prograding shelf margins. In the area around salt domes (2.5-mi radius from margin of salt stock) preferred orientations of faults and lineaments match regional trends. However, domal fault and lineament orientations are dispersed to a greater degree than regional values. Dispersion is greatest in areas where salt domes are abundant and shallow. The radial orientation of many faults around salt structures causes this dispersion of regional fault orientation. There was no difference in density of faults between regional and domal areas when mapped at a scale of 1 inch to 4,000 ft. There is insufficient data to determine if this absence of density difference is an artifact of map scale, procedure, or is real.

Both ductile and brittle processes expose strata over Damon Mound salt dome. An Oligocene reef facies, the Heterostegina limestone, is preserved in a down-dropped fault block over the upper part of the cap rock. Relief over the crest of the salt stock localized reef growth over those salt domes with sufficient positive surface expression, and currently this limestone exhibits about 6,000 ft of structural relief at Damon Mound. In addition to brittle deformation of the limestone, Late Pleistocene strata are warped over the crest of Damon Mound as a result of dome growth. Actual uplift of the salt dome has caused most of this warping of Late Pleistocene strata because drape compaction can account for only about 2 ft of differential elevation. Structural calculations indicate that short-term growth rates for Damon Mound since the Late Pleistocene were 2 ft (0.6 m) per 1,000 yr, whereas post-Miocene rates were 0.3 ft (0.08 m) per 1,000 yr. This recent short-term growth rate was approximately one order of magnitude greater than long-term rates, suggesting relatively recent pulses of rapid salt dome uplift.

Cap Rock

Cap rocks commonly overlie the crest and drape down the upper flanks of shallow salt domes. Cap rocks undergo a range of complex natural and man-induced processes that would affect the long-term stability of a toxic waste facility utilizing solution-mined caverns in salt. Characteristics and processes within cap rocks that are of greatest concern are (1) subsidence or collapse of voids, (2) lost-circulation zones, and (3) drill holes that penetrate the supercap, cap rock, and salt.

The potential for subsurface and surface disruption owing to natural and man-induced removal of large volumes of material from the cap rock is a critical concern. Domes with a history of significant Frasch sulfur mining are sites where large volumes of material have been removed from cap rocks. Of the ten domes in Texas with significant sulfur production (in excess of 1 million long tons), eight have definite surface subsidence or collapse directly

correlated to areas of sulfur production; the other two domes have subsidence probably related to sulfur production.

The surface expression of subsurface collapse includes two end-member geomorphic forms--broad, bowl-shaped depressions and steep-walled collapse sinks--that developed as a result of trough subsidence and caving, respectively. Other differentiating variables include rate of subsidence, dip of subsurface units, and the cohesion of the units overlying the zone of initial collapse.

Both types of collapse have affected the surface over domes with significant sulfur production. Boling Dome is an example of a dome with abundant surface subsidence over the area of sulfur production. In 1983 a circular collapse feature developed on the surface over Boling Dome at the site of a well drilled in 1927. During cap-rock drilling a cavity was encountered with a vertical extent exceeding 106 ft. Apparently the naturally formed cavern, possibly weakened by dissolution and caving, collapsed as a result of drill-hole penetration, allowing ingress of shallow ground water. The surface over Orchard Dome displays arcuate and circular collapse features over the area of sulfur production and circular collapse features over individual production wells.

Lost-circulation zones in cap rock are areas of concern because they can readily transmit fluids and because they are potential zones of collapse. That lost-circulation zones transmit fluids is evidenced by their use as high-volume saltwater disposal zones, and by the presence of associated minerals, oil, and sulfur. Long-term injection tests at Barbers Hill Dome revealed that lost-circulation zones there have transmissivities exceeding 500,000 g/d/ft.

Data developed for this report indicate that cap-rock lost-circulation zones at Boling, Barbers Hill, and Spindletop Domes are hydrologically connected to surrounding strata. Hydrologic connection is indicated by a correlation between periods of high-volume injection into cap rocks with changes in water chemistry in fresh-water sands surrounding the dome, and by increased oil production associated with deeper saltwater sandstones. In

addition to evidence indicating active export of water injected into cap rocks, geologic data reveal that cap rocks received both shallow (fresh) ground water and basinal (saline) fluids. Oil in cap rocks and supracap sands indicates upward migration of fluids from deep-basinal sources. Sulfur indicates that the strong reducing conditions associated with oil alternated with oxidizing conditions. Similarly, petrographic evidence of calcite dissolution and reprecipitation reveal active fresh-water diagenesis.

In addition to being hydrologically complex, some cap rocks are lithologically complex. The most common lithologic sequence within cap rocks from top to bottom is (1) calcite, (2) transitional calcite, gypsum, sulfur, and anhydrite, and (3) anhydrite. Lost-circulation zones can occur anywhere within cap rocks, but are concentrated at the top of the calcite zone, in the transitional zone, and at the base of the anhydrite zone immediately overlying the salt stock.

Cap rocks form from the bottom up, in part by accumulation of the residuum from salt dissolution at the diapir crest. This formative mechanism compresses within cap rocks the insoluble strata present within salt stocks. In addition to the depositional salt stratigraphy, any flanking strata that were sheared off and incorporated within the salt stock are liable to be preserved in the cap rocks. The presence of extradomal, terrigenous elastics within the cap rock at Boling Dome is explained in part by incorporation through this mechanism. Terrigenous clastic sediments within the anhydrite cap rock at Boling Dome are probably evidence that similar terrigenous elastics are included within the underlying salt stock, probably by shearing along the salt-sediment interface. Cap-rock stratigraphy can therefore provide powerful clues to the heterogeneity of the underlying salt stock.

Structure within the cap rock strongly influences fluid transmission and structural stability of both the salt stock and surrounding strata. Cap-rock structure includes lost-circulation zones, veins, faults, shear planes, and zones of incorporated exotic blocks of strata. At Boling Dome, structural analysis of cores reveals cap-rock structure and vein

orientation centered at about a 45° dip. The dip of the cap-rock - salt-stock interface and surrounding strata is also 45°. We infer that structure and vein orientation within the cap rock are controlled by the dip of the surrounding cap-rock - salt-stock interface. Such structural fabric and faulting promote cross-formational flow and migration of basinal fluids through the cap rock. These data explain why sulfur deposits are concentrated on the downdip "shoulders" of salt domes, where the dips of the cap-rock - salt-stock interface are often about 45°.

Artificial penetrations by exploration and production drill holes are also potential pathways for connecting shallow fresh-water aquifers and deep saline aquifers, possibly allowing rapid salt or cap-rock dissolution by fresh water. Approximately 20,000 drill holes penetrate the cap rock at Boling Dome. Although most of these drill holes penetrate only part way into the cap rock, a large number (greater than 100 holes) probably penetrate to the top of the salt stock.

Thus, cap rocks exhibit a very complicated evolutionary history. We think that those cap rocks with abundant sulfur production are among the most complex cap rocks because of the additional consequences induced by man's resource production.

Cap-Rock Hydrology

If a waste storage cavern lost integrity, it would probably lose waste into the cap rock over the salt stock. To predict the fate of waste leaking into a cap rock we examined cap-rock hydrogeology, focusing our attention on Barbers Hill and Boling Domes. The following lines of evidence suggest that cap rocks with lost-circulation zones pose serious threats to the long-term integrity of waste storage caverns in associated salt stocks:

- (1) natural fluids in lost-circulation zones within cap rocks can attack cements and casings,
- (2) wells completed through lost-circulation zones lack the outer barrier of cement within the zone of lost-circulation,
- (3) some lost-circulation zones are hydraulically connected to sandstone aquifers in strata surrounding the salt stock, and
- (4) lost-circulation zones may

be rich in sulfates and are capable of aggressively attacking cements and casing strings. Wells completed through lost-circulation zones are less secure than conventional wells because a liner is substituted in place of cement that normally would have been circulated to the surface.

Cap rock at Barbers Hill salt dome acts as a single, highly permeable integrated aquifer, based on analysis of interference tests during brine well injection. Transmissivities of the cap rock at Barbers Hill exceed 500,000 g/d/ft. Cap rocks with extensive lost-circulation zones appear to have good hydraulic connection with adjacent sands. At Barbers Hill Dome the hydraulic connection between the cap rock and surrounding sands is indicated by (1) a lost-circulation zone at the interface between cap rock and the horizontal planar crest of the salt stock, (2) the equivalent static water levels within the cap rock and surrounding fresh-water aquifers (Lower Chicot and Evangeline aquifers), (3) the response of oil-producing sands along the deep flank to high-volume brine injection in the cap rock, (4) equilibrium water levels in the cap rock during high-volume brine injection in the cap rock, and (5) long-term deterioration in water quality of fresh-water sands near Barbers Hill owing to addition of Na^+ and Cl^- .

Water is injected into the cap rock at Boling Dome at 315°F to produce sulfur. Injection rates have ranged from 4 million to 10 million g/d for the last 55 years. Contours of bottom-hole temperatures of water in strata surrounding the salt stock indicate that anomalously high-temperature waters have migrated 1 to 2 mi from the area of sulfur production.

Even with the injection of 1.5 billion (at Barbers Hill) to 2.4 billion (at Boling) barrels (bbl) of fluid into their respective cap rocks, it is difficult to prove unequivocally migration into surrounding strata. It would be difficult to detect a small quantity (less than thousands of bbl) of waste leaking from a hypothetical waste repository into the cap-rock lost-circulation zone without an extensive monitoring system. Domes with lost-circulation zones in the cap rock are not ideally suited for waste disposal in solution-mined caverns in

salt. Such lost-circulation zones must be completely isolated from the well bores that transmit toxic materials. Problems associated with lost-circulation zones would be attenuated by injecting cement until the zone is structurally supported and proves to be hydrologically tight.

ACKNOWLEDGMENTS

Thanks are extended to many helpful individuals in various State and Federal agencies and to industry representatives who provided data and access to information. The following personnel of the Railroad Commission of Texas provided ready access to files and helped compile data: J. W. Mullican (Director, Underground Injection Control), D. M. Jorgensen, R. Ginn, and L. L. Savage. Texas Water Commission (formerly the Texas Department of Water Resources) personnel were extremely helpful, including B. Knape (water resources research), L. Falconieri and C. Butler (remote sensing data from Texas Natural Resources Information System), and R. Heimann (geophysical log library).

Discussions with the following industry representatives were very helpful: K. Allen, J. Machado, and E. Voorhees (Fenix and Scisson, Inc.), H. J. Morgan (PB-KBB Inc.), F. Samuelson and G. P. Eager (Texasgulf Inc.), C. Brassow (United Resource Recovery, Inc.), W. Ehni (formerly with Geotronics Inc.), and M. Miller (Miller and Associates). Texasgulf Inc. graciously donated core from the cap rock of Boling Dome. T. Simons of Damon Quarry permitted access to cap rock at Damon Mound Dome.

The manuscript was word processed by the authors. They extend special thanks to the entire BEG computing staff, especially Elizabeth D. Orr, Gerry White, Dan Fowler, and Jack W. Lund under the supervision of Mike P. Roberts, who labored long hours with a new computer system, a new word processing system, and a whole host of new hardware and software. Dorothy C. Johnson did final word processing under the supervision of Lucille C. Harrell. Illustrations were drafted by Annie Kubert, Joel L. Lardon, Kerza A. Prewitt, and

T. B. Samsel III under the supervision of Richard L. Dillon. The manuscript was reviewed by Edward C. Bingler, Charles W. Kreitler, and Jules R. DuBar; their timely comments are acknowledged. Editing was by Mary Ellen Johansen.

Funding for this research was provided by the Texas Water Commission under interagency contract no. IAC(84-85)-2203.

RESEARCH REPORTS

SUBSIDENCE OVER TEXAS SALT DOMES

by

W. F. Mullican III

CONTENTS

INTRODUCTION	21
MECHANISMS OF SUBSIDENCE	22
Trough Subsidence	22
Subsurface Caving	24
Chimneying	24
Plug Caving	26
Controlling Factors	26
NATURAL SUBSIDENCE	28
Diapiric Salt	28
Bedded Salt	29
MAN-INDUCED SUBSIDENCE	30
Sulfur Mining	31
Mechanisms	31
Salt Mining	32
Solution-Brine Wells	32
Room-and-Pillar Mines	34
Oil and Gas Production	35
SUBSIDENCE OVER INDIVIDUAL SALT DOMES IN TEXAS	35
Procedures	36
Boling Dome	39
Activities	39
Subsidence Related to Sulfur Mining	43
Other Subsidence at Boling Dome	50
Orchard Dome	51
Chronology of Sinkholes	54
Moss Bluff Dome	60

Spindletop Dome	60
Other Domes	62
CONCLUSIONS	66
REFERENCES	67

Figures

1. Section over steeply dipping bed showing migration of surface subsidence	23
2. Migration of subsurface caving	25
3. Location map of 1979 U-2 color-infrared photography flights	37
4. Precipitation data, Fort Bend County	38
5. Local topography, and location of (a) Boling, (b) Clemens, (c) Hoskins Mound, (d) Long Point, (e) Moss Bluff, and (f) Orchard Domes	44-49
6. Map of sinkhole locations and salt structure on top of cap rock, Boling Dome	52
7. Fence diagram, Orchard Dome	53
8. Map of chronological development of subsidence features, Orchard Dome	56
9. Ground-level view of collapse sinkhole, Orchard Dome	59
10. Black-and-white copy of U-2 color-infrared photography, Orchard Dome	59
11. Map of man-induced subsidence, Moss Bluff Dome	61
12. Lateral and vertical extent of man-induced subsidence, Spindletop Dome	63
13. Map of man-induced subsidence, Fannett Dome	65

Tables

1. Terrain signature of color-infrared film	36
2. Sulfur production and subsidence data	40
3. Sinkhole evolution, Orchard Dome	55

INTRODUCTION

Subsidence is the sinking of the earth's surface that results from several natural and man-induced processes. Subsidence is an important indicator of structural instability of the surface over a salt dome, and thus the study of subsidence is an important element in evaluating the suitability of salt domes as repositories for toxic chemical waste disposal. This section of Phase III research involved remote sensing methods to detect land-surface subsidence associated with natural salt diapiric processes and man-induced resource recovery, and to determine processes likely to reduce the stability and integrity of hydrologic and structural barriers over individual salt diapirs.

Natural subsidence is commonly present over shallow diapirs. Such subsidence is evidenced by localized saline lakes and depressions over dome crests. Man-induced subsidence over salt diapirs has been documented since the early history of resource development of salt diapirs. This subsidence is associated with the production of sulfur, oil and gas, and brine. Sulfur production has caused the most dramatic subsidence and collapse in domal areas.

Hydrologic and structural barriers can be affected by natural and man-induced land-surface subsidence and consequently disrupt waste storage. Adverse effects would include extensive structural damage to buildings, pipelines, manifolds, well heads, and casing strings. Damage to subsurface and surface equipment at a storage site would release toxic waste into the natural environment. Subsidence over salt domes delineates subsurface zones where natural hydrologic barriers may be disrupted. The collapse of aquitards and aquicludes would enhance fluid movement as a result of fracturing. Meteoric ground water could be recharged at a greater rate over the dome crest and descend toward the dome, thereby accelerating dissolution of the cap rock and salt stock. Also, in the event of

cavern failure, migration of fluids and contaminants away from the dome would also be enhanced by transport through fractures in the aquitard.

MECHANISMS OF SUBSIDENCE

Obert and Duvall (1967) defined subsidence as the end result of three types of deformation that can act as a set or individually. These forces of deformation are (1) closure from elastic deformation, (2) closure from inelastic deformation, and (3) closure owing to fracturing and subsequent porosity increase of overlying rock that acts to fill the opening. Subsidence ensues after natural or man-induced processes remove subsurface material and create an unstable void or opening. Gravity-driven processes then act to close the opening. Four processes that may contribute to closure and subsidence as described by Obert and Duvall (1967) are (1) trough subsidence, (2) subsurface caving, (3) chimneying, and (4) plug caving. These processes and the extent of land-surface subsidence they initiate are determined by several factors, including rock profile and rock properties.

Trough Subsidence

Trough subsidence is gentle downwarping centered over the subsurface zone of excavation. Subsurface subsidence is initiated by downward flexing of the roof span over the voids. Subsurface subsidence usually propagates vertically through unconsolidated or incompetent, thin-bedded sedimentary deposits. Deere (1961) and Lee and Strauss (1969) reported trough subsidence after a brief period of sulfur production over an unnamed salt dome in Texas. Surface expression of subsidence shifted relative to the zone of extraction (fig. 1). Experimental and analytical analyses of trough subsidence are abundant (Rellensmann, 1957; Obert and Duvall, 1967; Ege, 1984).

Problems arise when experimental models are used to predict occurrence and magnitude of trough subsidence over salt domes, owing to variables such as thickness, rock

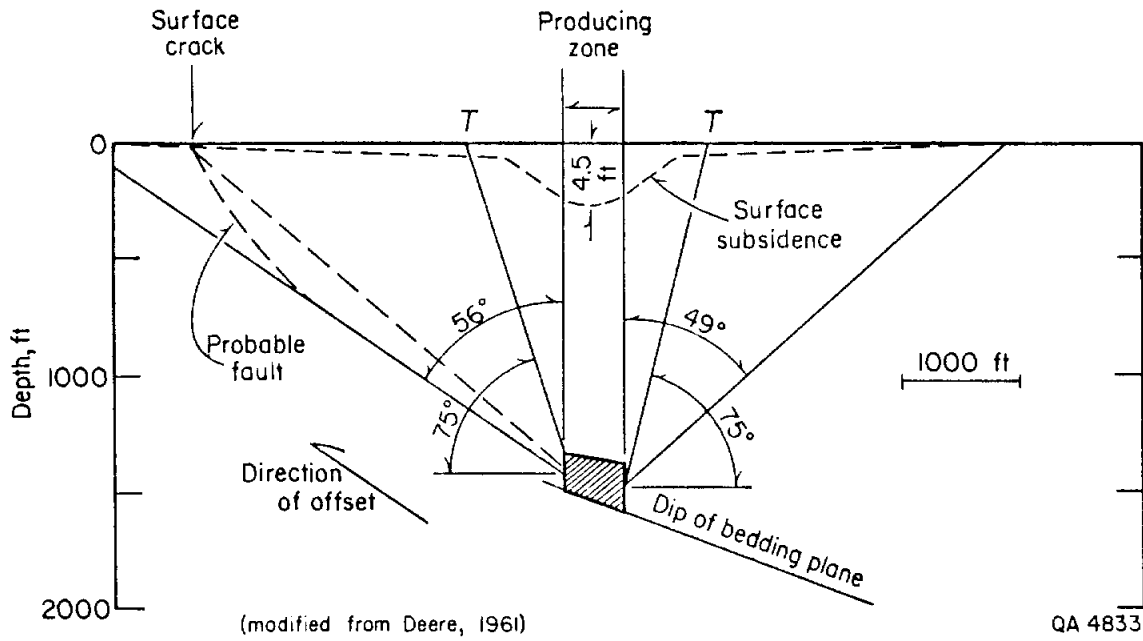


Figure 1. Section over steeply dipping bed showing migration of surface subsidence and points of maximum tension, T. (After Deere, 1961).

type, amount of support, and structure. For example, experimental modeling of trough subsidence often assumes structurally horizontal bedding. Sulfur intervals in cap rock may be horizontal, vertical, or any intermediate orientation. With trough subsidence, the zone affected by downwarping over the zone of excavation or solution increases as the disturbed zone migrates to the surface. Horizontal, isotropic bedding results in equal displacement radially from the excavation zone. Steeply dipping beds introduce significant variations that affect propagation of the disturbed zone. Lateral migration of the disturbed zone will be greatest along the dip of the beds. This results in migration toward the center of the salt dome when the flank structure dips away from the center.

Subsurface Caving

Caving is roof failure into the subsurface void or cavern, followed by upward migration of the zone of broken rock (fig. 2). Caving propagates through a variety of processes, including chimneying, plug caving, and piping (Allen, 1969). Caving is initiated when the strength of the roof span is exceeded by excavation. The overburden then fails by slabbing into the open void. Caving is prevalent in incompetent rocks such as fractured shales. Unconsolidated or poorly cemented rocks, which commonly overlie salt domes, are also conducive to caving. The area of caving in plan view either remains constant or decreases in extent as caving migrates to the surface (fig. 2). Caving may also migrate along the dip of bedding planes or along other geologic features such as igneous dikes (Boyum, 1961).

Chimneying

Chimneying is a type of caving that covers a relatively small area and rapidly migrates to the surface. Constant cross-sectional area is maintained during vertical migration of the broken zone to the surface. This mechanism of subsidence can migrate upward through 1,000 ft (300 m) of overburden in a matter of days (Obert and Duvall,

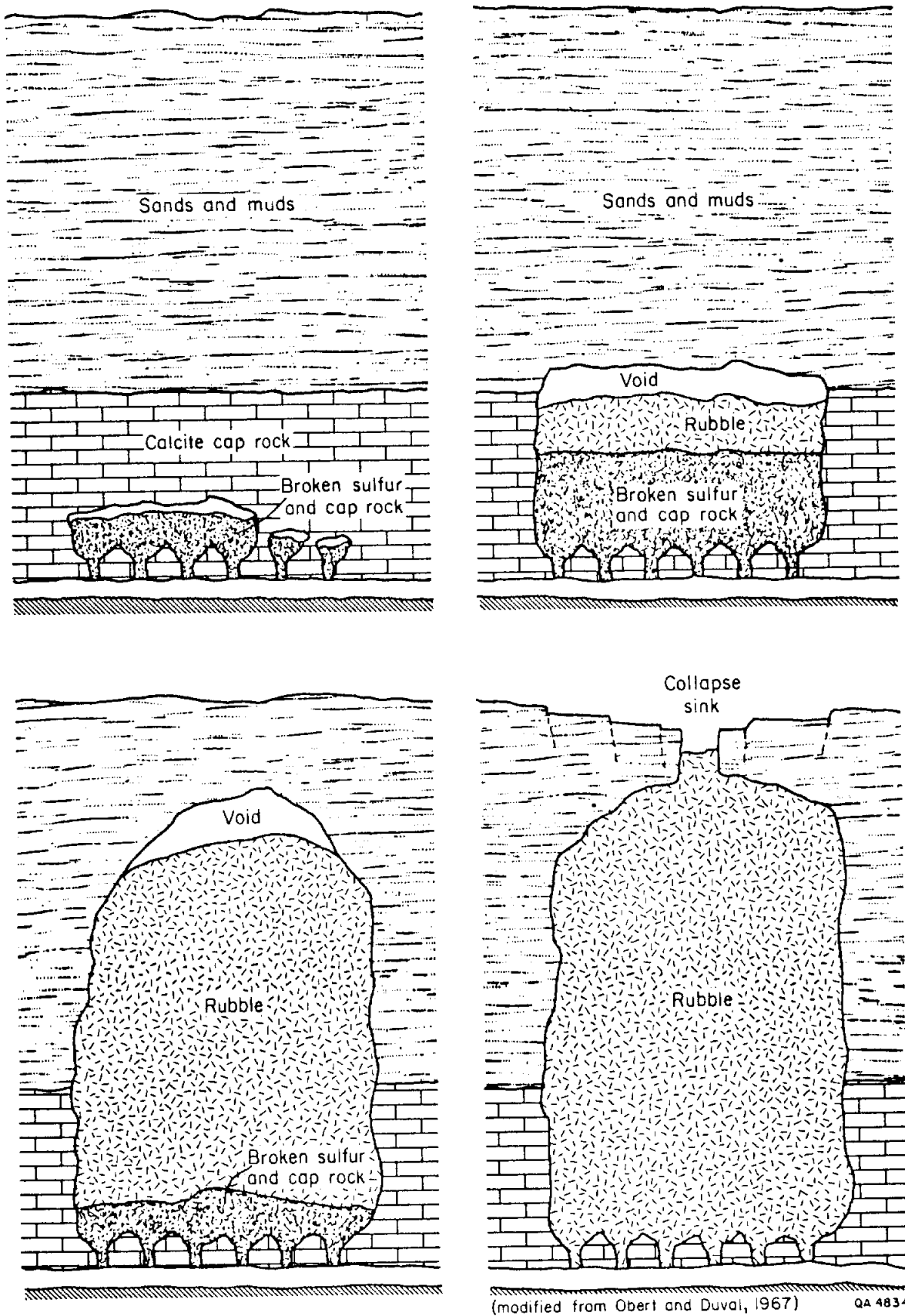


Figure 2. Migration of subsurface caving towards surface expression of collapse. (Modified from Obert and Duval, 1967).

1967). Chimneying is the mechanism of subsidence that has the strongest tendency to migrate concordant to the dip of bedding.

Plug Caving

Plug caving is the failure of overburden as a cohesive unit from the roof of the subsurface opening to the surface. Plug caving provides the most dramatic and potentially catastrophic mechanism of subsidence. It causes no apparent volume expansion and surface expression is roughly equivalent in area to the subsurface zone of failure. Plug caving is differentiated from the similar process of chimneying by a greater consolidation of the failed material.

Controlling Factors

Land-surface subsidence associated with salt domes results from (1) natural or man-induced dissolution of the salt stock, (2) natural or man-induced removal of cap-rock materials, and (3) oil, natural gas, and ground-water pumpage from superdomal strata. Two and possibly three different subsidence mechanisms operate under these conditions. Subsidence from oil and gas or ground-water production is a result of the removal of intergranular support from the host reservoir. Removal initiates differential compaction within the shallow reservoirs, which are typically composed of unconsolidated or poorly cemented Pleistocene and Holocene sediments.

Subsidence originating in the salt stock or cap rock results from void or cavern failure that occurs when void expansion exceeds roof strength. If this failure is of sufficient magnitude it will be expressed at the surface in the form of subsidence. Caving is the usual mechanism active in the collapse of voids or caverns due to solution or room-and-pillar mining methods. When the roof span of the void or cavern exceeds the strength of overlying strata, downwarping and collapse of the roof are initiated. The resulting broken rock will undergo a significant increase in volume owing to the creation of fracture and breccia porosity. If the original void is small or the distance to the surface is large,

the volume increase that the shattered rock undergoes during breakage will fill the void and support the roof span. If, however, the void is large enough or the distance to the surface is small enough, collapse will continue to the surface.

Surface expression of subsidence from downwarping or subsurface collapse is dependent on the size of the initial void or cavern and the distance from the void to the surface (Obert and Duvall, 1967). Downwarping and collapse initiate a sequence of events that must occur in order for subsidence to take place. Generally, downwarping of overburden characterizes trough subsidence, whereas overburden collapse into the subsurface void characterizes various types of caving. Stefanko (1973) reported the size of the span roofing the void or cavern as most critical to the potential for collapse. Prediction of rate and magnitude of subsidence is complicated by the large number of factors affecting mechanisms of subsidence. Factors listed by Chang and Nair (1974) are (1) rock profile, (2) rock properties, (3) location, size, and shape of the opening, (4) presence of faults, shear zones, bedding planes, and other geologic discontinuities, (5) presence of other openings, (6) initial stress state, and (7) any artificial support in the openings. The contrasting rock properties of cap rock and typically unconsolidated domal overburden illustrate the complexity of variables affecting subsidence. Subsurface caving is most prevalent in cap-rock void filling because of the brittle nature of the rock. Downwarping is a dominant process in the unconsolidated ductile overburden.

In some reported cases of man-induced subsidence, vertical and horizontal movement may continue long after the termination of production. One proposed explanation is the compaction and settling of broken rock that may be active for extended periods of time after caving ceased (Wassman, 1980).

NATURAL SUBSIDENCE

Natural subsidence in the form of collapse sinks and broad solution troughs are associated with diapiric and bedded salt. The variety of surface expressions indicates that natural solution mechanisms probably include both trough subsidence and subsurface caving.

Diapiric Salt

Natural subsidence is present over salt domes as a result of the dissolution of salt and possibly cap rock. Salt dissolves in contact with fresh or undersaturated saline ground waters. The amount of surface and subsurface water, the influx of fresh water, and the length of exposure to these active waters determine the degree of dissolution in individual diapiric environments.

In extremely arid environments with limited hydrologic interaction, the rate of salt movement toward the surface exceeds the amount of salt removal from dissolution. This is illustrated in the arid environments of northeastern Spain where rates of diapiric growth have exceeded rates of dissolution. Literally mountains of salt are exposed at the surface above the surrounding plains (Sellards, 1930).

Salt dissolution is active in more humid environments associated with fresh groundwater and surface-water systems. Dissolution and removal of salt is at a rate faster than the salt is being replaced from structurally lower source beds. Several of the shallow domes in the East Texas Basin have topographic depressions located over the crest of the domes indicating the area of maximum dissolution and subsidence (Powers, 1926; Fogg and Kreitler, 1980; Collins, 1982). Five diapirs in the East Texas Basin have surface salines that indicate potentially active dissolution (Fogg and others, 1982).

Topographic lows suggest minor subsidence centered over Keechi, Oakwood, Palestine, and Grand Saline Domes in the East Texas diapir province (Collins, 1982; Fogg

and others, 1982). Similarly, Lake Port is reported to be an area of natural subsidence located approximately 1 mi (1.6 km) west of the center of Butler Dome (Powers, 1926).

Kolb (1977) reported that some of the domes in the Northern Louisiana Basin are also overlain by topographic lows, for example, Rayburn and Vacherie. Although two possible scenarios are presented, he concluded that domes overlain by topographic lows have been tectonically inactive for a long period of time. The depressions are a result of extensive dissolution followed by collapse of the salt and overburden.

Lake Peigneur, Louisiana has been attributed to subsidence resulting from the natural dissolution of the underlying Jefferson Island salt dome (Harris, 1908; O'Donnell, 1935). Autin (1984) noted that all of the Five Islands salt domes in Louisiana have at least some surficial expression of natural dissolution and subsidence.

Bedded Salt

Natural dissolution and subsidence also occur in several evaporite basins containing bedded salt in Texas, New Mexico, Louisiana, and Kansas. Gustavson and others (1980) reported that salt dissolution in the Anadarko, Dalhart, and Palo Duro Basins is an active process, as expressed by the numerous salt seeps, springs, and salt pans present in the Texas Panhandle. Approximately 2.8×10^6 tons of dissolved solids are removed each year (Gustavson and others, 1980). Of this figure, 66 percent is from salt dissolution and 34 percent is from gypsum and anhydrite. Surface expression of these dissolution processes includes (1) 250 ft (75 m) of regional subsidence north of the Canadian River, (2) folding and brecciation of strata overlying the bedded salts, (3) chimney features filled with collapsed breccias, and (4) ancient and modern sinkholes (Gustavson and others, 1980). Stratigraphic studies suggest that dissolution and subsidence have been active since the Late Cretaceous.

One of the more dramatic modern subsidence features related to the natural dissolution of bedded salt developed in Winkler County, Texas on June 3, 1980

(Baumgardner and others, 1982). Wink Sink formed as a result of dissolution of salt in the Permian Salado Formation. By June 5, the dimensions of the sink were 360 ft (110 m) in diameter, 110 ft (34 m) deep, and had an estimated volume of $5.6 \times 10^6 \text{ ft}^3$ ($1.6 \times 10^5 \text{ m}^3$). Natural dissolution of the salt was probably hydrologically controlled by the underlying Permian Capitan Reef trend. A 52-year-old abandoned well bore inside the area affected by the sink may also have acted to enhance dissolution and subsequent collapse (Baumgardner and others, 1982).

Natural dissolution of bedded salt has also been reported in Kansas (Walters, 1978). The Wellington lost-circulation zone is an interval of partial to total dissolution of the Wellington Salt extending more than 100 mi (160 km). Abrupt changes in salt thickness range from 200 ft (61 m) of salt on the west side, to a total absence of salt on the east side of the trend. The lost-circulation zone is the result of partial collapse of overburden into void spaces created by the dissolution of salt. The surface expression of this salt dissolution includes subparallel sinks and valleys. The trend has been migrating westward with the dissolution of the salt front since the early Pleistocene (Walters, 1978).

MAN-INDUCED SUBSIDENCE

The same subsidence features that naturally form over subsurface deposits of salt have been associated with man's recovery of natural resources, including sulfur, brine, and oil and gas. Subsidence related to man's activity results from extraction of subsurface material and subsequent removal of support. The risk of damage to surface and subsurface structures owing to man-induced subsidence and collapse has promoted a substantial body of literature (Minor, 1925; Pratt and Johnson, 1926; Sellards, 1930; Winslow and Doyel, 1954; Winslow and Wood, 1959; Gabrysch, 1969; Gabrysch and Bonnet, 1975; Kreitler, 1976a; Ratzlaff, 1982; Gabrysch, 1984).

Sulfur Mining

Fourteen domes in the Houston diapir province have had sulfur production. All of the 10 domes with sulfur production greater than 1 million long tons (LT) have surface subsidence. Remote sensing, mapping, and field surveys documented subsidence associated with sulfur production.

Cap rock commonly contains extensive primary and secondary porosity. Hanna and Wolf (1934) noted that some cap rock may have up to 50 percent cavities and voids. These porous zones are often the intervals where sulfur is located. Frasch sulfur mining in domal cap rock creates and enlarges underground openings as sulfur is removed. To reduce stress, subsurface subsidence will act by bending overlying strata or closing the opening through collapse. Structural movement and deformation may continue until a depression forms at land surface.

Two types of land surface subsidence were observed over sulfur-productive domes-- broad subsidence bowls and collapse sinks. Trough subsidence of Obert and Duvall (1967) has a small vertical component of movement compared to an extensive horizontal component (small vertical to horizontal ratio). Broad subsidence bowls are best illustrated at Moss Bluff, Fannett, Hoskins Mound, and Spindletop Domes. In contrast, circular collapse sinks and arcuate- or crescent-shaped sinkholes are related to various caving processes and have a relatively greater vertical component of movement. Collapse sinks and arcuate bands of subsidence with large vertical movements occur at Boling and Orchard Domes.

Mechanisms

Differences in surface subsidence at sulfur-mined domes can best be explained by the contrasting structural attitude of sulfur-producing zones and by the distribution of sulfur. Broad subsidence bowls occur where productive intervals are relatively flat lying and measured thickness of the sulfur intervals approaches true thickness (thickness perpend-

icular to bedding plane). This results in subsidence bowls with widespread horizontal movement and vertical movement proportional to the thickness of the producing interval. Circular to arcuate subsidence observed at Boling and Orchard Domes is the result of thick massive sulfur and steep dip. Instead of being relatively flat lying, sulfur zones are very steep around the flank of the dome. Observed thickness of productive intervals is much greater than true thickness. With this type of subsidence, the vertical component exhibits much greater movement, while the horizontal component remains localized.

The nature of the sulfur deposits will also influence the type of surface subsidence. Sulfur may occur in the cap rock as one of two end members: (1) evenly disseminated throughout the cap-rock matrix or (2) thick, continuous beds. If the mined area is producing from a disseminated zone of sulfur, the probable surface expression will be trough subsidence analagous to production of ground water. If sulfur is produced from a thick, continuous bed, caving will dominate.

Salt Mining

Salt mining has resulted in extensive and occasionally catastrophic subsidence. Salt is mined from bedded salt and salt domes by solution-brine wells and room-and-pillar rock-salt mines. In Texas, two domes have active underground salt mines and seven domes have active solution-brine wells. Thirteen salt domes have had brine- and rock-salt mines (Seni and others, 1984b,c). Subsidence has not been documented over room-and-pillar salt mines in Texas.

Solution-Brine Wells

Historically, salt brining operations were plagued by subsidence and collapse. Salt brining operations active at Palestine Dome in the East Texas diapir province from 1904 to 1937 resulted in 15 known collapse structures (sinkholes) (Fogg and Kreitler, 1980). These sinkholes are typically circular, water-filled depressions with diameters 27 to 105 ft (8 to

32 m) and depths 2 to 15 ft (0.6 to 4.5 m). The Palestine Salt and Coal Company mined salt from this dome using the then standard brining procedure of (1) drilling and cementing production casing in the cap rock, (2) drilling into salt 100 to 150 ft (30 to 50 m) below the cap rock, (3) injecting fresh water to dissolve the salt, and (4) removing saturated salt water with compressed air.

Fogg and Kreitler (1980) concluded that (1) a one-to-one relationship exists between collapse features and the location of old brine wells (not all of the potential collapse features have been expressed at the surface although each collapse feature can usually be correlated to a brine well), (2) a long time may elapse between termination of mining operations and appearance of collapse features (one collapse feature formed at least 41 years after mining operations ceased), and (3) the presence of an active hydrologic system was either created or enhanced by collapse features.

Fogg and Kreitler (1980) described a hydrologic model for Palestine Dome consisting of (1) ground-water recharge in the hills surrounding Duggey's Lake, (2) downward movement of this water into the dome, (3) active dissolution of the salt stock, (4) discharge of resultant saline waters into Duggey's Lake and proximal sinkholes. The Office of Nuclear Waste Isolation eliminated Palestine Dome from further consideration as a potential candidate for the storage of nuclear waste because not all of the historical brine wells could be located, and thus future locations of collapse could not be predicted (Patchick, 1980).

Grand Saline Dome, a site of active salt mine operations since the 1800's, also experienced recent collapse. On April 2, 1976, a sinkhole appeared at the edge of town (Martinez and others, 1976). Maximum size of this sinkhole was 80 ft (24 m) in diameter. This sinkhole probably developed around an abandoned solution-brine well. Collapse may have been enhanced by a sewer line discharging into the old cavity (Science Applications, Inc., 1977).

The area around a former shaft of a rock-salt mine located at Blue Ridge Dome collapsed in 1949 after conversion to a solution-brine well (Science Applications, Inc., 1977; Seni and others, 1984a). Uncontrolled solution mining of the cavern resulted in rock failure and collapse. In addition to the loss of the cavern, several buildings at the surface were lost. Engineering procedures have been developed to prevent this type of failure. These procedures include casing the cap rock and leaving a thick salt roof.

Historically, salt mining operations in Texas have resulted in the failure and collapse of 10 brine and salt cavern facilities (Seni and others, 1984b). Modern practices associated with solution mining of salt for brine and for cavern storage space have improved such that minimal surface subsidence, detectable only with sensitive instruments, occurs.

Room-and-Pillar Mines

Although subsidence has not been documented over room-and-pillar salt mines in Texas, the room-and-pillar mine at Jefferson Island, Louisiana was flooded when an inaccurately drilled well penetrated a salt mine, drained a lake into the mine, and forced its abandonment (Autin, 1984). On November 18, 1980, Texaco initiated drilling of a scheduled 7,990 ft (2,435 m) test well along the south flank of the dome approximately 50 to 165 ft (15 to 50 m) from the salt stock. On November 20, the drill pipe became stuck and experienced a total loss in circulation of drilling fluids. Approximately one hour later the drilling rig began to tilt owing to active subsidence and was immediately evacuated. Three hours later Lake Peigneur had emptied into the resulting sinkhole along with the drilling rig, a supply barge, and other pieces of oil field equipment. The maximum dimensions of the sinkhole were 1,300 ft (400 m) in width and covered a surface area of 0.30 mi² (0.91 km²). Rapid flooding of the Jefferson Island salt mine coincided with the events at the surface. A detailed summary of this subsidence catastrophe was reported by Autin (1984).

Oil and Gas Production

Man-induced subsidence over Texas salt domes owing to oil and gas production was first reported at Goose Creek oil field in Harris County (Minor, 1925). At the time of his report the field had produced almost 50 million bbl of oil from production intervals between 1,000 ft (305 m) and 4,200 ft (1,280 m). The field covered about 1,000 acres. Subsidence was reported to range from an original level of 2 ft (.6 m) above mean high tide to 3 ft (.9 m) below mean high tide. Subsidence was attributed to the extraction of oil, gas, water, and sand, and possibly to clay dehydration and pressure loss (Minor, 1925; Pratt and Johnson, 1926).

Oil and gas production can also cause sinkholes to form rapidly (Sellards, 1930). On October 9, 1929, a large sinkhole developed 1,500 ft (457 m) northeast of the crest of Sour Lake salt dome. By 1929, production figures for Sour Lake field totaled 73,340,000 bbl of oil, along with unreported large amounts of water.

Sellards (1930) used four field observations to document subsidence: (1) breaks in the earth, (2) newly submerged land, (3) local depressions, and (4) submergence as indicated by inhibited timber growth (otherwise unexplained groups of dead trees). These types of observations are still effective indicators of subsidence along the Texas Coastal Plains.

SUBSIDENCE OVER INDIVIDUAL SALT DOMES IN TEXAS

Natural and man-induced subsidence associated with salt domes was documented for this report using conventional black-and-white and U-2 color-infrared (CIR) photography, and U.S. Geological Survey topographic maps and field surveys. Subsidence was confirmed over 20 of the 30 domes. The principal cause of significant subsidence was Frasch sulfur mining. Of 14 domes with significant sulfur production, 12 had areas of subsidence. Subsidence is also associated with solution mining of brine to a lesser degree. Regionally, oil and gas production, along with ground-water pumpage, appears most active off the

flanks of the diapir. This type of compactional subsidence is strongly expressed off of the flanks of diapirs because of the tremendous amount of oil and gas trapped in reservoirs on the steep flanks of the domes.

Procedures

Specific photography used for this study was originally supported by Flight Requests #0774a (Shelton, Environmental Protection Agency) and #0047 (Ferry, NASA/Ames Research Center) under the FY 1980 Airborne Instrumentation Research Program plan. Flight paths for the two photography missions are mapped in figure 3. Rainfall totals and monthly averages for the four months prior to these flights are included in figure 4. Color-infrared is valuable for detecting subsidence under certain environmental conditions. Various subsidence signatures were (a) circular ponds full of water (Orchard Dome), (b) tonal anomalies--usually dark compared to rest of area (Boling and Stratton Ridge Domes), (c) distinctive loss or absence of vegetation (Clemens and Fannett Domes), (d) scarp-like slump expression (Hoskins Mound Dome), and (e) arcuate- or crescent-shaped swamps around all or part of the flanks of a diapir (Hull Dome).

Wet conditions prior to these flights, combined with the relatively flat topography of the coastal plain, aided interpretation of subsidence with remotely sensed data. Table 1 lists observed signatures of color-infrared photography in this study (Sabins, 1978).

Table 1. Terrain signature of color-infrared film (Sabins, 1978).

<u>Subject</u>	<u>Signature on color-infrared film</u>
<u>Healthy Vegetation</u>	
Broadleaf type	Red to magenta
Needle-leaf type	Reddish brown to purple
<u>Stressed Vegetation</u>	
Prevision stage	Darker red

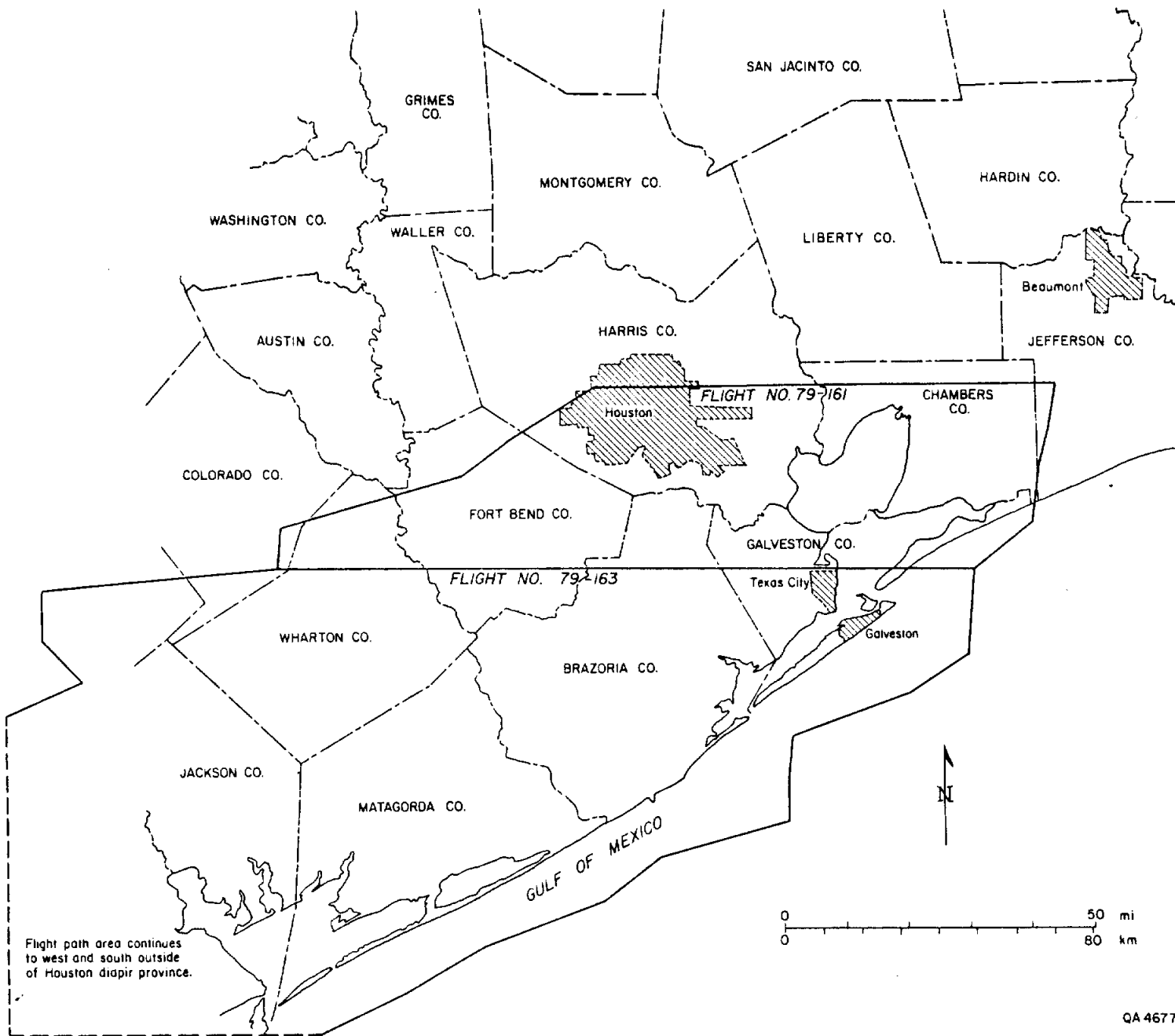


Figure 3. Location map of 1979 U-2 color infrared photography flights used in remote sensing.

Precipitation Data

for periods preceding aerial photography

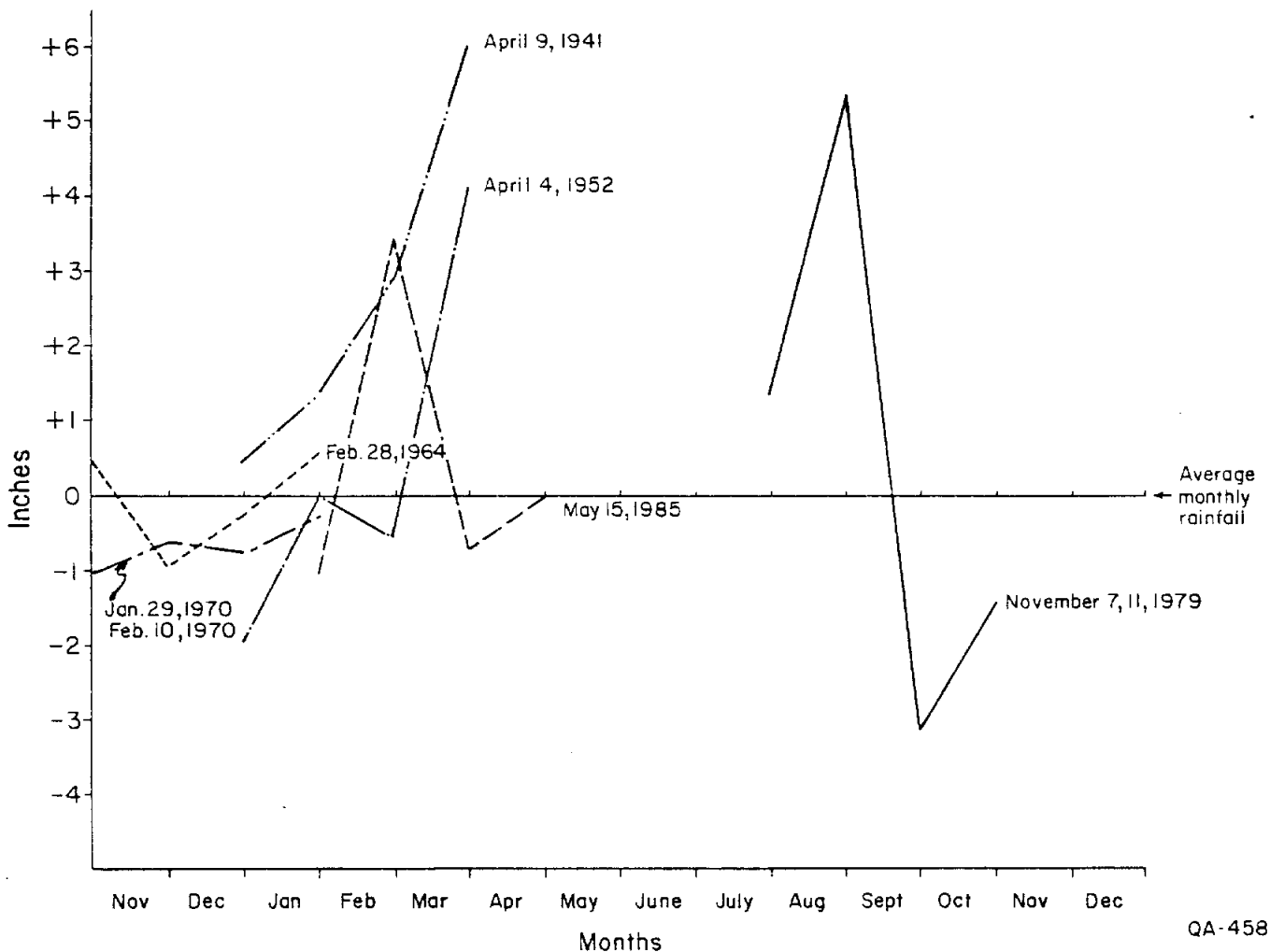
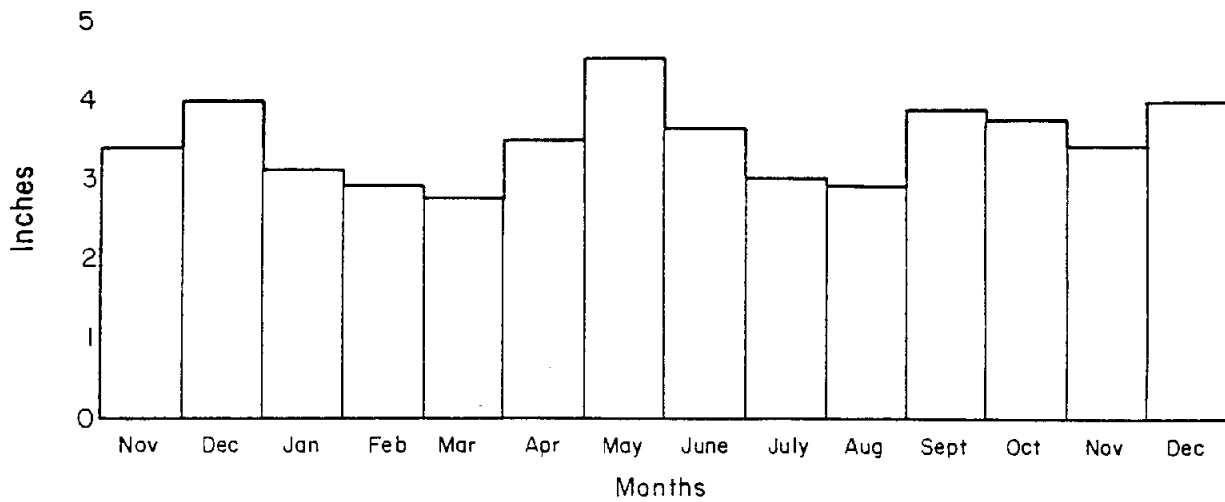


Figure 4. Precipitation data recorded in Fort Bend County for 4 months preceding aerial photography over Orchard Dome. Upper graph shows average monthly rainfall. Lower graph shows deviation from average monthly rainfall for individual photographic missions. Note the absence of any significant or systematic difference in rainfall amounts among dates prior to photography.

Visual stage	Cyan
Autumn leaves	Yellow to white
Clear water	Dark blue to black
Silty water	Light blue
Damp ground	Distinct dark tones
Shadows	Black with few details visible
Water penetration	Green and red bands good: IR bands poor
Contacts between land	Excellent discrimination

Boling Dome

Boling Dome is located in Wharton and Fort Bend Counties, Texas. Minimum depth to cap rock and salt is 380 ft (116 m) and 975 ft (297 m), respectively. It is the largest salt diapir along the Gulf Coastal Plain, with major and minor axis lengths of 25,400 ft (7,742 m) and 16,200 ft (4,938 m) and a planar crest area of $2.39 \times 10^8 \text{ ft}^2$ ($2.2 \times 10^7 \text{ m}^2$).

Activities

Virtually every aspect of mineral recovery is active at Boling Dome (table 2). Natural gas is stored in solution-mined caverns in the salt stock. Valero Inc., operates four gas-storage caverns at Boling Dome with a combined volume of 10,000,000 bbl (at 3,800 psig, 10,000,000 bbl will contain 250,000,000,000 ft^3 of natural gas). Brine disposal into sands flanking the dome is also currently active at Boling Dome. Since 1950, nine saltwater disposal wells (SWD) have been permitted by the Railroad Commission of Texas (RRC). Three of these wells have been operated by Valero Inc., to dispose brines created during storage-cavern construction.

Sulfur production at Boling Dome is one of the most impressive examples of mineral production from salt domes. Four companies, Texasgulf Inc., Baker-Williams, Duval

Table 2. Sulfur production and subsidence data from 14 sulfur domes in the Houston diapir province.

Dome with Sulfur Production	County	Cumulative Production LT to 1/1/83 (unpublished)	Cumulative Production LT to 1/1/88 (from Ellison, 1971)	Duration of Sulfur Production	Cumulative Oil Production to 1/1/85 (in 1000 bbls)	Number of Solution-Mined Storage Caverns
Boling	Wharton-Fort Bend	7.86 x 10 ⁷	6.32 x 10 ⁷	1928-Present	36,177	4
Gulf	Matagorda	1.28 x 10 ⁷	1.26 x 10 ⁷	1919-1936 1965-1970	0.48	0
Hoskins Mound	Brazoria	1.09 x 10 ⁷	1.09 x 10 ⁷	1923-1955	6,020	0
Spindletop	Jefferson	9.84 x 10 ⁶	6.85 x 10 ⁶	1952-1976	153,788	0
Moss Bluff	Liberty-Chambers	9.31 x 10 ⁶	5.27 x 10 ⁶	1948-1982	2,319	5
Long Point	Fort Bend	8.97 x 10 ⁶	5.22 x 10 ⁶	1930-1938 1946-1982	71	0
Orchard	Fort Bend	5.49 x 10 ⁶	5.24 x 10 ⁶	1938-1970	23,041	0
Bryan Mound	Brazoria	5.0 x 10 ⁶	5.0 x 10 ⁶	1912-1935 1967-1968	17	16
Fannett	Jefferson	3.48 x 10 ⁶	1.94 x 10 ⁶	1958-1977	52,384	5
Clemens	Brazoria	2.97 x 10 ⁶	2.97 x 10 ⁶	1937-1960	72	17
Nash	Fort Bend-Brazoria	3.22 x 10 ⁵	2.08 x 10 ⁵	1954-1956 1966-1969	5,109	0
High Island	Galveston	1.47 x 10 ⁵	3.68 x 10 ⁴	1960-1962 1968-1971	140,297	0
Damon Mound	Brazoria	1.40 x 10 ⁵	1.40 x 10 ⁵	1953-1957	21,956	0
Big Creek	Fort Bend	1.71 x 10 ³	1.45 x 10 ³	1925-1926	25,114	0

Table 2. (cont.)

Dome with Sulfur Production	County	SUBSIDENCE					Comments	
		P = Present	A = Absent	1979 Color-Infrared Aerial Photography	Field Confirmation 1985	RRC, TDWR, and Other		Aerial Extent Land-Surface Subsidence (ft ²)*
Boling	Wharton-Fort Bend	P	P	P	P	P	6.08 x 10 ⁷	Greatest producer of sulfur from Gulf Coast domes
Gulf	Matagorda	P	P	No access	A	-insufficient data-		Portion of sulfur field now covered by Mine Lake
Hoskins Mound	Brazoria	P	P	P	P	-insufficient data-		Subsidence includes slump escarpment over north part of dome
Spindletop	Jefferson	P	Not covered	P	P	2.55 x 10 ⁷		Subsidence from oil and gas production in addition to sulfur production
Moss Bluff	Liberty-Chambers	P	P	P	P	2.03 x 10 ⁷		Discrete subsidence bowls
Long Point	Fort Bend	P	P	P	A	-insufficient data-		Obscure subsidence owing to construction of levees
Orchard	Fort Bend	P	P	P	A	5.31 x 10 ⁶		Only area of large crescent sink measured; 20-22 small circular collapse sink-holes also present
Bryan Mound	Brazoria	A	P	no access	A	-insufficient data-		First sulfur-producing dome in Texas

Table 2. (cont.)

SUBSIDENCE

P = Present
A = Absent

Dome with Sulfur Production	County	U.S.G.S. Topographic Sheet	1979 Color-Infrared Aerial Photography	Field Confirmation 1985	RRC, TDWR, and Other	Aerial Extent Land-Surface Subsidence (ft ²)	Comments
Fannett	Jefferson	A	not covered	P	P	3.96×10^7	Subsidence from oil and gas production in addition to sulfur production
Clemens	Brazoria	P	P	no access	A	-insufficient data-	
Nash	Fort Bend-Brazoria	A	P	no access	A	-insufficient data-	
High Island	Galveston	A	P	no access	A	-insufficient data-	Subsidence from oil and gas production
Damon Mound	Brazoria	A	A	A	A	A	No evidence of subsidence
Big Creek	Fort Bend	A	A	A	A	A	No evidence of subsidence

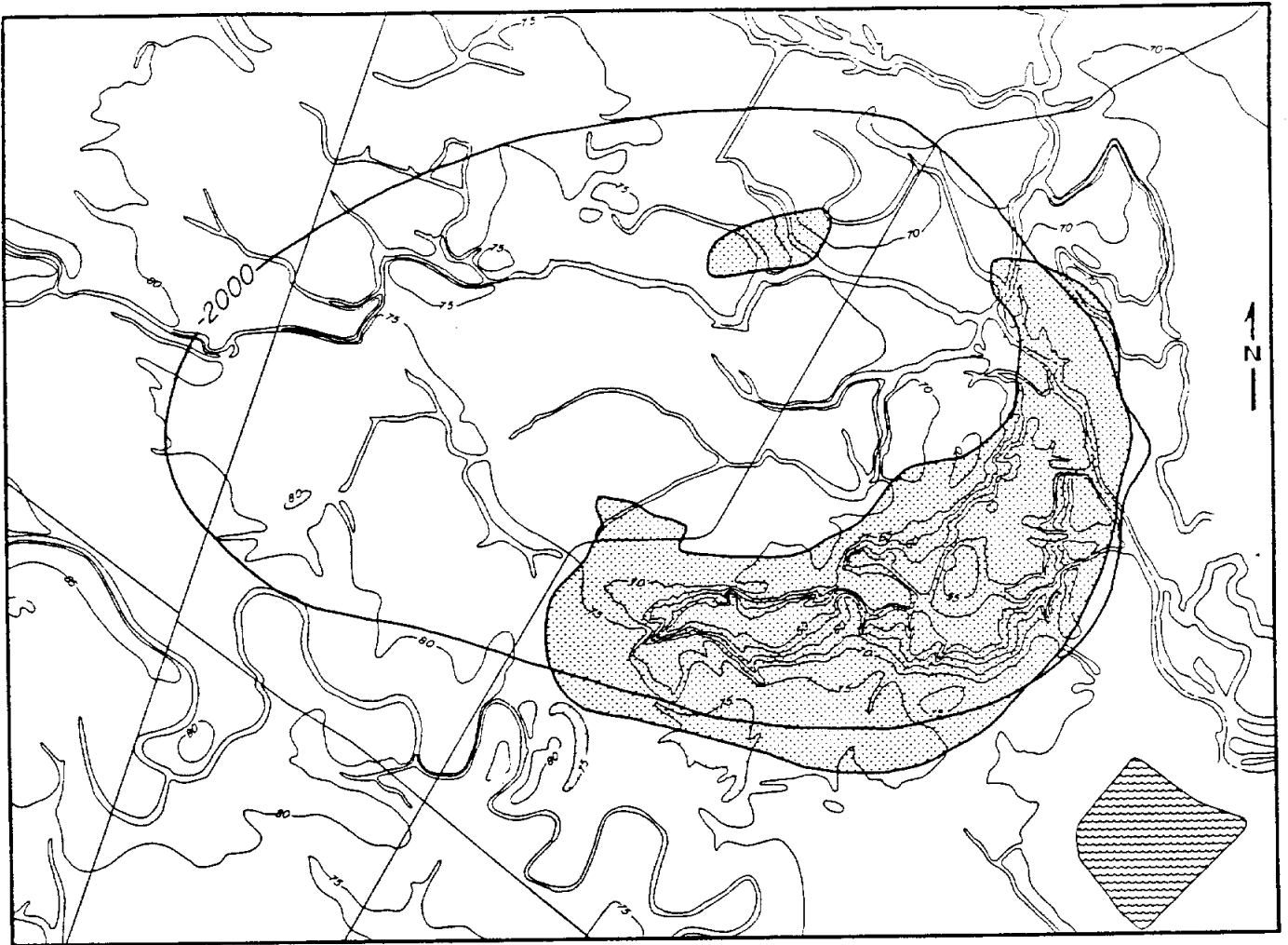
*1 acre = 4.36×10^4 ft²
1 km² = 1.08×10^7 ft²

Sulphur and Potash, and Union Sulphur, began operating sulfur facilities at Boling Dome in 1928. The Texasgulf Inc. facilities at Boling are the only active salt dome sulfur operations in Texas. The latest cumulative figure for sulfur production at Boling (1983, unpublished) is 7.81×10^7 LT. Boling Dome has produced more sulfur than any other Texas diapir. Sulfur production is from the crest of the cap rock to deep down the flank of the cap.

Subsidence Related to Sulfur Mining

Boling Dome was also found to have more man-induced subsidence than any other dome in Texas. Records of changes in surface topography observed through aerial photography, field investigations, and topographic maps illustrate the subsidence that primarily occurred from Frasch mining of sulfur. Other possible contributing factors to the subsidence at Boling are (1) oil and gas production, (2) brining operations, and (3) natural dissolution of the salt stock and cap rock.

Subsidence is directly related to sulfur production. The area of land-surface subsidence at Boling has been defined by closed contours less than the regional elevation (75 ft) over the known extent of the sulfur field (fig. 5a). Greatest vertical movement for this area was 35 ft (10.7 m) based on 1953 topographic maps. Using these parameters, the volume of subsidence at Boling is 7.83×10^8 ft³ (2.22×10^7 m³). Cantrell (1953) reported production figures for Boling of 3.8×10^7 LT of sulfur. The subsidence volume was converted to equivalent sulfur production based on sulfur density (129 lb/ft³; 2.07 g/cm³) yielding 4.6×10^7 LT of equivalent sulfur. Thus, the mass of known sulfur in 1953 (3.8×10^7 LT) is 83 percent of the equivalent sulfur calculated from the subsidence volume. This loss may be due to (1) subsidence from oil production at Boling Dome field, which produces from superdomal strata and geographically overlaps the sulfur field, (2) dissolution of salt and/or cap rock due to various hydrologic interactions, and (3) collapse of some initial porosity in voids or caverns after removal of structural support



(a)

EXPLANATION



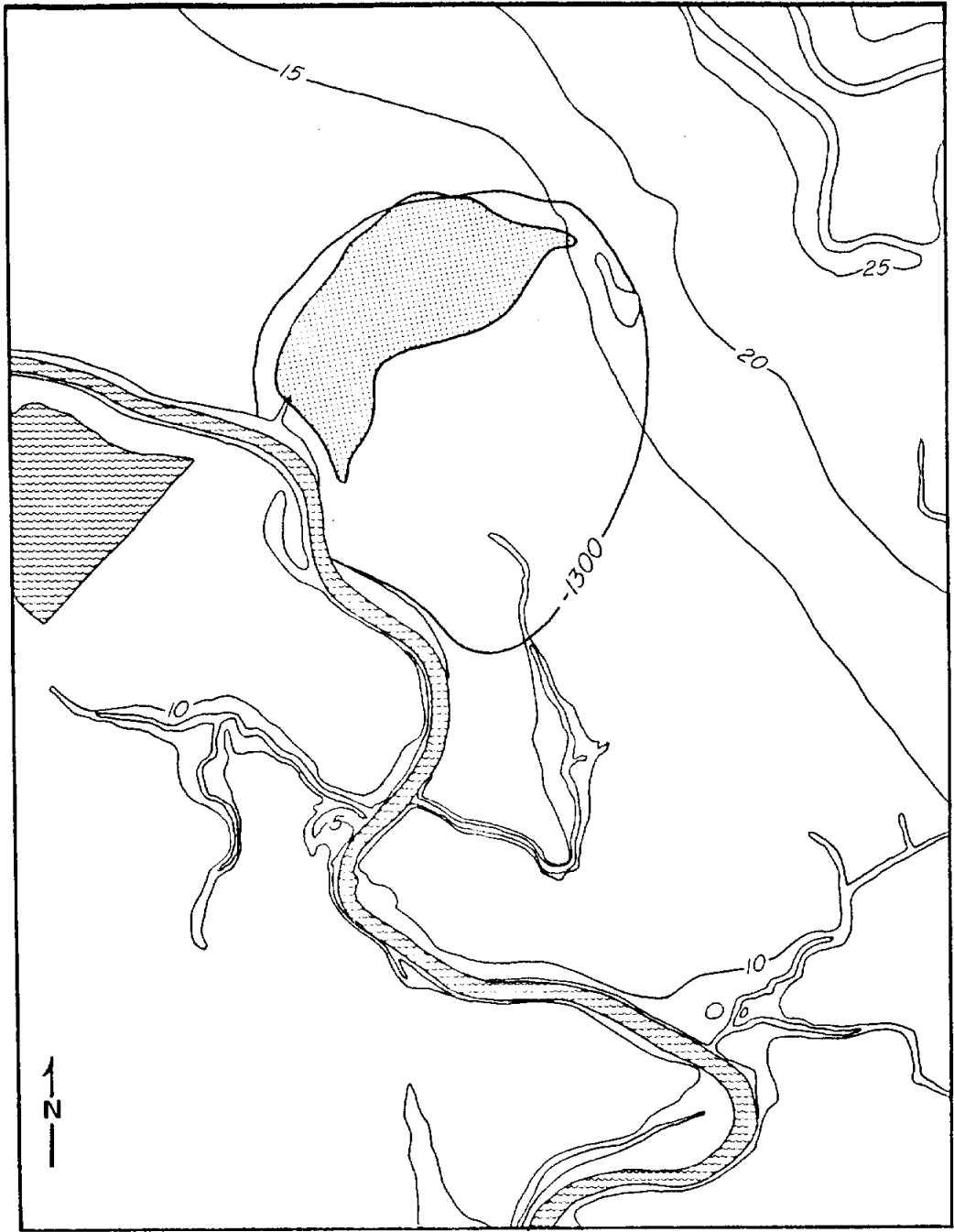
- | | | | |
|----------|-------------------------|---|------------------------|
| --2000-- | Salt structure contour |  | Sulfur mining area |
| —30— | Surface topography (ft) |  | Water/evaporating pond |

Figure 5. Local topography and location of sulfur field at
a) Boling Dome



0 1 mi
0 1 km

(b)

EXPLANATION

- 2000-- Salt structure contour
- 30--- Surface topography (ft)
- [Stippled Box] Sulfur mining area
- [Hatched Box] Water/evaporating pond

Figure 5. Local topography and location of sulfur field at
b) Clemens Dome

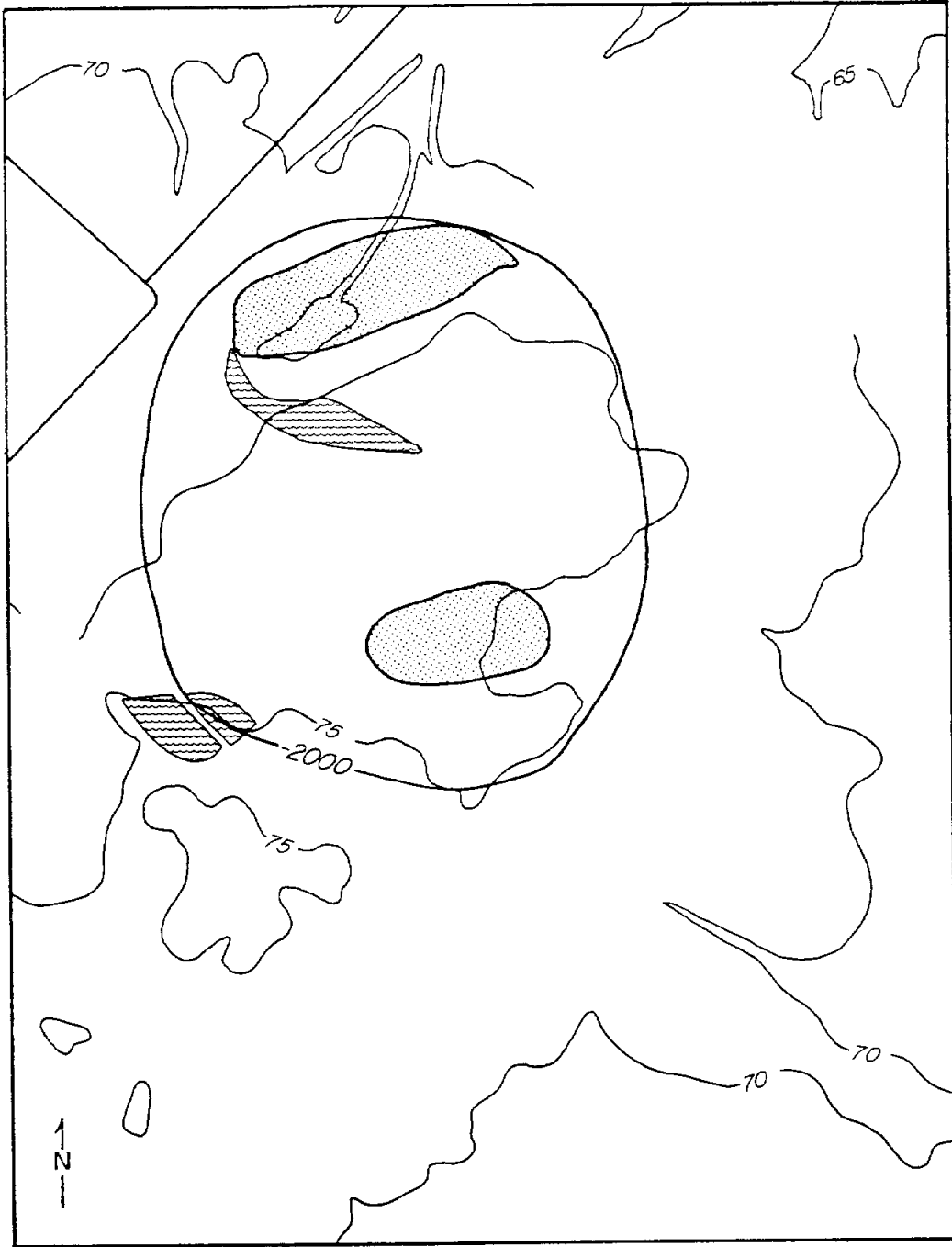


(c)

EXPLANATION

- 2000-- Salt structure contour
- 30--- Surface topography(ft)
- [Hatched Box] Sulfur mining area
- [Hatched Box] Water/evaporating pond

Figure 5. Local topography and location of sulfur field at c) Hoskins Mound Dome



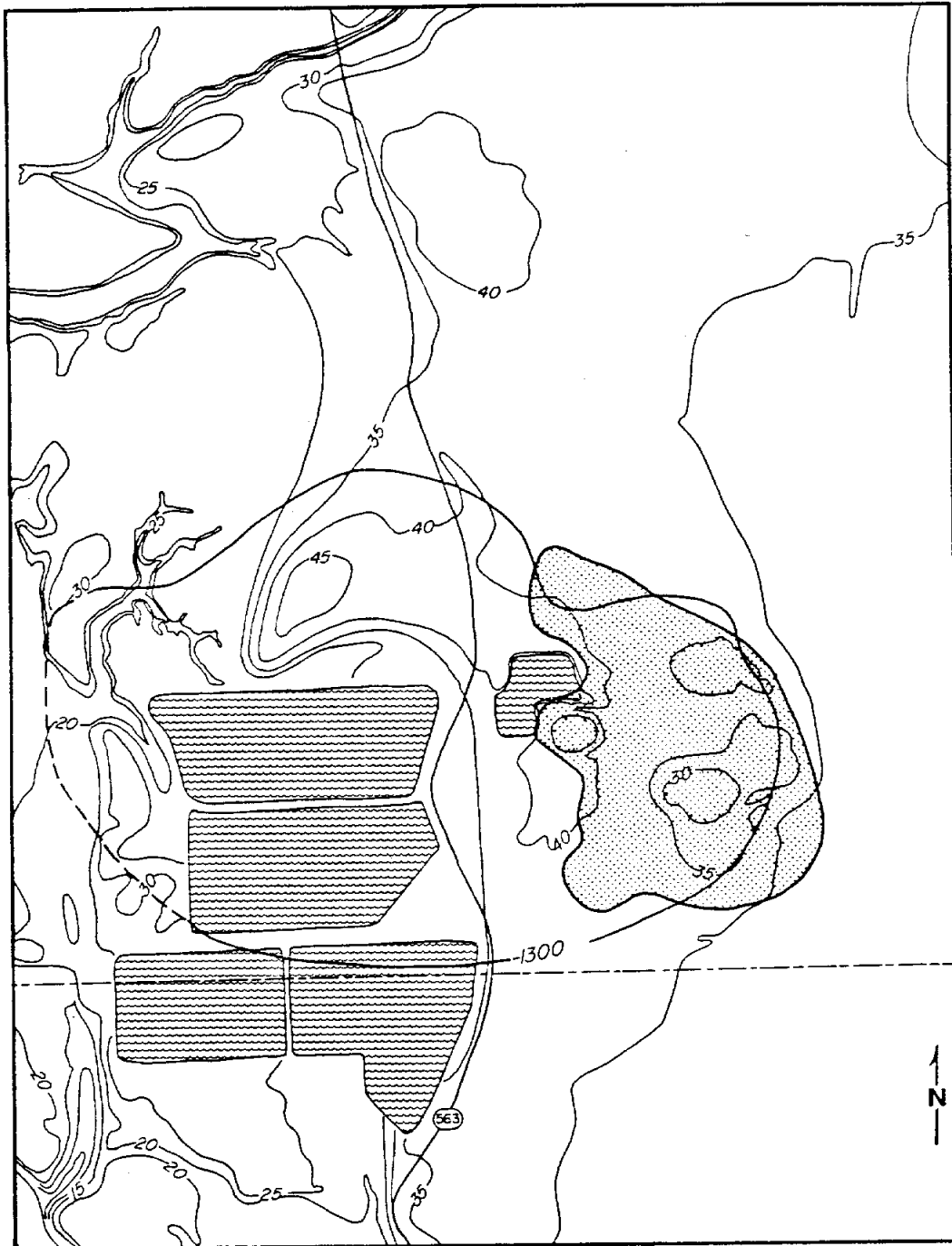
0 1 km 1 mi

(d)

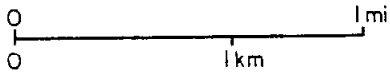
EXPLANATION

- 2000-- Salt structure contour
- 30--- Surface topography (ft)
- [Stippled Box] Sulfur mining area
- [Horizontal Lines Box] Water/evaporating pond

Figure 5. Local topography and location of sulfur field at
d) Long Point Dome



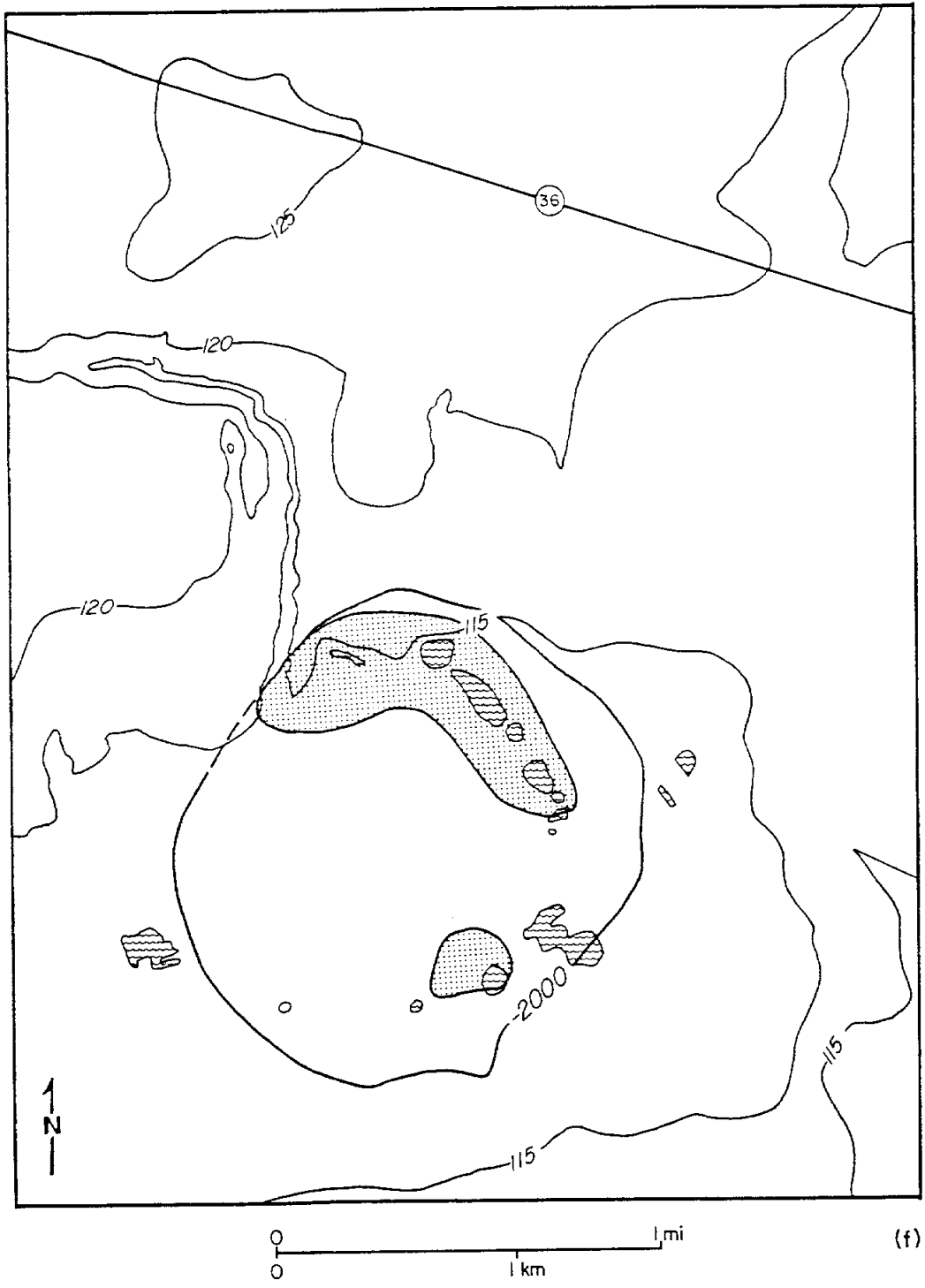
(e)



EXPLANATION

- 2000-- Salt structure contour
- 30--- Surface topography (ft)
- [Stippled Box] Sulfur mining area
- [Hatched Box] Water/evaporating pond

Figure 5. Local topography and location of sulfur field at Moss Bluff Dome



EXPLANATION

- | | |
|---------------------------------|------------------------|
| --2000-- Salt structure contour | Sulfur mining area |
| —30— Surface topography (ft) | Water/evaporating pond |

Figure 5. Local topography and location of sulfur field at f) Orchard Dome.

supplied by sulfur. The collapse of these natural voids is thought to account for most of the missing volume ($3.74 \times 10^6 \text{ m}^3$).

Sulfur production at Boling Dome has been accomplished through the drilling of over 20,000 wells (F. Samuelson, personal communication, 1985). Well spacings for sulfur wells are typically 100 ft (30 m). These boreholes, along with subsurface and surface collapse and trough subsidence, modify the hydrologic environment that must be understood to study salt dome stability and integrity. The surface expression of subsidence over the Boling sulfur field generally fits Obert and Duvall's (1967) description of trough subsidence. Subsurface caving is also present at Boling Dome. This disruption and 20,000 well bores create a highly porous zone. The aquitard that naturally restricts ground water around the diapir is altered in unknown ways in this zone.

Other Subsidence at Boling Dome

The large size of Boling Dome and the localized nature of sulfur production might be used as an argument that the stability and hydrology of other areas of the dome are not affected by sulfur production. However, the presence of catastrophic sinkholes and the continuity of thermal anomalies in the cap rock over the crest of the dome (Seni, this report) indicate partial hydrologic communication over most of the dome crest.

On August 12, 1983, a sinkhole approximately 250 ft (76 m) in diameter and 25 ft (7.6 m) deep formed over the crest of Boling Dome along FM 442. The sinkhole, located approximately 3 mi east of Boling townsite, caused roadway collapse and flooding within the sinkhole. The sink is located outside the area of sulfur mining. Although no one explanation could be documented as the sole reason for the collapse, evidence from previous drilling records suggests a large natural cavern collapsed (Dreyer and Schulz, 1984).

The B. Monroe Well No. 1 was drilled in 1927 by Gulf Production Company. The well is located near the middle of the sinkhole. The driller's log for this well recorded a void or

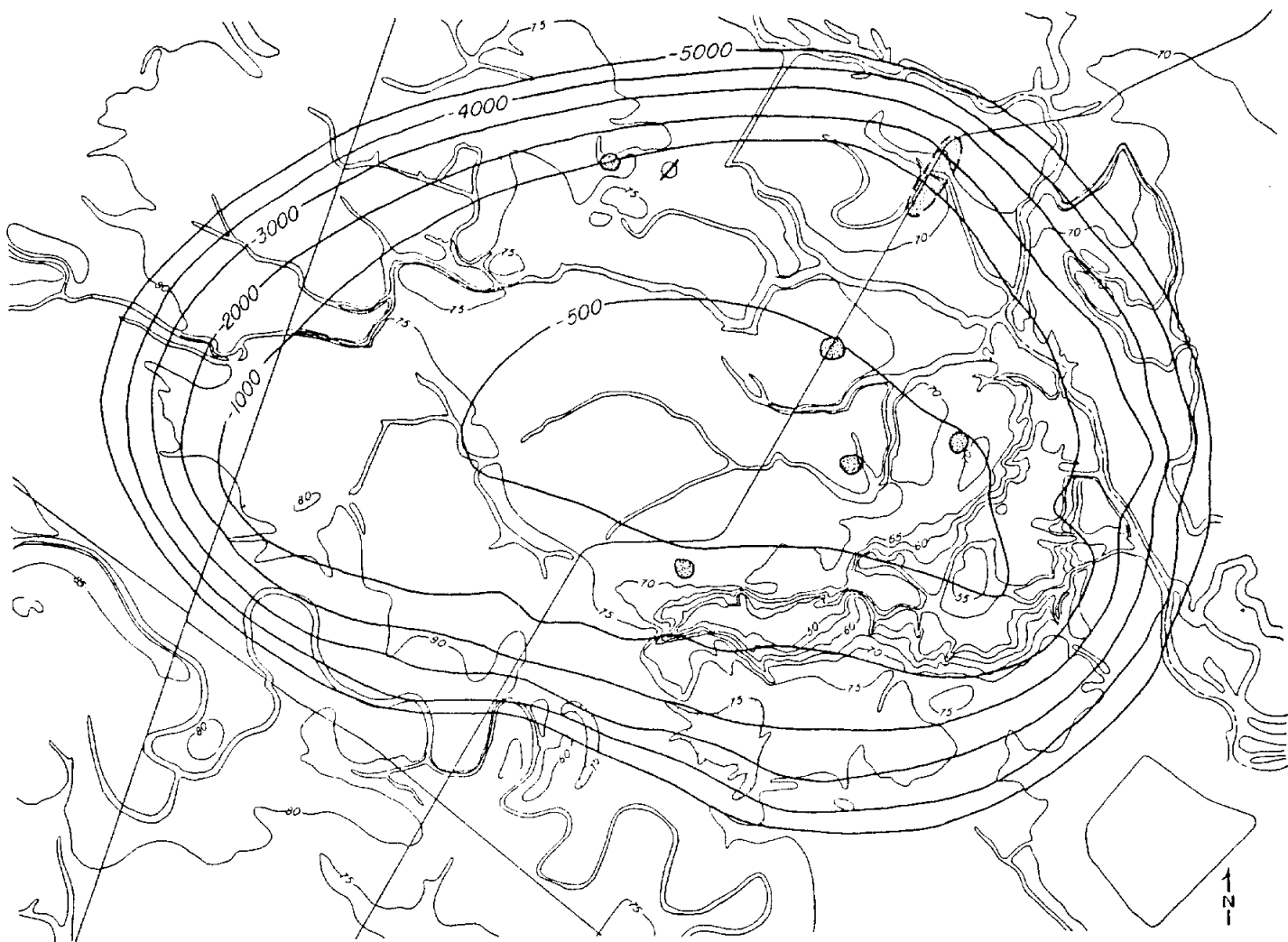
cavern at least 106 ft in vertical extent while drilling from 679 ft (207 m) to 785 ft (239 m). Plugging techniques used during this time period were probably not effective in isolating the well bore. Collapse ensued after one or a combination of the following factors: (1) transport of sediment from the well bore and enlargement of the roof span, (2) roof slabbing of the cavern, (3) natural collapse of the original cavern, or (4) vibration-induced collapse owing to traffic on the overlying roadway. Other sinkholes have also been reported over Boling Dome (fig. 6).

Orchard Dome

Orchard Dome (figs. 5b and 7), located in Fort Bend County, is approximately 17 mi (27 km) due north of Boling Dome. Minimum depths to cap rock and salt are 285 ft (87 m) and 375 ft (114 m), respectively. Major and minor axis lengths are 7,000 ft (2,134 m) and 6,200 ft (1,890 m), with planar crest area approximately $2.7 \times 10^7 \text{ ft}^2$ ($2.5 \times 10^6 \text{ m}^2$).

Mineral recovery at Orchard Dome has been active since the initial discovery of sulfur in 1924 (Ellison, 1971). As with Boling Dome, sulfur and oil and gas have been the primary minerals targeted for production (table 2). Duval Sulfur and Potash Co. actively mined sulfur at Orchard from 1938 to 1970. Sulfur production has dramatically affected the local surface topography and hydrology over and around the dome, as evidenced by six trough subsidence features and 20 to 22 collapse sinkholes.

The position of sulfur zones in the cap rock has influenced the type of subsidence at Orchard Dome. Sulfur at Orchard Dome was restricted to the deep cap-rock flanks of the salt stock. The sulfur-productive interval from 1,000 ft (305 m) to 3,156 ft (962 m) was the deepest Frasch mining operation in the world (Hawkins and Jirik, 1966). The flank position and steep structural attitude influenced the type and magnitude of subsidence at Orchard Dome that resulted from sulfur production.



EXPLANATION

- 500-- Dome structure contour (ft)
- Sinkhole
- Depression
- ∅ Lost rig
- 75— Surface topography (ft)

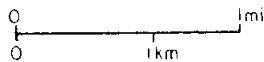
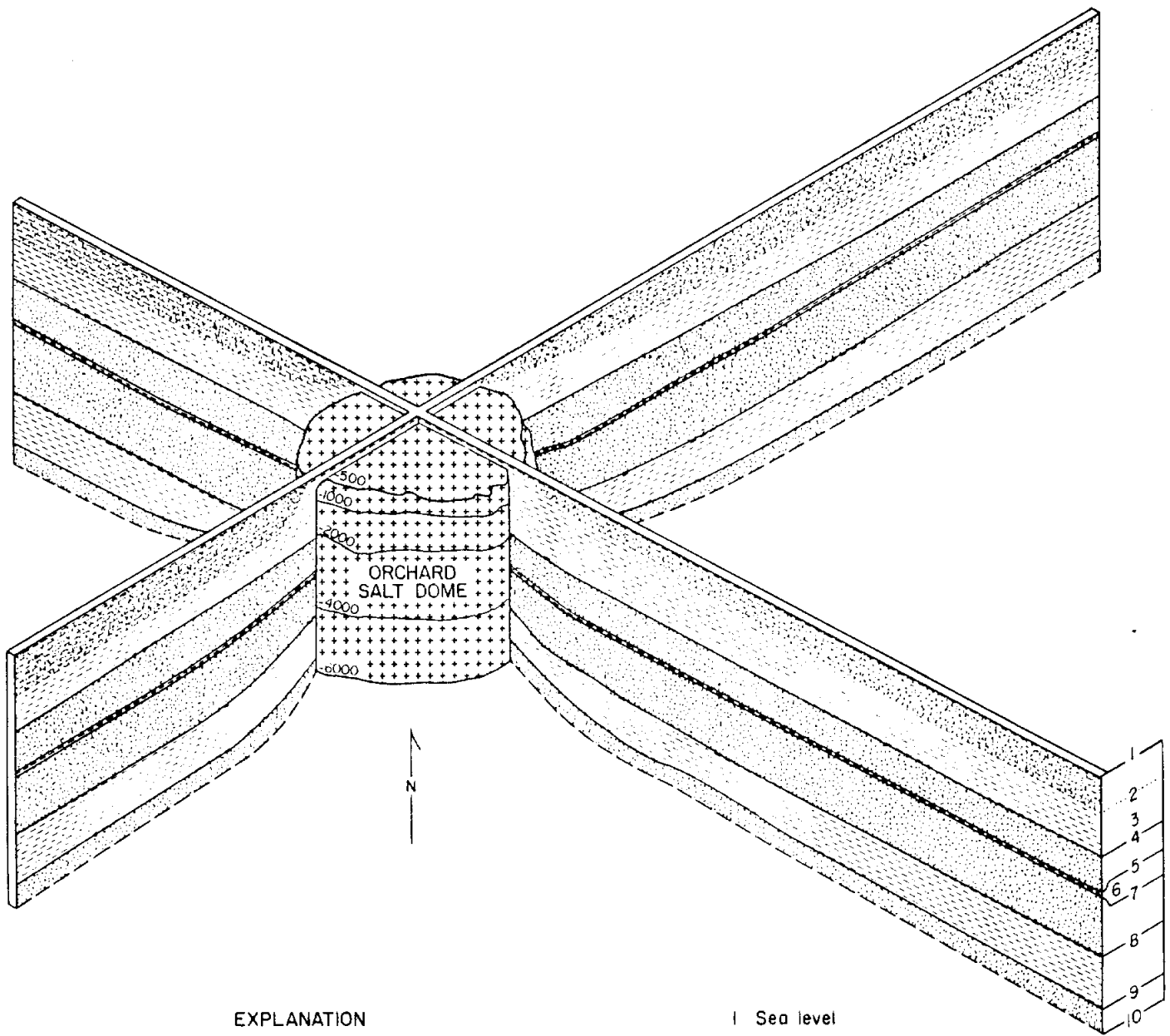

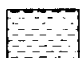
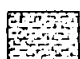


Figure 6. Map of sinkhole locations and structure on top of cap rock at Boling Dome, Wharton and Fort Bend Counties, Texas.



EXPLANATION

-  Sand, sandstone; subordinate mud, mudstone
-  Mud, mudstone; subordinate sand, sandstone
-  Mixed fresh water sands and muds

0 2000 4000 6000 8000 ft
 0 500 1000 1500 2000 m

No vertical exaggeration
 -4000 Salt structure contours,
 C) variable, feet below
 sea level

- 1 Sea level
- 2 Base of fresh water
- 3 Post-Miocene strata
- 4 Top of Upper Miocene
- 5 Top of Oligocene
- 6 Anahuac
- 7 Top of Frio
- 8 Top of Vicksburg
- 9 Top of Yegua
- 10 Base of control

QA 4680

Figure 7. Fence diagram of Orchard Dome area. Unit thicknesses taken from regional isopach data.

Chronology of Sinkholes

A sequence of topographic maps, aerial photos, and U-2 color-infrared photos were assembled to document subsidence at Orchard Dome during the period between 1929 and 1985 (table 3). A brief summary of each data set follows.

The earliest data prior to sulfur production was the 1929 U.S. Army Corps of Engineers Tactical Map for the Rosenberg area. No topographic evidence of natural or man-induced subsidence was present in 1929. However, reports from various Duval Sulphur and Potash engineers indicate that before sulfur production could begin in 1938, drainage ditches had to be constructed from the dome to the Brazos River to drain water from a natural depression over the crest of the dome. Salt marshes around the west flank of the dome also indicate possible natural dissolution of the salt stock. The 1941 photographs show one sinkhole (sinkhole #1), approximately 100 ft (30 m) in diameter, three years after the beginning of sulfur production (fig. 8). No other evidence of subsidence related to mineral production was observed.

The 1952 data, 14 years after the beginning of sulfur production, show increasingly large areas of subsidence at Orchard Dome. Six new sinkholes developed since 1941, including one large crescent sinkhole (sinkhole #2) along the northeast flank of the dome. This was also the major sulfur-producing area. The morphology of sinkhole #2 provides evidence for the mechanisms and magnitude of subsidence that may result from withdrawal of mineral resources associated with salt domes. At least two and possibly three types of subsidence described by Obert and Duvall (1967) occur within sinkhole #2. Most of the area covered by sinkhole #2 and other crescent sinkholes around the perimeter of the dome is the result of trough subsidence. However, within the crescent sink are circular areas of caving and/or chimney subsidence.

Sinkhole #2 is located domeward of the main concentration of sulfur wells mapped by the RRC. The exact distance of migration of subsidence toward the center of the dome is not precisely known because limits of sulfur production are vague. One sinkhole over the

Table 3. Sinkhole evolution at Orchard Dome.

Date of Coverage	Type of Data	Number of circular sinkholes over crest	Number of crescent sinkholes around flank	Surface area of Sinkhole #2 (ft ²)	Percentage increase in size of Sinkhole #2	Comments
1929	U.S. Army Corps of Engineers Tactical Topographic Map Rosenberg Area	0	0	--	--	No indication of natural subsidence around dome
April 9, 1941	Black and White A.S.C.S. 1" = 1667'	1	0	--	--	Salt marsh on west flank clearly defined
April 4, 1952	Black and White A.S.C.S. 1" = 1667'	4	3	1.3 x 10 ⁶	--	First occurrence of Sinkhole #2
February 28, 1964	Black and White A.S.C.S. 1" = 1667'	13	6	2.27 x 10 ⁶	75	First occurrence of Sinkhole #3 = rig collapse sinkhole
January 29, 1970 February 10, 1970	U.S.G.S. 7.5" Topographic Sheet - Orchard 1" = 2000'	14	6	2.51 x 10 ⁶	11	Sinkhole #2 fully connected
November 7, 1979	NASA - Ames	16	6	5.3 x 10 ⁶	111	Sinkhole #2 now covers approximately 18% of dome
November 11, 1979	1" = 5417' Aerochrome Infrared					
May 15, 1985	BEG - Coastal Salt Domes Reconnaissance Flight - Variable Scales	20-22	6	--	--	Cannot accurately determine size changes owing to distortion from oblique view

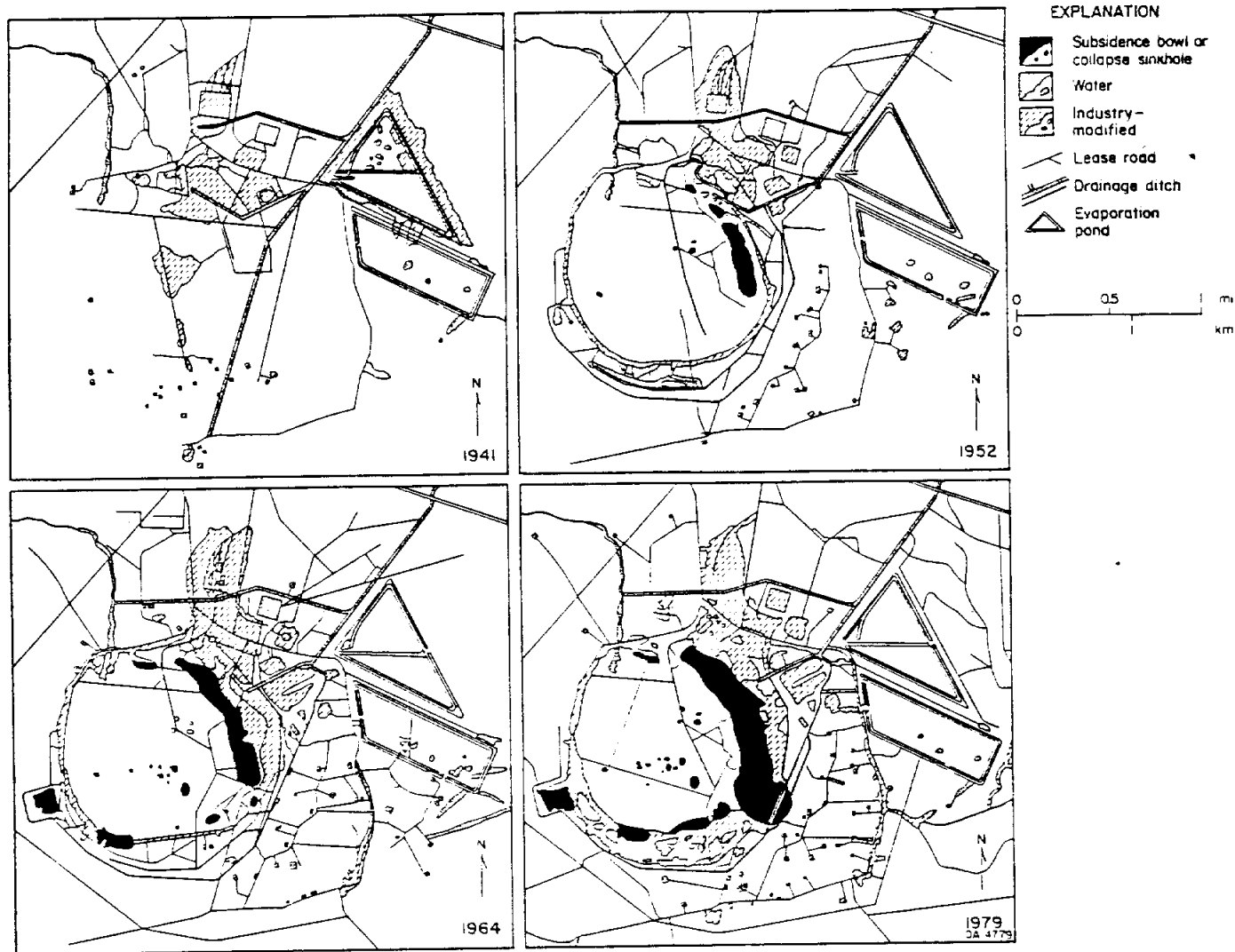


Figure 8. Map showing chronological development of subsidence features at Orchard Dome, Fort Bend County, for a) 1941, b) 1952, c) 1964, and d) 1979. Data for a, b, and c taken from black-and-white aerial photographs, scale 1:20,000. Data for d from color infrared photography, scale 1:65,000.

southern portion of the dome seems to suggest that circular chimney features developed naturally and then trough subsidence developed. This chronology could not be determined at sinkhole #2.

All of the sinkholes present over the central portion of the dome are circular and cover much smaller areas than the crescent sinkholes surrounding the perimeter of the dome. These sinkholes exhibit the characteristics of subsidence resulting from plug caving or chimneying processes. Most of the circular sinkholes over the central portion of the dome coincide with the location of early test wells. As postulated for the FM 442 sinkhole at Boling Dome, an improperly plugged well bore may act as a conduit for ground-water movement and transport of support materials.

The 1964 data indicate increases in sinkhole numbers and also amount and rate of growth for sinkhole #2. Twelve sinkholes developed between 1952 and 1964 and the surface area of sinkhole #2 increased 75 percent. One of the most interesting events in sinkhole evolution at Orchard Dome occurred during the interval between 1952 and 1964. The 1964 photos indicate a new sinkhole (sinkhole #3) appeared south of sinkhole #2. Sinkhole #3 (fig. 9) has a different character, including (1) steep walls of considerable depth and (2) absence of water filling the sinkhole. Carl Eller, former production engineer with the sulfur operations for Duval Sulphur and Potash at Orchard, provided a history of this sinkhole (Eller, personal communication, 1985). In the late 1950's and early 1960's the sinkhole was the location of a steam-powered, skid-mounted, sulfur production rig. It had been producing sulfur at maximum capacity from a stratigraphically thick, almost near-vertical sulfur zone. A common engineering procedure used to recover expensive production casing after sulfur was depleted was to cut the casing string above the production casing shoe and then pull the casing string out of the borehole for salvage or reuse. To sever the casing, dynamite charges were set off at the lowest depth of free casing. When the dynamite charge was exploded at this location, collapse quickly occurred, totally engulfing the production rig. There was enough warning for rig personnel to

evacuate with no injuries. This method of casing recovery was abandoned after this incident.

Field investigations at Orchard Dome confirm the unusual character of sinkhole #3. All other sinkholes had water levels within 10 ft (3 m) of ground level. Sinkhole #3, however, had a water level approximately 35 ft (10.6 m) below ground level. The present vertical subsidence is about 35 ft (10.6 m). The walls of the sinkhole now dip 32°--when the sinkhole formed they were near vertical. Further study is needed to determine possible explanations for the differences in water levels between sinkhole #3 and the other sinkholes at Orchard Dome.

The 1970 USGS Orchard topographic sheet (fig. 5b) illustrates: (1) presence of both trough subsidence and caving or chimney subsidence in the crescent sinkholes around the flank of the dome and (2) an increase (11 percent) in surface area for sinkhole #2. The time of this coverage coincides with the termination of sulfur production at Orchard Dome.

The 1979 U-2 color infrared photography (fig. 10) provides an excellent illustration of continued subsidence after the termination of production. Since the termination of production, the surface area of sinkhole #2 increased 111 percent. Two new circular sinkholes also formed over the crest of the dome. Continued measurement of surface area covered by sinkhole #2 at Orchard could provide data for the subsidence potential of other salt domes with a past history of mineral recovery.

On May 15, 1985, a reconnaissance mission flew over Orchard Dome to observe and record any notable increases in the number or size of sinkholes previously discussed. Although photographic technique did not facilitate accurate measurements of increases in surface area for sinkhole #2, the number of sinkholes increased to 20 to 22 over the central area of the dome.



Figure 9. Ground-level view of collapse sinkhole at Orchard Dome. A sulfur production rig was lost in this sinkhole during initial collapse. Vertical distance from ground level to base of sinkhole is approximately 35 ft (11m).

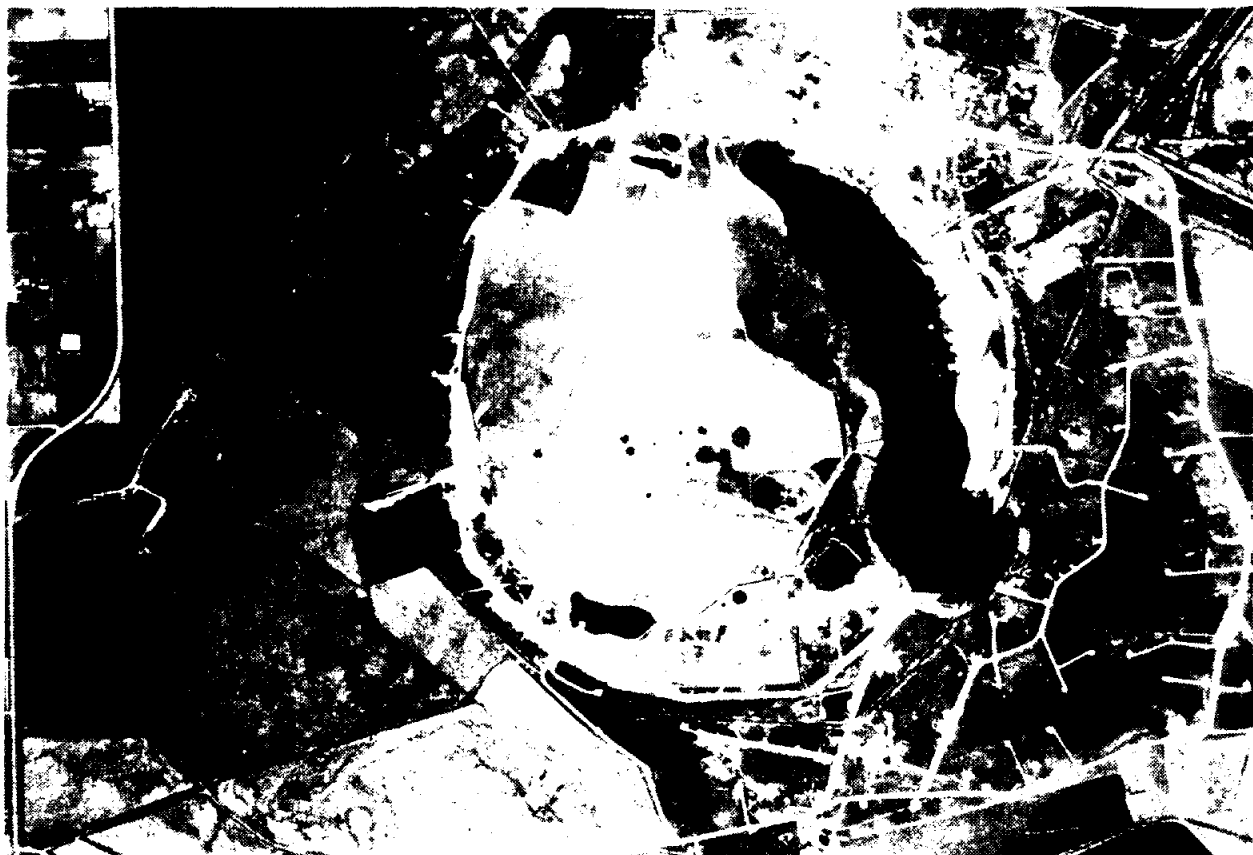


Figure 10. Black-and-white copy of U-2 color infrared photography over Orchard Dome, 1979. Scale 1:26,667.

Moss Bluff Dome

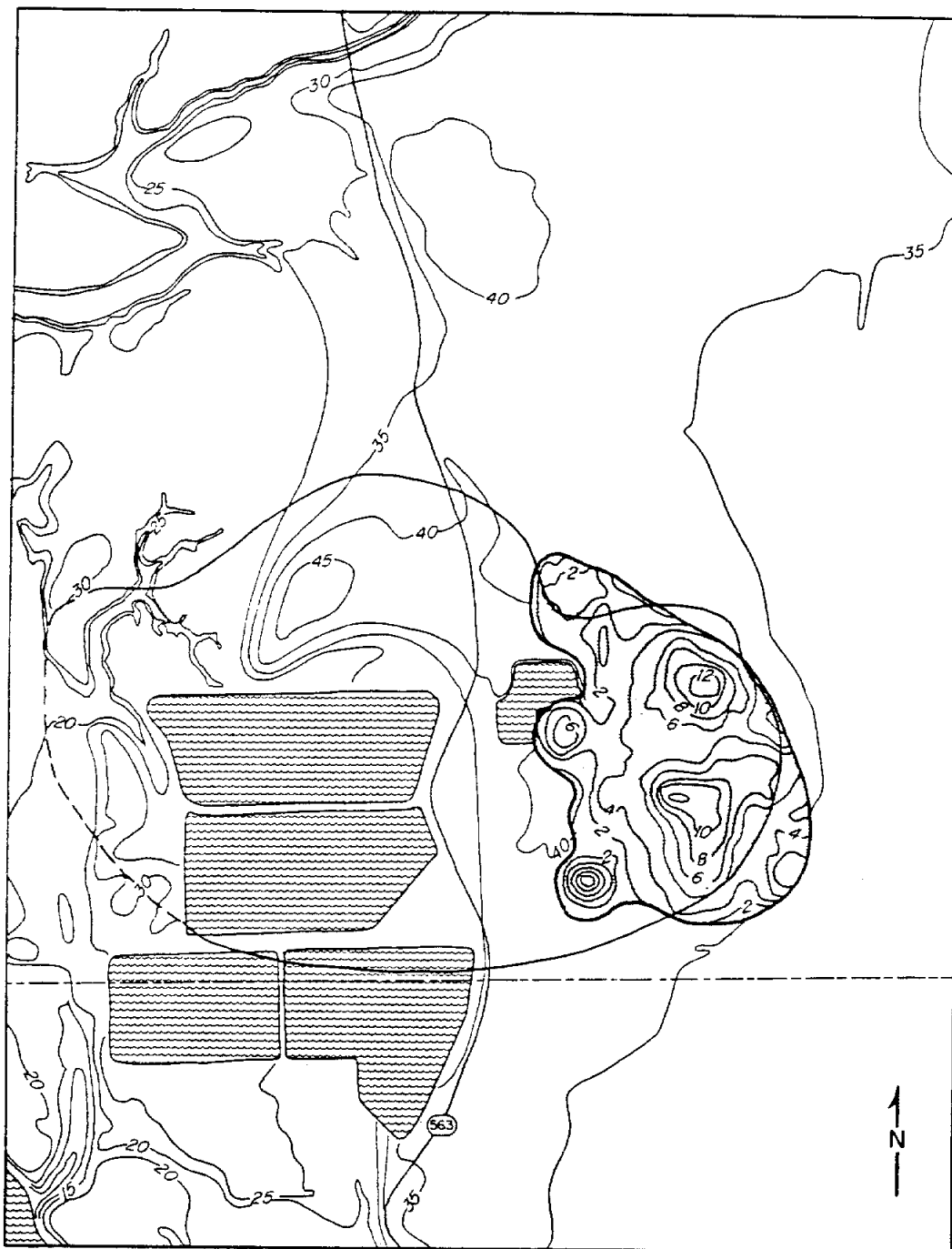
Moss Bluff Dome (fig. 5c) is located in Liberty and Chambers Counties, Texas, east of Houston. Shallowest measured depths to cap rock and salt are 600 ft (183 m) and 1,100 ft (335 m). Dimensions of the dome crest include the major axis of 13,400 ft (4,084 m), minor axis of 9,200 ft (2,804 m), and area of planar crest approximately $4.08 \times 10^7 \text{ ft}^2$ ($3.8 \times 10^6 \text{ m}^2$). Oil, gas, and sulfur production figures for Moss Bluff Dome are in table 2.

Moss Bluff Dome is the fifth largest sulfur-producing dome in Texas. Tonal anomalies, ponded water, field observations, topographic maps, and RRC documents confirmed the presence and extent of subsidence at Moss Bluff Dome primarily owing to sulfur production. Dark tonal anomalies were very strong over the production area. This indicates an increase in the soil moisture content at the time of coverage, which is a result of the low topography in the subsidence bowl. There was also an absence of normal vegetation over the entire area of the dome because of industrial activities during production.

The Shiloh 7.5' topographic sheet over the Moss Bluff area illustrates up to 10 ft (3 m) of subsidence over the sulfur field (fig. 5c). Three separate subsidence bowls with at least 12 ft (3.6 m) of vertical movement are shown in figure 11 (RRC hearing files, Docket No. 3-72,099). Maximum subsidence was 15 ft (4.6 m). Total surface area affected by subsidence after sulfur production was $1.2 \times 10^6 \text{ ft}^2$ (28 acres).

Spindletop Dome

Spindletop Dome is located in Jefferson County, Texas. Minimum depths to cap rock and salt are 700 ft (213 m) and 1,200 ft (366 m), respectively. Major and minor axis lengths are 6,300 ft (1,920 m) and 5,700 ft (1,737 m); area of planar crest is $2.57 \times 10^7 \text{ ft}^2$ ($2.39 \times 10^6 \text{ m}^2$). Subsidence over Spindletop Dome has been active for a long period of time. Until recently, this subsidence was a result of the tremendous amount of oil and gas



EXPLANATION

-  Dome outline (~1300 ft)
-  -35- Surface topography (ft)
-  Subsidence contours CI=2ft
-  Area of subsidence

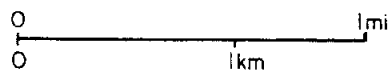


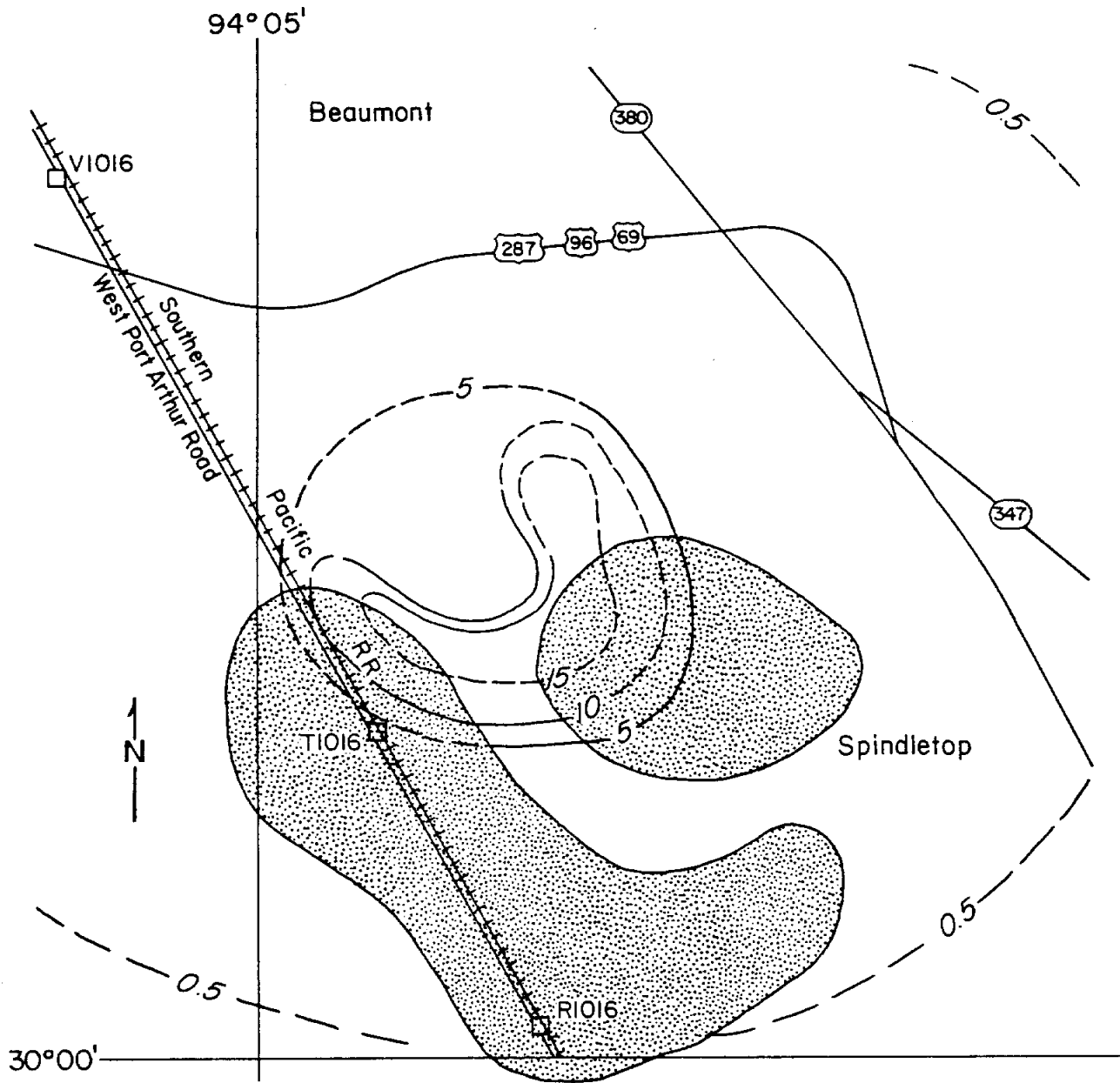
Figure 11. Map showing extent of man-induced subsidence over Moss Bluff Dome, Liberty and Chambers Counties, as a result of sulfur mining. Data from Railroad Commission of Texas.

produced from the various reservoirs situated over and around the dome. Cumulative oil production as of 1984 was 153,788,059 bbl. With the discovery of oil at Spindletop in 1901 sulfur was also discovered, although it was not recovered until 51 years later.

Field observations indicate that extensive subsidence has occurred from mineral recovery at Spindletop. Subsidence at the dome is considered to be a result of trough subsidence mechanisms. Ratzlaff (1982) reported that at least 15 ft (4.6 m) of subsidence has occurred over Spindletop Dome. Ten feet (3 m) of this vertical movement is attributed to sulfur mining, while 5 ft (1.5 m) is a result of oil, natural gas, and ground-water withdrawal (fig. 12). Wesselman (1971) also noted extremely localized subsidence occurring at Spindletop as a result of sulfur mining. One example of catastrophic subsidence occurred at Spindletop Dome when a sulfur production rig and tractor were almost lost in a sinkhole that had developed overnight (Science Applications, Inc., 1977).

Other Domes

In addition to Boling, Orchard, Moss Bluff, and Spindletop, eight other sulfur-productive domes display evidence of land-surface subsidence. Hoskins Mound Dome in Brazoria County produced 1.1×10^7 LT of sulfur from 1923 to 1955. Marx (1936) described sulfur production at Hoskins Mound Dome and noted the benefits of subsidence with regard to increased efficiency of sulfur production. Marx (1936) and the 1963 Hoskins Mound USGS topographic sheet illustrate subsidence over the northern portion of the field (fig. 5d). Surface contours from Marx (1936) present an even, circular, positive-mound topography. The 1963 topographic map records a distinctive 5- to 10-ft (1.5- to 3.0-m) irregular escarpment trending southwest-northeast over the dome. Field observations along this escarpment confirmed that relief exceeded 10 ft (3.0 m) in places along the escarpment.



EXPLANATION

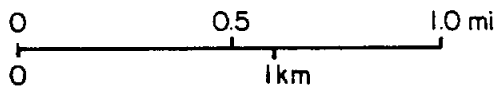
R1016 □ Bench-mark number

Oil field

—/0— Line of equal land-surface subsidence -- dashed where approximate (ft)

NOTE: Lines of equal subsidence are based on data from 1925 to 1977

Base from US Geological Survey topographic quadrangles



Modified from Ratzlaff (1982)

QA-459I

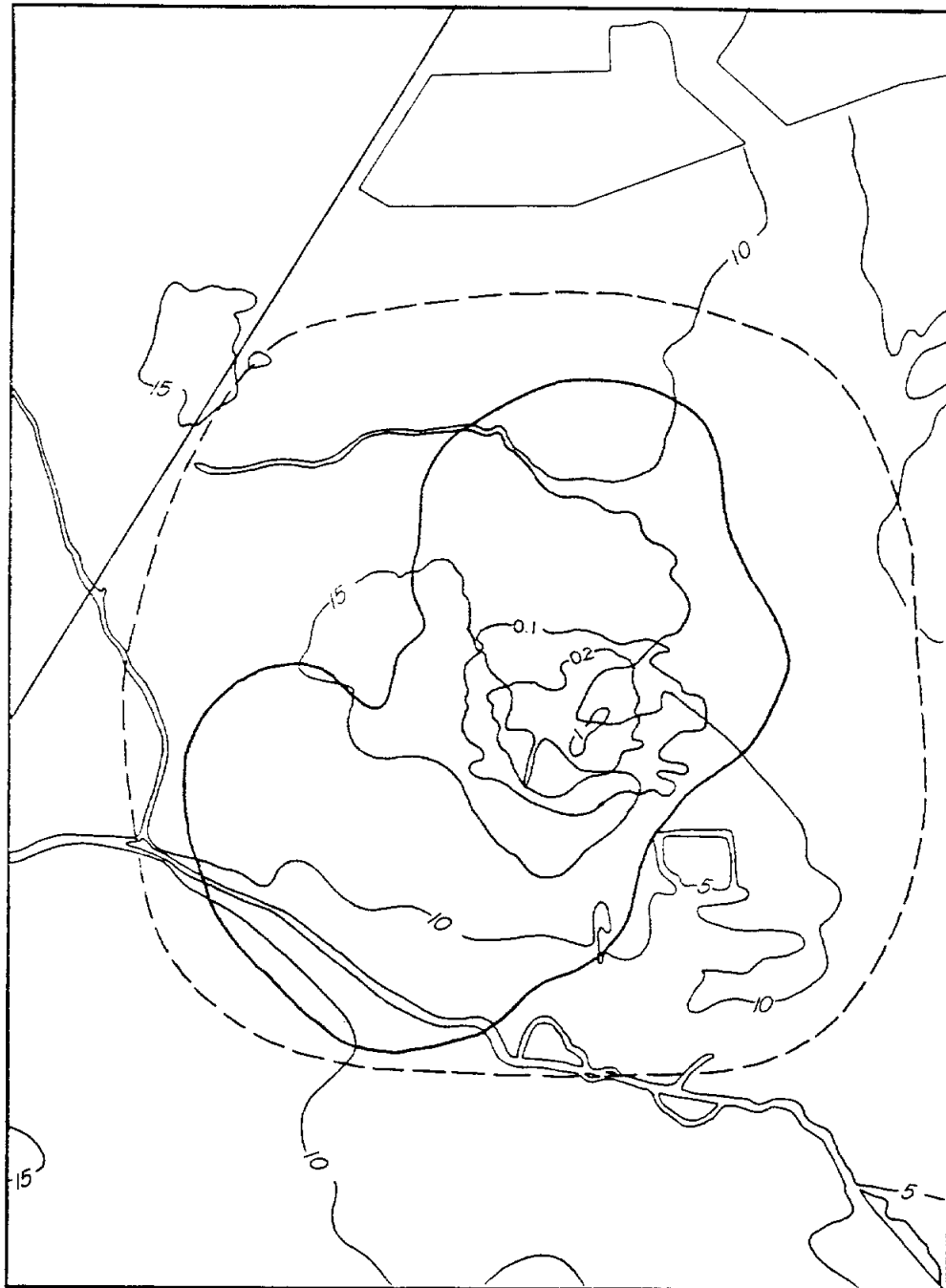
Figure 12. Lateral and vertical extent of man-induced subsidence from oil, gas, and sulfur production at Spindletop Dome, Jefferson County, Texas.

Fannett Dome in Jefferson County produced 3.48×10^6 LT of sulfur from 1958 to 1977 (table 2). CIR photography did not extend to the Fannett area. The 1962 Hamshire USGS topographic sheet covering the southwest portion of the sulfur field maps a 5-ft closed depression near the southeastern portion of the sulfur field. Evidence of subsidence was obtained from a series of maps delineating the extent of surface movement over the sulfur field (fig. 13). Area calculations of the extent of surface movement after one year of production were 4.0×10^7 ft² (RRC hearing file, Docket No. 3-38994). Total vertical movement for this same time period was 1 ft (.3 m) or less. Field observations over the southern area of sulfur production clearly illustrated the presence of subsidence. Production from the Fannett oil field may also have contributed to subsidence.

Long Point Dome (fig. 5e) in Fort Bend County produced 8.97×10^6 LT of sulfur during two periods of production from 1930 to 1938 and 1946 to 1982. The 1953 Smithers Lake USGS topographic sheet records a 5-ft depression over the northern area of sulfur production. CIR photography also illustrates possible subsidence with a dark tonal anomaly. Field observations confirmed the presence of several low topographic depressions over the sulfur field. Extensive levee construction and other surface disturbances related to sulfur operations, however, made confirmation of surface subsidence difficult.

Nash Dome in Fort Bend and Brazoria Counties displays limited evidence of subsidence related to sulfur production. Cumulative production figures for this dome were 2.0×10^5 LT of sulfur. CIR photography indicated subsidence by the presence of ponded water over the eastern portion of the sulfur field. Attempts to confirm subsidence in the field were unsuccessful.

High Island Dome in Galveston County produced 3.7×10^4 LT of sulfur. Oil and natural gas production, however, has been extensive, with cumulative oil figures of 138,867,419 bbl through 1984. Natural gas production for 1984 was 11,026,939 mcf. CIR photography delineates several areas of potential subsidence, although field observations failed to confirm their presence. High Island Dome is an example of compaction-driven



EXPLANATION

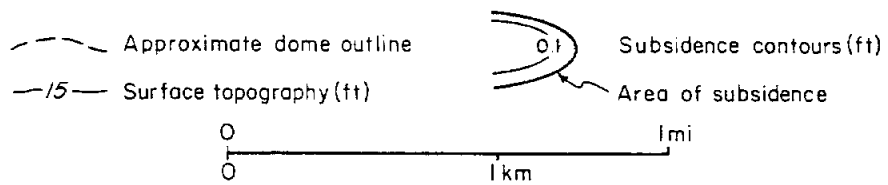


Figure 13. Map showing extent of man-induced subsidence over Fannett Dome, Jefferson County. Data from Railroad Commission of Texas.

trough subsidence related to oil and natural gas production rather than the more dramatic collapse features observed over other sulfur fields.

Bryan Mound Dome, also in Brazoria County, was the first commercial sulfur operation in Texas. Production at this dome was active from 1912 to 1935 with a cumulative production of 5.0×10^6 LT. The early production period, in conjunction with the close proximity to coastal wetlands, makes before-and-after documentation at Bryan Mound difficult. Lakes and marshes surrounding the dome and active surface faulting suggest early, sulfur-related subsidence.

Clemens Dome (fig. 5f) in Brazoria County produced sulfur from 1937 to 1960 with a cumulative production of 2.97×10^6 LT. A light tonal anomaly over the sulfur field on CIR photography indicates absence of vegetation. This area is also marked by a 5-ft closed depression on the 1953 Cedar Lane NE USGS topographic sheet. Attempts to gain access to the field area were unsuccessful.

Gulf Dome in Matagorda County produced sulfur from 1919 to 1936 and also from 1965 to 1970. Cumulative production for both time intervals was 1.28×10^7 LT of sulfur. Subsidence, either natural or man-induced, is inferred by the presence of Mine Lake over the crest of the dome. Maps of sulfur production reported by Myers (1968) show the field covering the crest of the dome. Because sulfur production covered the crest of the dome, Mine Lake must postdate sulfur production.

CONCLUSIONS

1. The land surface over many salt domes in Texas has subsided through natural and man-induced processes.
2. Frasch sulfur mining from cap rocks causes the most dramatic subsidence over salt domes.

3. Twelve of fourteen salt domes with sulfur production have evidence of land-surface subsidence.

4. Subsidence includes a continuum of processes that ranges between trough subsidence and subsurface caving.

5. Trough subsidence is a ductile deformation process centered over the zone of excavation. Subsidence bowls are the surface expression of trough subsidence. Moss Bluff, Fannett, and Spindletop Domes display surface subsidence bowls.

6. Subsurface caving is brittle failure through roof slabbing into a subsurface void. This process occurs spectacularly when relatively pure sulfur is extracted. Steep-walled collapse sinkholes are the surface expression of subsurface caving. Orchard Dome displays both collapse sinkholes and subsidence bowls.

7. The structural and hydrologic stability of a salt dome is compromised by subsidence processes and resultant deformation.

REFERENCES

- Allen, A. S., 1969, Geologic settings of subsidence, in Varnes, D. J., and Kiersch, G., eds., Reviews in engineering geology, volume II: Geological Society of America, p. 305-342.
- Autin, W. J., 1984, Observations and significance of sinkhole development at Jefferson Island: Louisiana Geological Survey, Department of Natural Resources, Geological Pamphlet No. 7, 75 p.
- Baumgardner, R. W., Jr., Hoadley, A. D., and Goldstein, A. G., 1982, Formation of the Wink Sink, a salt dissolution and collapse feature, Winkler County, Texas: The University of Texas at Austin, Bureau of Economic Geology Report of Investigations No. 114, 38 p.

- Boyum, B., 1961, Subsidence case histories in Michigan mines, in Hartman, H. L., ed., Proceedings, Fourth Symposium on Rock Mechanics, Pennsylvania State University, Mining Engineering Series.
- Cantrell, R. B., 1953, Boling Field, Fort Bend and Wharton Counties, Texas: American Association of Petroleum Geologists and Houston Geological Society Fieldtrip Guidebook, p. 87-96.
- Chang, C. Y., and Nair, K., 1974, Analytical methods for predicting subsidence above solution-mined cavities: Fourth Symposium on Salt, Northern Ohio Geological Society, Cleveland, Ohio, p. 101-117.
- Clanton, U. S., and Amsbury, D. L., 1976, Active faults in southeastern Harris County, Texas: Environmental Geology, v. 1, no. 3, p. 149-154.
- Collins, E. W., 1982, Surficial evidence of tectonic activity and erosion rates, Palestine, Keechi, and Oakwood salt domes, East Texas: The University of Texas at Austin, Bureau of Economic Geology Geological Circular 82-3, 39 p.
- Deere, D. U., 1961, Subsidence due to mining--a case history from the Gulf Coast region of Texas, in Hartman, H. L., ed., Proceedings, Fourth Symposium on Rock Mechanics, Pennsylvania State University, Mining Engineering Series, p. 59-64.
- Dreyer, B. V., and Schulz, C. E., 1984, Evaluation, repair, and stabilization of the Boling Sinkhole FM 442, Wharton County, Texas, in Beck, B. F., ed., Sinkholes: their geology, engineering and environmental impact: Proceedings, First Multidisciplinary Conference on Sinkholes, Orlando, Florida.
- Ege, J. R., 1984, Mechanisms of surface subsidence resulting from solution extraction of salt, in Holzer, T. L., ed., Reviews in engineering geology, volume VI: Geological Society of America, p. 203-221.
- Ellison, S. P., Jr., 1971, Sulfur in Texas: The University of Texas at Austin, Bureau of Economic Geology Handbook No. 2, 48 p.

- Fogg, G. E., and Kreitler, C. W., 1980, Effects of salt-brining on Palestine Dome, in Kreitler, C. W., and others, Geology and geohydrology of the East Texas Basin, a report on the progress of nuclear waste isolation feasibility studies (1979): The University of Texas at Austin, Bureau of Economic Geology Geological Circular 80-12, p. 46-54.
- Fogg, G. E., Kreitler, C. W., and Wuerch, H. V., 1982, Meteoric hydrology, in Kreitler, C. W., and others, Geology and geohydrology of the East Texas Basin, a report on the progress of nuclear waste isolation feasibility studies (1981): The University of Texas at Austin, Bureau of Economic Geology, report prepared for the U.S. Department of Energy under Contract No. DE-AC97-80ET46617, p. 12-27.
- Gabrysch, R. K., 1969, Land-surface subsidence in the Houston-Galveston Region, Texas: Proceedings, Tokyo International Symposium on Land Subsidence, ASH and AISH-UNESCO Publication No. 88, p. 43-55.
- _____, 1984, Ground-water withdrawals and land-surface subsidence in the Houston-Galveston Region, Texas, 1906-80: Texas Department of Water Resources Report 287, 64 p.
- Gabrysch, R. K., and Bonnet, C. W., 1975, Land-surface subsidence in the Houston-Galveston region, Texas: Texas Department of Water Resources Report 188, 19 p.
- Gustavson, T. C., Finley, R. J., and McGillis, K. A., 1980, Regional dissolution of Permian salt in the Anadarko, Dalhart, and Palo Duro Basins of the Texas Panhandle: The University of Texas at Austin, Bureau of Economic Geology Report of Investigations No. 106, 40 p.
- Hanna, M. A., and Wolf, A. G., 1934, Texas and Louisiana salt-dome caprock minerals: American Association of Petroleum Geologists Bulletin, v. 18, no. 2, p. 212-225.
- Harris, G. D., 1908, Rock salt: its origin, geological occurrences and economic importance in the state of Louisiana: Geological Survey of Louisiana, Baton Rouge, Bulletin No. 7, 259 p.

- Hawkins, M. E., and Jirik, C. J., 1966, Salt domes in Texas, Louisiana, Mississippi, Alabama, and offshore tidelands; a survey: U.S. Bureau of Mines Information Circular No. 8313, 78 p.
- Kolb, C. R., 1977, Topographic lows above domes, in Martinez, J. D., and others, eds., An investigation of the utility of Gulf Coast salt domes for the storage or disposal of radioactive wastes: Louisiana State University, Institute for Environmental Studies, Baton Rouge, p. 407-414.
- Kreitler, C. W., 1976, Lineations and faults in the Texas Coastal Zone: The University of Texas at Austin, Bureau of Economic Geology Report of Investigations No. 85, 32 p.
- Lee, K. L., and Strauss, M. E., 1969, Prediction of horizontal movements due to subsidence over mined areas: Proceedings, Tokyo International Symposium on Land Subsidence, ASH and AISH-UNESCO Publication No. 88, p. 512-523.
- Martinez, J. D., Thoms, R. L., Kupfer, D. H., Smith, C. J., Jr., Kolb, C. R., Newchurch, E. J., Wilcox, R. E., Manning, T. A., Jr., Romberg, M., Lewis, A. J., and Rovik, J. E., 1976, An investigation of the utility of Gulf Coast salt domes for isolation of nuclear wastes: Louisiana State University, Institute for Environmental Studies, Baton Rouge, Report No. ORNL-SUB-4112-25, prepared for U.S. Department of Energy, 329 p.
- Marx, A. H., 1936, Hoskins Mound salt dome, Brazoria County, Texas, in Barton, D. C., and Sawtelle, G., eds., Gulf Coast oil fields, a symposium on the Gulf Coast Cenozoic: American Association of Petroleum Geologists, p. 833-856.
- Myers, J. C., 1968, Gulf Coast sulfur resource, in Brown, L. F., Jr., ed., Fourth Forum on Geology of Industrial Minerals: The University of Texas at Austin, Bureau of Economic Geology Special Publication, p. 57-65.
- Minor, H. E., 1925, Goose Creek Oil Field, Harris County, Texas: American Association of Petroleum Geologists Bulletin, v. 9, no. 2, p. 286-297.
- Obert, L., and Duvall, W. I., 1967, Rock mechanics and the design of structures in rock: New York, John Wiley, 650 p.

- O'Donnell, L., 1935, Jefferson Island salt dome, Iberia Parish, Louisiana: American Association of Petroleum Geologists Bulletin, v. 19, no. 11, p. 1602-44.
- Patchick, P. F., 1980, The suitability of Palestine salt dome, Anderson County, Texas, for disposal of high-level radioactive waste: Office of Nuclear Waste Isolation, ONWI-74, 35 p.
- Powers, S., 1926, Interior salt domes of Texas: American Association of Petroleum Geologists Bulletin, v. 10, no. 1, p. 1-60.
- Pratt, W. E., and Johnson, D. W., 1926, Local subsidence of the Goose Creek oil field: Journal of Geology, v. 34, p. 577-590.
- Ratzlaff, K. W., 1982, Land-surface subsidence in the Texas Coastal Region: Texas Department of Water Resources Report 272, 26 p.
- Rellensmann, O., 1957, Rock mechanics in regard to static loading caused by mining excavation, in Behavior of materials of the earth's crust: Colorado School of Mines Quarterly, v. 52, no. 3, p. 35-49.
- Sabins, F. F., Jr., 1978, Remote sensing principles and interpretation: San Francisco, W.H. Freeman, 426 p.
- Science Applications, Inc., 1977, The mechanics and ecological impacts of the collapse of salt dome storage caverns: McLean, Virginia, Report No. 5-210-00-567-04.
- Sellards, E. H., 1930, Subsidence in Gulf Coastal Plains salt domes: University of Texas, Austin, Bureau of Economic Geology Bulletin No. 3001, p. 9-36.
- Seni, S. J., Mullican, W. F., III, and Hamlin, H. S., 1984a, Texas salt domes--aspects affecting disposal of toxic-chemical waste in solution mined caverns: The University of Texas at Austin, Bureau of Economic Geology, report prepared for Texas Department of Water Resources under interagency contract no. IAC(84-85)-1019, 94 p.

- _____ 1984b, Texas salt domes: natural resources, storage caverns, and extraction technology: The University of Texas at Austin, Bureau of Economic Geology, report prepared for Texas Department of Water Resources under interagency contract no. IAC(84-85)-1019, 161 p.
- Seni, S. J., Mullican, W. F., III, and Ozment, R. W., 1984c, Computerized inventory of data on Texas salt domes: The University of Texas at Austin, Bureau of Economic Geology, report prepared for Texas Department of Water Resources under interagency contract no. IAC(84-85)-1019, 34 p.
- Stefanko, R., 1973, Roof and ground control-subsidence and ground movement, in Cummins, A. B., and Given, I. A., eds., SME mining engineering handbook: Society of Mining Engineers of American Institute of Mining, Metallurgical, and Petroleum Engineers, v. 2, sec. 13, p. 2-9.
- Walters, R. F., 1978, Land subsidence in Central Kansas related to salt dissolution: Kansas Geological Survey Bulletin 214, 82 p.
- Wassmann, T. H., 1980, Mining subsidence in the East Netherlands: Fifth Symposium on Salt, Northern Ohio Geological Society, Cleveland, Ohio, p. 463-475.
- Wesselman, J. B., 1971, Ground-water resources of Chambers and Jefferson Counties, Texas, with a section on Quaternary Geology by Saul Aronow: Texas Department of Water Resources Report 133, 183 p.
- Winslow, A. G., and Doyel, W. W., 1954, Land-surface subsidence and its relation to the withdrawal of ground water in the Houston-Galveston region, Texas: Economic Geology, v. 49, p. 413-422.
- Winslow, A. G., and Wood, L. A., 1959, Relation of land subsidence to ground-water withdrawals in the upper Gulf Coast region, Texas: Mining Engineering, v. 11, no. 10, p. 1030-1034.

STATISTICAL ANALYSIS OF STRUCTURE
IN THE HOUSTON DIAPIR PROVINCE

by

W. F. Mullican III

CONTENTS

INTRODUCTION	76
PREVIOUS STUDIES	76
REGIONAL GEOLOGY	79
LOCAL GEOLOGY	81
DATA COLLECTION	81
STATISTICAL ANALYSIS	93
Regional Structure	100
Domal Structure	106
CONCLUSIONS	107
REFERENCES	108

Figures

1. Parameters used to differentiate regional and domal areas	83
2. Location map of data areas	84
3. Lineament patterns over domes	86
4. Fault patterns mapped at domes	87
5. Polar graphs of azimuth orientations for (a) regional faults, (b) domal faults, (c) regional lineaments, (d) domal lineaments, and (e) test faults	88-92
6. Bar graphs of azimuth orientations	96
7. Rectangular graph of fault and lineament azimuth	98
8. Polar graphs of length-weighted frequencies	99
9. Polar graph of frequency of domal axis azimuth	101
10. Histogram of significant windows	102
11. Frequency histogram of fault lineament and segment length	103

Tables

1. Fault types associated with salt structures	77
2. Growth fault characteristics	78

3. Structural parameters	82
4. Statistical data comparing for fault/lineament density	95
5. Structural data	104

INTRODUCTION

The Houston diapir province is part of the Tertiary Gulf Coast Basin. The structural fabric of the area is dominated by regional strike-oriented, down-to-the-coast, normal growth faults (contemporaneous faults of Bruce, 1973) and salt structures in various stages of evolution (predominantly salt diapirs) (Bornhauser, 1958; Murray, 1961). The potential exists in a shallow diapiric environment for the opening of hydrologic pathways along fault planes through the cap rock to the salt stock, thereby initiating or enhancing active dissolution (Balk, 1936; Barton, 1936; Ferguson and Minton, 1936; Dreyer and Schulz, 1984). Cause-and-effect relationships between major growth faults and domal faults, and their potential for hydrologic interaction with cap rocks is an integral component of salt dome stability (Seni and others, 1984a). If a domal area has a significant increase in mean fault or lineament density, the potential for hydrologic interaction and dissolution of the salt stock along faults through the cap rock could significantly decrease salt dome stability.

This study examines the structural and statistical relationships between regional structural trends and salt diapirs in the Houston diapir province. It is intended to quantify the aspects of those relationships, including fault patterns and densities, that may potentially influence the stability of salt domes and thus their suitability as toxic chemical waste storage sites.

PREVIOUS STUDIES

For this study surface faults and lineaments were compared with subsurface faults in the Houston diapir province in regional and domal areas. Surface faults, fracture lines, and/or photo lineaments have previously been correlated with deep-seated salt domes and regional subsurface faults (DeBlieux and Shepherd, 1941; Desjardins, 1952; Miller, 1961; Weaver and Sheets, 1962; Reid, 1973; Fisher and others, 1972; Kreitler, 1976; Clanton and Amsbury, 1976).

When an individual salt body evolves from a pillow stage to a diapir stage, both local and regional structure are affected. The distortion of structural grain by diapirism has been studied extensively (Halbouty and Hardin, 1956; Murray, 1961; Halbouty, 1979; Ewing, 1983a; Jackson and Seni, 1983; Jackson and Galloway, 1984). The degree of structural distortion effected by diapirism is variable and dependent on diapiric growth rates and stage of diapir evolution.

Growth faults and salt diapirs are often geographically and structurally related, but their mutual dependency has not been established. This is evident when one compares the Coastal Bend growth fault trend where diapirs are absent with the East Texas diapir province where salt diapirs are present and growth faults are absent (Seni and others, 1984a). Syndepositional movement of growth faults and salt diapirs led Jackson and Galloway (1984) to classify the Tertiary Gulf Coast Basin as the world's type area for currently active growth tectonics. Growth faulting is the structural term used to describe the well-established contemporaneous normal faults characterized by thickening of sediments in the downthrown fault block. Periods of active faulting can be determined by the age of thickened sediments (Kupfer, 1974). The age of salt-withdrawal induced faulting can also be used to indicate timing of diapiric growth (Hughes, 1960).

Faulting in domal areas may be a direct result of local diapirism or be regional in nature, thus influencing or masking diapiric fault patterns (Murray, 1961). Although radial faults may dominate domal areas, Murray (1961) described seven fault types associated with salt structures (table 1). Carver (1968) summarized seven common characteristics of growth faults in the Tertiary Gulf Coast Basin (table 2).

Table 1. Fault types associated with salt structures (Murray, 1961).

- (1) Normal faulting with single offset
- (2) Normal faulting with multiple offsets
- (3) Grabens

- (4) Horsts
- (5) Radial faulting
- (6) Peripheral or tangential faulting
- (7) Reverse or thrust faulting

Table 2. Growth fault characteristics (Carver, 1968).

- (1) Fault traces are arcuate, normally concave toward the coast, and associated with areas of active subsidence.
- (2) Average dip of growth faults is 45° and decreases with depth.
- (3) Growth faults are normal faults and are commonly downthrown on the Gulf side.
- (4) Growth faults tend to have increased displacement with depth. It has been postulated that below this zone of maximum displacement there is an interval where decreasing throw is present, but confirmation of this is beyond resolution of data.
- (5) Movement along a vertically curved fault plane causes sediments in the downthrown block to slump and form rollover and reverse drag.
- (6) Age of fault trends decreases coastward, as do major deltaic trends, changes in thickness, regional dip, and sedimentary facies.

Several experimental studies have dealt with mechanisms of faulting in various diapiric environments (Balk, 1936; Currie, 1956; Horsfield, 1980; Withjack and Scheiner, 1982). These studies examined the relationship between fault patterns around the domes and regional and local stresses. Withjack and Scheiner (1982) described three types of faults over domes: (1) normal, (2) strike-slip, and (3) reverse. They concluded that regional strain, either extensional or compressional, and the plan shape of the salt stock significantly affected domal fault patterns. In areas dominated by regional extension stresses, as in the Tertiary Gulf Coast Basin, normal faults with down-to-the-basin offset are the most common fault type. Most faults mapped in domal areas were oriented radially about the diapir. This observation is supported by the dispersion in preferred orientation of fault azimuths recorded in domal areas for this study. Detailed mapping of fault patterns

in domal areas would aid the interpretation of various fault types and help establish their influence on dome stability.

Dix and Jackson (1981) reported that shallow salt diapirs in the southern portion of the East Texas diapir province had a statistically significant influence on regional lineament patterns. This influence was twofold. First, there was an increase in the dispersion of preferred orientation (fluctuation of preferred orientation of Cloos, 1947) of lineaments with respect to regional patterns and, second, the density of lineaments increased. These deviations from regional trends were attributed to increased fracturing and faulting of domal overburden (Dix and Jackson, 1981).

REGIONAL GEOLOGY

Structural style and configuration of the Texas Gulf Coast Basin have been controlled by a sequence of three geologic regimes. In a broad sense these were (1) Triassic-Jurassic rifting and spreading of North and South America from Europe and Africa with deposition of restricted-marine salt and evaporite, (2) Cretaceous carbonate deposition, and (3) Cenozoic terrigenous clastic deposition (Kupfer, 1974). The northern Tertiary Gulf Coast Basin inherited its margin from the Paleozoic Ouachita tectonic belt (Martin, 1976). This area was still continental as late as Triassic time. Basin filling was facilitated by subsidence due to spreading and subsequent cooling of the crust (Jackson and Seni, 1983). Another explanation offered by Kupfer (1974) is that subsidence in local areas such as the Houston diapir province was accomplished through a dynamic process involving a phase change in the Moho (Kennedy, 1959).

This basin, like many other basins developing along divergent margins, underwent extensive salt and evaporite deposition during early stages of rifting and breakup. Gulf Coast salt was deposited in a restricted, subsiding, linear Jurassic basin characteristic of initial stages of rifting (Kupfer, 1974). Salt deposition had ceased before Cretaceous time

when sufficient expansion of the basin had occurred to create open-marine conditions required for carbonate deposition.

The Houston diapir province extends without break to the east into the Louisiana diapir province. Throughout the Mesozoic this area received distal continental slope deposits; during the early Cretaceous carbonate sedimentation became dominant (Martin, 1976). Most of the basin filling occurred during the Tertiary from the late Paleocene to the beginning of the Pleistocene as a result of massive influx of terrigenous clastics (Winkler and Edwards, 1983) from areas to the north and west during Laramide continental uplift.

Environments of deposition that dominate basin filling are fluvial- and wave-dominated delta systems (Galloway and Hobday, 1983). These sediments continue to fill the Tertiary Gulf Coast Basin, which has subsided from 10,000 to 60,000 ft (3 to 20 km) (Kupfer, 1974). In some areas of the basin more than 50,000 ft (12 km) of predominantly fluvial-deltaic sediments were deposited as a result of rapid episodic subsidence (Salvador and Buffler, 1983). Although deposition was essentially continuous throughout Tertiary time, major influxes of sediment occurred during (1) the Eocene (Wilcox and Yegua deposits), (2) the Oligocene (Vicksburg deposits), and (3) the Miocene (Frio deposits).

Movement along growth faults, which are products of large-scale, deep-seated gravity sliding along ancient continental shelf margins, is maintained primarily by gravity and differential compaction (Bornhauser, 1958; Murray, 1961; Cloos, 1968; Winker and others, 1983; Jackson and Galloway, 1984). The precise catalysts initiating structural movement remain unclear. Gravity sliding is facilitated by deltaic progradation over prodelta muds at the shelf margin for two reasons: (1) the undercompacted nature of underlying prodelta muds and (2) the focus of deposition at the crest of the slope (Jackson and Galloway, 1984). The potential of gravity sliding and downslope movement resulting in buckling at the toe of the slope are important factors in Tertiary Gulf Coast geology.

LOCAL GEOLOGY

This project included structural analysis of 41 salt domes in the Houston diapir province. Of these, 26 (63%) penetrated the subsurface map horizon used for structural control (table 3). The cap rock of only one diapir in the study area, Damon Mound, is partially exposed at the surface (Hurlburt, 1946). Average depths to cap rock and salt for domes in this province are 1,222 ft (372 m) and 3,346 ft (1,020 m), respectively. Average cap-rock thickness is 414 ft (126 m) for all domes and is 568 ft (173 m) for domes shallower than 4,000 ft.

DATA COLLECTION

For this project the orientation and length of straight-line segments of surface lineaments and subsurface faults in the Houston diapir province were computed. When compiling the data bases certain assumptions were made. Foremost is that lineaments are geologic features that may illustrate surface traces of subsurface faults (O'Leary and others, 1976; Caran and others, 1982). Although faults in domal areas are shorter and have less displacement compared to regional growth faults, we also assumed that with intense well control, domal faults have been mapped with the same attention to density, orientation, and length as have regional growth faults.

Faults and lineaments were analyzed separately as domal and regional data sets. The domal area was defined by a 2.5-mi (4.0-km) radius from the salt stock - country rock interface (fig. 1). This is the controlled area defined by the Texas Department of Water Resources for disposal permits. Data sets were separated into three areas to aid analysis of regional variations in structural strike, dome density, and local tectonic features. The three regions are those defined by the Environmental Geologic Atlas of the Texas Coastal Zone (EGATCZ) as covering a majority of the Houston diapir province: Beaumont-Port Arthur (BPA), Houston-Galveston (HG), and Bay City-Freeport (BCF) (fig. 2) (Fisher and

Table 3. Structural parameters used in statistical analysis.

Region	Area km ² (mi ²)	Regional Fault Segments TCL(m)*	Domal Fault Segments TCL(m)	Regional Lineaments TCL(m)	Domal Lineaments TCL(m)	Faults in Test Area TCL(m)	Diapirs in Data Area (Dome Code: Appendix 1)	Shallow Diapirs with depth to crest <4,000 ft (Dome Code: Appendix 1)
Beaumont - Port Arthur (BPA)	5,954 (2,300)	506 1,584,960	137 357,015	79 2,095,693	44 299,321	34 82,542	AR, BI, CL, FN, HI, HR, HU, OR, PN, SO, SP	AR, BI, FN, HI, HU, SO, SP
Houston - Galveston (HG)	7,515 (2,903)	954 3,009,511	226 518,128	78 1,689,319	37 302,977	77 150,731	BB, BL, CP, DN, ES, HM, LL, MA, MB, MY, PJ, RF, SH, SL, SR, SU, TH, WE	BB, BL, HM, MB, PJ, SL, SR
Bay City - Freeport (BCF)	8,160 (3,152)	772 3,264,871	101 281,672	71 1,850,682	23 203,089	30 131,149	AL, BC, BM, BO, CM, DM, GU, HK, LP, MK, NA, WC	AL, BC, BM, BO, CM, DM, GU, HK, LP, MK, NA, WC

* Total cumulative length of fault or lineament segments recorded in meters.

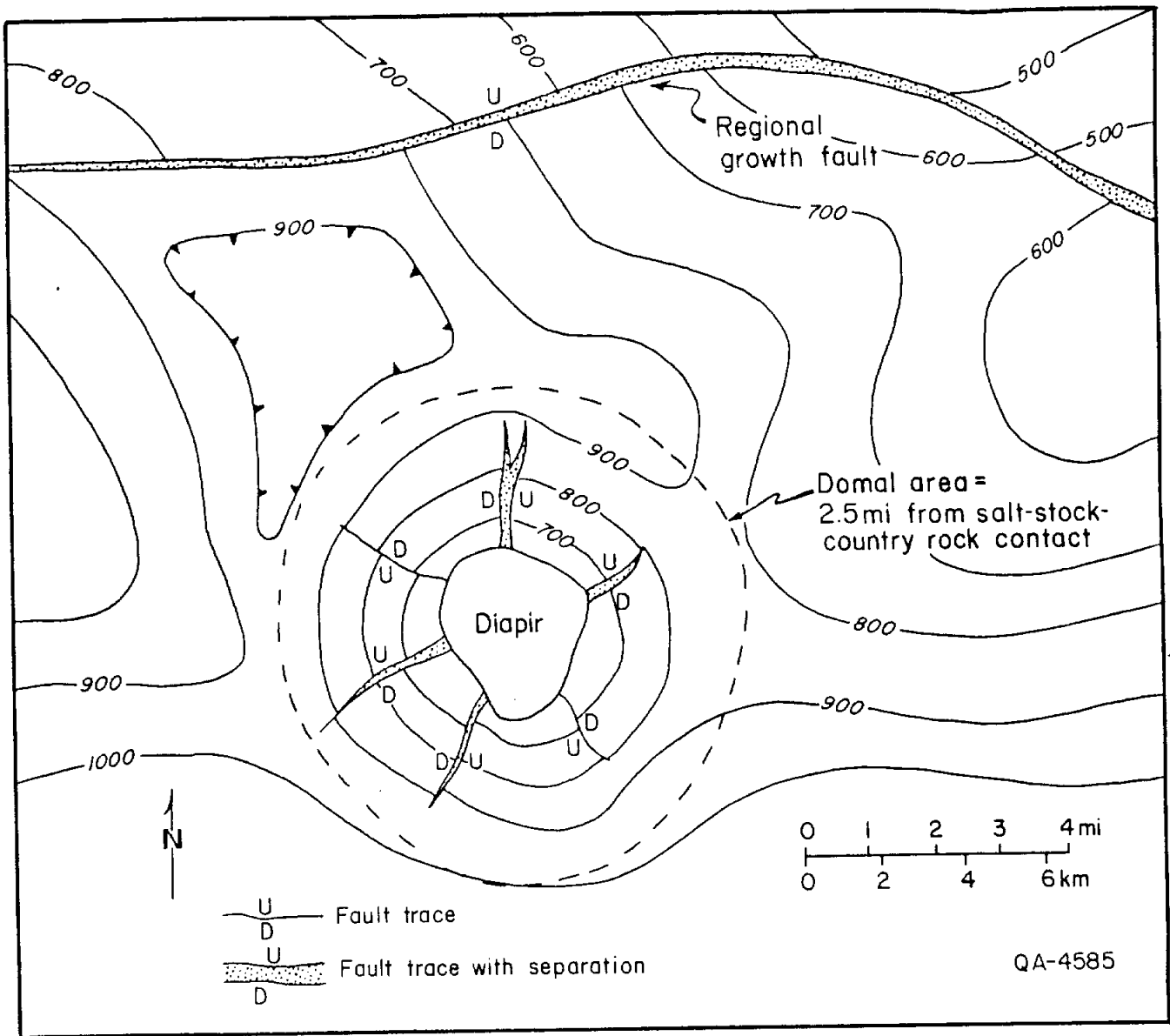
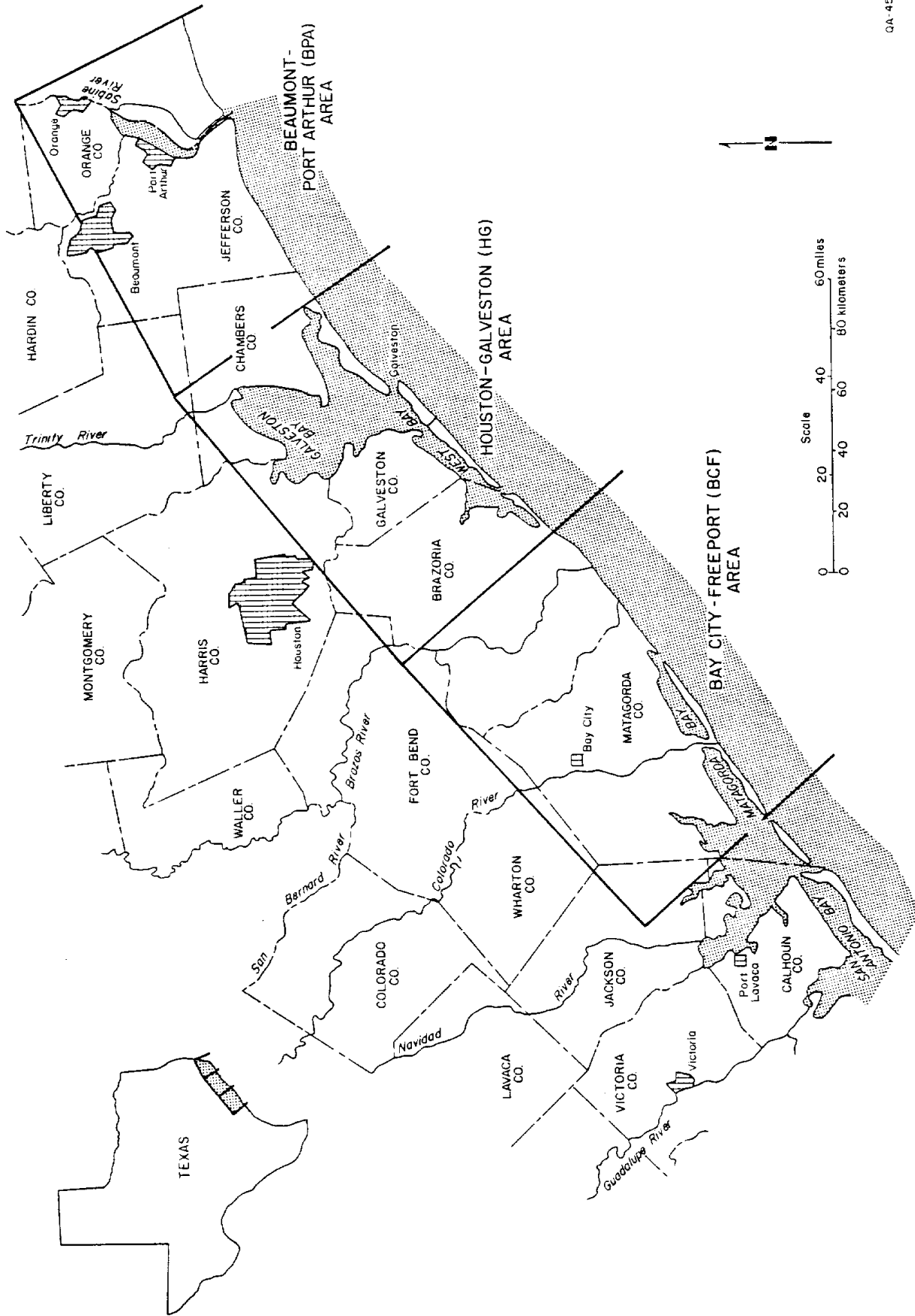


Figure 1. Parameters used to differentiate regional and domal areas during statistical analysis.



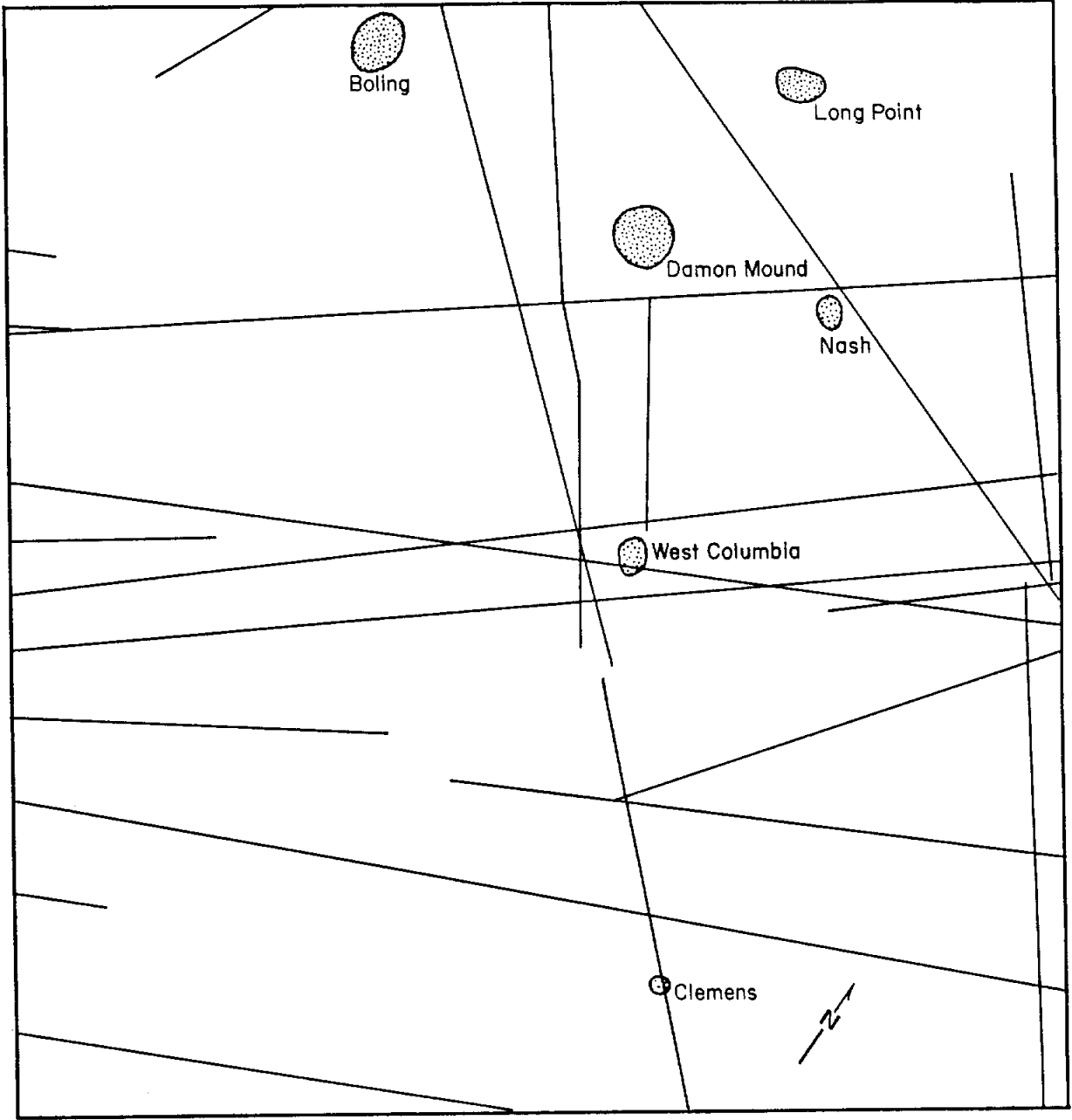
GA-4596

Figure 2. Location map of data areas covering Houston diapir province used in statistical analysis (modified from Fisher and others, 1972).


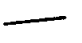
others, 1972; 1973; McGowen and others, 1976). Four data sets were compiled for each EGATCZ region. In addition, one nondomal test area was analyzed for each region. Data sets compiled for analysis are (1) regional subsurface faults, (2) domal subsurface faults, (3) regional surface faults and lineaments, (4) domal surface faults and lineaments, and (5) a test case using regional subsurface faults. Surface faults and lineaments were taken directly from the Physical Property Map enclosed with each EGATCZ map set (fig. 3). Subsurface fault data (fig. 4) are from unpublished maps developed for the Tectonic Map of Texas (Ewing, 1983b). Data pertaining to the study area is in table 3.

Data processing was accomplished using a series of three computer programs designed for structural analysis. Phase One involved entering the data by digitizing the lineaments and faults. Curved faults were digitized as a series of straight-line segments. Straight-line segments of arcuate growth faults were separated by inflection points. The azimuth of adjacent segments deviated less than 10° . Each data set was digitized using BEG Program DIGLIN (GS0020.00.00) on a Tektronix 4054 graphics computer. The data were then stored on permanent files. Phase Two involved computer processing of raw data sets. The length and azimuth of fault segments and lineaments were measured with BEG Program Baumlin.

Program ROSENET (Williams, 1980) was modified for BEG application in structural analysis and renamed ROSEDIA (GR0020.00.00). Phase Three used ROSEDIA to plot results. ROSEDIA generates two different types of polar graphs. The "section diagram" is an analog of a histogram with all azimuths in 10° windows of observation combined and plotted as a unit. Two section diagrams are plotted for each data set. They are (1) number of azimuths and (2) cumulative length of azimuths. "Boundary diagrams" are designed to plot moving averages where fixed intervals are scanned through the data set at user-defined increments. Two plots are also generated for boundary diagrams--one plot for number of azimuths and one plot for cumulative length of azimuths (Williams, 1980) (fig. 5a through e).



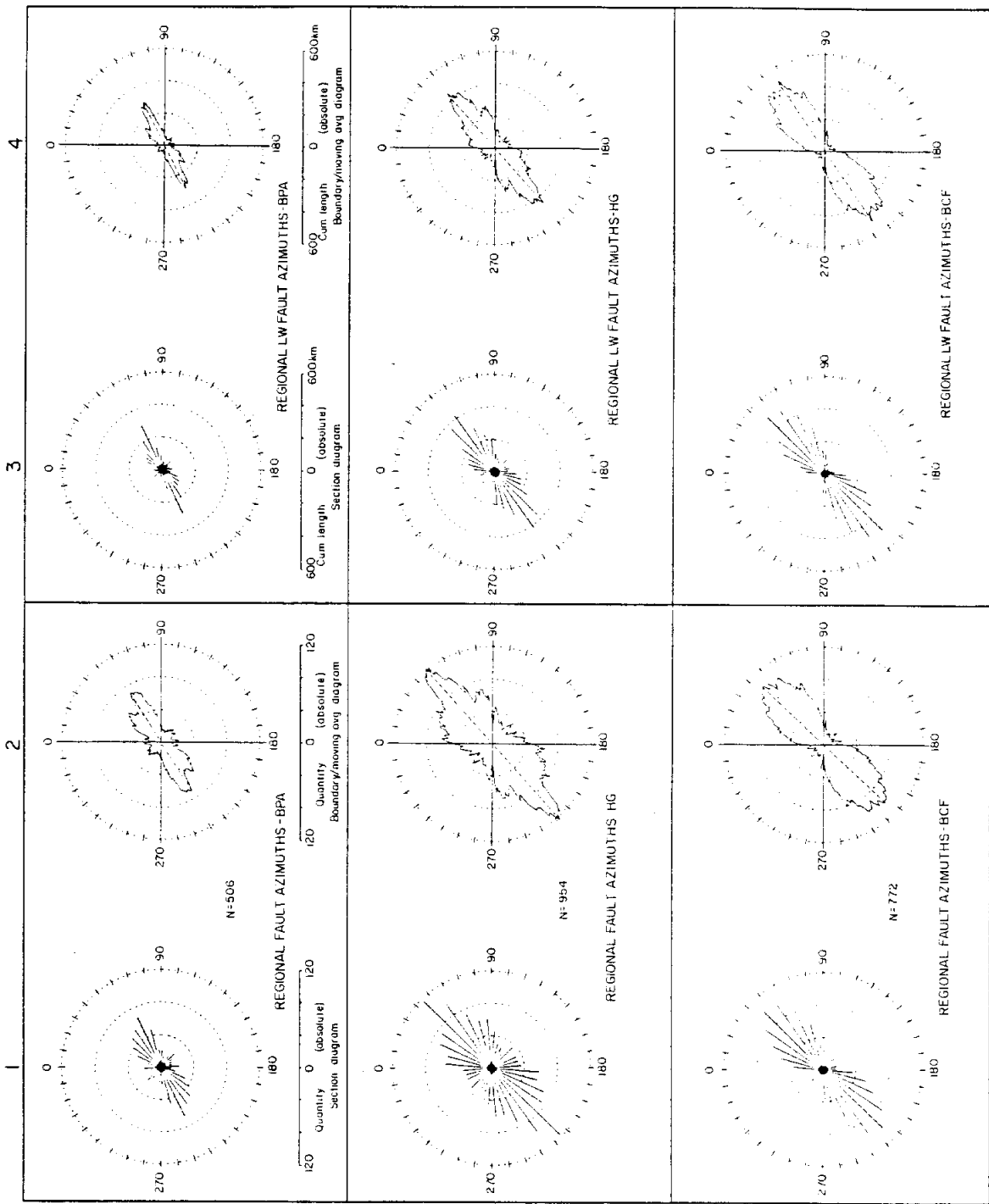
EXPLANATION

 Diapir
  Structural lineament or surface fault

0 1 2 3 4 5mi
 0 2 4 6 8 km

QA-4586

Figure 3. Lineament patterns over Boling, Long Point, Damon Mound, Nash, West Columbia, and Clemens Domes.



(a)

Figure 5. Polar graphs of azimuth orientations for a) regional faults. Columns 1 and 3 are section diagrams. 2 and 4 are boundary diagrams.

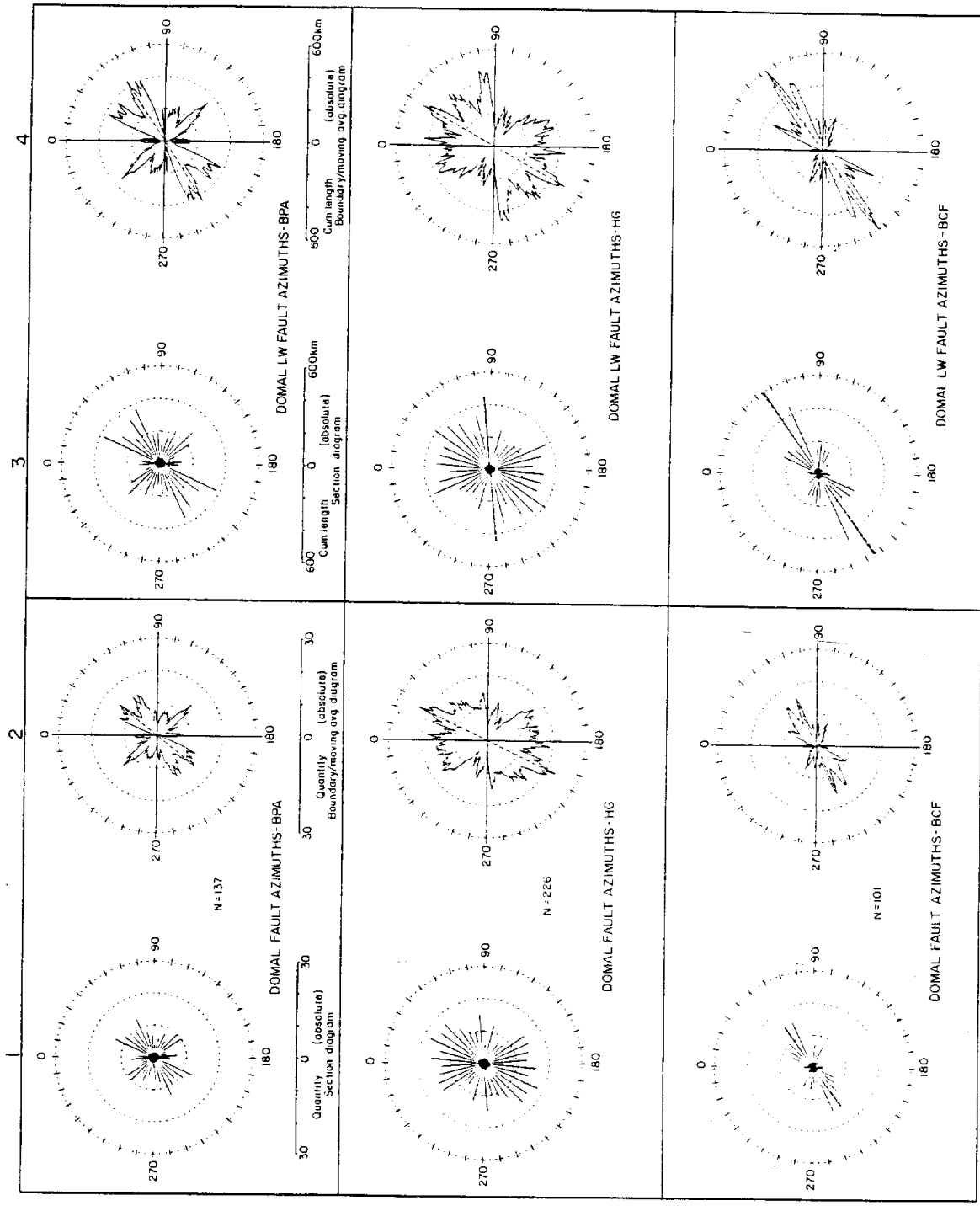


Figure 5. Polar graphs of azimuth orientations for b) domal faults. Columns 1 and 3 are section diagrams, 2 and 4 are boundary diagrams.

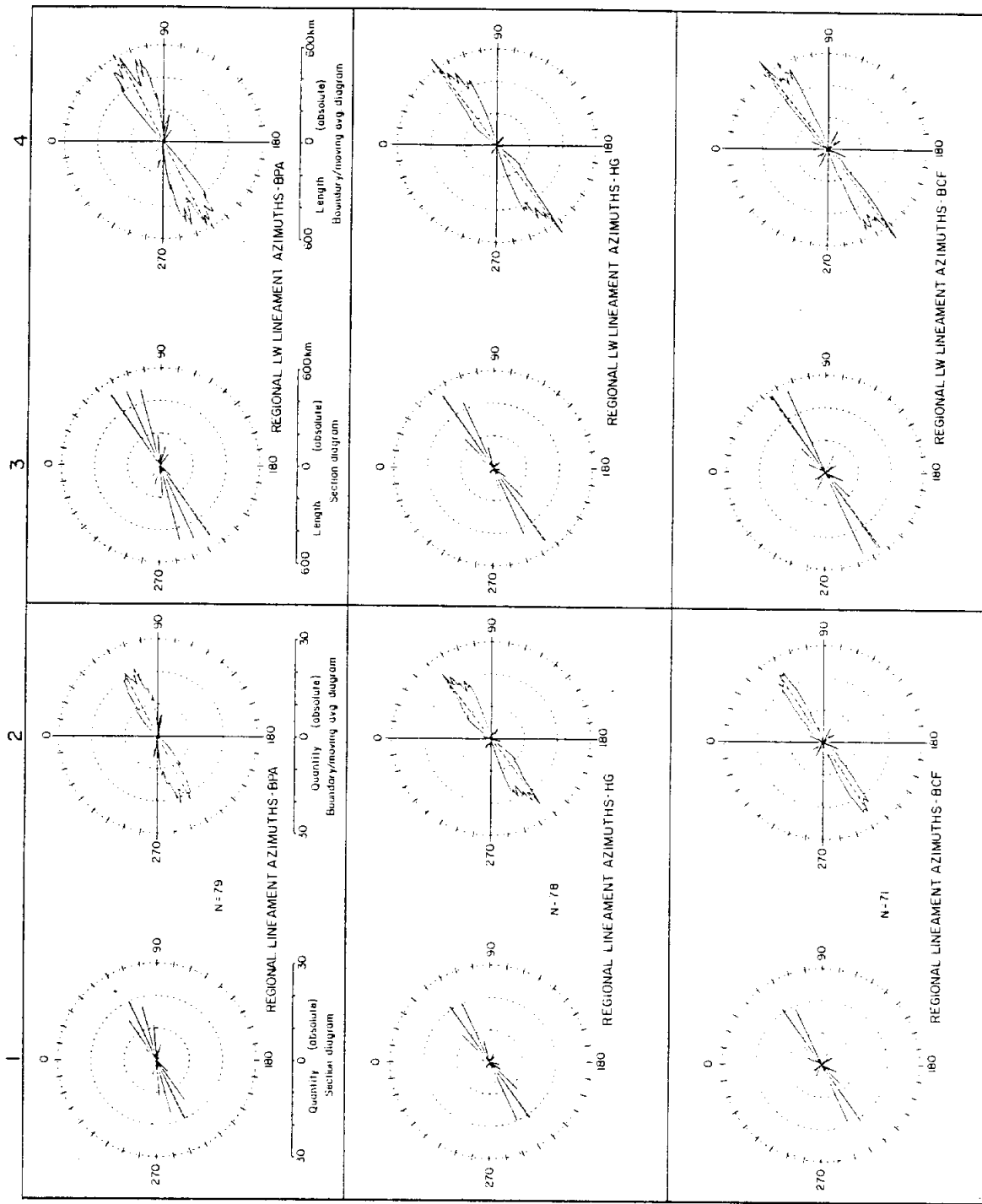
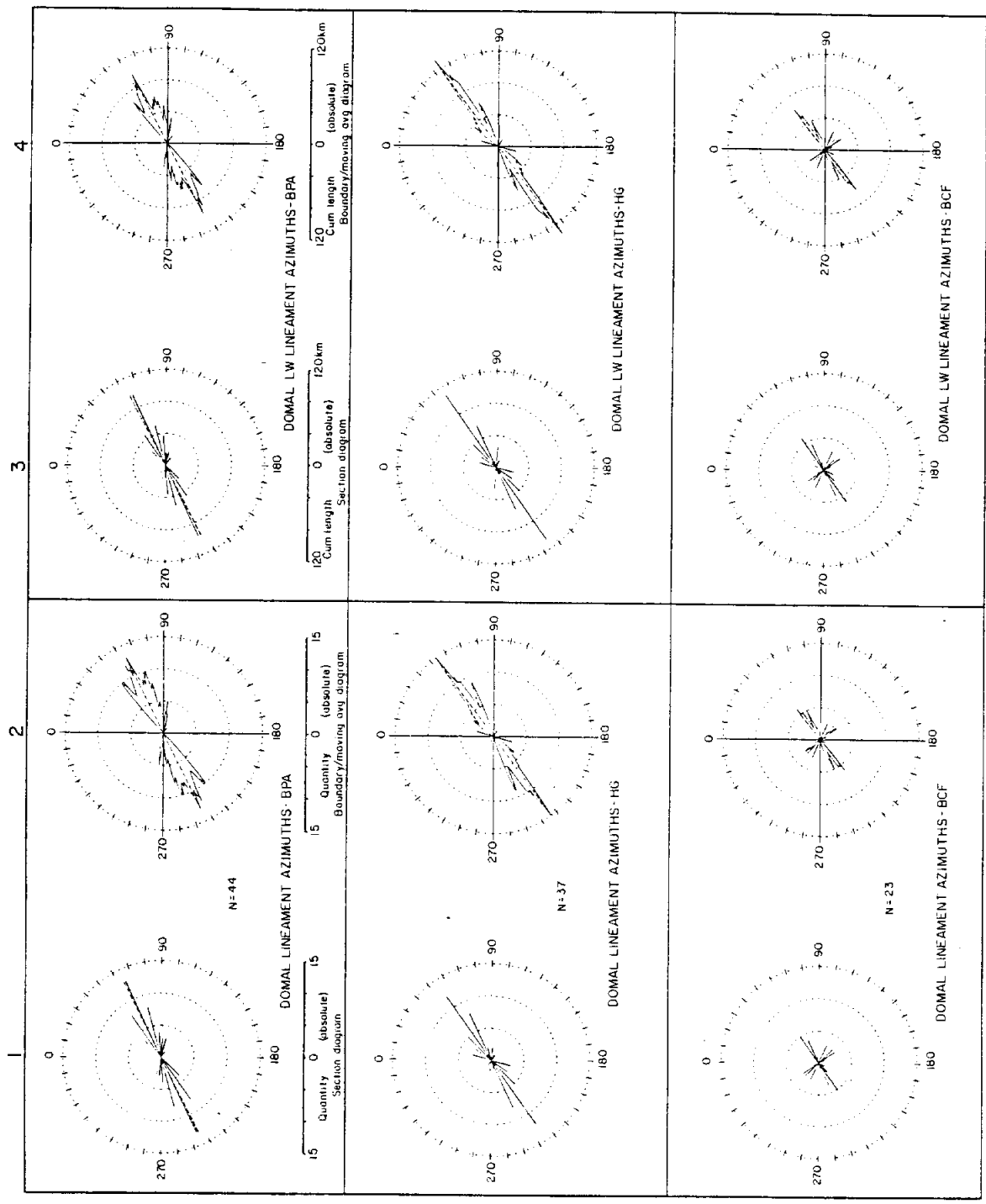


Figure 5. Polar graphs of azimuth orientations for c) regional lineaments. Columns 1 and 3 are section diagrams, 2 and 4 are boundary diagrams. (c)



(d)

Figure 5. Polar graphs of azimuth orientations for d) domal lineaments. Columns 1 and 3 are section diagrams, 2 and 4 are boundary diagrams.

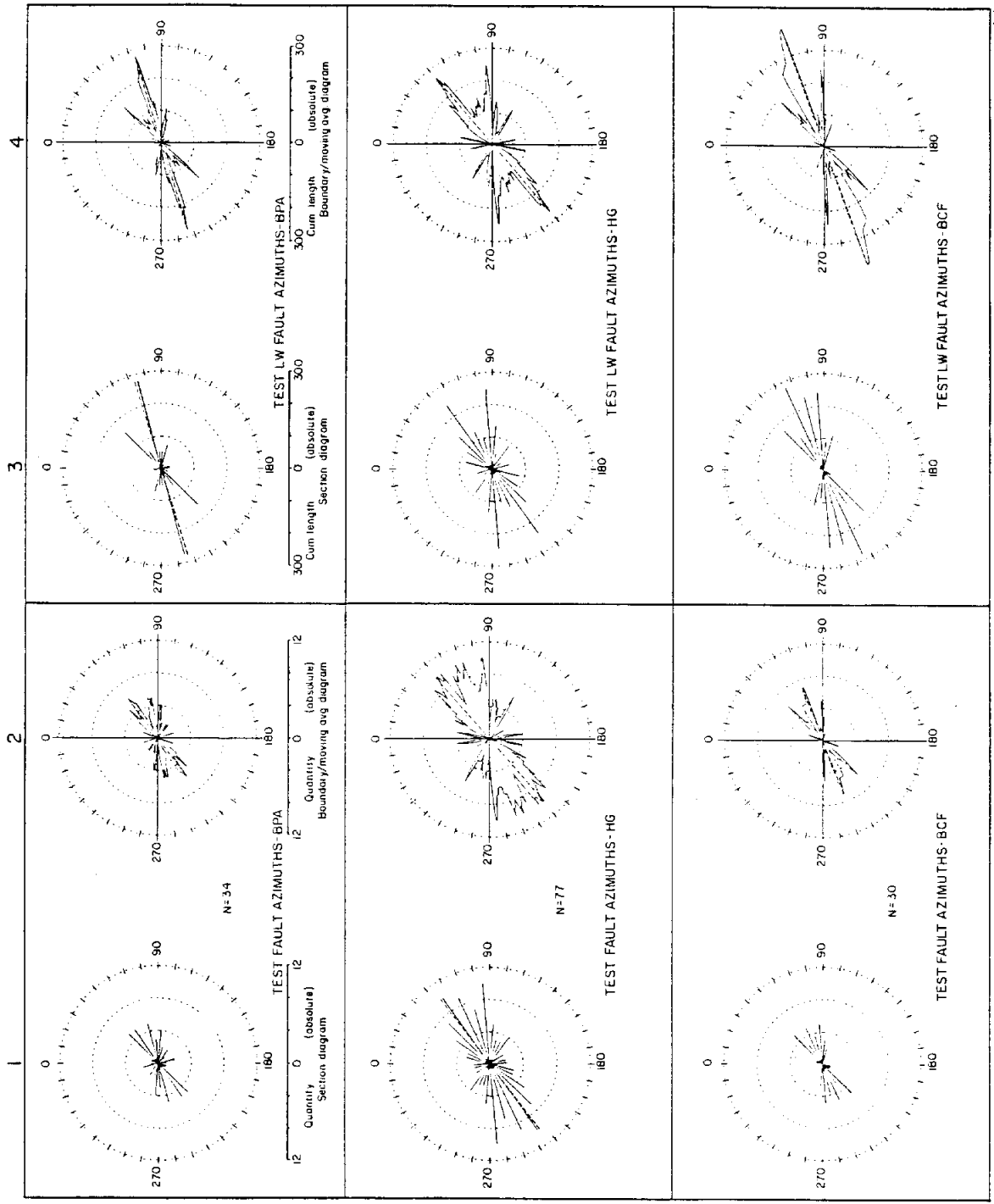


Figure 5. Polar graphs of azimuth orientations for e) test faults (nondomal).
 Columns 1 and 3 are section diagrams, 2 and 4 are boundary diagrams.

(e)
 QA-4595

STATISTICAL ANALYSIS

Different statistical tests were applied to the computer-generated data to evaluate geologic significance and to determine levels of confidence for potential correlations. Methodology was based on the techniques used by Dix and Jackson (1981). The initial task was to determine the optimum window size (the defined angle of observation) and those windows with a greater-than-average cumulative length value. Windows that were too narrow were found to be numerically cumbersome and difficult to synthesize. Windows that were too wide did not differentiate groups of significant data effectively. After testing several different window sizes or increments, data sets were analyzed using 10° windows of observation for the total range of observation (Dix and Jackson, 1981). This was also the precision applied to the division of curved faults into straight-line fault segments.

Windows found to be greater than average were not always found to be statistically significant at an acceptable level, as defined by Dix and Jackson (1981). They showed that randomly generated numbers can illustrate greater-than-average peaks with no geological significance. This was found to be especially true in the analysis of data sets with small populations.

To determine geologic significance, the chi squared (χ^2) one-sample nonparametric test was applied to each window with a greater-than-average value (Siegel, 1956; Vistelius, 1966). χ^2 tests were based on percent cumulative length of greater-than-average windows to analyze cumulative length of fault and lineament azimuths and azimuth frequency.

Using the χ^2 test for intervals with two or more continuous windows of greater-than-average length-weighted frequencies, 16 of 20 windows tested were determined to be significant at the 95-percent level of confidence, whereas 15 of 20 were significant at the

99-percent level. Figure 10 is a frequency histogram of 10° window segments found to be statistically significant at the 99-percent level of confidence.

A reported relationship in the East Texas diapir province is that a statistically significant increase in mean lineament densities exists for southern diapirs (Dix and Jackson, 1981). To test for this type of relationship around Gulf Coast diapirs, mean-fault and mean-lineament densities were calculated for the five data types. F- and t-tests were then applied to determine if relationships (increases in lineament or fault densities) previously reported in other areas (Dix and Jackson, 1981) were also applicable in this study.

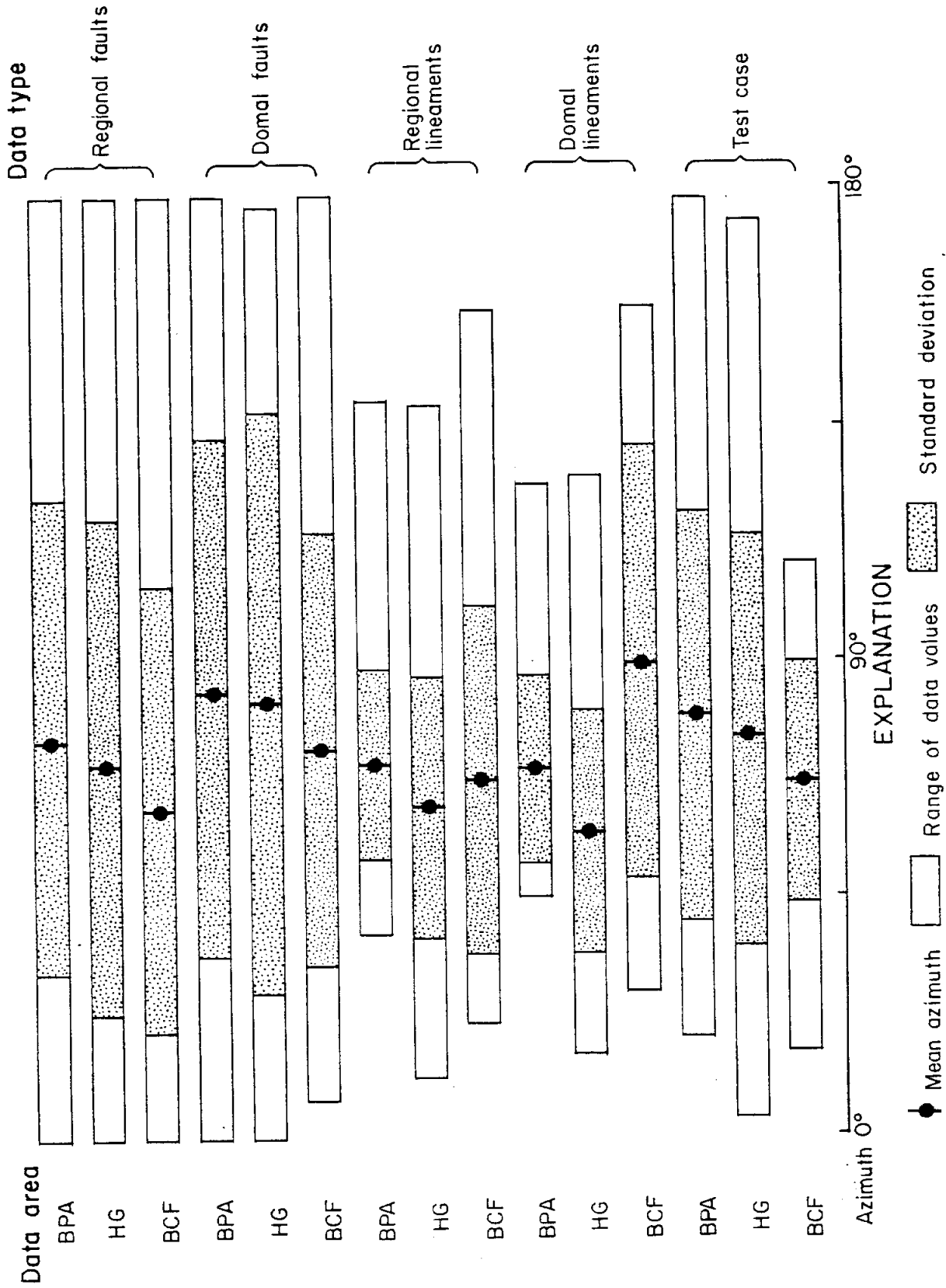
Population tests (F- and t-tests) indicated that no statistically significant differences in mean lineament or fault densities were detected among any of the five data types (table 4). This could be a result of any of five different factors, including (1) failure to include diapiric circular faults as part of the domal data sets, (2) potential inability to consistently detect domal faults with the same accuracy as regional faults, (3) standardized size of domal areas may fail to adequately cover area of faulting resultant from diapirism, (4) shorter length of domal faults is mathematically overwhelmed by regional length of growth faults in statistical analysis, and (5) that there is in fact no difference in mean lineament or fault densities. Detailed study of these different factors would be beneficial in confirming or revising density relationships.

Previous studies on populations of faults indicate the importance of mean azimuth orientation and standard deviation. Wermund and others (1978) used the magnitude of standard deviation to differentiate between synthetic and antithetic fracture patterns in a bimodal structural environment. Although significant bimodal peaks were the exception and not the rule for this study, analysis from this technique did illustrate some relationships. Figure 6 is a rectangular graph of mean azimuth orientations, standard deviations, and minimum-maximum values for individual data sets.

Table 4. Statistical data comparing fault/lineament density in regional and domal areas.

Data Set	Data Sets (n)	Fault or Lineament Segments (n)	Mean Fault/Lineament Density (km/km ²)	Standard Deviation among Data Sets	F test* (95% level)	t test* (99% level)
Regional faults	3	2232	.36	.075	equivalent variances	no significant difference in means
Domal faults	3	464	.33	.050	equivalent variances	no significant difference in means
Regional lineaments	3	228	.26	.075	equivalent variances	no significant difference in means
Domal lineaments	3	104	.23	.066	equivalent variances	no significant difference in means
Test case	3	141	.14	.041	equivalent variances	no significant difference in means

*F test and t test modified from Davis (1973); Dix and Jackson (1981). Equivalence comparisons based on all possible combinations.



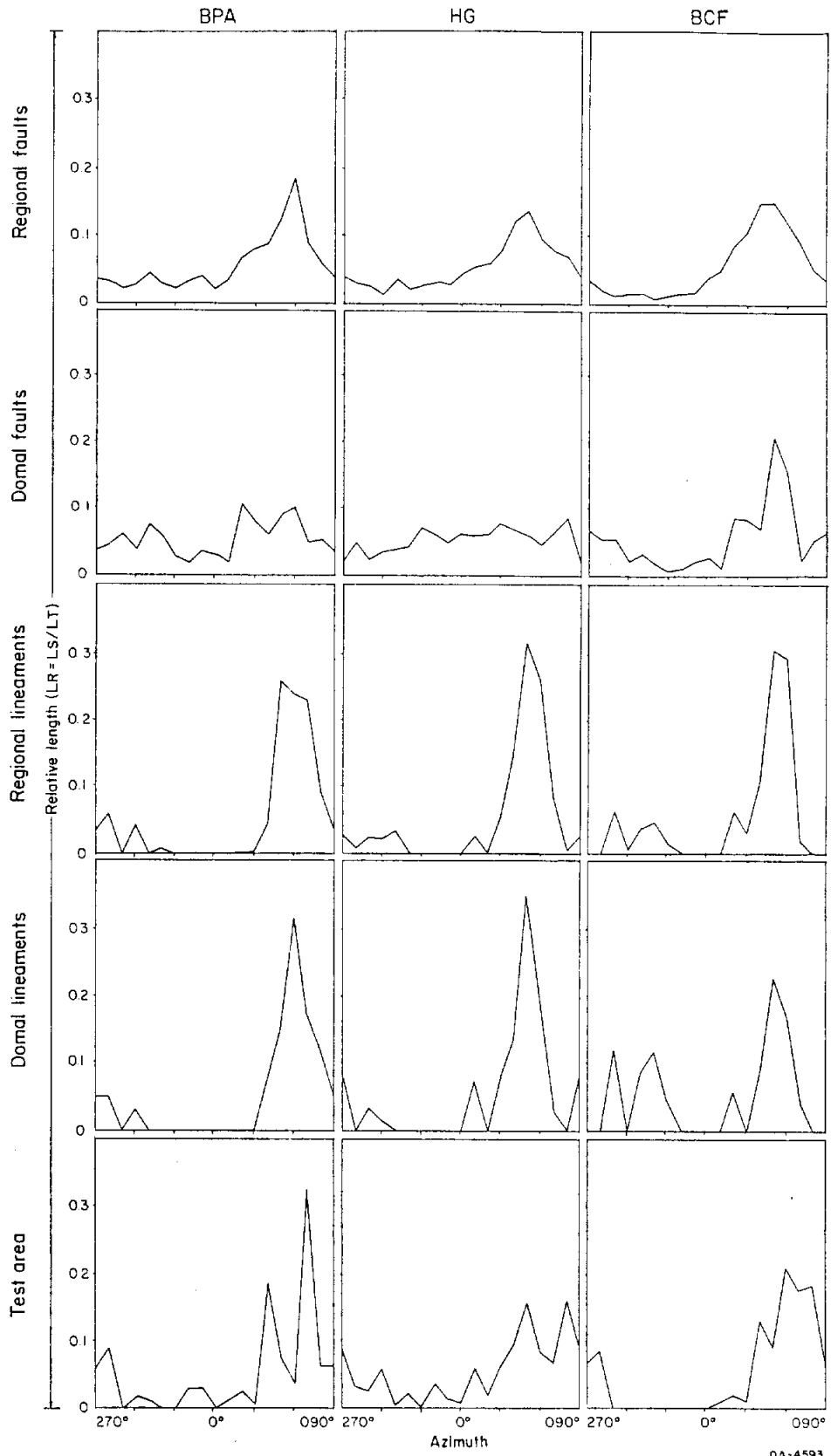
QA-4584

Figure 6. Bar graphs of azimuth orientations including mean value, minimum-maximum value, and standard deviation computed for data sets.

Rectangular graphs illustrate the relationship between azimuth orientation and relative fault or lineament length (LR) (fig. 7). LR is computed using the equation $LR=LS/LT$, where LS is equal to the cumulative fault or lineament length for 10° windows of observation and LT is equal to total cumulative length of faults or lineaments for entire data sets (Dix and Jackson, 1981). Peak azimuth orientation and movement among various data sets are highlighted using this method of presentation.

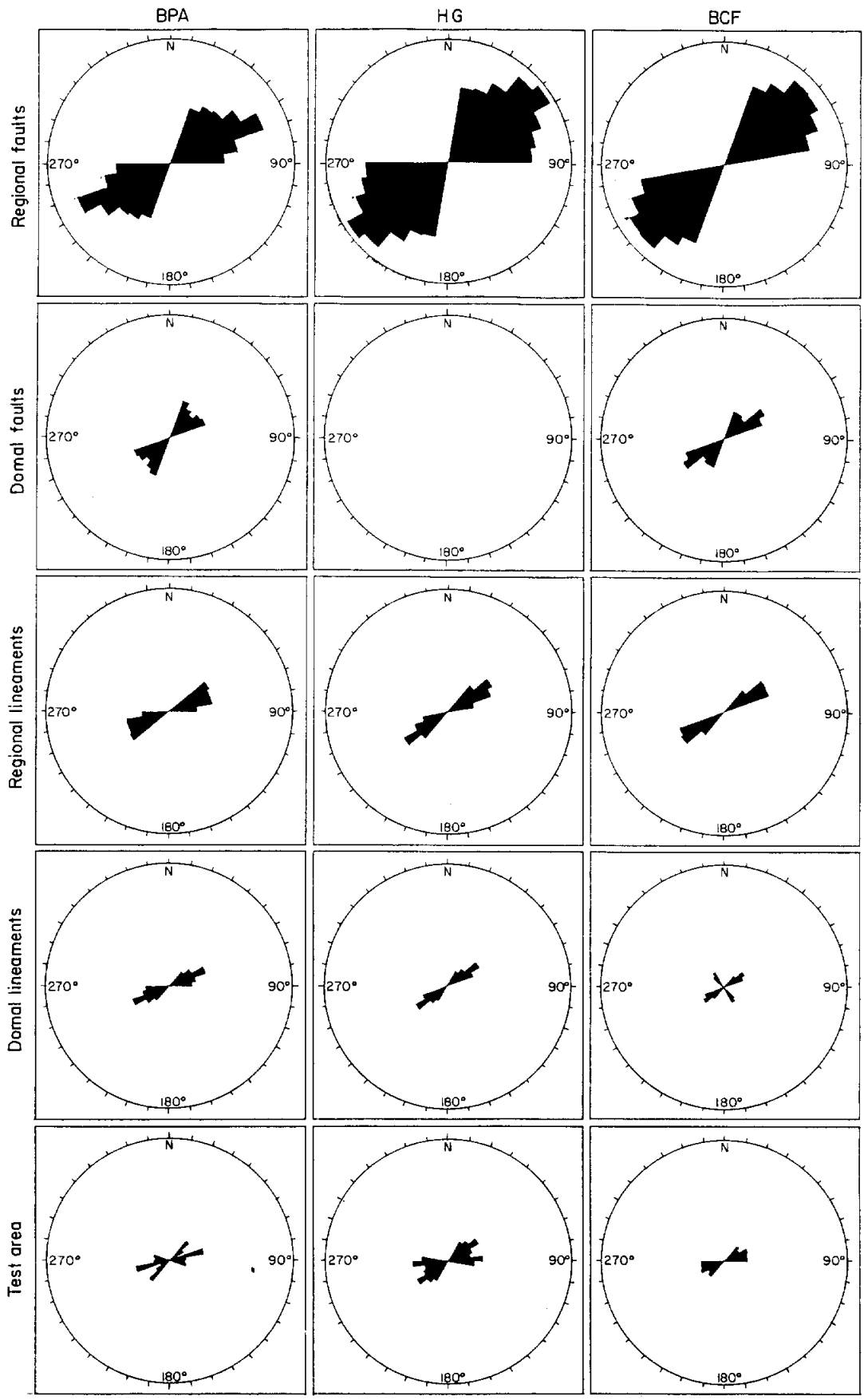
Subsurface faults as a group have a mean standard deviation of 46.5° , whereas surface faults and lineaments have a mean standard deviation of 26.5° . This 43-percent difference in standard deviation is best explained by the great difference in length between the two structural components measured--faults and lineaments. Figure 11 illustrates the difference in length for the two components measured. Average fault segment length for regional and domal fault data sets were 11,499 ft (3,505 m) and 8,405 ft (2,562 m), respectively, whereas average lengths of regional and domal lineaments were 81,201 ft (24,750m) and 26,046 ft (7,939 m), respectively. This difference in length is the result of different mapping techniques used to delineate faults and lineaments. The BCF domal lineament data set was the only lineament data set that recorded a standard deviation comparable to fault data sets. This illustrates the increased influence of diapirism at the surface in regions with shallow diapirs because BCF has the greatest number of shallow diapirs. This analysis was particularly effective in showing the movement of mean azimuth orientation from west to east through the various data types.

Another method employed for analyzing relative strength and orientation of regional growth fault trends was through a series of polar graphs plotting the square root of F for greater-than-average windows at the 99-percent level of confidence (fig. 8). F is length-weighted frequency for the window observed (Frost, 1977). In several different data sets, weighting of azimuth frequency by its cumulative length provided a more accurate representation of the overall magnitude of faulting. This is a result of the methodology



QA-4593

Figure 7. Rectangular graph showing relation between relative fault or lineament length (L_R) and fault or lineament azimuth.



Length-weighted (\sqrt{F}) azimuth

0 3 6 \sqrt{F}

QA-4594

Figure 8. Polar graphs of fault and lineament azimuth orientation using square root of length-weighted frequencies (\sqrt{F}) for data sets.

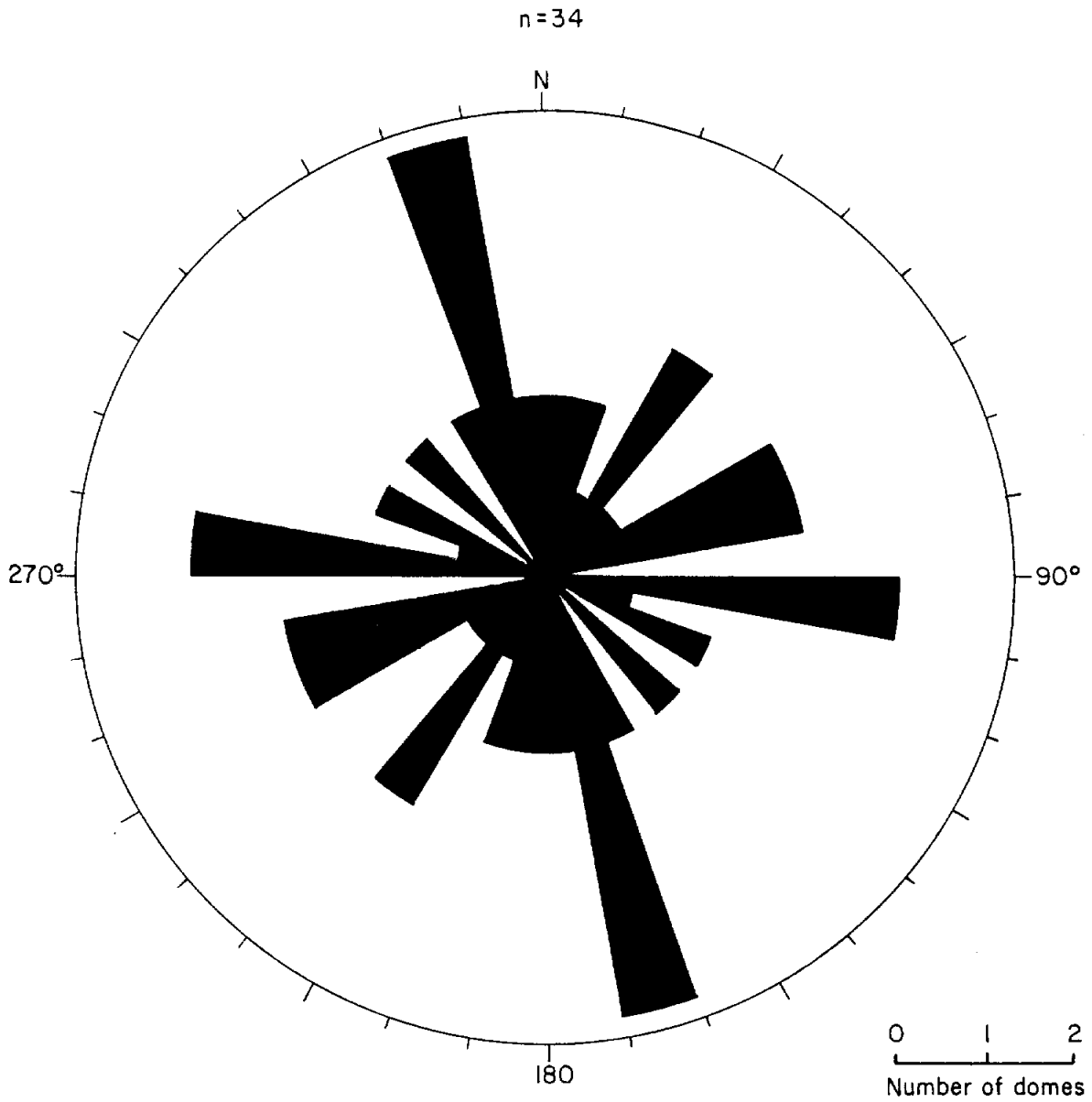
used for the data processing of subsurface faulting. Measuring the azimuth of large arcuate growth faults necessitated their division into straight-line segments. Fault segments were weighted with respect to cumulative length to better represent longer faults, which have greater displacement. Length and frequency scales were normalized to aid comparison among types of data. The square root of F is used, because when F or F^2 is used, the area under the curve defining greater-than-average peaks is exaggerated (Vistelius, 1966; Dix and Jackson, 1981).

Although circular faults (Kupfer, 1963) separating country rock from salt stock were not included in the main data base, their orientations were plotted. Figure 9 is a polar graph of major axis orientation for diapirs in the Houston diapir province. The dominant orientation in this province is perpendicular to regional strike, whereas a minor trend does parallel regional strike.

Regional Structure

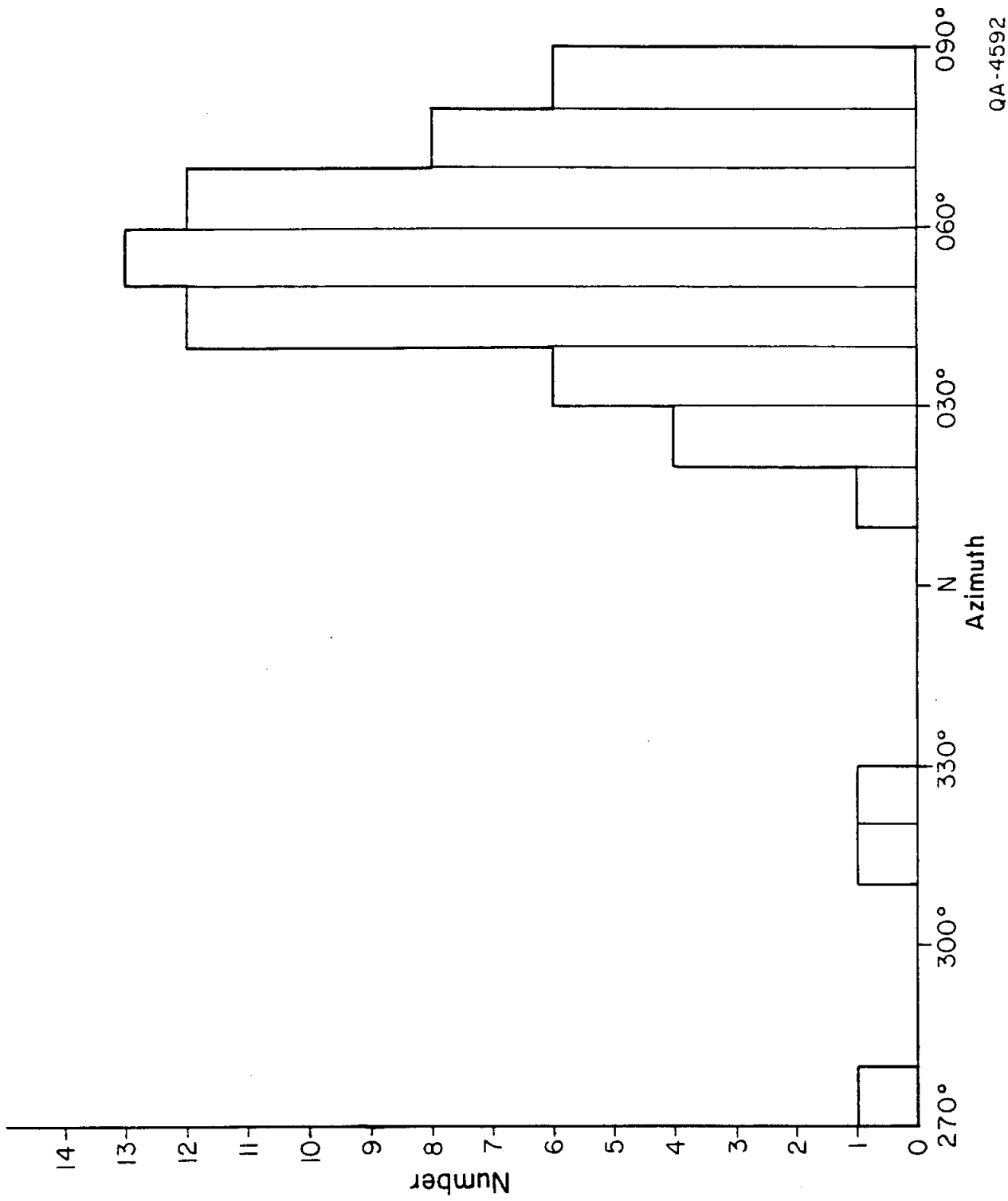
Section and boundary diagrams generated from the various data sets document several different structural features of the Houston diapir province (fig. 5, table 5). Maximum azimuth strength for regional data sets was almost parallel for each data area. BPA regional data sets had a maximum azimuth strength of 60° to 69° for faults and 50° to 59.9° for lineaments. In HG, both faults and lineaments recorded a maximum value of 50° to 59.9° . In the BCF area the maximum fault azimuth was 40° to 49.9° , and the lineaments equaled 50° to 59.9° .

These data demonstrate the overwhelming influence of regional depositional strike (50° - 65°) on the preferred orientation of structural features of the Houston diapir province. BPA and BCF have slight fluctuations between regional mean subsurface fault azimuth and regional mean surface lineament azimuth. These slight fluctuations might indicate that modern surface fault and lineament azimuths have shifted slightly since deposition of subsurface units used in this study. This difference could be used as evidence



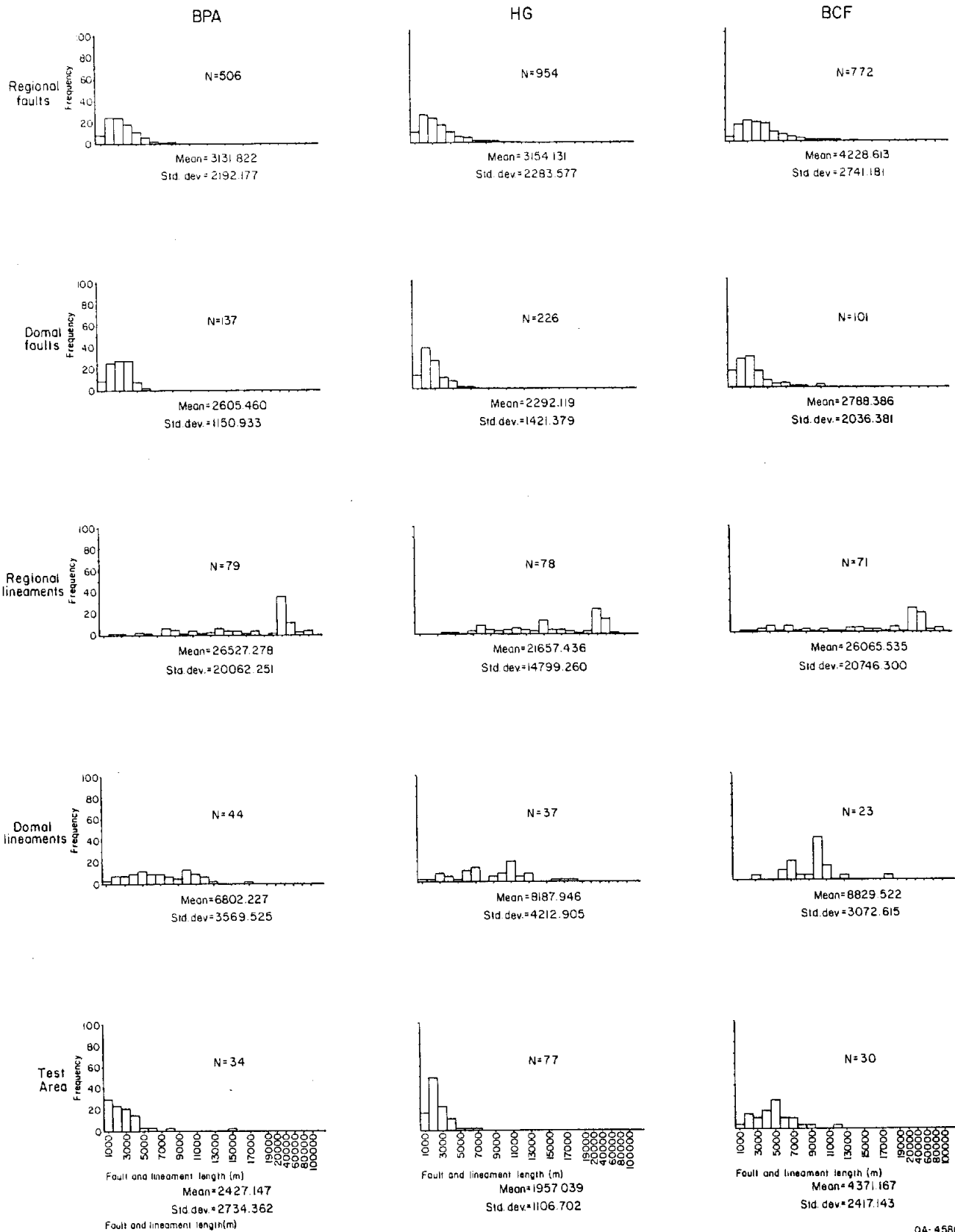
QA-4590

Figure 9. Polar graph showing frequency of major axis azimuths for salt diapirs in the Houston diapir province.



QA-4592

Figure 10. Histogram of greater-than-average 10° windows significant at 99% level of confidence.



QA-4588

Figure 11. Frequency histogram comparing fault and lineament segment length for different data sets.

Table 5. Structural data from statistical analysis.

Data Set	Fault or Line Segments	Mean Azimuth (°)	Min - Max Azimuth (°)	Standard Deviation (°)	Total Cumulative Length (m)	Azimuth with Maximum Cumulative Length (°)	Frequency of Fault or Lineament Segments for Maximum Cumulative Length Window	Azimuth Window above Average at 99% Level of Confidence (χ^2 test)
BPA Regional Faults	506	76.7	.1-179.4	45.0	1.58 x 10 ⁶	60-69.9	67	20-89.9
BPA Domal Faults	137	85.0	.7-178.7	49.0	3.57 x 10 ⁵	20-29.9	13	-----
BPA Regional Lineaments	79	71.0	38.8-139.7	18.0	2.09 x 10 ⁶	50-59.9	15	50-89.9
BPA Domal Lineaments	44	70.3	45.6-124.1	18.3	2.99 x 10 ⁵	60-69.9	13	40-89.9
BPA Test	34	80.4	19.5-178.1	39.2	8.2 x 10 ⁴	70-79.9	5	40-59.9 70-289.9
HG Regional Faults	954	71.5	.0-179.4	47.5	3.01 x 10 ⁶	50-59.9	96	10-89.9
HG Domal Faults	226	83.5	.1-177.2	55.0	5.18 x 10 ⁵	80-89.9	15	-----
HG Regional Lineaments	78	63.3	11.0-139.4	24.9	1.69 x 10 ⁶	50-59.9	21	40-79.9
HG Domal Lineaments	37	58.0	15.6-125.3	23.3	3.03 x 10 ⁵	50-59.9	12	30-69.9
HG Test	77	75.5	4.2-173.7	38.6	1.51 x 10 ⁵	80-89.9	10	30-279.9
BCF Regional Faults	772	63.2	.8-179.7	41.7	3.26 x 10 ⁶	40-49.9	101	20-79.9
BCF Domal Faults	101	73.8	7.8-179.5	40.6	2.82 x 10 ⁵	50-59.9	15	20-69.9
BCF Regional Lineaments	71	68.1	21.6-157.1	33.3	1.85 x 10 ⁶	50-59.9	21	40-69.9
BCF Domal Lineaments	23	89.9	27.7-157.1	41.4	2.03 x 10 ⁵	50-59.9	5	40-69.9 310-329.9

Table 5. (cont.)

Data Set	Fault or Line Segments	Mean Azimuth ($^{\circ}$)	Min - Max Azimuth ($^{\circ}$)	Standard Deviation ($^{\circ}$)	Total Cumulative Length (m)	Azimuth with Maximum Cumulative Length ($^{\circ}$)	Frequency of Fault or Lineament Segments for Maximum Cumulative Length Window	Azimuth Window above Average at 99% Level of Confidence (χ^2 test)
BCF Tests	30	67.5	16.4-109.0	22.9	1.31×10^5	60-69.9	5	40-89.9
Regional Faults	2232	69.8	.0-179.7	45.3	7.85×10^6			
Domal Faults	464	81.8	.1-179.5	50.5	1.16×10^6			
Regional Lineaments	228	67.5	11.0-157.1	25.9	5.63×10^6			
Domal Lineaments	104	70.3	15.6-157.2	28.9	8.05×10^5			
Test Faults	141	75.0	4.2-178.1	36.1	3.64×10^5			

for a slight change in depositional strike as it influences regional structural trends. Rectangular graphs of LR versus azimuth orientation illustrate consistent patterns, which were obvious within both data types and data areas. With the exception of HG domal faults, each data set expresses maximum peak orientation parallel to the trend of regional depositional strike.

Domal Structure

Maximum azimuth peak orientation for domal faults varied from trends established in regional data sets. These peaks were (1) 20° to 29.9° for BPA, (2) 80° to 89.9° for HG, and (3) 50° to 59.9° for BCF.

All five greater-than-average peaks determined not to be geologically significant (at 99-percent level of confidence) were from data sets compiled for domal areas. This indicates domal faults have greater variation in azimuth orientation than faults in regional areas. This corresponds with results previously reported for lineaments in southern domal areas for the East Texas diapir province (Dix and Jackson, 1981). Cloos (1968) documented similar observations (dispersion of preferred orientation) from his experimental analysis of Gulf Coast fracture patterns.

Domal lineaments were virtual duplicates of regional lineament diagrams, maximum azimuth strength being equal and only the magnitude representing different scales. One exception was statistically significant--bimodal peak orientation for BCF domal lineaments.

Domal lineaments record a much stronger expression of regional structural trends than domal faults. The azimuths of BFC domal lineaments have bimodal peaks oriented at 50° to 59.9° and 320° to 329.9° . All 12 diapirs in BCF have depths to domal material less than 4,000 ft. This allows a greater probability for surface expression of diapirism than if their crests were deeply buried. The bimodal peak orientation is the probable expression of domal influence at the surface. Similarly, 38 percent and 63 percent of the diapirs in the

HG and BPA areas, respectively, have depths to salt less than 4,000 ft with no bimodal peaks for domal lineament azimuths. One conclusion of this relationship is that structure in areas with shallow diapirs (depth of crest less than 4,000 ft) has a greater surface expression (surface faults and lineaments) of domal influence than in areas with deeper domes.

Polar graphs of the square root of F also illustrate development of bimodal structural grain in BCF domal lineaments present in other analyses. Another point to note is the irregular nature of the curve illustrated in smaller data sets. The increase in well-defined curve development with progressively larger data sets confirms conclusions regarding the inherent pitfalls of small data sets in structural analysis (Dix and Jackson, 1981). The erratic profile of fault azimuth observed in test areas from different statistical analyses when compared with smooth curves for regional faults can be best explained by the relatively small size of data sets in the test areas and their ability to generate random peaks of no geologic significance.

CONCLUSIONS

Regional structural trends in the Houston diapir province are revealed by the azimuth of subsurface faults and surface lineaments. The mean azimuth orientation varies from 40° to 59.9° in BCF to 50° to 69.9° in BPA. Regional trends of fault and lineament azimuths are dispersed in local areas around diapirs. The dispersion of both fault and lineament azimuths increases in domal areas where domes are shallow.

From the BCF to BPA areas, regional structural trends align with depositional strike. Regional fault azimuth is influenced by depositional strike along ancient prograding shelf margins. The azimuth of domal subsurface faults has greater dispersion than that of regional faults in the Houston diapir province. The strongest expression of this relationship

is seen in the Houston-Galveston area. This is probably a result of the large number of domes (18), abundant shallow domes, and subsequently larger size of the data set.

There was not an increase in the mean lineament or fault densities for domal areas as was observed in a previous study (Dix and Jackson, 1981) for the East Texas diapir province. Two possible explanations are offered. The absence of any increase in mean lineament or fault density indicates that structural processes in domal areas are no stronger for those parameters measured than regional processes. Processes related to dome growth may act slowly enough so that the surrounding unconsolidated strata deform ductilely rather than through brittle (fault) deformation (M.P.A. Jackson, personal communication, 1985). Alternatively, the result may be that an artifact of data analysis methodology introduced factors masking an increase in fault density for domal areas. Confirmation or revision of the density results reported here are important to the overall goal of determining dome stability and integrity because of the greater potential for hydrologic conduits over domes with increased fault densities. Further study is needed to determine if any one or combination of factors possibly influencing this analysis significantly affect density results.

REFERENCES

- Balk, R., 1936, Structure elements of domes: American Association of Petroleum Geologists Bulletin, v. 20, no. 1, p. 51-67.
- Barton, D. C., 1936, Surface fracture system of South Texas, in Barton, D.C., and Sawtelle, G., eds., Gulf Coast oil fields, a symposium on the Gulf Coast Cenozoic: American Association of Petroleum Geologists, p. 251-269.
- Bornhauser, M., 1958, Gulf Coast tectonics: American Association of Petroleum Geologists Bulletin, v. 42, no. 2, p. 339-370.
- Bruce, C. H., 1973, Pressured shale and related sediment deformation: American Association of Petroleum Geologists Bulletin, v. 57, no. 5, p. 878-886.

- Caran, S. C., Woodruff, C. M., Jr., and Thompson, E. J., 1982, Lineament analysis and inference of geologic structure--examples from the Balcones/Ouachita trend of Texas: The University of Texas at Austin, Bureau of Economic Geology Geological Circular 82-1, 12 p.
- Carver, R. E., 1968, Differential compaction as a cause of regional contemporaneous faults: American Association of Petroleum Geologists Bulletin, v. 52, no. 3, p. 414-419.
- Clanton, U. S., Jr., and Amsbury, D. L., 1976, Active faults in southeastern Harris County, Texas: Environmental Geology, v. 1, no. 3, p. 149-154.
- Cloos, E., 1947, Oolite deformation in the Southern Mountain Fold, Maryland: Geological Society of America Bulletin, v. 58, p. 843-918.
- _____ 1968, Experimental analysis of Gulf Coast fracture patterns: American Association of Petroleum Geologists Bulletin, v. 52, no. 3, p. 420-444.
- Currie, J. B., 1956, Role of concurrent deposition and deformation of sediments in development of salt-dome graben structures: American Association of Petroleum Geologists Bulletin, v. 40, no. 1, p. 1-16.
- Davis, J. C., 1973, Statistics and data analysis in geology: New York, John Wiley, 550 p.
- DeBlieux, C. W., and Shepherd, G. F., 1941, Photogeologic exploration along the Louisiana Wilcox-Fault trend (abs.): Gulf Coast Association of Geological Societies Transactions, v.1, p. 42.
- Desjardins, L., 1952, Aerial photos of multiple surface faults may locate deep-seated salt domes: Oil and Gas Journal, v. 51, no. 13, p. 82-84.
- Dix, O. R., and Jackson, M. P. A., 1981, Statistical analysis of lineaments and their relation to fracturing, faulting, and halokinesis in the East Texas Basin: The University of Texas at Austin, Bureau of Economic Geology Report of Investigations No. 110, 30 p.
- Dreyer, B. V., and Schulz, C. E., 1984, Evaluation, repair, and stabilization of the Boling Sinkhole FM 442, Wharton County, Texas, in Beck, B.F., ed., Sinkholes: their geology,

engineering and environmental impact: Proceedings, First Multidisciplinary Conference on Sinkholes, Orlando, Florida.

Ewing, T. E., 1983a, Growth faults and salt tectonics in the Houston diapir province--relative timing and exploration significance: Gulf Coast Association of Geological Societies Transactions, v. 33, p. 83-90.

_____, 1983b, compiler, in preparation, Tectonic map of Texas: The University of Texas at Austin, Bureau of Economic Geology, scale 1:750,000.

Ferguson, W. B., and Minton, J. W., 1936, Clay Creek salt dome, Washington County, Texas: American Association of Petroleum Geologists Bulletin, v. 20, no. 1, p. 68-90.

Fisher, W. L., McGowen, J. H., Brown, L. F., Jr., 1972, Environmental geologic atlas of the Texas Coastal Zone--Galveston-Houston area: The University of Texas at Austin, Bureau of Economic Geology, 91 p.

Fisher, W. L., Brown, L. F., Jr., McGowen, J. H., and Groat, C. G., 1973, Environmental geologic atlas of the Texas Coastal Zone--Beaumont-Port Arthur area: The University of Texas at Austin, Bureau of Economic Geology, 93 p.

Frost, R. T. C., 1977, Tectonic patterns in the Danish region (as deduced from a comparative analysis of magnetic, Landsat, bathymetric and gravity lineaments): Geologie en Mijnbouw, v. 56, no. 4, p. 351-362.

Galloway, W. E., Ewing, T. E., Garrett, C. M., Tyler, N., and Bebout, D. G., 1983, Atlas of major Texas oil reservoirs: The University of Texas at Austin, Bureau of Economic Geology Special Publication, 139 p.

Galloway, W. E., and Hobday, D. K., 1983, Terrigenous clastic depositional systems: applications to petroleum, coal, and uranium exploration: New York, Springer-Verlag, 416 p.

Halbouty, M. T., 1979, Salt domes, Gulf region, United States and Mexico (2d ed.): Houston, Gulf Publishing, 561 p.

- Halbouty, M. T., and Hardin, G. C., Jr., 1956, Genesis of salt domes of Gulf Coastal Plains: American Association of Petroleum Geologists Bulletin, v. 40, no. 4, p. 737-746.
- Horsfield, W. T., 1980, Contemporaneous movement along crossing conjugate normal faults: Journal of Structural Geology, v. 2, no. 3, p. 305-310.
- Hughes, D. J., 1960, Faulting associated with deep-seated salt domes in the northeast portion of the Mississippi salt basin: Gulf Coast Association of Geological Societies Transactions, v. 10, p. 154-173.
- Hurlburt, E. M., 1946, Limestone on Damon Mound, Brazoria County, Texas: University of Texas, Austin, Bureau of Economic Geology Bulletin 4301, p. 265-269.
- Jackson, M. P. A., and Galloway, W. E., 1984, Structural and depositional styles of Gulf Coast Tertiary continental margins: application to hydrocarbon exploration: American Association of Petroleum Geologists, Continuing Education Course Note Series No. 25, 226 p.
- Jackson, M. P. A., and Seni, S. J., 1983, Geometry and evolution of salt structures in a marginal rift basin of the Gulf of Mexico, East Texas: Geology, v. 11, p. 131-135.
- Kennedy, G. C., 1959, The origin of continents, mountain ranges, and ocean basins: American Science, v. 47, p. 491-504.
- Kreitler, C. W., 1976, Lineations and faults in the Texas Coastal Zone: The University of Texas at Austin, Bureau of Economic Geology Report of Investigations No. 85, 32 p.
- Kupfer, D. H., 1963, Structure of salt in Gulf Coast domes, in Bersticker, A. G., ed., First Symposium on Salt, Northern Ohio Geological Society, Cleveland, Ohio, p. 104-123.
- Kupfer, D. H., 1974, Environment and intrusion of Gulf Coast salt and its probable relationship to plate tectonics, in Coogan, A. H., ed., Fourth International Symposium on Salt, Northern Ohio Geological Society, Cleveland, Ohio, p. 197-213.
- Martin, R. G., 1976, Geologic framework of northern and eastern continental margins, Gulf of Mexico, in Bouma, A. H., Moore, G. T., and Coleman, J. M., eds., Beyond the shelf

break: American Association of Petroleum Geologists Marine Geology Committee
Short Course, v. 2.

McGowen, J. H., Brown, L. F., Jr., Evans, T. J., Fisher, W. L., and Groat, C. G., 1976,
Environmental geologic atlas of the Texas Coastal Zone--Bay City-Freeport area:
The University of Texas at Austin, Bureau of Economic Geology, 98 p.

Miller, B. C., 1961, Photogeology: New York, McGraw-Hill, 248 p.

Murray, G. E., 1961, Geology of the Atlantic and Gulf Coastal province of North America:
New York, Harper and Brothers, 692 p.

O'Leary, D. W., Friedman, J. D., and Pohn, H. A., 1976, Lineament, linear, lineation: some
proposed new standards for old terms: Geological Society of America Bulletin, v. 87,
no. 10, p. 1463-1469.

Reid, W. M., 1973, Active faults in Houston, Texas: The University of Texas at Austin,
Ph.D. dissertation, 122 p.

Salvador, A., and Buffler, R. T., 1983, The Gulf of Mexico Basin, in Palmer, A. R., ed.,
Perspectives in regional geological synthesis: Geological Society of America, DNAG
Special Publication 1, p. 157-162.

Seni, S. J., Mullican, W. F., III, and Hamlin, H. S., 1984a, Texas salt domes--aspects
affecting disposal of toxic-chemical waste in solution-mined caverns: The University
of Texas at Austin, Bureau of Economic Geology, report prepared for the Texas
Department of Water Resources under interagency contract no. IAC(84-85)-1019,
94 p.

Seni, S. J., Mullican, W. F., III, and Hamlin, H. S., 1984b, Natural resources, storage
caverns, and extraction technology: The University of Texas at Austin, Bureau of
Economic Geology, report prepared for the Texas Department of Water Resources
under interagency contract no. IAC (84-85)-1019, 161 p.

Siegel, S., 1956, Nonparametric statistics for the behavioral sciences: New York, McGraw-
Hill, 312 p.

- Vistelius, A. B., 1966, Structural diagrams: New York, Pergamon Press, 178 p.
- Weaver, P., and Sheets, M. M., 1962, Active faults, subsidence, and foundation problems in the Houston, Texas area, in Rainwater, E. H., and Zingula, R. P., eds., Geology of the Gulf Coast and Central Texas and guidebook of excursions: Houston Geological Society Field Excursion Guidebook, p. 254-265.
- Wermund, E. G., Cepeda, J. C., and Luttrell, P. E., 1978, Regional distribution of fractures in the southern Edwards Plateau and their relationship to tectonics and caves: The University of Texas at Austin, Bureau of Economic Geology Geological Circular 78-2, 14 p.
- Williams, J. D., 1980, Rosenet: a Fortran IV program for production of Rose Diagrams compatible with Gould or Calcomp plotting facilities: Computers and Geosciences, v. 6, p. 95-103.
- Winker, C. D., Morton, R. A., Ewing, T. E., and Garcia, D. D., 1983, Depositional setting, structural style, and sandstone distribution in three geopressured geothermal areas, Texas Gulf Coast: The University of Texas at Austin, Bureau of Economic Geology Report of Investigations No. 134, 60 p.
- Winker, C. D., and Edwards, M. B., 1983, Unstable progradational elastic shelf margins: Society of Economic Paleontologists and Mineralogists, Special Publication No. 33, p. 139-157.
- Withjack, M. O., and Scheiner, C., 1982, Fault patterns associated with domes--an experimental and analytical study: American Association of Petroleum Geologists Bulletin, v. 66, no. 3, p. 302-316.

PETROGRAPHY AND STRUCTURE OF CAP ROCK
WITH EMPHASIS ON CORE FROM BOLING SALT DOME, TEXAS

by
S. J. Seni

CONTENTS

INTRODUCTION. 118

 Summary of Major Findings. 121

 Significance of Findings. 123

CAP-ROCK FACIES. 123

 Facies Relationships. 125

 Calcite Cap Rock 136

 Normal Calcite Cap Rock 136

 Proto-Cap Rock 140

 Proto-Cap-Rock - True Cap-Rock Contact 142

 Anhydrite Cap Rock. 146

 Discussion 148

CAP-ROCK STRUCTURE 153

 Methodology 153

 Calcite Cap Rock 158

 Anhydrite Cap Rock. 162

 Mechanisms 162

POROSITY, PERMEABILITY, AND FLUID TRANSPORT 163

 Fluid Transport 167

REFERENCES 169

APPENDIX. List of Wells 172

Figures

1. Location map, Boling Dome. 119

2. Location map of domes, fence diagrams, and cross sections 120

3. Cross section, Boling Dome	122
4. Lithologic logs from domes in Texas	124
5. Cross section, Moss Bluff Dome	126
6. Cross sections, Hoskins Mound Dome	127
7. Cross sections and fence diagram, Stratton Ridge Dome	128
8. Cross section, Sugarland Dome	129
9. Cross section, cap-rock facies, Boling Dome	131
10. Fence diagram (A) and cross sections A-A' (B) and B-B' (C), Boling Dome . . .	132-134
11. Photograph of anhydrite cap-rock - salt-stock contact	135
12. Photograph of typical true calcite cap rock, Boling Dome	137
13. Photograph of light and dark parallel-banded calcite cap rock, Boling Dome. . .	138
14. Photomicrograph of calcite pseudospar, Boling Dome	139
15. Photograph of calcite proto-cap rock, Boling Dome	141
16. Photomicrograph of proto-cap rock, Boling Dome	143
17. Photograph of true calcite - proto-cap-rock contact	144
18. Photomicrograph of true calcite - proto-cap-rock contact	145
19. Photograph of anhydrite cap rock, Boling Dome	147
20. Photomicrograph of anhydrite cap rock, Boling Dome	149
21. Schematic diagram of cap-rock evolution, Boling Dome	151
22. Photograph of calcite cap-rock fault, Boling Dome	157
23. Cross section, Boling Dome	159
24. Photograph of small sulfur veins in calcite cap rock, Boling Dome	160
25. Orientation of veins, faults, and bedding, Boling Dome	161
26. Photograph of collapse sink, FM442, Boling Dome	166
27. Geothermal gradient, Boling Dome	168

Tables

1. Vein orientations in calcite and anhydrite cap rock 154

2. Whole core and core plug permeability analyses 165

INTRODUCTION

Boling Dome is in Wharton and Fort Bend Counties on the western margin of the Houston diapir province (figs. 1 and 2). Boling Dome hosts the only Frasch sulfur operation from domal cap rock currently active in Texas. This dome is also the proposed site for a toxic waste disposal facility utilizing solution-mined caverns in salt (United Resource Recovery, Inc., 1983). Cores from approximately 100 closely spaced sulfur production holes (fig. 1) loaned by Texasgulf Sulfur, Inc. form the basis for this study. Cap-rock facies and mineralogy were also studied for 10 other domes in Texas, including Allen, Barbers Hill, Big Hill, Damon Mound, Gyp Hill, Hockley, Hoskins Mound, Hull, Oakwood, and Stratton Ridge (fig. 2). This petrologic study is a small part of a project commissioned by the Texas Department of Water Resources to examine the technical merits of toxic waste disposal in solution-mined caverns. During the course of the study it became quickly apparent that cap rocks were a dynamic component of salt domes and that a complex range of chemical and physical processes associated with cap rock could affect the suitability of salt domes for toxic waste disposal. Indicators that such processes are probably ongoing include occurrence of oil in fractures within cap rock, sulfate-rich mineralizing water, and high temperature anomalies around domes, but proof of present activity is difficult to document unequivocally.

This study of cap-rock core from Boling Dome was designed (1) to determine the stratigraphy and facies of cap rock by microscopic examination of core slabs, petrographic analysis of thin sections, SEM analysis, and geochemical analysis, (2) to determine the structure of cap rock by analysis of the orientations of veins, bedding, joints, vugs, and faults in core slabs, (3) to compare these findings with those from other cap rocks, and (4) to integrate these findings with the overall assessment of the suitability of domes in general and Boling Dome in particular for toxic waste disposal.

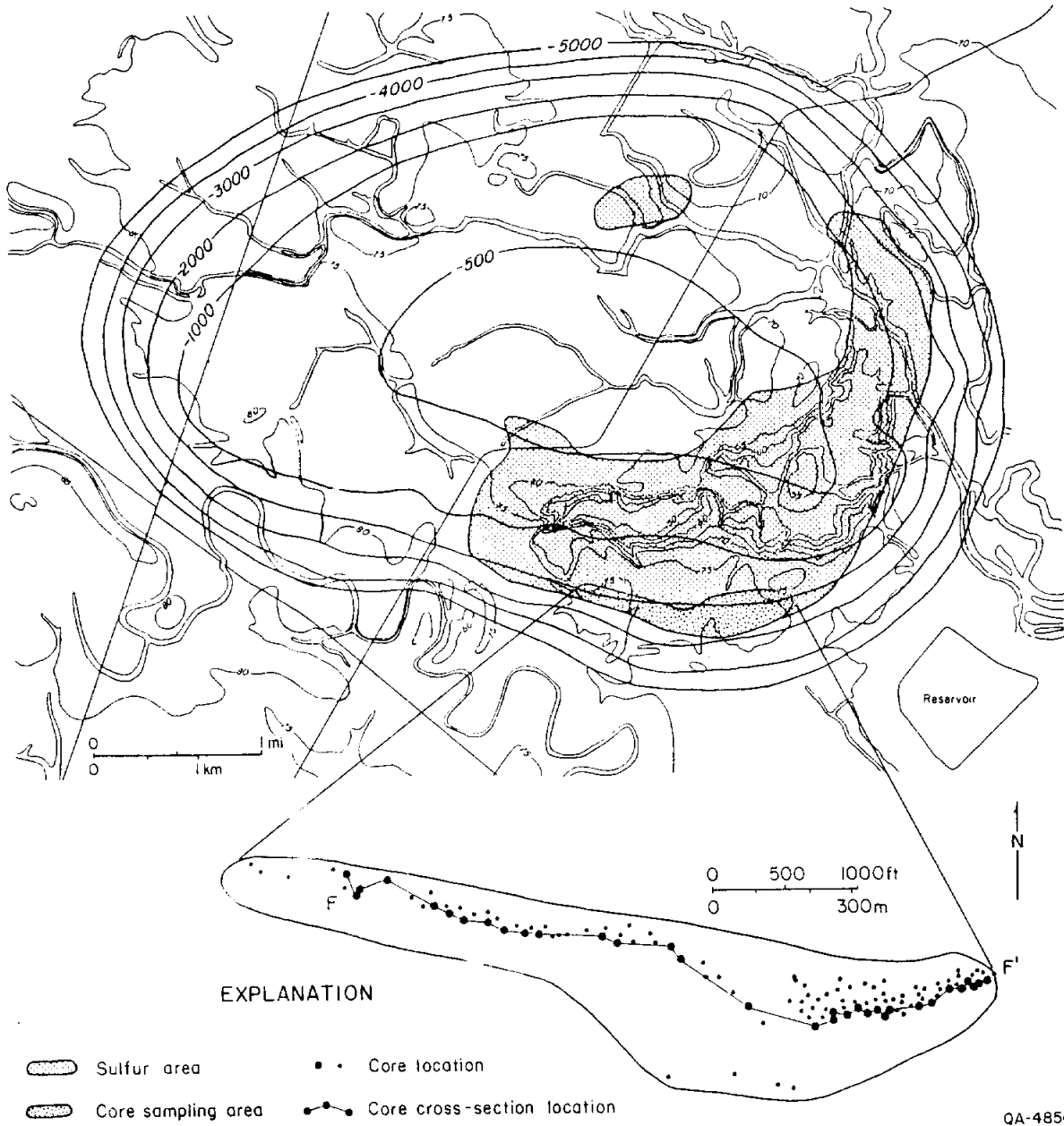
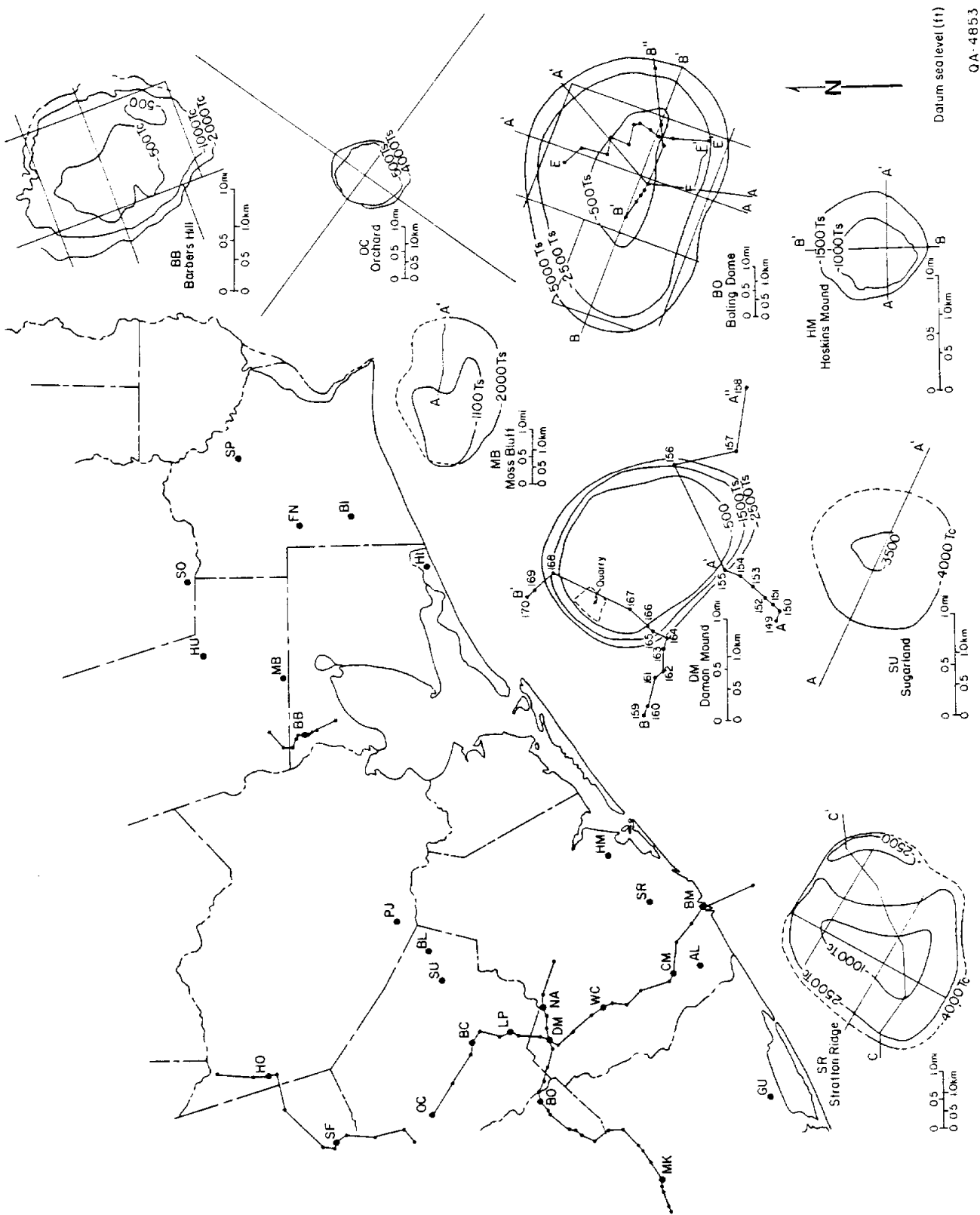


Figure 1. Location map of cores, cross section F-F', and area of sulfur production in relation to salt structure contours of Boling Dome.

QA-4854



QA-4853

Figure 2. Location map of domes, fence diagrams, and cross sections described in this report.

Cores from Boling Dome that were examined for this study came from the area of active sulfur mining. More than 20,000 core holes have been drilled for production of sulfur by the Frasch method (F. Samuelson, Texasgulf Inc., personal communication, 1985). The cores used in this study are in a relatively narrow band oriented along the strike of dome structure on the southern dome flank (fig. 1). The cores are located along a transect from the dome "shoulder," characterized by a break in slope from the much steeper dip of the deep salt flank to the nearly horizontal dome crest (fig. 3).

Summary of Major Findings

Major findings of this study are: (1) veins and faults within the cap rock are extension fractures that opened as a result of shear between the salt stock and surrounding country rock; (2) the dip orientation of veins, faults, and bedding within the cap rock is induced by the 45° dip of the country-rock - cap-rock - salt-stock interface; (3) the density of veins and faults is similar between the anhydrite and calcite sections; (4) as a result of migration of hot waters injected during sulfur mining, the sediments surrounding the cap rock are anomalously hot; (5) many episodes of calcite precipitation, dissolution, brecciation, and reprecipitation are indicated by resedimented breccias, vugs, and multiple closed and open vein fillings; (6) much of the cap rock of Boling Dome in the area studied incorporates previously deposited terrigenous clastics; (7) terrigenous clastics occur in both the calcite and anhydrite sections of the cap rock; (8) if the anhydrite in cap rock is the accumulated residuum from salt dissolution, as most researchers agree, then terrigenous clastics present within the anhydrite section must have been incorporated by the salt stock, probably by shearing during dome growth; (9) terrigenous clastics within the calcite section are being replaced by calcite; (10) calcite microspar replaces the clayey matrix of the terrigenous sandstones and possibly the more resistant coarse-fraction detritus as well; (11) intergradations of calcitic terrigenous clastics and "normal" true calcite cap rock indicate that much of the calcite in the true calcite cap rock replaced previously deposited

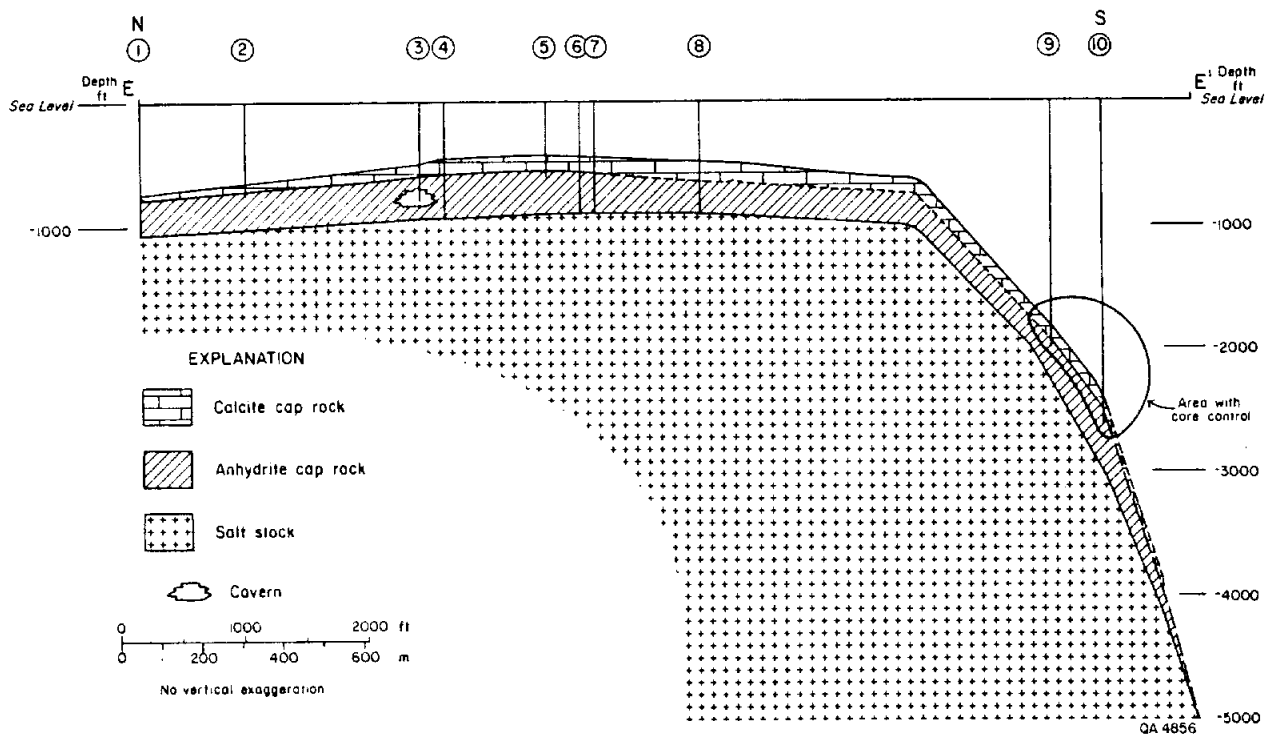


Figure 3. Cap-rock cross section E-E', Boling Dome. Dip-oriented section is from crestal area to deep flank. Data in part supplied by Texasgulf Sulfur, Inc.

terrigenous clastics; (12) some terrigenous clastics within the calcite section were originally deposited over the crest of the cap rock and were incorporated within the cap rock through calcite replacement and neomorphism.

Significance of Findings

These findings support the conclusion that the cap rock is a dynamic component of the salt dome, especially at Boling Dome. The abundance of vugs, caverns, open veins, mineralized veins and faults, faults with oil within the cap rock, and temperature anomalies in sediments surrounding the cap rock as a result of sulfur mining, all indicate that the cap rock at Boling Dome is not a barrier to fluid migration. The approximately 45° slope of the cap-rock - salt-stock interface exerted a powerful influence on the structure within the cap rock and hence on sulfur mineralization and facies distribution. Additionally, the presence of terrigenous clastics within the cap rock indicates that the salt stock, especially around the margin of the dome, may include large blocks of sediment incorporated during dome growth. If a waste repository were to be designed at Boling Dome, much engineering effort would be required to completely isolate the cap rock and to assure site-specific structural integrity.

CAP-ROCK FACIES

Cap rocks overlie the crest of shallow salt domes and drape the upper flanks (Murray, 1966). Cap rocks are lithologically diverse, commonly composed of an upper calcite zone, a central transitional zone of calcite, gypsum, sulfur, and anhydrite, and a basal zone of anhydrite (Goldman, 1925, 1933; Taylor, 1938; Martinez, 1980). The range of lithologic variability is shown for cap rocks from 10 Texas domes in figure 4. Although a single well or core can give valuable information about the lithology of the cap rock for that one hole (for example, Kreitler and Dutton, 1983), the more holes one has access to, the more

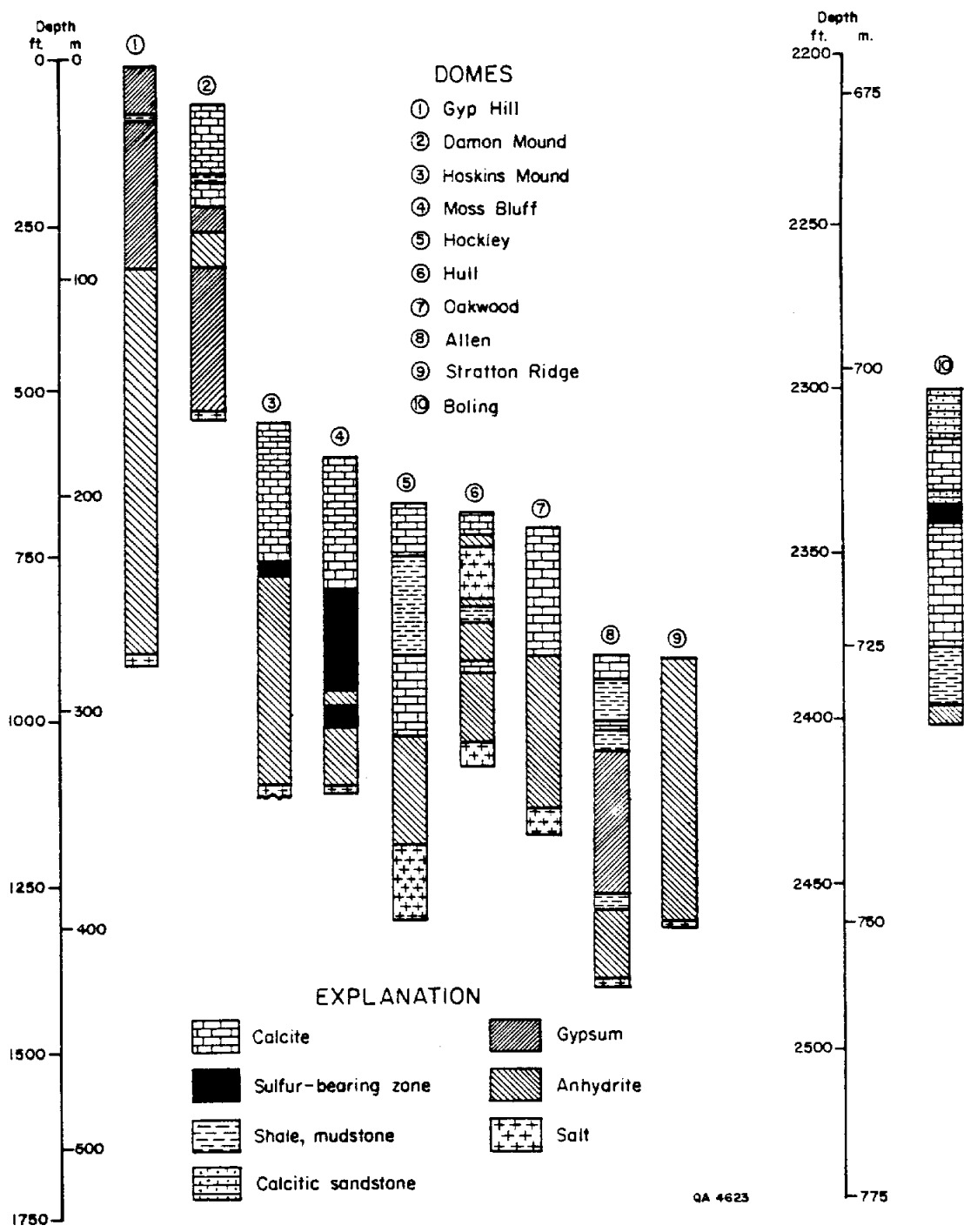


Figure 4. Lithologic logs from domes in Texas; 1. Gyp Hill Dome—Joy Manufacturing (Kreitler and Dutton, 1983); 2. Damon Mound Dome—Texas Exploration #R-246; 3. Hoskins Mound Dome—Freeport Sulfur Co. #29 (Marx, 1936); 4. Moss Bluff Dome—Texasgulf Sulfur Inc., Sergeant #9 (Railroad Commission of Texas Hearings Files Docket # 3-72,099); 5. Hockley Dome—Freeport Sulfur Co. #6 (Walker, 1974); 6. Hull Dome—Freeport Sulfur Co. #4 (Walker, 1974); 7. Oakwood Dome—Law Engineering Testing Co. LETCO TOG #1 (Kreitler and Dutton, 1983); 8. Allen Dome—Freeport Sulfur Co. #14 (Walker, 1974); 9. Stratton Ridge Dome—Tolar Well #1; 10. Boling Dome—Texasgulf Sulfur Inc., Abendroth #602.

complex the cap rock appears (Walker, 1974). The following section describes the vertical and lateral relationships of facies or zones within the cap rock.

Facies Relationships

A detailed cross section of cap rock at Moss Bluff Dome (fig. 5) illustrates some of the facies variability and helps us to understand the genesis of cap rock at the dome. The calcite cap rock thins toward the center of the dome and thickens to a maximum over the dome shoulder. Thickness of anhydrite is relatively constant over the dome crest, but anhydrite thins dramatically in a narrow band around the shoulder. The sulfur-bearing zone extends in a broad band from the area where the anhydrite is thin to the cap-rock center. The distribution of these cap-rock facies indicates that the zone of the most intense anhydrite alteration to calcite was on the dome shoulder. Distribution of sulfur between this anhydrite minimum zone and the center of the cap rock indicates that fluids penetrated from the area of maximum anhydrite alteration toward the interior of the dome. The hummocky upper contact of the calcite zone does not mimic the more regular upper surface of the anhydrite zone. It is likely that some of the sediments over the dome were replaced by calcite. The cap-rock shoulder may represent a mixing zone where hot, deep, basinal fluids discharge up the diapir flanks and react with cool, meteoric waters recharging over the dome crest (Price and others, 1983). The zone of mixing probably migrated back and forth across the margin of the cap rock in response to variations in recharge and discharge, thus producing the very complex diagenesis associated with cap rocks, especially at the shoulder of the salt stock. For purposes of comparison, cross sections of cap rocks from Hoskins Mound, Stratton Ridge, and Sugarland Domes are shown in figures 6, 7, and 8.

Cap-rock facies relationships present at Boling Dome are similar to the generalized model and to Moss Bluff Dome, but with additional complexities that stem from having so much core data from a relatively restricted area of the dome. Many of these cores

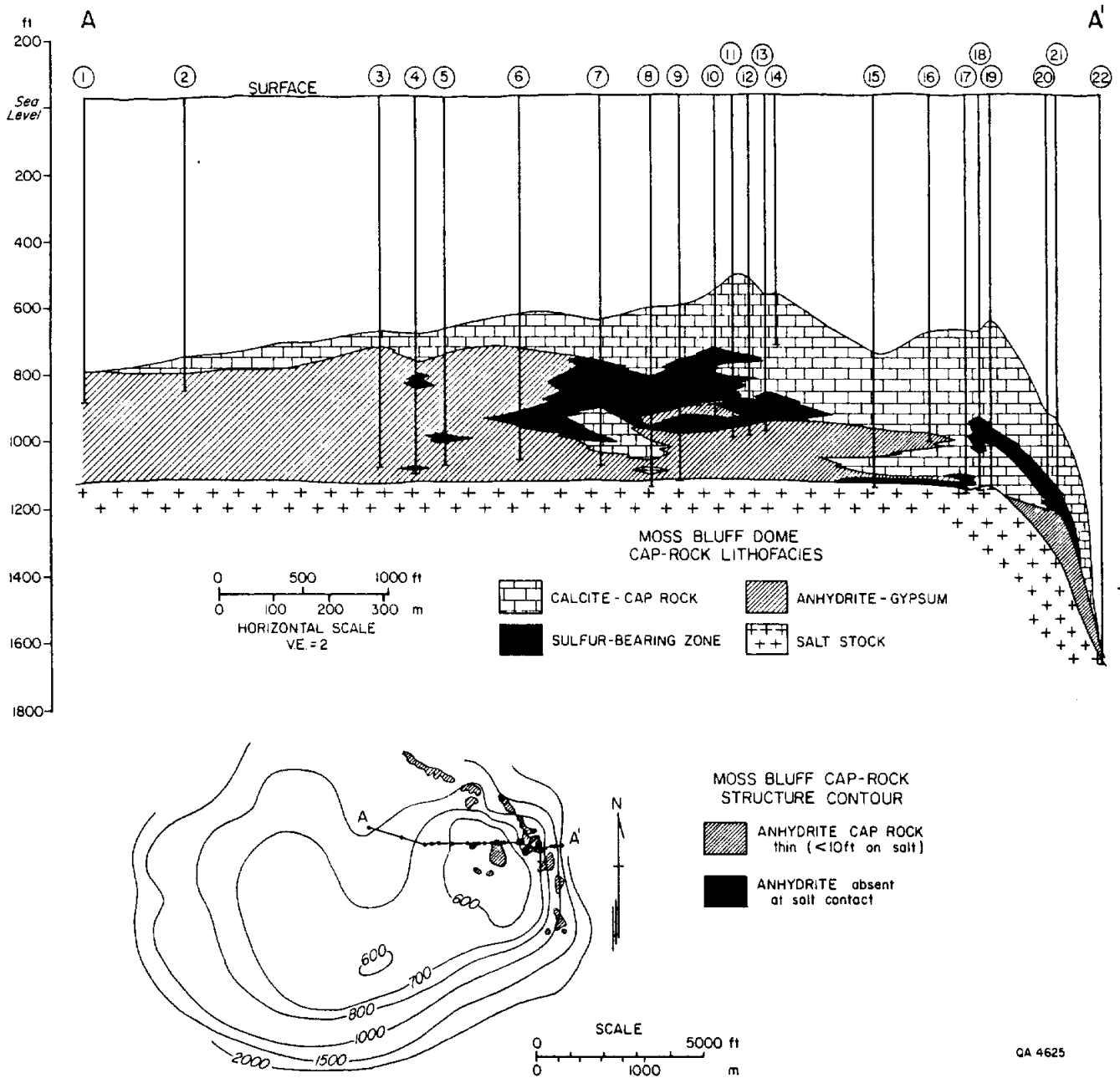


Figure 5. Cross section cap-rock facies, Moss Bluff Dome. Dip-oriented section shows interrelations of various cap-rock facies. Contact between salt stock and cap rock is strikingly horizontal and planar. Data synthesized and modified from Railroad Commission of Texas Hearing Files Docket # 3-72,099.

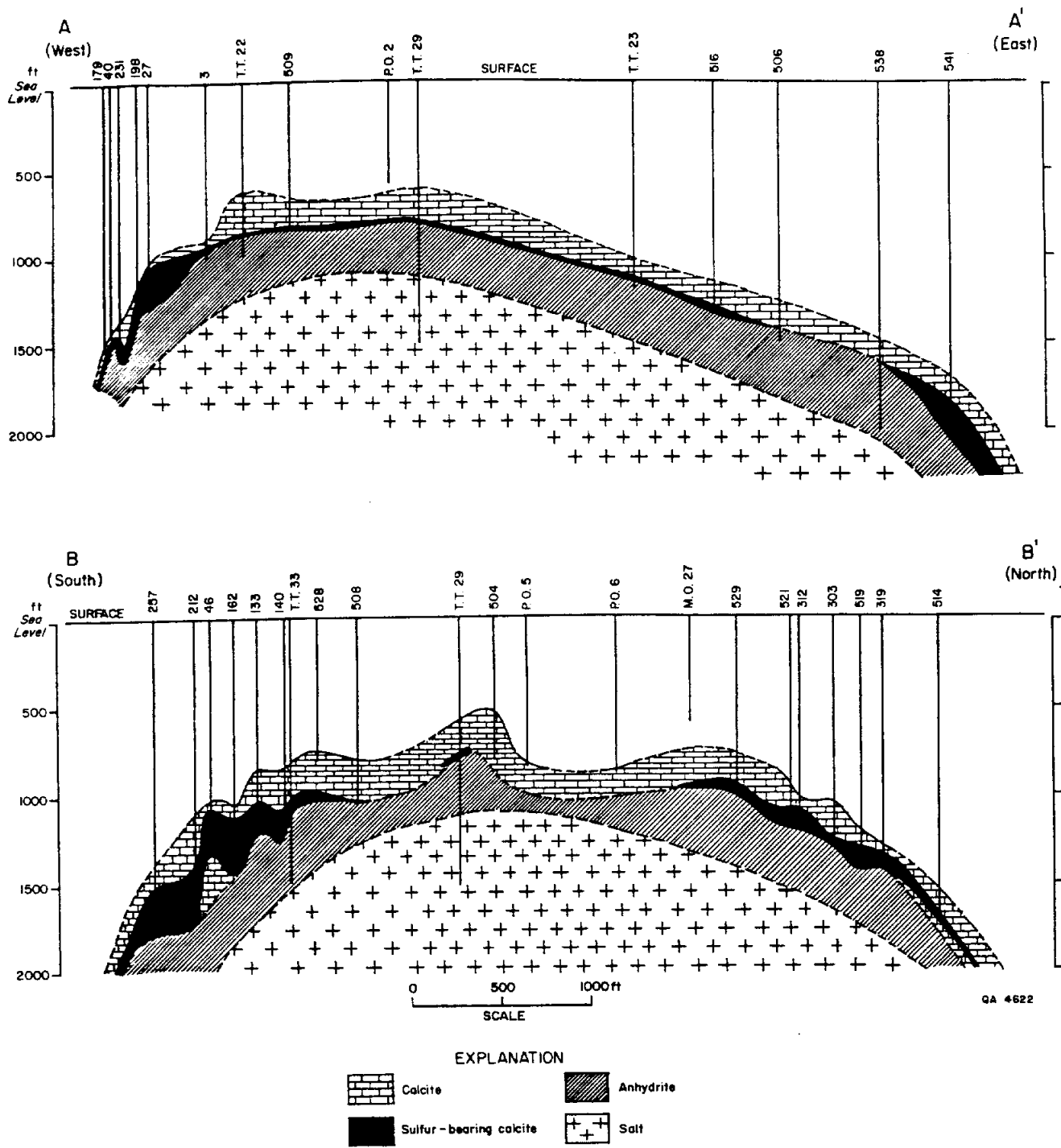
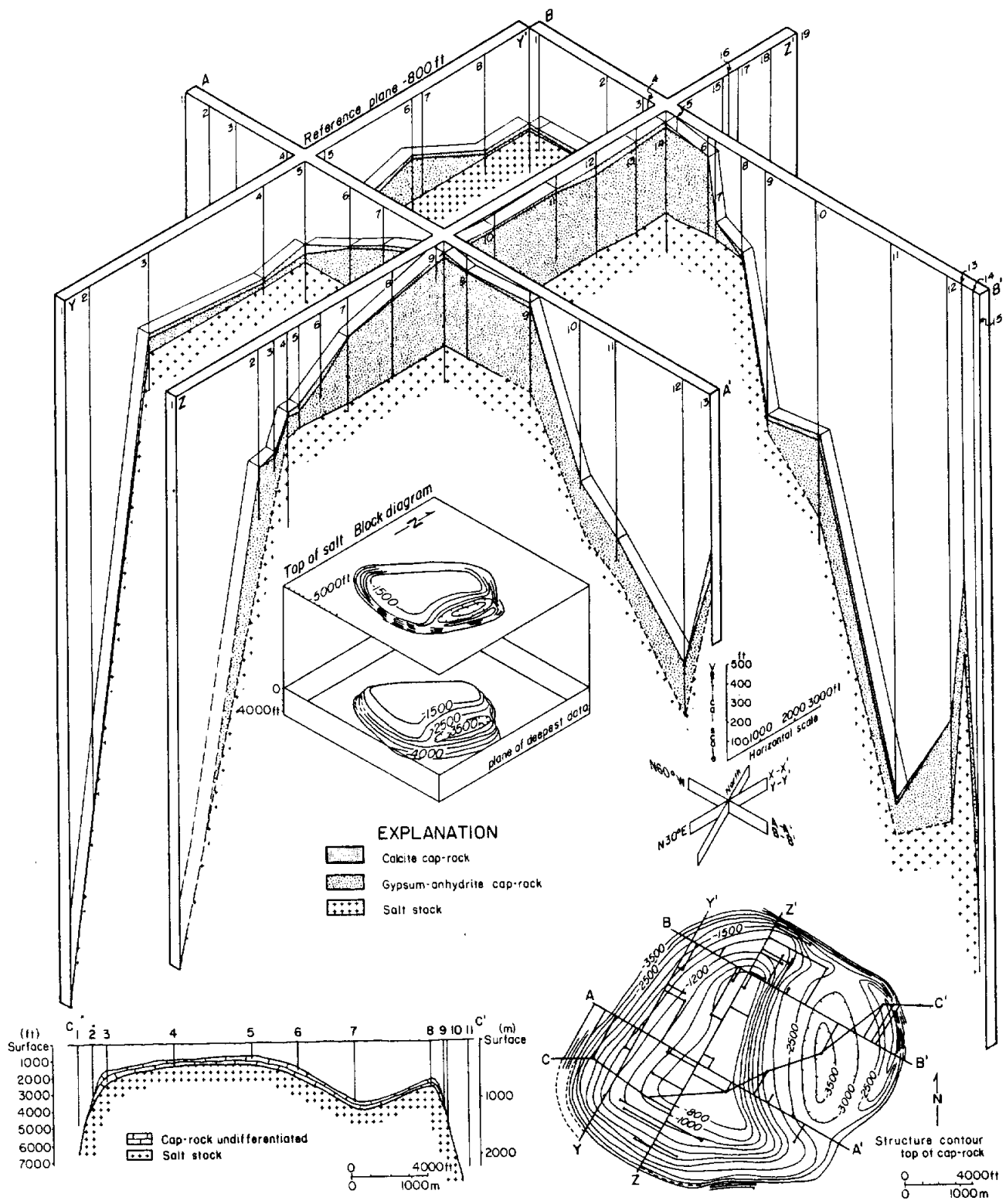


Figure 6. Cross section cap-rock facies, Hoskins Mound Dome. Note arched contact between salt stock and cap rock. Marx (1936) described abundant terrigenous clastics within the cap rock at Hoskins Mound. After Marx (1936).



QA-4631

Figure 7. Cross section and fence diagram cap-rock facies, Stratton Ridge Dome. Three-dimensional block diagram illustrates complex structure of contact between salt stock and cap rock. Nature and origin of structural depression is not known.

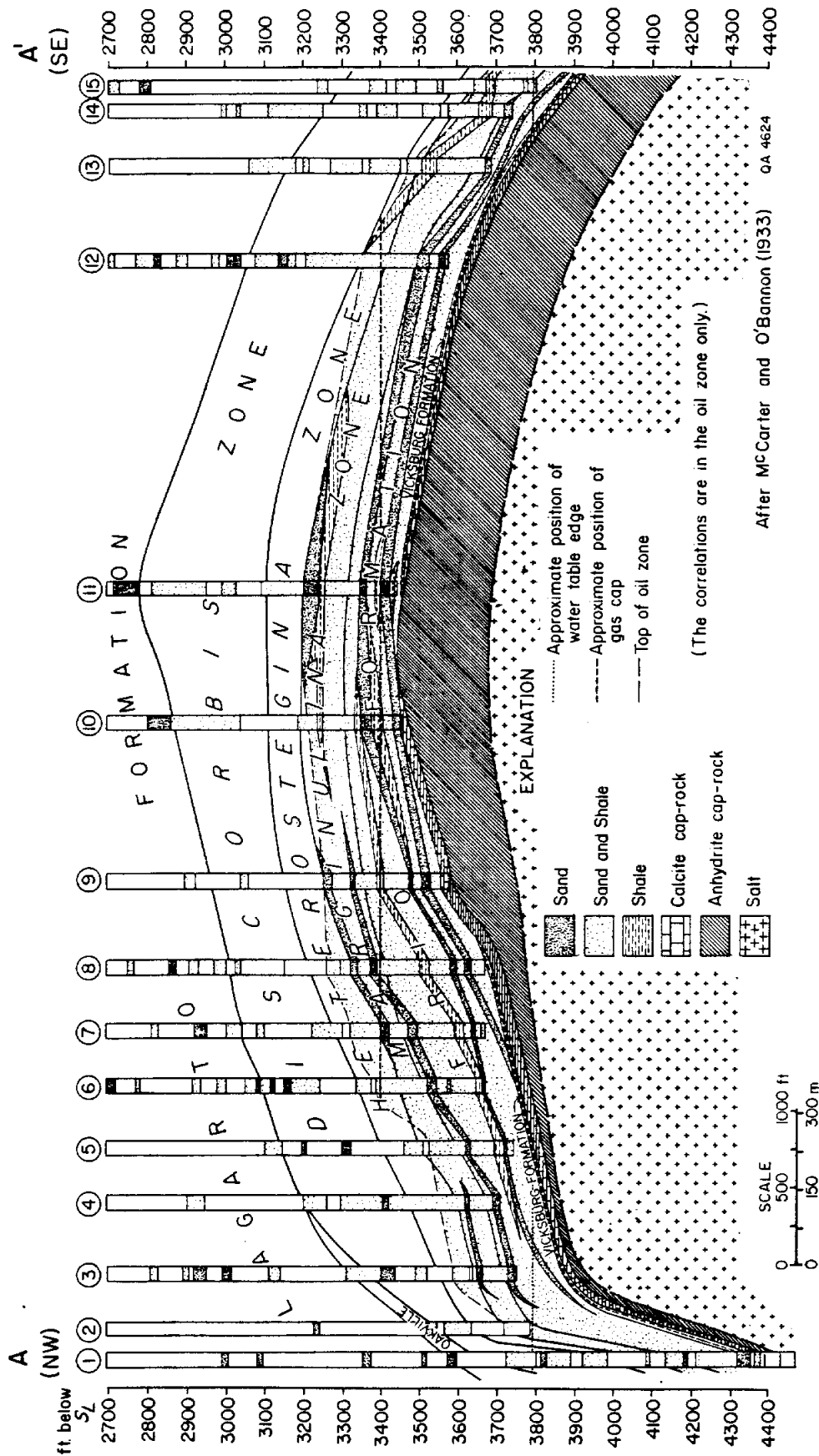


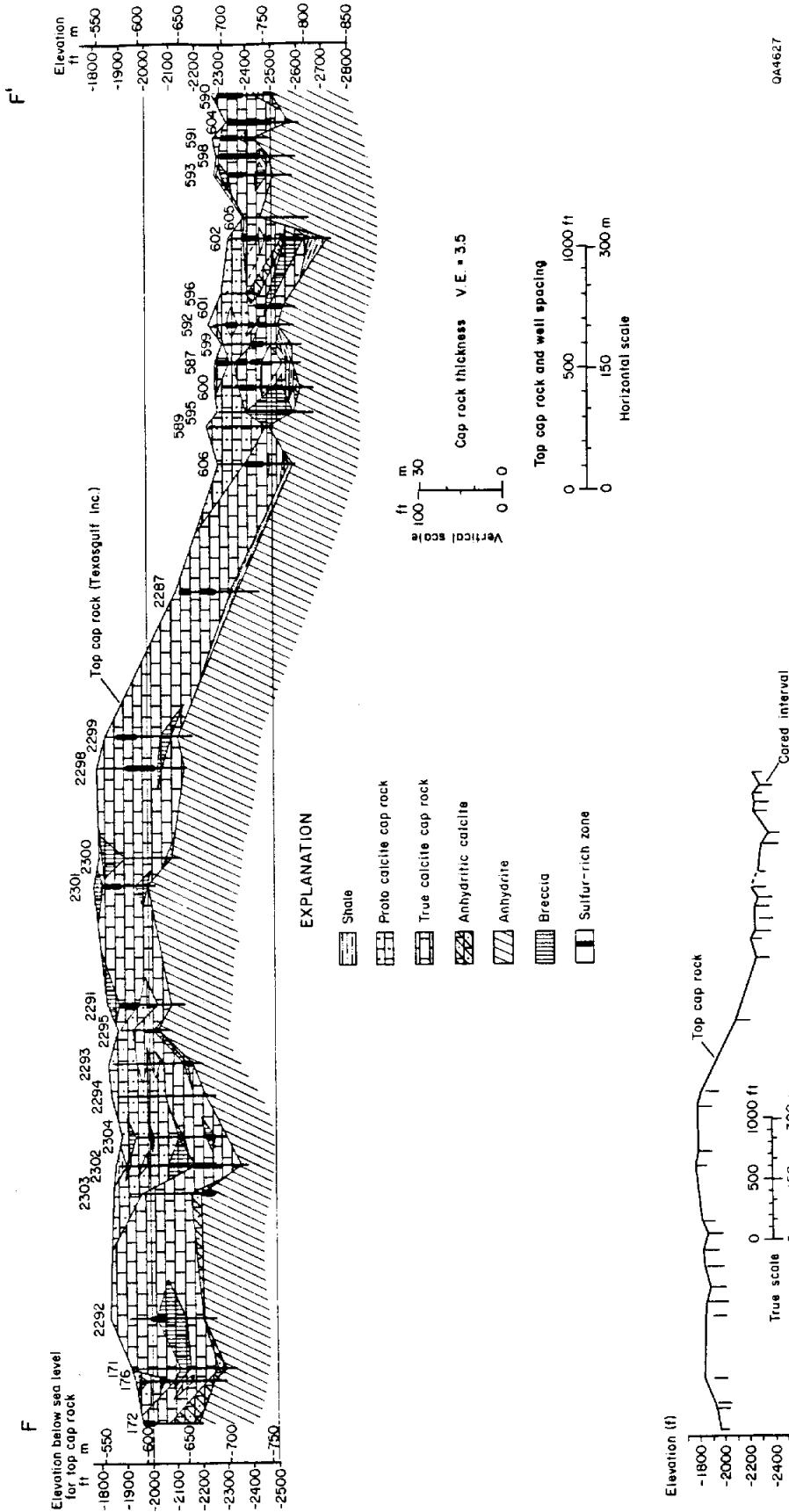
Figure 8. Cross section cap-rock facies and over dome strata, Sugarland Dome. Stratal thinning indicates growth of dome during deposition of Oligocene and Miocene units. Calcite cap rock thins over the crest of dome, but thinning is probably controlled by diagenetic reactions and not erosion. Crest of dome is much deeper than domes in Figures 5, 6, and 7. After McCarter and Bannon (1933).

completely penetrate the calcite facies, but on average only penetrate the upper 15 ft (4.6 m) of the anhydrite facies. A cross section of 33 wells spaced 168 ft (51 m) apart on average illustrates facies variations along a 6,000-ft (1,830-m) arc of the southern flank of the dome (fig. 9).

Figure 10a is a fence diagram that gives a broad perspective of the cap-rock and supradomal strata at Boling Dome. Sand-rich units pinch out over the crest of the dome (figs. 10b,c) where a 100- to 200-ft- (30- to 60-m-) thick mud-dominated unit directly overlies the cap rock. This relatively low-permeability unit has aided trapping of hydrocarbons and may have influenced the preservation of abundant sulfur resources.

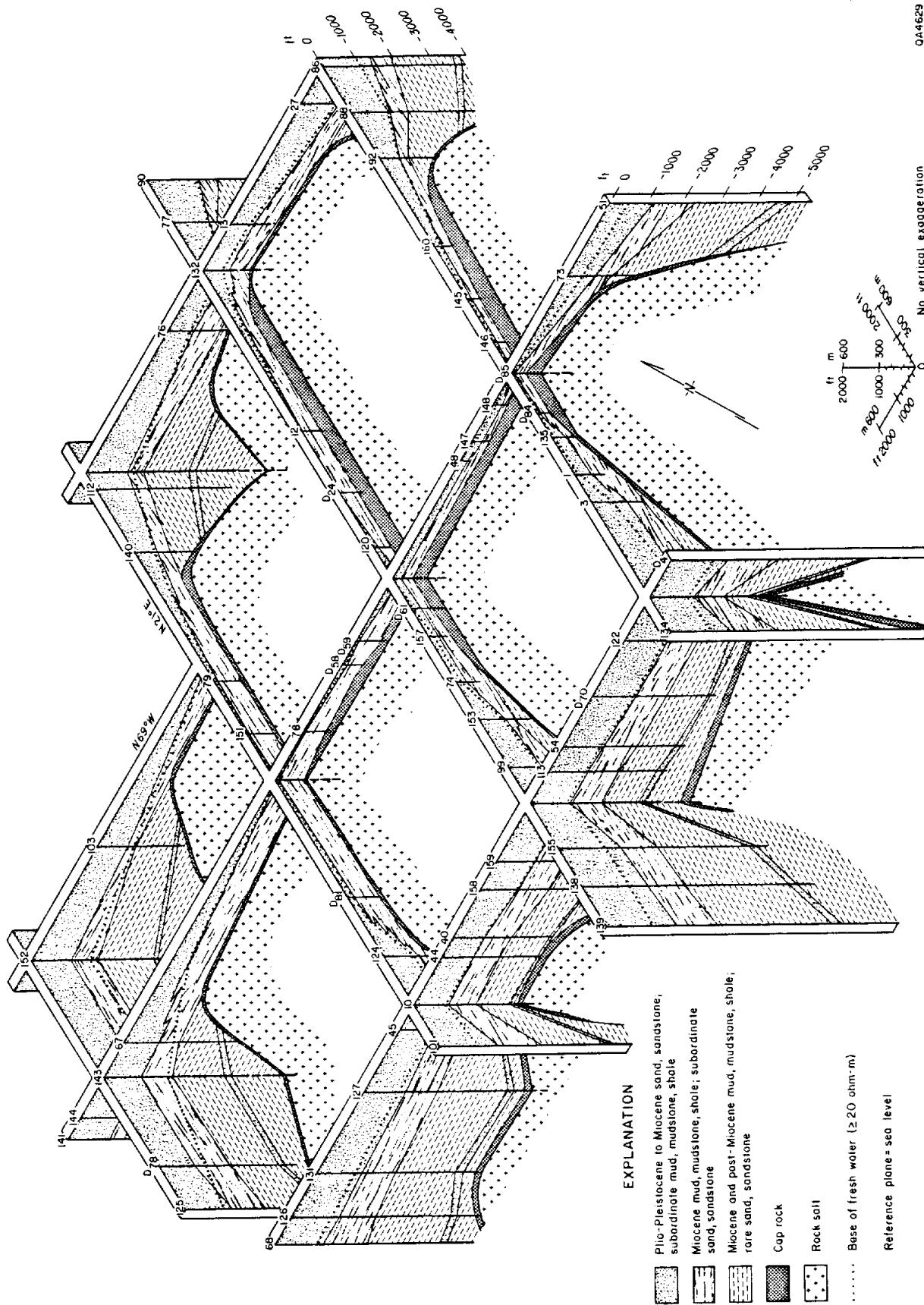
Correlatable lithologic facies within the cap rock at Boling Dome include (1) calcitic quartz sandstone, (2) calcitic shale, (3) calcite, and (4) anhydrite. Sulfur may be present in any facies but is most abundant in the calcite facies. Brecciation is also common. The calcite facies is commonly most brecciated and the anhydrite facies least brecciated. In terms of distribution, the calcitic quartz sandstone facies occurs near the top and interfingers with the pure calcite facies. Calcitic shale is common within the upper part of the anhydrite facies and immediately above the anhydrite. Over much of the dome the contact between anhydrite and the salt stock (fig. 11) is sharp and tight (F. Samuelson, personal communication, 1985).

The zones of calcitic sandstone are up to 100 ft (30 m) thick and extend over 1,000 ft (300 m) along strike as discrete pods within the cap rock. They are part of the cap rock proper. These zones are here termed "proto-cap rock" to distinguish them from false cap rocks, which are not properly part of the cap rock but are calcite-cemented units surrounding the dome or cap rock. Proto-cap rock may evolve with additional diagenesis and replacement by calcite to true calcite cap rock. Proto-cap rock interfingers with pure true calcite cap rock. However, the distribution of proto-cap rock in a dip sense is unknown. Sulfur is abundant throughout the pure calcite zone but less common in the proto-cap rock.



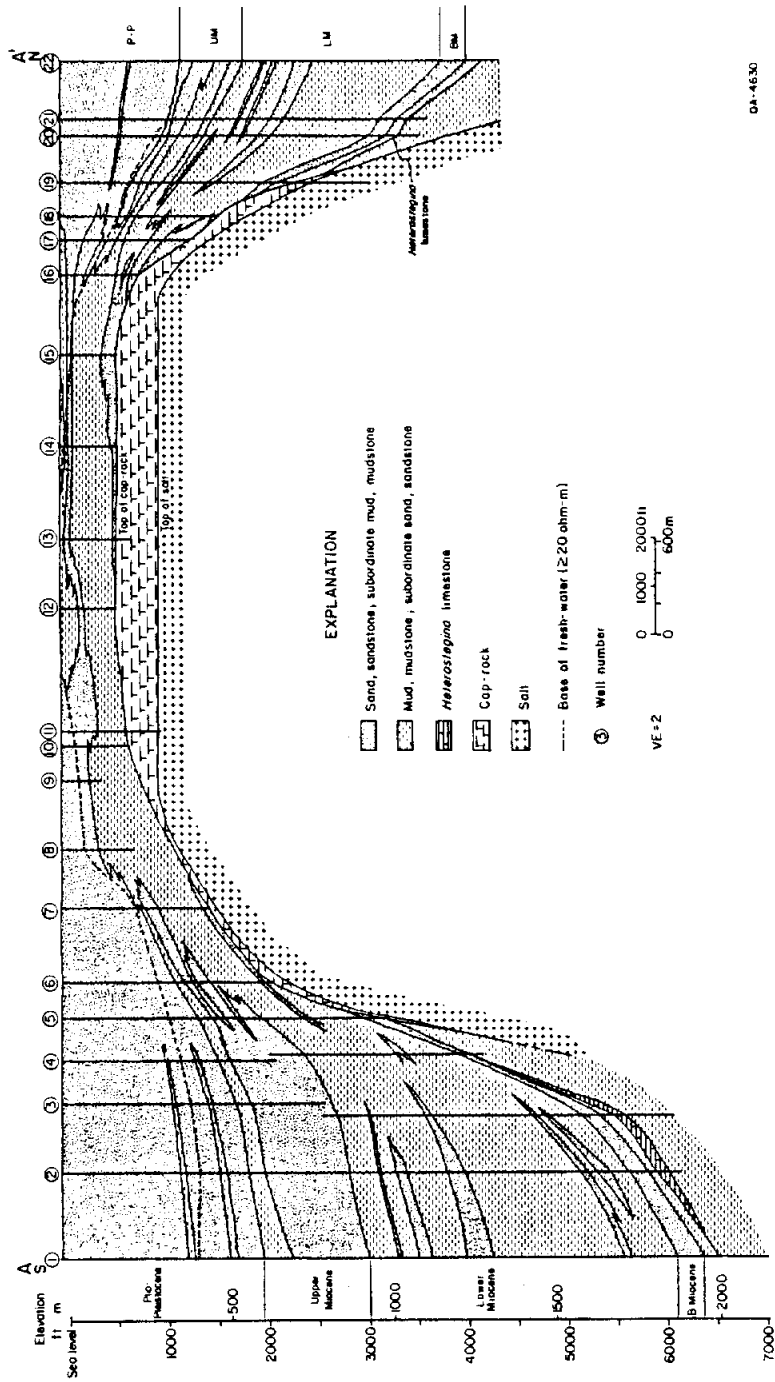
0A4627

Figure 9. Cross section cap-rock facies, Boling Dome. Cross section based on binocular and petrographic examination of core. Terrigenous clastics comprise 25-33% of calcite facies. Shaly terrigenous clastics also occur at contact between calcite and anhydrite cap rocks and within anhydrite cap rock.



044629

Figure 10. Fence diagram (A) and cross sections A-A' (B) and B-B' (C) of cap rock and over dome strata, Boiling Dome. Over dome strata are predominately mud or mudstone. Most Miocene sand units pinch out at the shoulder of the dome.



DA-4630

Figure 10.(B)

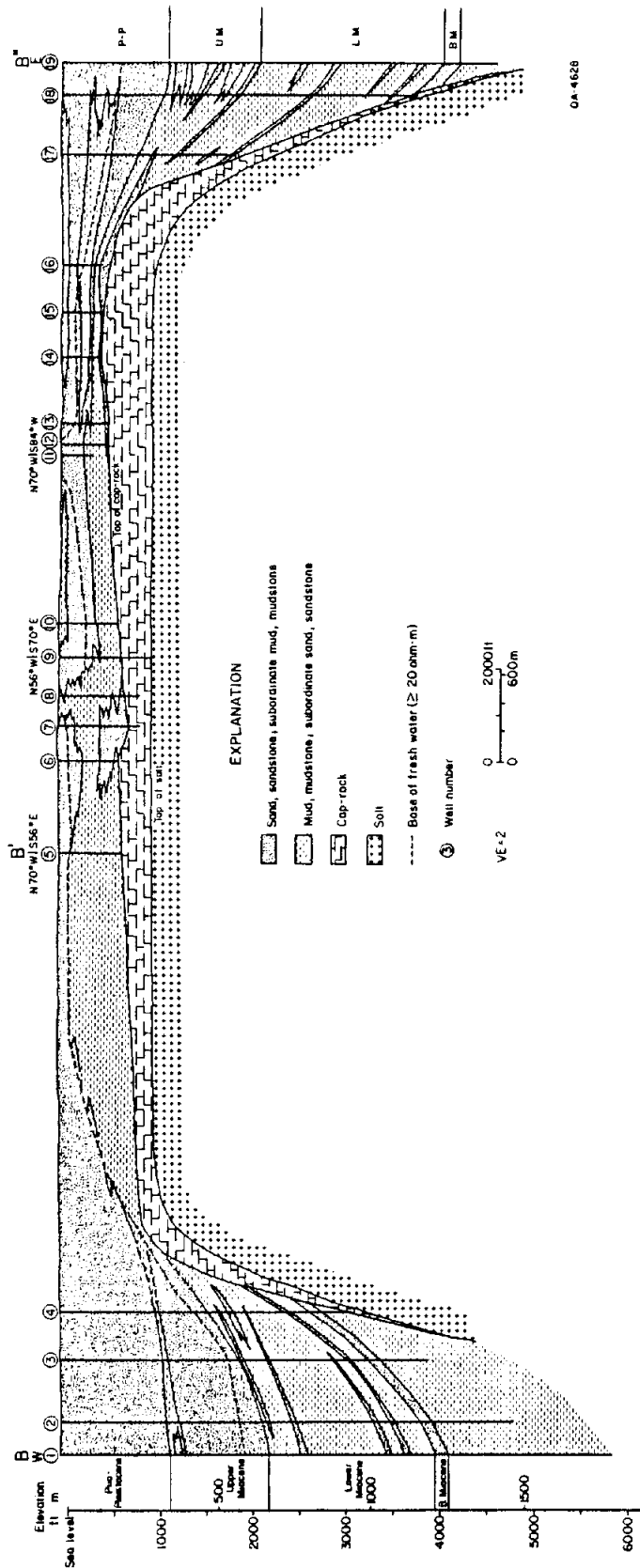


Figure 10. (C)



Figure 11. Photograph of contact between anhydrite cap rock and salt stock, Boling Dome.

The transitional zone at Boling is poorly developed. The contact between the calcite and the anhydrite is commonly sharp over a distance of millimeters to decimeters. There is very little gypsum to mark the transition from calcite to anhydrite. Incorporated shale occasionally marks the contact between the calcite and anhydrite zones.

The following discussion of cap-rock facies will concentrate on the "normal" or "true" calcite cap rock and on the anhydrite facies.

Calcite Cap Rock

The calcite section at Boling Dome includes the traditional dark and light true calcite cap rock (fig. 12). The alternating dark and light banding of calcite that is so characteristic of some other cap rocks, for example at Oakwood Dome (Kreitler and Dutton, 1983), is rare at Boling except near the base of the calcite section (fig. 13). In addition, the upper calcite cap rock contains zones of incorporated terrigenous clastics (proto-cap rock), abundant veins of calcite spar and sulfur, brecciated zones of resedimented calcite, and void spaces ranging in size from 0.1-mm intergranular pores to caverns of unknown dimensions. On the average there are 0.7 veins and faults/ft (2.2 veins and faults/m) of core in the calcite cap rock. Any void space whose dimension approaches the size of the core (5 inches) will not be recovered in its original condition. The percentage recovery of the calcite section was about 50 percent, the lowest of any cap-rock facies at Boling Dome.

Normal Calcite Cap Rock

The normal calcite cap rock at Boling Dome is a light to dark-gray, fine to medium calcite. Most of the calcite is termed pseudospar (Folk, 1965). Calcite grain size may commonly be quite uniform (0.05 to 0.2 mm) (fig. 14). Crystal shape varies from anhedral to rhombic. The centers of the larger calcite grains (0.1 to 0.2 mm) often have internal ghosts at the center of the crystal, suggesting the calcite replaced some precursor mineral.



Figure 12. Photograph of typical true calcite cap rock, Boling Dome. Pseudospar calcite is dark. Light veins are calcite spar. Note that the dip angle of the spar vein is near vertical. Texasgulf Sulfur Inc., Well #2311, depth 2074 ft (cm scale).



Figure 13. Photograph of light and dark parallel-banded calcite near base of Dome. Texasgulf Sulfur Inc., Well #2314, depth 2147 ft (cm scale).

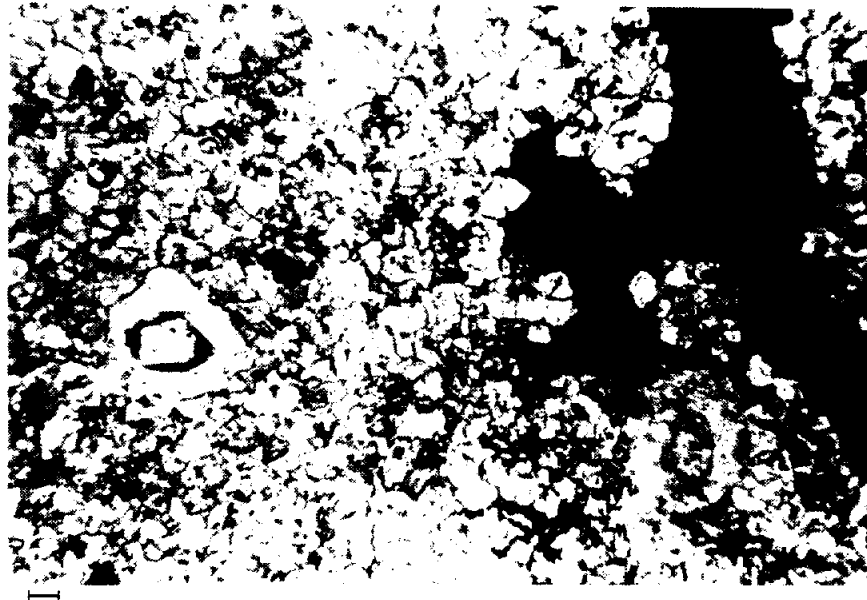


Figure 14. Photomicrograph of calcite pseudospar in true calcite cap rock. Note that calcite crystals are anhedral and subequal in size 0.2–0.3 mm. Larger porphyroblasts of calcite (center left and below dark sulfur) are 1.0–2.0 mm with central area surrounded by dark halo suggesting central area was replaced by calcite or possible neomorphism of original finer grained calcite. Large dark area to right is sulfur crystal. Texasgulf Sulfur Inc., Well #2294, depth 1974 ft (0.1 mm scale).

A dark, opaque, spherical mineral, presumed to be pyrite framboids, is sprinkled in the central parts of the crystals.

Many veins of calcite and sulfur are associated with the calcite section of the cap rock (fig. 12). The veins are typically white calcite spar, with late-stage euhedral crystals of sulfur commonly precipitating as the last mineral phase. Monomineralic veins of either pure calcite or sulfur are also common, with a tendency for the percentage of sulfur within a vein to increase as the vein size decreases. The veins of calcite spar usually contain white, coarse crystalline, cm-sized anhedral crystals. Crystal terminations are usually scalenohedrons or may be blocky and trigonal. The frequency of veins in the terrigenous clastics within the calcite cap rock is less than the frequency of veins within the pure calcite cap rock. Many veins have open interiors, suggesting that the vein-filling minerals precipitated in open voids. In contrast, most of the veins in the anhydrite facies are diffuse planes where sulfur replaces anhydrite. Details on vein orientation are described under "Cap-Rock Structure."

Proto-Cap Rock

Terrigenous clastics within the calcite cap rock are medium to light-gray calcareous strata cemented by a variable but high percentage of finely crystalline calcite (fig. 15). In hand specimens, the terrigenous clastic facies can resemble the true calcite cap rock quite closely, including the presence of veins of calcite spar and sulfur. The percentage calcite in the terrigenous clastic rocks ranges from 40 to 80 percent. Twenty-five to thirty-three percent of the volume of the calcite cap rock in the area studied is composed of terrigenous clastics. The rock may be described as either calcitic very fine sandstone or quartz-bearing sandy fine to medium calcilutite, depending on percentage calcite. All the calcite is authigenic. Quartz is the primary detrital component, chert is common, and feldspars are rare. This association of fine-grained calcite matrix and coarse-grained terrigenous (siliciclastic) components is uncommon as a depositional fabric. The mixture of



Figure 15. Photograph of proto cap rock, Boling Dome. Terrigenous clastics, calcite. Unusual circular patches have different percentages of terrigenous clastics and calcite. Patches appear to have been burrows. Original matrix of terrigenous clay has been replaced by microspar. Calcite content approximately 80 percent. Texasgulf Sulfur Inc., Well #595, depth 2030 ft (cm scale).

the carbonate and detrital components strongly suggests that the carbonate replaced the original matrix material, probably clay minerals.

The calcite is unusually fine grained, 0.01 to 0.1 mm microspar to pseudospar (Folk, 1965). Most of the calcite matrix is clayey microspar 0.01 to 0.03 mm (fig. 16). The grains are anhedral masses to somewhat dirty rhombs. Clay minerals occur with the calcite, commonly as coatings around individual calcite crystals. Na-smectite is the predominant clay mineral.

Proto-Cap-Rock - True Cap-Rock Contact

As one traverses the boundary from calcite sandstone proto-cap rock into true calcite cap rock, the grain size of the calcite increases through neomorphism and the quartz disappears (fig. 17). The calcite first replaces the original clay-rich matrix of the sandstones, then neomorphism causes the grain size of the calcite to increase as impurities are segregated into discrete layers and zones. Actual replacement of quartz by calcite is more difficult to document. Contacts between true calcite and calcitic sandstones are commonly marked by large euhedral porphyroblasts of rhombohedral calcite (1.0 to 2.0 mm) floating in a sea of pseudospar (0.1 to 0.3 mm). Many of these large grains have central ghosts about the same size and shape as clastic grains in the surrounding rock (fig. 18). A few of the porphyroblasts contain small remnants of quartz or feldspar grains. SEM grain mounts were used to study the surface morphology of grains from the area of the contact between true cap rock and proto-cap rock. Although inconclusive, the surface morphology of the detrital feldspar grains have increased surface roughness suggestive of active dissolution. Quartz grains include well-developed quartz overgrowths and authigenic bipyramids.

Uncommon mineral species that may be significant include authigenic quartz and sulfide minerals, principally pyrite. The authigenic quartz fills pores flanking the side of large veins. The quartz is clearly authigenic, as it occurs in single euhedral bipyramids

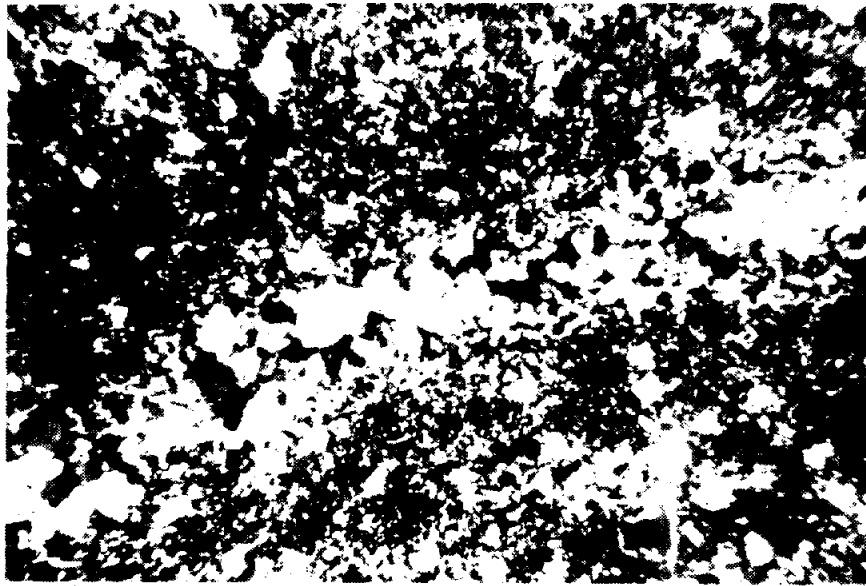


Figure 16. Photomicrograph of proto cap rock, Boling Dome. Very fine and fine sand-sized quartz and chert grains float in a matrix of microspar calcite. Crystal size of microspar is 0.02–0.05 mm. Central area is vein of calcite pseudospar and spar. Boundary between vein and microspar matrix is diffuse with gradually increasing grain size toward center of vein. Texasgulf Sulfur Inc., Well #587, depth 2455 ft (0.1 mm scale).



BOLING CAP ROCK
TEXASGULF SULFUR WELL 599
DEPTH 2440.0 FT

Figure 17. Photograph of contact between true calcite cap rock and proto cap rock, Boling Dome. True cap rock is light, pseudospar calcite (base of sample), whereas proto cap is dark microspar cemented quartz sandstone. Contact is marked by dark 1-2 mm euhedral porphyroblasts of rhombohedral calcite. These large crystals often have central remnant of quartz. Texasgulf Sulfur Inc., Well #599, depth 2440 ft (cm scale).

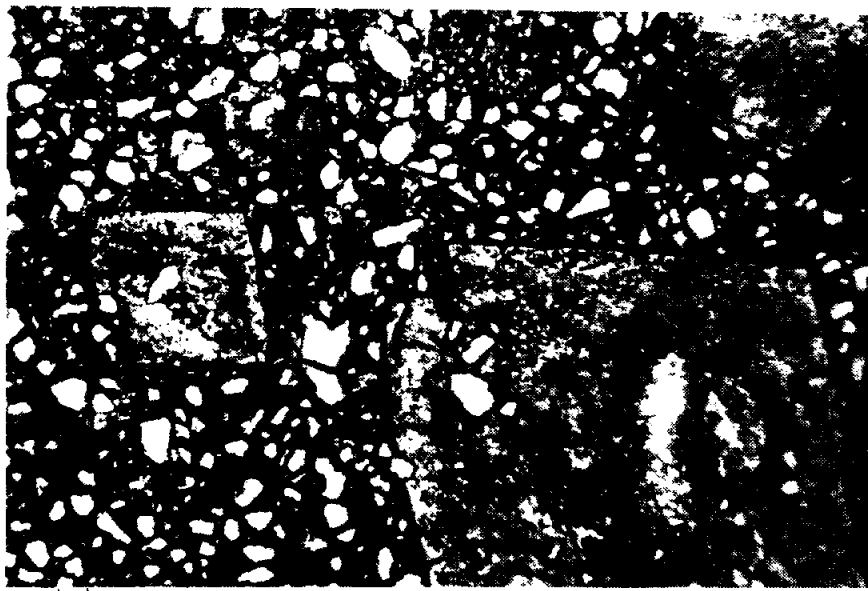


Figure 18. Photomicrograph of area near contact between true calcite cap rock and proto cap rock, Boling Dome. Porphyroblasts of calcite mentioned in Figure 17 are shown. Rhombohedral calcite is stained red with allizarn red S. Remnant microcrystalline quartz grain, with calcite-filled pits, is clearly visible in center of crystal. Original outline of quartz crystal is shown by dark rim. Texasgulf Sulfur Inc., Well #599, depth 2440 ft (0.1 mm scale).

(0.05 to 0.2 mm) and in 2 to 3 mm rosettes with sharp crystal boundaries. If large-scale dissolution of quartz is postulated to transform the calcitic sandstone into true calcite cap rock, then large-scale transport of dissolved silica is required. However, occurrence of the authigenic quartz only indicates that silica is precipitating in the cap-rock environment. No evidence from SEM observations indicates large-scale dissolution of sand-sized quartz.

The sulfide minerals present in the cap rock include pyrite, chalcopyrite, and possibly sphalerite. Sulfide seams are up to 1 cm thick, but are rare. Pyrite occurs in cubic masses up to 2.0 cm across. Spherules of an opaque mineral presumed to be pyrite are 0.01 to 0.02 mm in diameter within dark calcite grains and segregated in dark laminae 1 to 2 mm thick.

Anhydrite Cap Rock

The anhydrite cap rock is a dense, dark-gray rock predominantly composed of anhydrite (fig. 19). Individual crystals of anhydrite are euhedral and idiomorphic. They occur as interlocking grains cemented by anhydrite. Near the contact with the calcite facies, anhydrite may be cemented by calcite. Grain size varies from 0.2 to 0.5 mm. Whereas the calcite cap rock is extremely heterogeneous with respect to mineralogy and structure, the anhydrite cap rock is much simpler. This simplicity, however, may be a function of the underrepresentation of the anhydrite cap rock within the core suite studied. Usually less than 15 ft (5 m) of the upper anhydrite cap rock is drilled. However, recovery of the anhydrite averaged 90 percent. Distribution of mineralogical and structural zones within the main body of the anhydrite is unknown.

All the minerals found in the calcite cap rock are also present in the anhydrite cap rock. Anhydrite, however, comprises 90 percent of the rock volume. The terrigenous clastics occur in anhydrite as shale or shaly sandstones. The calcite is present as an authigenic cement concentrated near the contact with the calcite cap rock. Calcite veins are not common and very large veins, so common in the calcite cap rock, are absent. Veins

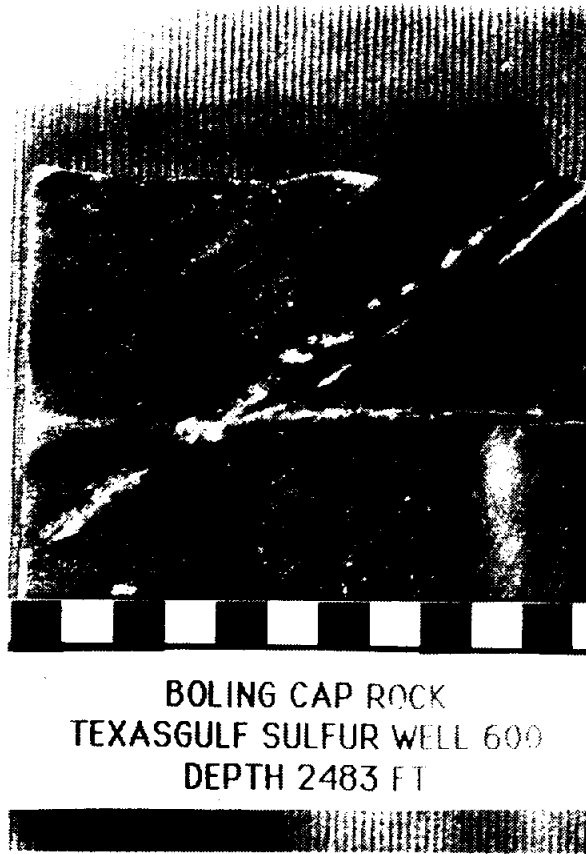


Figure 19. Photograph of anhydrite cap rock, Boling Dome. Light vein of sulfur cutting core at 55° is typical of diffuse sulfur vein in anhydrite. Horizontal light vein normal to axis of core is a coring-induced fracture. Faint concentric bands are saw marks. Texasgulf Sulfur Inc., Well #600, depth 2483 ft (cm scale).

of sulfur are common in anhydrite but are very different from those present in the calcite cap rock. The sulfur veins uniformly replace anhydrite and are not void fillings (fig. 20).

Terrigenous clastics occur within the anhydrite cap rock and at the contact between the anhydrite and calcite cap rocks (fig. 19). Clastics in the anhydrite are shale- or clay-rich in contrast with clastics in the calcite part of the cap rock, which have the clayey matrix replaced by calcite. Clayey very fine sandstone is also present in the anhydrite. The abundance of clay is the principal difference between clastics in the anhydrite and those within the calcite cap rock.

Discussion

One of the most interesting aspects of the cap rock at Boling Dome is the relative abundance of incorporated detrital material within the cap rock. Calcitic sandstone and the calcitic shale are two of the extradomal facies within Boling Dome cap rock. The calcitic sandstone is associated with the calcite facies, and the calcitic shale and shaly, very fine sandstone are associated with the anhydrite facies. The mechanism by which this material is incorporated within the cap rock has important implications for the structural stability of the dome and the growth mechanism of the cap rock. Murray (1966) noted that some cap rocks are characterized by abundant incorporated terrigenous clastic material. In fact, the very earliest workers on cap rocks (Goldman, 1925; Teas, 1931) thought cap rocks, including the anhydrite, were of sedimentary origin. The origin of anhydrite cap rock as a dissolution residuum from solution of the upper parts of the salt stock was accepted by most cap-rock researchers (Goldman, 1933, 1952; Taylor, 1938; Feely and Kulp, 1957) on the basis of the flat-topped solution table that decapitates folds at the top of the salt stock. There is also compositional similarity between residues in the salt stock and residues in the anhydrite cap rock (Martinez, 1980). Sulfate in the anhydrite is reduced by sulfate-reducing bacteria (Feely and Kulp, 1957; Sassen, 1980; Kreitler and Dutton, 1983) in the presence of hydrocarbons. Geochemically significant reaction products include



Figure 20. Photomicrograph of anhydrite cap rock, Boling Dome. Euohedral anhydrite (lightest gray) and gypsum crystals are separated by small euohedral pores (fuzzy, dark gray). Irregular medium gray crystals are sulfur. Top—plain polarized light, bottom—crossed nicols. Texasgulf Sulfur Inc., Well #171, depth 2097 ft (0.1 mm scale).

CO₂ and H₂S. Geologically significant products are calcite, free sulfur, and pyrite (Sassen, 1980).

Additional mechanism(s) are necessary to account for the incorporation of significant quantities of terrigenous clastics within cap rocks over salt stocks. The data indicate that a three-stage process of cap-rock evolution is involved. First, the movement of ductile salt and sediments along the margins of the dome allows shear to mechanically incorporate the shaly clastics within the salt stock. Second, salt dissolution accretes the clastics to the base of the cap rock within the anhydrite section. Third, upward migrating basinal fluids, including hydrocarbons, foster the replacement of anhydrite by calcite and precipitation of calcite within the sediments overlying the cap rock. The upward migration of basinal fluids and hydrocarbons is indicated by the distribution of oil in deep Oligocene strata, in cap-rock fractures, and in Miocene and Pliocene strata over the dome crest.

Extradomal facies within the cap rock have been incorporated by one or two mechanisms (fig. 21): basal accretion and replacement of overlying sediment by calcite. The salt definitely incorporated the shale facies and conveyed it to the top of the dome. The shale was accreted with the anhydrite to the base of the cap rock as salt was dissolved. Assuming the anhydrite in the cap rock is a residuum product of salt dissolution (Goldman, 1933; Taylor, 1938; Feely and Kulp, 1957; Murray, 1966; Kreitler and Dutton, 1983), and because the shale is commonly surrounded by anhydrite, the shale that is now surrounded by anhydrite must have originally been surrounded by salt. Hockley Dome (fig. 4) is another dome with shale within the anhydrite. This shale is concentrated around the exterior margin of the cap rock. These facts support the conclusion that the shale was probably incorporated into the margins of the salt stocks by shearing during dome growth. Kupfer (1974, 1980) described similar anomalous zones of sediments concentrated along shear zones within salt stocks in Louisiana. These shear zones in salt cause major problems during mining, including gas blowouts (Thoms and Martinez, 1980), fluid production, and slabbing (Kupfer, 1980).

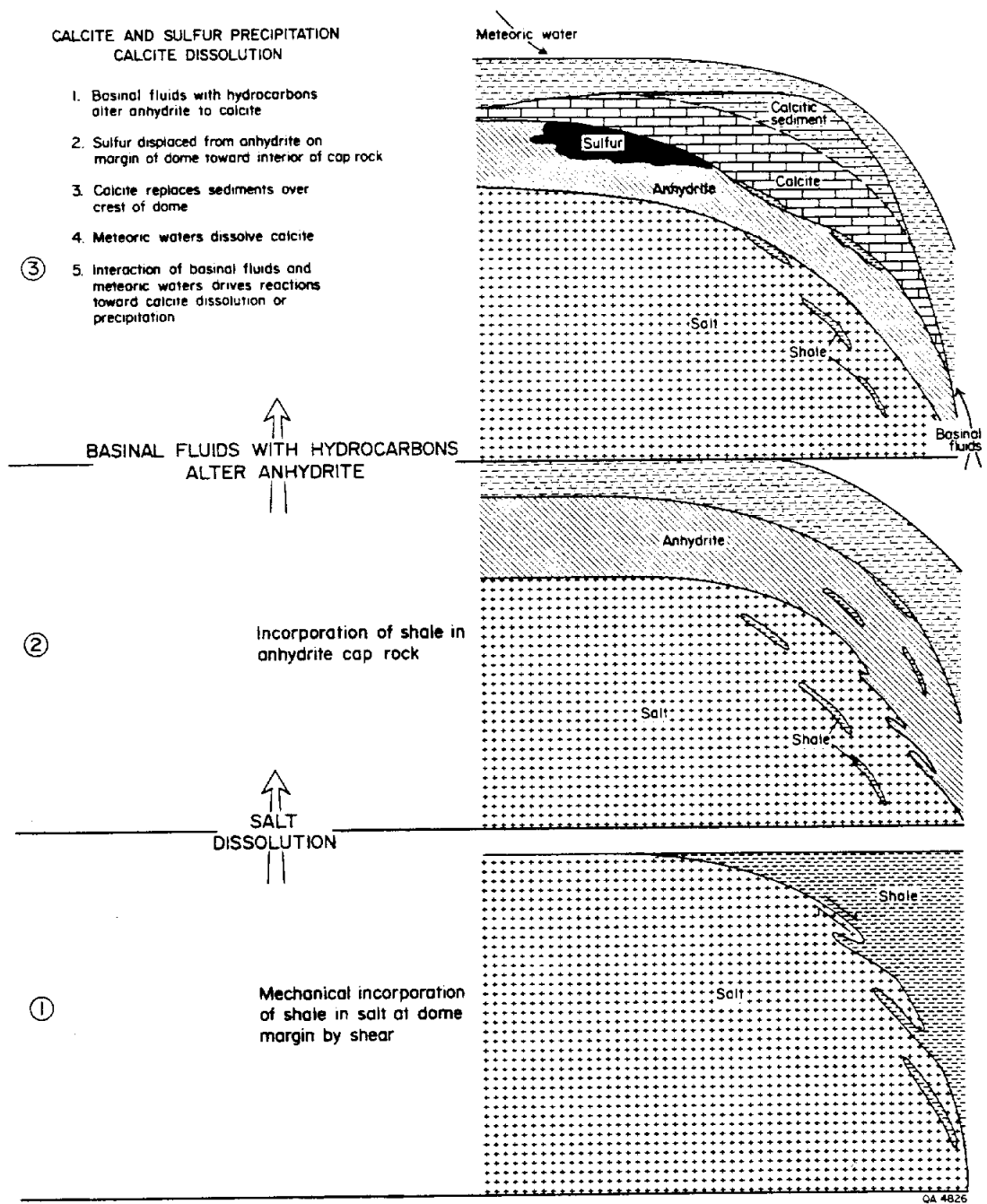


Figure 21. Schematic diagram of cap-rock evolution, Boling Dome.

If the salt stock could raft up shale, the stock could probably also bring up sandstone. Sandstones and sandy mudstones could be incorporated within the calcite section by a continuation of basal accretion. When fluids bearing hydrocarbons enter the cap rock and alter anhydrite to calcite, sandstones and sandy mudstones originally surrounded by anhydrite become surrounded by calcite. The fine-grained clayey matrix is replaced by calcite at this stage. The quartz, however, is more resistant to replacement. The quartz in the calcitic sandstones remains within the fine-grained calcite of the proto-cap rock. According to this hypothesis, sandstones would have been rafted up by the salt stock, survived subsequent salt dissolution and anhydrite replacement, and arrived at the top of the cap rock as relatively undigested pods of quartz sand within a calcite matrix. Admittedly, this proposed journey sounds rather farfetched.

The calcitic sandstone facies may have been incorporated by upward growth of the calcite facies through calcite precipitation and replacement. Calcitic sandstone is currently concentrated near the top of the cap rock. This argues for upward growth of the calcite facies through the overlying sediments by a dissolution-precipitation and replacement process. The absence of any sandstone associated with the anhydrite facies and the absence of any shale in the calcite section indirectly indicates that the calcite sandstones were incorporated by upward growth of the calcite facies by matrix replacement.

Intergradation of the calcitic sandstone with the pure calcite and lateral equivalence of the two facies are evidence that at least some pure "normal" calcite evolved by replacement of overlying strata. Although the boundary between the two facies is often abrupt over 1 mm to 10 mm (fig. 17), some detrital grains show equivocal evidence of progressive replacement by calcite across the zone (fig. 16). The association of finer grained quartz with cap rock containing a greater percentage calcite may represent an inherited depositional fabric where finer grained quartz was originally associated with more clay-rich sediments. There is, however, no compelling evidence that "true" calcite cap rock evolved from replacement of quartz in "proto" cap rock. Replacement of clay

minerals by calcite is thermodynamically easier and more clearly documented petrographically. Variations in the distribution of quartz-rich proto-cap rock may represent depositional variations in the lithology of strata deposited over the dome crest. True calcite cap rock in the upper parts of the cap rock may have completely replaced former mudstones, whereas calcite sandstones in the proto-cap rock are the residuum of calcite replacement of sand-dominated channel sands.

CAP-ROCK STRUCTURE

Salt diapirs are major structural discontinuities with cap rocks positioned at the interface between the upper part of salt stocks and the surrounding strata. Shear is strongly developed at this interface between relatively stationary or downbuilding strata (Bornhauser, 1958) and salt that is moving up relative to the strata. By analyzing the structure within cap rocks we can better understand the mechanism controlling vein and fault development and orientation and better predict the distribution of veins and faults in less explored areas.

Methodology

Cap-rock structure was studied in the cap-rock core loaned by Texasgulf Inc. Cores were unoriented by azimuth and are assumed to be vertical. The dip angle was measured for various structural features, including veins, bedding, vugs, and faults. The features were measured for each well and segregated by depth and facies, including calcite, anhydrite, and terrigenous clastics. Table 1 summarizes the raw data for calcite and anhydrite facies for each well.

Veins were the main structural feature measured (fig. 12). Faults are presumed to be abundant in the cap rock (fig. 22), but their orientation and density were difficult to

Table 1. Vein orientations in calcite and anhydrite cap rock for wells on core cross section (fig. 9).

Facies	Vein Dip Angle	Well 171	Well 176	Well 589	Well 590	Well 592	Well 593	Well 595	Well 597	Well 598	Well 599	Well 600	Well 601	
Anhydrite	Degrees													
	0-9	3	0	0	0	0	1	0	0	1	0	0	0	
	10-19	7	0	0	0	1	1	0	0	1	0	0	1	
	20-29	6	1	0	0	2	0	1	0	3	0	0	6	
	30-39	5	3	1	0	1	0	1	1	8	0	0	3	
	40-49	1	2	1	0	8	3	4	3	10	0	1	0	
	50-59	0	1	4	3	4	1	0	2	5	2	0	0	
	60-69	0	2	4	0	0	0	0	0	0	0	2	6	
	70-79	0	0	0	3	0	2	0	0	2	2	0	1	
	80-89	0	0	0	0	0	0	3	0	0	0	0	1	
	sum		22	9	10	6	16	11	6	6	30	4	9	10
	footage		5	15	4	2	13	22	22	10	30	10	21	15
	density of veins/ft		4.40	0.60	2.50	3.00	1.23	0.50	0.27	0.60	1.00	0.40	0.43	0.67
Calcite	Degrees													
	0-9	13	6	3	4	1	3	17	7	2	2	9	5	
	10-19	16	18	4	4	0	3	6	8	2	5	5	3	
	20-29	14	17	7	5	2	5	7	4	2	9	6	4	
	30-39	13	6	7	6	0	3	6	12	8	6	10	5	
	40-49	10	11	9	5	5	5	11	6	7	10	24	0	
	50-59	18	5	8	1	3	2	12	2	7	7	16	0	
	60-69	11	5	8	0	0	0	5	0	0	1	7	0	
	70-79	14	4	6	0	0	0	2	0	0	2	4	0	
	80-89	12	3	0	0	0	0	1	0	0	4	1	0	
	sum	121	75	52	25	11	21	67	67	39	34	41	82	17
	footage	105	55	67	69	35	67	75	75	45	60	45	44	30
	density of veins/ft	1.15	1.36	0.78	0.36	0.31	0.31	0.89	0.89	0.87	0.57	0.91	1.86	0.57

Table 1. (cont.)

Facies	Vein Dip Angle	Well 602	Well 603	Well 604	Well 605	Well 606	Well 607	Well 613	Well 2287	Well 2291	Well 2292	Well 2293	Well 2294
Anhydrite	Degrees												
	0-9	0	0	1	2	0	0	0	0	0	0	0	0
	10-19	0	0	2	0	0	0	0	0	0	0	0	0
	20-29	0	1	8	3	0	0	2	0	0	2	1	0
	30-39	0	4	7	2	0	2	4	1	0	0	1	0
	40-49	5	6	1	11	1	7	5	8	1	0	7	5
	50-59	0	2	0	11	1	5	2	4	2	0	3	2
	60-69	1	0	0	4	0	4	0	0	4	0	2	0
	70-79	0	0	1	0	0	2	0	0	0	0	0	0
	80-89	0	1	0	0	0	0	0	0	0	0	0	0
	sum	6	14	20	33	2	20	13	13	7	2	14	7
	footage	4	19	11	57	7	51	6	22	15	13	10	13
	density of veins/ft	1.50	0.74	1.82	0.58	0.29	0.39	2.17	0.59	0.47	0.15	1.40	0.54
Calcite	Degree												
	0-9	11	No Data	6	5	0	0	1	2	4	6	3	11
	10-19	9		10	3	0	0	2	0	15	5	2	6
	20-29	6		3	6	0	3	5	3	7	9	6	5
	30-39	7		5	2	1	7	8	1	6	6	3	5
	40-49	1		12	4	0	2	3	5	3	7	11	8
	50-59	0		4	1	1	1	1	6	5	7	7	1
	60-69	1		1	0	3	1	2	1	1	2	9	1
	70-79	1		2	1	1	1	0	0	1	2	5	3
	80-89	5		2	2	3	0	0	0	0	2	6	2
	sum	41		45	24	9	15	22	18	42	46	52	42
	footage	53		74	18	28	21	33	60	60	75	85	90
	density of veins/ft	0.77		0.61	1.33	0.32	0.71	0.67	0.30	0.70	0.61	0.61	0.47

Table 1. (cont.)

Facies	Vein Dip Angle	Well 2295	Well 2298	Well 2299	Well 2300	Well 2301	Well 2302	Well 2303	Well 2304	Well 2311	Well 2312	Well 2313	Well 2314
Anhydrite	Degrees												
	0-9	2	0	0	0	0	0	1	0	2	1	0	0
	10-19	0	0	0	0	0	0	1	0	1	3	0	0
	20-29	0	0	0	0	0	0	0	0	2	2	1	0
	30-39	0	0	0	0	0	0	1	0	6	5	2	1
	40-49	1	0	0	0	0	1	6	0	5	7	1	2
	50-59	1	0	1	0	1	0	0	0	14	5	4	0
	60-69	4	0	3	2	2	0	1	0	4	0	7	0
	70-79	2	0	4	4	1	0	1	0	2	1	1	2
	80-89	1	0	2	0	0	0	0	0	5	6	0	0
	sum	11	0	10	6	4	1	11	0	41	30	16	5
	footage	15	3	15	8	9	8	30	6	15	47	5	8
	density of veins/ft	0.73	0.00	0.67	0.75	0.44	0.13	0.37	0.00	2.73	0.64	3.20	0.63
Calcite	Degrees												
	0-9	7	3	0	8	3	4	8	3	5	3	9	7
	10-19	3	8	0	10	2	9	8	3	12	6	10	5
	20-29	3	9	0	15	5	10	12	2	11	7	4	7
	30-39	2	5	2	9	2	10	4	5	7	6	1	11
	40-49	2	6	4	7	4	8	11	5	9	8	1	20
	50-59	0	4	0	6	3	11	8	8	12	8	0	3
	60-69	0	5	4	2	5	7	4	8	7	8	0	4
	70-79	0	1	1	5	4	1	3	5	11	6	5	2
	80-89	0	12	1	2	8	2	5	2	4	11	6	6
	sum	17	53	12	64	36	62	63	41	78	63	36	65
	footage	45	75	85	67	60	117	75	112	95	45	91	112
	density of veins/ft	0.38	0.71	0.14	0.96	0.60	0.53	0.84	0.37	0.82	1.40	0.40	0.58



Figure 22. Photograph of calcite cap rock, Boling Dome. Apparent thrust fault is in calcite and late stage vein fill of calcite spar is displaced. Texasgulf Sulfur Inc., Well #2298, depth 1962 ft (cm scale).

analyze because of the poor recovery associated with the faults. We conclude that intense veining is one expression of faulting.

Calcite Cap Rock

A greater volume of the calcite facies has been structurally and diagenetically altered than the anhydrite facies. Brecciation is very common in the calcite section, but absent in the anhydrite facies except in the shear zones (fig. 23). Veins occur at all scales up to the size of the core (5 inches). Although vein length is unknown, the similarity in vein swarms in adjacent wells suggests that they may extend many meters. Undoubtedly, veins larger than the core diameter are present, especially in brecciated zones.

Most veins in the calcite section are open-void fills. The largest number of veins within the calcite facies are primarily calcite, often with a late-stage fill of sulfur (fig. 12). These veins tend to have parallel sides with up to 10 cm of separation. Veins composed solely of sulfur are also common, but tend to be shorter and thinner than the pure calcite and calcite-sulfur veins. The smaller pure sulfur veins tend to be sharply bound, stretched parallelograms with lengths of a few mm to cm and widths about 10 to 50 percent of the length (fig. 24). These veins are oriented more vertically than the larger calcite veins and often in an echelon sets. Dip of veins is difficult to measure precisely because of the short length; overall dips range from vertical to 45° . This type of sulfur vein represents an extension fracture (for example, De Sitter, 1964).

Mean orientation of veins in the calcite facies shown in figure 25 is 39° . Dip was measured relative to the vertical axis of the core. Variation in dip of these veins with respect to depth is shown in figure 25. There is a progressive increase in variability of dip (the standard deviation increases) for these veins as the calcite facies becomes shallower. Mean dip shows very little change, from 36° for the deepest wells to 40° for the shallowest wells.

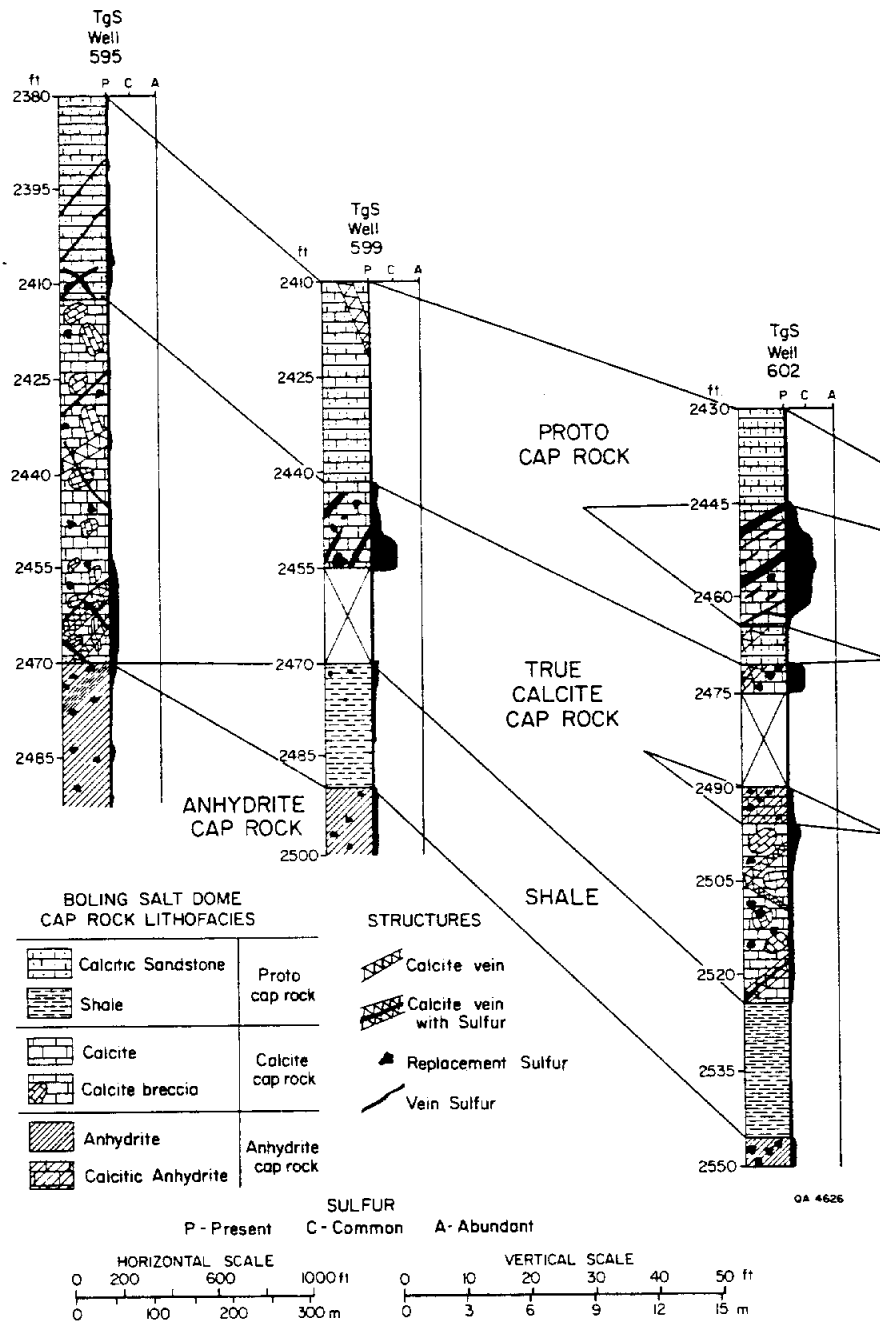
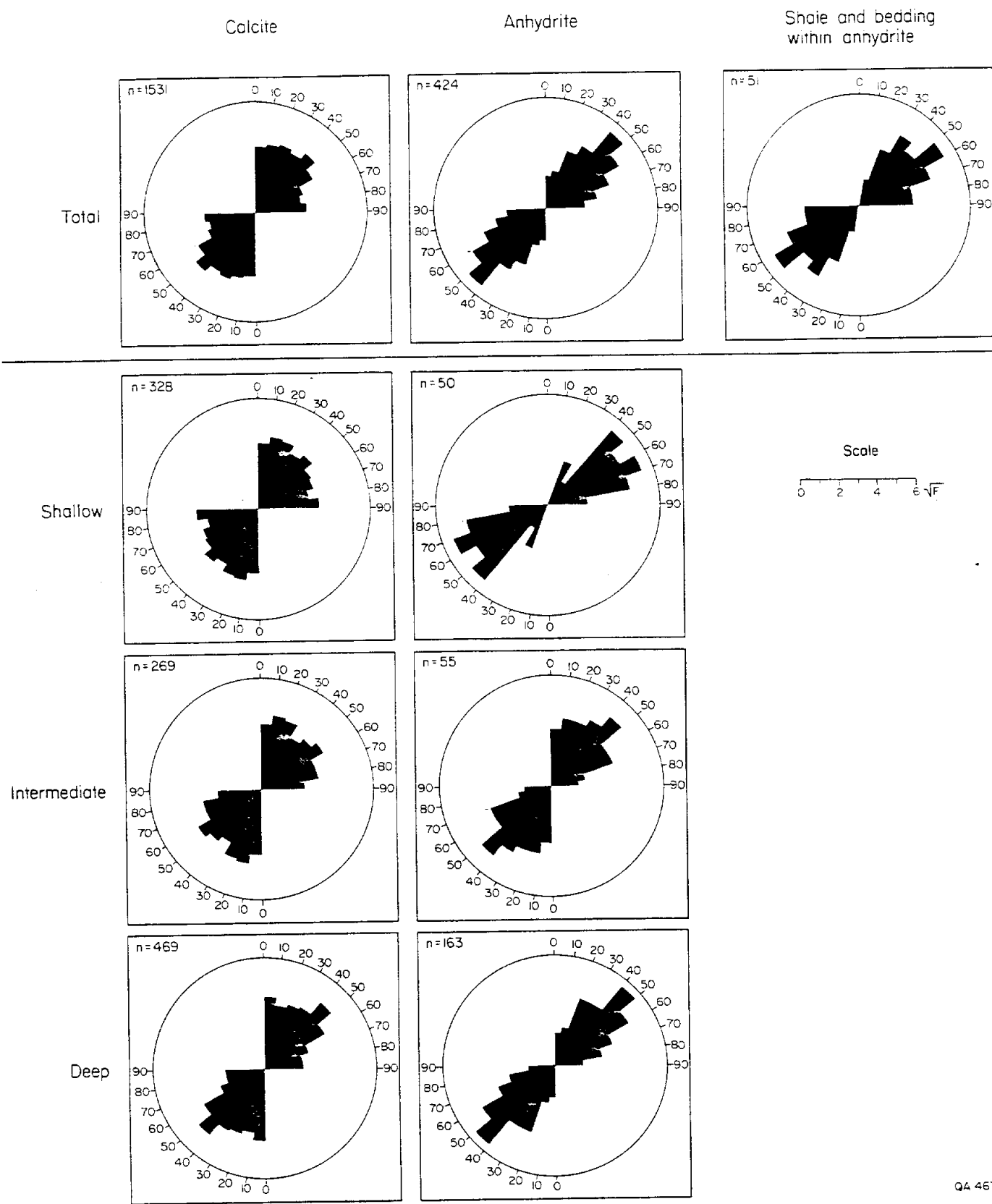


Figure 23. Cross section of cap rock, Boling Dome. Brecciated zones in calcite cap rock are correlated between wells spaced approximately 100 ft (30 m) apart.



Figure 24. Photograph of small veins of sulfur in calcite cap rock, Boling Dome. Veins have rhombohedral form and are arranged in an echelon sets. Texasgulf Sulfur Inc., Well #593, depth 2439 ft (cm scale).



QA 4673

Figure 25. Orientation of veins, faults, and bedding, Boling Dome. Mean orientation is shown for calcite cap rock, anhydrite cap rock, and for bedding and shale within anhydrite cap rock. Variations in dip of veins and faults are shown for calcite and anhydrite cap rock.

Anhydrite Cap Rock

The veins and faults within the anhydrite facies are very different from those present in the calcite facies (compare fig. 12 with fig. 19). Diffuse veins of sulfur that replaced anhydrite are the most common vein type in anhydrite. Faults or shear planes with slickensides, oil, and often shale are common in the anhydrite. Orientation of veins and faults in anhydrite clustered very tightly about a mean of 47° (fig. 25). The mean density of veins and faults in the anhydrite cap rock is 0.8/ft (2.5/m). The orientation of shale bedding within the anhydrite and anhydrite layering is also tightly clustered about a mean of 51° . Unlike the calcite section, there is no systematic variation with depth in the orientation or spread of dip within the anhydrite section.

Mechanisms

Vein orientations were compared to the orientation of ideal fractures in both compressional and extensional regimes to understand the mechanism controlling vein formation. Faults that form in compressional regimes are conjugate sets separated by less than 90° and generally by 60° . The angle between the compressive force and the resultant fractures is about 30° (when the compression is directed vertically and fractures measured from the vertical) (Billings, 1972). Faults that form by extension are separated by 120° and thus form at 60° to the direction of extension (with extension oriented normal to the vertical and fractures measured from the vertical) (Billings, 1972). Most veins at Boling Dome cap rock have, or originally had, open centers. Many smaller veins are short rhombohedral-shaped fractures in an echelon sets. The modal (most common 10° class) dip orientation for the veins in Boling cap rock is 45° . The shale bedding and anhydrite layering within anhydrite dips at 51° . The preponderance of open veins indicates that the cap rock is under an extensional stress regime. However, the fracture dip angles fall midway between the angle that would be expected in either a horizontally directed extensional or vertically directed compressive regime operating on horizontal strata.

Shear is the probable mechanism controlling fault and vein orientation because of the parallelism between cap-rock orientations and the orientation of the major local shear zone at the cap-rock contact. Additionally, shear has aligned the dip of shale bedding and anhydrite layering (fig. 25), which would not be possible with simple extension or compression.

Cap-rock veins developed from shear fractures as a result of extensional stresses that developed at the interface between the dome and the surrounding rock. There are at least two lines of evidence suggesting that the veins in Boling cap rocks principally result from shear. The cap-rock - salt-stock interface in the area where the core was recovered dips about 45° . This interface is a shear zone between the salt stock and the surrounding strata. The shear results from the relative movement of salt past the surrounding strata. We also think that this shear is responsible for having incorporated shale within the salt stock and then within the cap rock. As the surrounding shale slides by the salt stock, the salt, being less viscous, will tend to get smeared along the contact. The salt - country-rock contact may develop salt extensions that eventually coalesce and incorporate shale with the salt (fig. 21). Exotic blocks of country rock concentrated along the margins of salt stocks are thought to arise in this manner. Additionally, conjugate joint, vein, and fault sets were not observed as would be expected if they were the result of either simple compression or extension. Also, although structures that looked like thrust faults were present, they were extremely rare.

POROSITY, PERMEABILITY, AND FLUID TRANSPORT

Void spaces are an important component of the calcite section of the cap rock. The porosity and permeability of the calcite cap rock are very high, but difficult to measure accurately without large-scale hydrologic pumping tests (Smith, this volume). In contrast, plug and core permeabilities are much lower when a much smaller section of the cap rock

is sampled (table 2). Whole-core permeability within calcite cap rock varied over four orders of magnitude. One curious result was that vertical permeability exceeded horizontal permeability (measured for the same sample) from one to three orders of magnitude.

Core-plug and whole-core permeabilities within the anhydrite section are lower than those measured in the calcite section. Within the anhydrite, cap-rock reservoir conditions at a local scale from over mm to cm approach isotropic and homogeneous ideals. These conditions do not typify the aquifer conditions throughout the anhydrite section or the calcite section lengths greater than 2 ft (0.5 m). For example, the density of faults and veins in the calcite and anhydrite sections is 0.7 and 0.8/ft (2.2 and 2.5/m), respectively.

Meaningful estimates of percentage void space are not possible owing to poor recovery of the cap-rock sections with the highest percentage of void space. Porosity and permeability measurement of whole core and core plugs must be analyzed in the context that the major zones of maximum porosity and permeability in lost-circulation zones and caverns are not recovered during coring.

Approximate percentage recovery for the calcite section was 50 percent, whereas recovery for the anhydrite section was 90 percent. Although no large, poorly recovered zones within the anhydrite section were encountered in the wells used in this study, very large caverns have been encountered at Boling Dome (Mullican, Subsidence over Texas Salt Domes, this report). An oil exploration well drilled in 1927 encountered a cavern in the anhydrite section with at least 106 ft (32 m) of vertical extent. The hole was abandoned because of lost-circulation problems and forgotten until 1983. The site around the forgotten hole catastrophically collapsed on August 11, 1983, destroying a 250-ft (80-m) section of County Road 442 (fig. 26). It is unknown what processes caused the cavern to collapse (Dreyer and Schulz, 1984).

The true calcite cap rock is much more porous than the calcitic sandstones. The porosity in the calcite cap rock includes intergranular pores and fracture porosity

Table 2. Whole core and core plug permeability analyses.

Sample number	Well number	Depth (ft)	Orientation	Permeability* (md)	Sample type	Lithology
1	171	2,039	Vertical	14.180	Core	True calcite cap rock --pseudospar
2	171	2,039	Horizontal	0.018	Core	True calcite cap rock --measured along vein
3	2289	1,970	Vertical	4.250	Core	True calcite cap rock --abundant veins of spar
4	2289	1,970	Horizontal	0.004	Core	True calcite cap rock --random vein orientations
5	588	2,379	Horizontal	0.001	Core	Proto calcite cap rock --parallel to vertical veins
6	588	2,379	Horizontal	0.005	Core	Proto calcite cap rock --perpendicular to vertical vein
7	588	2,379	Vertical	0.090	Core	Proto calcite cap rock --measured along vein
8	2314	2,025	Horizontal	0.0356	Plug	Proto calcite cap rock --small vugs, breccia
9	2314	2,025	Vertical	0.173	Plug	Proto calcite cap rock --small vugs
10	2313	2,058	Horizontal	0.167	Plug	True calcite cap rock --large vein, open spar
11	2313	2,058	Vertical	0.001	Plug	True calcite cap rock --large vein, open spar
12	2313	2,065	Horizontal	0.244	Plug	White calcite spar within large vein
13	2314	2,150	Horizontal	0.0418	Plug	Anhydrite cap rock --tight, no fractures
14	2314	2,150	Vertical	0.275	Plug	Anhydrite cap rock --intersected sulfur vein @ 45° to the axis of the core

*Liquid permeability measured under the following test conditions: temperature-ambient; pore pressure-900 psi; confining pressure-2000 psi; permeating fluid-3000 mg/l NaCl brine. Pore pressure based on hydrostatic pressure at 0.45 psi/ft; confining pressure based on lithostatic pressure of 1 psi/ft.



Figure 26. Photograph of collapse sink, FM 442, Boling Dome on 16 August 1983. Water depth was approximately 23 ft (7 m). Concentric extension fractures are arrayed around the periphery of the sink. Sink formed over the site of a well drilled in 1927 that intersected a cavern 106 ft (32 m) tall within the anhydrite cap rock.

associated with the open veins. The porosity within the fractures is thought to be much greater than intergranular porosity. The porosity of the calcitic sandstones is reduced by the precipitation of the fine-grained calcite, by the less abundant veins, and by fractures.

Fluid Transport

Large volumes of superheated water are injected into the cap rock at Boling Dome to produce sulfur by the Frasch process. The superheated water melts the sulfur, which is then pumped to the surface with compressed air. The water is currently injected at the rate of about 4 million g/d. Historically, peak injection rates were about 10 million g/d (F. Samuelson, personal communication, 1985). Temperature of injection waters is about 315°F (157°C). To use water efficiently, bleed-water wells withdraw most of the injected water from the cap rock when the temperature drops below the temperature needed to melt the sulfur. Bleed-well temperatures are usually 150°F (66°C). Bottom-hole temperatures from wells completed in sands above and around the cap rock indicate anomalous temperature conditions owing to probable convective transport of the heat by fluids migrating out of the cap rock. Figure 27 shows the geothermal gradient around the area of sulfur production. Regional geothermal gradient is about 1°F/100 ft (18°C/km). Around domes the geothermal gradient roughly doubles. Geothermal gradients mapped around Boling Dome exceed 10°F/100 ft (180°C/km) in the shallow sediments over the cap rock. The gradients decline with increasing depth. As expected, the area of maximum temperature gradient coincides with the area of sulfur production. However, arcuate plumes of high gradient also extend around the margin of the dome and extend to the southeast from the sulfur mining area. These plumes reveal zones of preferential water transport and likely are zones of maximum porosity and permeability. The unevenness of the high-temperature area indicates that simple thermal conduction is not the dominant mechanism of heat transport. Heat convection by fluid transport, especially along porous

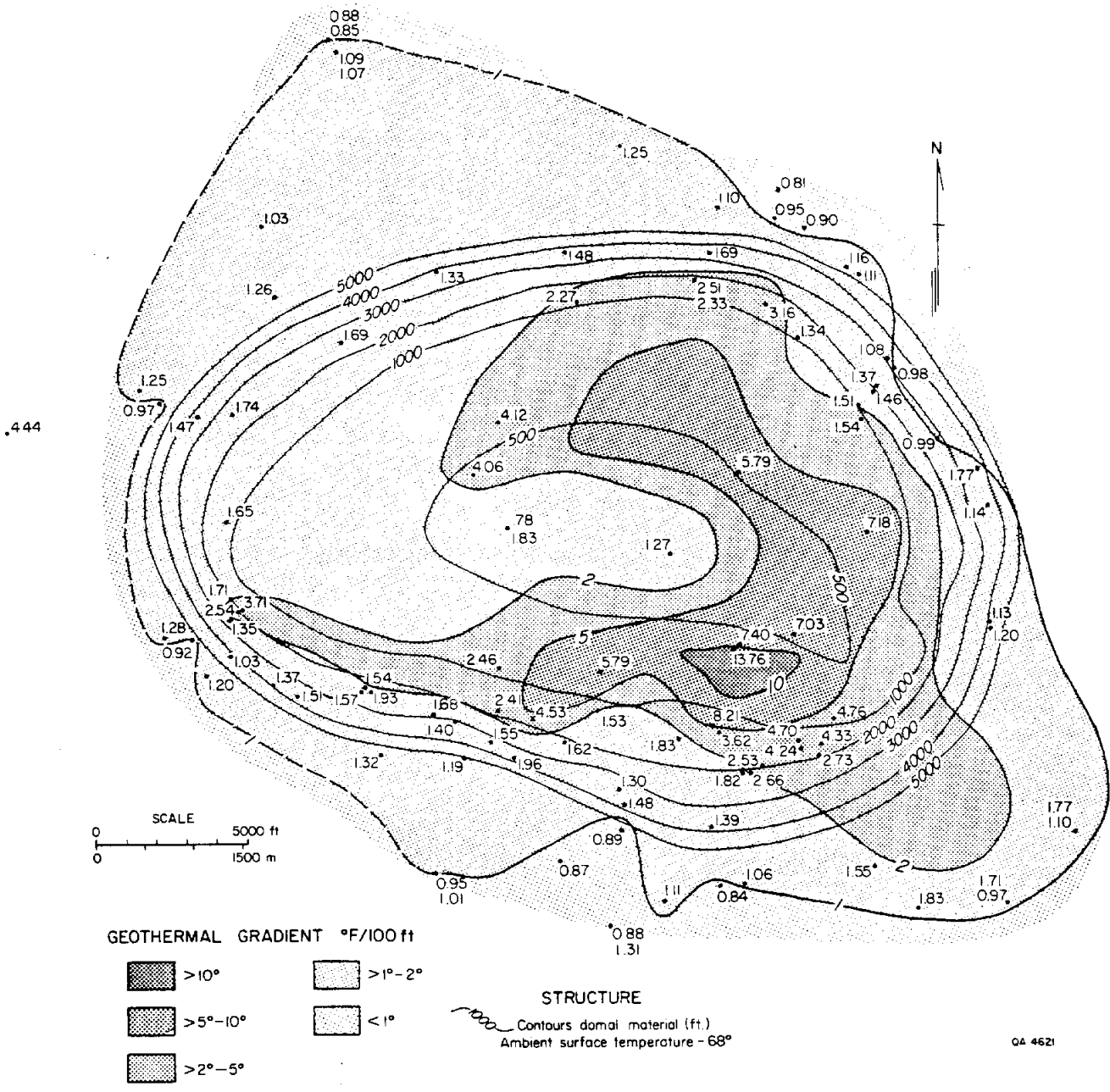


Figure 27. Geothermal gradient, Boling Dome. Intense heat anomaly is in sediments over the cap rock centered about the area of sulfur mining. Arcuate extensions outline areas of heat export through convective transport of ground water.

and permeable zones, is the probable dominant mechanism controlling distribution of heat flow and export of heat from cap rocks into surrounding strata.

REFERENCES

- Billings, M. P., 1972, Structural geology: Englewood Cliffs, New Jersey, Prentice-Hall, 606 p.
- Bornhauser, M., 1958, Gulf Coast tectonics: American Association of Petroleum Geologists Bulletin, v. 42, no. 2, p. 339-370.
- De Sitter, L. U., 1964, Structural geology: New York, McGraw-Hill, 351 p.
- Dreyer, B. V., and Schulz, C. E., 1984, Evaluation, repair and stabilization of the Boling sinkhole FM 442, Wharton County, Texas, in Beck, B. F., ed., Sinkholes--their geology, engineering and environmental impact: Proceedings, First Multidisciplinary Conference on Sinkholes, sponsored by Sinkhole Research Institute, Univ. Central Florida, p. 353-357.
- Feely, H. W., and Kulp, J. L., 1957, Origin of Gulf Coast salt-dome sulfur deposits: American Association of Petroleum Geologists Bulletin, v. 41, no. 8, p. 1802-1853.
- Folk, R. L., 1965, Some aspects of recrystallization in ancient limestones, in Pray, L. C., and Murray, R. C., eds., Dolomitization and limestone diagenesis, a symposium: Society of Economic Paleontologists and Mineralogists Special Publication, no. 13, p. 14-48.
- Goldman, M. I., 1925, Petrography of salt dome cap rock: American Association of Petroleum Geologists Bulletin, v. 7, no. 1, p. 42-78.
- _____ 1933, Origin of the anhydrite cap rock of American salt domes: U.S. Geological Survey Professional Paper 175, p. 83-114.

- _____ 1952, Deformation, metamorphism, and mineralization in gypsum-anhydrite caprock, Sulfur Salt Dome, Louisiana: Geological Society of America Memoir 50, 169 p.
- Kreitler, C. W., and Dutton, S. P., 1983, Origin and diagenesis of cap rock, Gyp Hill and Oakwood Salt Domes, Texas: The University of Texas at Austin, Bureau of Economic Geology Report of Investigations No. 131, 58 p.
- Kupfer, D. H., 1974, Boundary shear zones in salt stocks, in Coogan, A. H., ed., Proceedings, Fourth Symposium on Salt, Northern Ohio Geological Society, Cleveland, Ohio, v. 1, p. 215-225.
- _____ 1980, Problems associated with anomalous zones in Louisiana salt stocks, USA, in Coogan A. H. and Hauber, L., eds., Proceedings, Fifth Symposium on Salt, Northern Ohio Geological Society, Cleveland, Ohio, v. 1, p. 119-134.
- Martinez, J. D., 1980, Salt dome caprock--a record of geologic processes, in Coogan, A. H., and Hauber, L., eds., Proceedings, Fifth Symposium on Salt, Northern Ohio Geological Society, Cleveland, Ohio, v. 1, p. 143-151.
- Marx, A. H., 1936, Hoskins Mound salt dome Brazoria County, Texas: American Association of Petroleum Geologists Bulletin, v. 20, no. 2, p. 155-178.
- McCarter, W. B., and O'Bannon, P. H., 1933, Sugarland oil field, Fort Bend County, Texas: American Association of Petroleum Geologists Bulletin, v. 17, no. 11, p. 1362-1386.
- Murray, G. E., 1966, Salt structures of Gulf of Mexico Basin--a review: American Association of Petroleum Geologists Bulletin, v. 50, no. 3, p. 439-478.
- Price, P. E., Kyle, J. R., and Wessel, G. R., 1983, Salt-dome related zinc-lead deposits, in Kisvarsanyi, G., and others, eds., Proceedings, International Conference on Mississippi Valley-Type Lead-Zinc Deposits, University of Missouri, Rolla, p. 558-571.
- Sassen, R., 1980, Biodegradation of crude oil and mineral deposition in a shallow Gulf Coast salt dome: Organic Geochemistry, v. 2, p. 153-166.

- Taylor, R. E., 1938, Origin of the cap rock of Louisiana salt domes: Louisiana Geological Survey Bulletin 11, 191 p.
- Teas, L. P., 1931, Hockley salt shaft, Harris County, Texas: American Association of Petroleum Geologists Bulletin, v. 15, no. 4, p. 465-469.
- Thoms, R. L., and Martinez, J. D., 1980, Blowouts in domal salt, in Coogan, A. H., and, Hauber, L., eds., Proceedings, Fifth Symposium on Salt, Northern Ohio Geological Society, Cleveland, Ohio, v. 1, p. 405-411.
- United Resource Recovery, Inc., 1983, Application of United Resource Recovery, Inc., to dispose of waste by well injection at the Boling salt dome: Submitted by Keysmith Corp., Austin, Texas, 121 p.
- Walker, C. W., 1974, The nature and origin of cap rock overlying Gulf Coast salt domes, in Coogan, A. H., ed., Proceedings, Fourth Symposium on Salt, Northern Ohio Geological Society, Cleveland, Ohio, v. 1, p. 169-195.

Appendix. List Of Wells

Moss Bluff Dome
Cross Section A-A'

County	Cross Section Well Number	Well Name
Liberty	1	Moss Bluff Storage Ventures Test Hole #1
	2	Texasgulf Sergeant #13
	3	Texasgulf Sergeant #48
	4	Texasgulf Sergeant #801
	5	Texasgulf Sergeant #47
	6	Texasgulf Sergeant #63
	7	Texasgulf Sergeant #62
	8	Texasgulf Sergeant #945
	9	Texasgulf Sergeant #950
	10	Texasgulf Sergeant #360
	11	Texasgulf Sergeant #345
	12	Texasgulf Sergeant #359
	13	Texasgulf Sergeant #249
	14	Texasgulf Sergeant #245
	15	Texasgulf Sergeant #993
	16	Texasgulf Sergeant #155
	17	Texasgulf Sergeant #671
	18	Texasgulf Sergeant #1023
	19	Texasgulf Sergeant #681
	20	Texasgulf Sergeant #685
	21	Texasgulf Sergeant #933
	22	Texasgulf Sergeant #80

Appendix (cont.)
Stratton Ridge Dome
Cross Section A-A'

County	Cross Section Well Number	Well Name
Brazoria	1	Empire #3
	2	Empire #2
	3	Empire #1
	4	Freeport Sulfur #1 Brock
	5	Humble #1
	6	Freeport Sulfur #1 Storrie
	7	Freeport Sulfur #2 Brock
	8	Freeport Sulfur #3 Brock
	9	Freeport Sulfur #4 Seaburn
	10	Roxana #1
	11	Roxana #2
	12	Roxana #3
	13	Humble #B-2

Cross Section B-B'

Brazoria	1	Freeport Sulfur #2 Storrie
	2	Freeport Sulfur #7 Brock
	3	Castell #1
	4	Union Sulfur #1 Brock
	5	Dow Chemical #1
	6	Freeport Sulfur #1
	7	Number 4
	8	Number 6
	9	Farish #3
	10	Freeport Sulfur #2
	11	Bowman #1
	12	Cockrell #2
	13	Rycade #1
	14	Rycade #4
	15	Rycade #3

Appendix (cont.)
 Stratton Ridge Dome
 Cross Section C-C'

County	Cross Section Well Number	Well Name
Brazoria	1	Empire #3
	2	Empire #2
	3	Empire #1
	4	Roxana #4
	5	Freeport Sulfur #4 Seaburn
	6	Roxana #2
	7	Bowman #1
	8	Rycade #1
	9	Rycade #4
	10	Rycade #3
	11	Rycade #2

Cross Section Y-Y'

Brazoria	1	Empire #3
	2	Empire #2
	3	Freeport Sulfur #4 Brock
	4	Freeport Sulfur #1 Brock
	5	Humble #1
	6	Freeport Sulfur #1 Storrie
	7	Pruit et al. #2-A
	8	Freeport Sulfur #2 Storrie

Appendix (cont.)
 Stratton Ridge Dome
 Cross Section Z-Z'

County	Cross Section Well Number	Well Name
Brazoria	1	Gulf #2
	2	Freeport Sulfur #1 Seaburn
	3	Freeport Sulfur #1 Tolar
	4	Brine Well #6
	5	Freeport Sulfur #1 Storrie
	6	Freeport Sulfur #2 Seaburn
	7	Roxana #4
	8	Dow Chemical #9 Brock
	9	Freeport Sulfur #4 Seaburn
	10	Freeport Sulfur #3 Brock
	11	Union Sulfur #1 Brock
	12	Freeport Sulfur #6 Brock
	13	Dow Chemical #1
	14	Freeport Sulfur #1
	15	Number 5
	16	Number 2
	17	Number 6
	18	Freeport Sulfur #2
	19	Number 10

Appendix (cont.)
 Boling Salt Dome
 Cross Section A-A'

County	Cross Section Well Number	Well Name
Wharton	1	Pan American Prod. Co. #2 Brooks-Gary
	2	Josey & Halbouty #1 Gary Estate
	3	Texas Co. #A-18 Taylor
	4	Greenbriar Corp. #5-B J. B. Gary Estate
	5	Greenbriar Corp. #4-B J. B. Gary Estate
	6	Texas Co. #8-A S. T. Taylor
	7	Texas Co. #A-14 Taylor
	8	Texas Co. #2 S. T. Taylor
	9	Thomas H. Abell et al. #2 Texasgulf Sulfur Fee
	10	Neaves Pet. Dev. Co. #10 B. M. Floyd
	11	Rose Tex Oil Co. #1 Ruth C. Harrison
	12	Atlantic Oil Prod. Co. #1 Ruth Harrison
	13	Sun Oil Co. #7 E. W. Thomas
	14	Longmire & Beall #1 S. L. Bay
	15	Hyde Prod. Co. #1 Joe Robbins et al.
	16	Claude Knight #2 Fojtik
	17	Leigh J. Sessions #1 Joe Davidek
	18	George Hyde #1 Frank Sitta
	19	G. R. Gentry #3 Sitta
	20	Wellco Oil Co. #3-W Frank Sitta
Fort Bend	21	Callery & Hurt #1 Texasgulf Sulfur Fee
	22	John B. Coffee #4 Texasgulf Sulfur Fee
	23	Callery & Hurt #1 Kasperek
	24	Midland Oil Co. #1 P. F. Coulter

Appendix (cont.)
 Boling Salt Dome
 Cross Section B-B'-B''

County	Cross Section Well Number	Well Name
Wharton	1	Luling Oil & Gas Corp. and Royal Oil and Gas Corp. #1 Urbanovsky and Outlar
	2	Kennon & Cantrell #1 L. B. Outlar
	3	Universal Pet. Corp. #1 Hawes
	4	McKenzie Bros. Oil and Gas Co. #1 Cora Riggs
	5	Roy R. Gardner #2 R. G. Hawes
	6	Sun Oil Co. #3 E. W. Thomas
	7	Sun Oil Co. #5 E. W. Thomas
	8	Sun Oil Co. #6 E. W. Thomas
	9	Sun Oil Co. #7 E. W. Thomas
	10	Preston E. Anderson #B-1 Anderson
	11	Texasgulf Sulfur Co. #12 McCarson
	12	Texasgulf Sulfur Co. #10 McCarson
	13	Texasgulf Sulfur Co. #4 McCarson
	14	Texasgulf Sulfur Co. #A-2 W. H. Keller
	15	Texasgulf Sulfur Co. #5 Feltz
	16	L. Patterson #14 S. L. Bay
	17	Texasgulf Sulfur Co. #5 S. L. Bay Blk. 1
Fort Bend	18	Texas Co. #2 E. C. Farmer
	19	Coastal Minerals Inc. #C-37 J. R. Farmer

Appendix (cont.)
 Boling Salt Dome
 Cross Section C-C'

County	Cross Section Well Number	Well Name
Wharton	1	E. L. Buckley #1 Texasgulf Sulfur Fee
	2	Danciger Oil & Ref. Co. #6 A. A. Mullins
	3	Danciger Oil & Ref. Co. #4 A. A. Mullins
	4	Danciger Oil & Ref. Co. #3 A. A. Mullins
	5	Danciger Oil & Ref. Co. #7 A. A. Mullins
	6	Danciger Oil & Ref. Co. #1 A. A. Mullins
	7	Danciger Oil & Ref. Co. #1 Autrey
	8	Danciger Oil & Ref. Co. #1 Hawes Est.
	9	Texas Co. #A-14 Taylor
	10	Greenbriar Corp. #1 J. Brooks Gary Est.
	11	Texas Co. #2-B S. T. Taylor
	12	M. J. Halbouty #1 Gary-Hogg

Appendix (cont.)
 Boling Salt Dome
 Cross Section D-D'

County	Cross Section Well Number	Well Name
Wharton	1	Smith & Smith #2 Loudie T. Mick
	2	Sinclair Prairie Oil Co. #1 W. R. Taylor
	3	Beall Oil Co. #2 R. H. Vineyard
	4	Kirby Pet. Co. #2 Dagley
	5	Kennon & Cantrell #1 C. Hackstedt
Fort Bend	6	Callery & Hurt #1 Kasperek
	7	Sun Oil Co. #1 H. R. Farmer Est.

Cross Section E-E'

Wharton	1	Duval Sulfur #16
	2	Duval Sulfur #676
	3	GP Co. #1
	4	Duval Sulfur #19
	5	Miller #2
	6	Duval Sulfur #105
	7	Duval #5
	8	Duval #97
	9	Texasgulf Sulfur #2298
	10	Texasgulf Sulfur #602

Appendix (cont.)
 Boling Salt Dome F-F'Core Cross Section

County	Cross Section Well Number	Well Name
Wharton	1	Texasgulf Sulfur Taylor #172
	2	Texasgulf Sulfur Taylor #176
	3	Texasgulf Sulfur Taylor #171
	4	Texasgulf Sulfur Chase #2292
	5	Texasgulf Sulfur Chase #2303
	6	Texasgulf Sulfur Chase #2302
	7	Texasgulf Sulfur Chase #2304
	8	Texasgulf Sulfur Chase #2294
	9	Texasgulf Sulfur Chase #2293
	10	Texasgulf Sulfur Chase #2295
	11	Texasgulf Sulfur Chase #2291
	12	Texasgulf Sulfur Chase #2301
	13	Texasgulf Sulfur Chase #2300
	14	Texasgulf Sulfur Chase #2298
	15	Texasgulf Sulfur Chase #2299
	16	Texasgulf Sulfur Chase #2297
	17	Texasgulf Sulfur Abendroth #606
	18	Texasgulf Sulfur Abendroth #589
	19	Texasgulf Sulfur Abendroth #595
	20	Texasgulf Sulfur Abendroth #600
	21	Texasgulf Sulfur Abendroth #587
	22	Texasgulf Sulfur Abendroth #599
	23	Texasgulf Sulfur Abendroth #592
	24	Texasgulf Sulfur Abendroth #601
	25	Texasgulf Sulfur Abendroth #596
	26	Texasgulf Sulfur Abendroth #602
	27	Texasgulf Sulfur Abendroth #605
	28	Texasgulf Sulfur Abendroth #593
	29	Texasgulf Sulfur Abendroth #598
	30	Texasgulf Sulfur Abendroth #591
	31	Texasgulf Sulfur Abendroth #604
	32	Texasgulf Sulfur Abendroth #590

**GEOLOGY AND HYDROGEOLOGY,
BARBERS HILL SALT DOME, TEXAS**

by

H. S. Hamlin

CONTENTS

INTRODUCTION	184
Major Findings	188
GENERAL GEOLOGY	189
Dome Geometry	189
Cap Rock	191
Stratigraphy	195
Structure	203
Growth History	205
HYDROGEOLOGY	208
Hydrogeologic Units	209
Burkeville Aquitard	209
Evangeline Aquifer	211
Chicot Aquifer	212
Hydrochemistry	213
Ground-Water Salinity	214
Hydrochemical Facies	219
Temporal Changes in Composition and Salinity	222
REFERENCES	223
APPENDICES	
1. Barbers Hill Driller's Logs	229
2. Barbers Hill Electric Logs	232

Figures

1. Location map, Barbers Hill Dome	185
2. Structure-contour map, Barbers Hill Dome	186
3. General distribution of cap-rock facies and porous zones, Barbers Hill Dome	190

4.	Distribution of lost-circulation zones in the upper part of Barbers Hill caprock	194
5.	Dip-oriented structural cross section, Barbers Hill area	197
6.	Structure-contour map, top of Frio Formation	199
7.	Generalized net sand map, lower Chicot aquifer	202
8.	Well-control index map, Barbers Hill Dome	204
9.	Fence diagram, Barbers Hill Dome	207
10.	Distribution of total dissolved solids in water wells around Barbers Hill.	215
11.	Distribution of chloride concentrations in water wells around Barbers Hill.	216
12.	Piper diagrams of water-well chemical analyses, Barbers Hill area	221
13.	Graph of dissolved ions concentrations in public water supply	228

Tables

1.	Stratigraphic column, Barbers Hill area	196
2.	Hydrogeologic units, Barbers Hill area	210
3.	Total dissolved solids and chloride concentrations in water wells, Barbers Hill area	217

INTRODUCTION

Many Texas salt domes support multiple uses by man. Some of these uses are hydrocarbon production and storage, salt and cap-rock mining, brine production and disposal, as well as surficial concentrations of industrial and municipal facilities. Should disposal of toxic chemical waste be added to this list? Barbers Hill Dome is a leading example of a Texas coastal dome with a long and complex history of resource recovery, including oil production, storage of hydrocarbons in solution-mined caverns in salt, and disposal of brines into cap-rock lost-circulation zones. In this section, the general hydrogeologic and geologic conditions around Barbers Hill Dome are described. These data were analyzed to determine what, if any, influence this resource recovery has had on the hydrogeologic system. With this analysis, we will be able to better understand the long-term effects of proposed toxic waste disposal in domes.

Barbers Hill salt dome is located in northwestern Chambers County, Texas, 20 mi (32 km) east of Houston and 5 mi (8 km) northeast of Baytown (fig. 1). A hill rising 40 ft (12 m) above the surrounding flat-lying coastal plain overlies the dome (fig. 2). The City of Mont Belvieu (population 1,500) covers the eastern half of Barbers Hill, and the surface facilities of the world's largest salt-cavern hydrocarbon storage operations occupy the western half. Nine companies store almost 160 million bbl of light hydrocarbons in about 137 caverns in Barbers Hill Dome (Seni and others, 1984a, 1984b).

Barbers Hill Dome has a multifaceted history of use by the oil and gas industry. A large, mature (discovered in 1916) oil field surrounds the dome. Oil is trapped in Eocene to Miocene strata truncated or pinched out against the dome flanks. Annual production is over 400,000 bbl, and accumulative oil production to January 1, 1985, is 129,273,134 bbl (Railroad Commission of Texas).

Salt-cavern storage operations began in the 1950's. Solution-brine production began about this same time, and a number of brine caverns have been converted to hydrocarbon

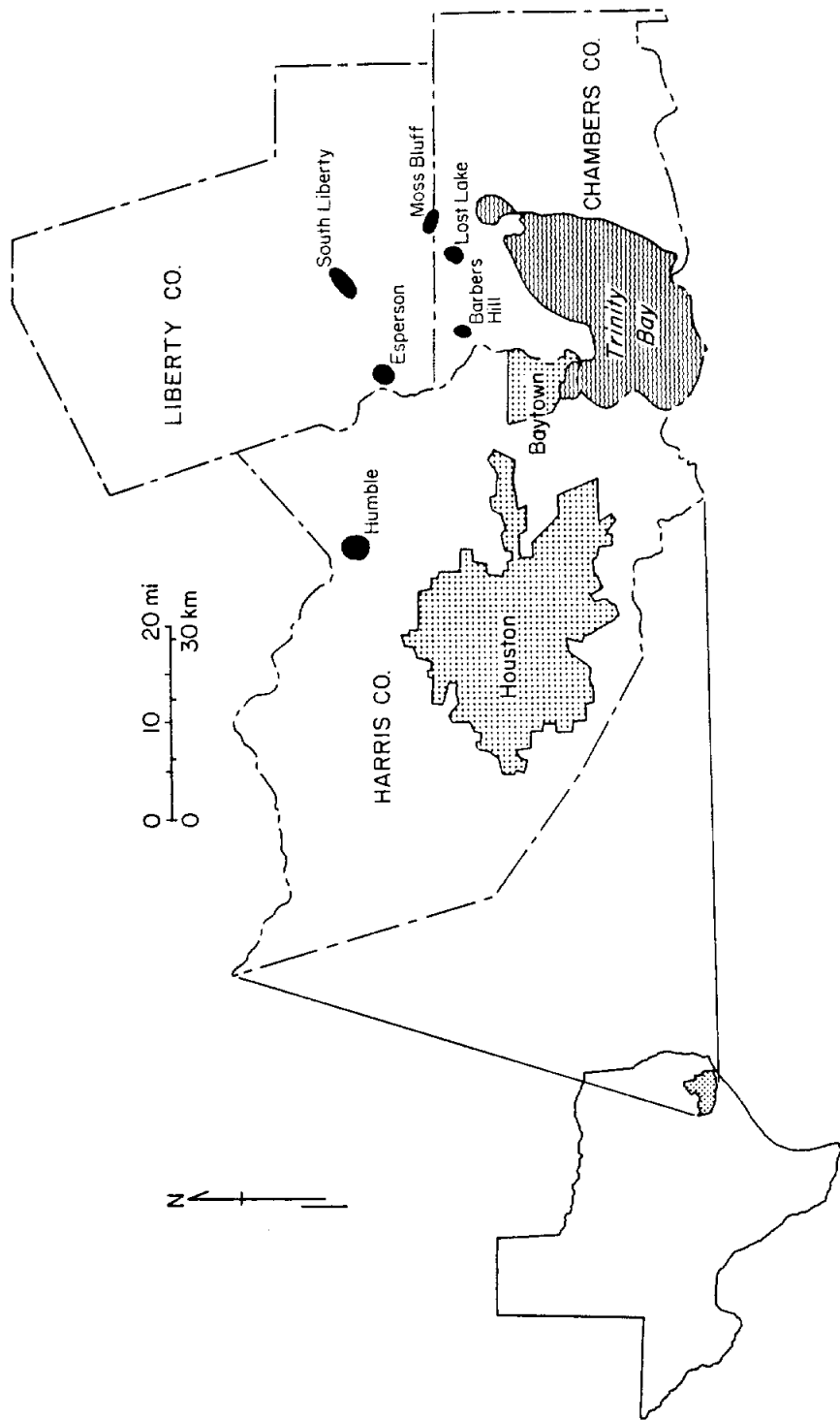


Figure 1. Location map, Barbers Hill salt dome, surrounding domes, and population centers.

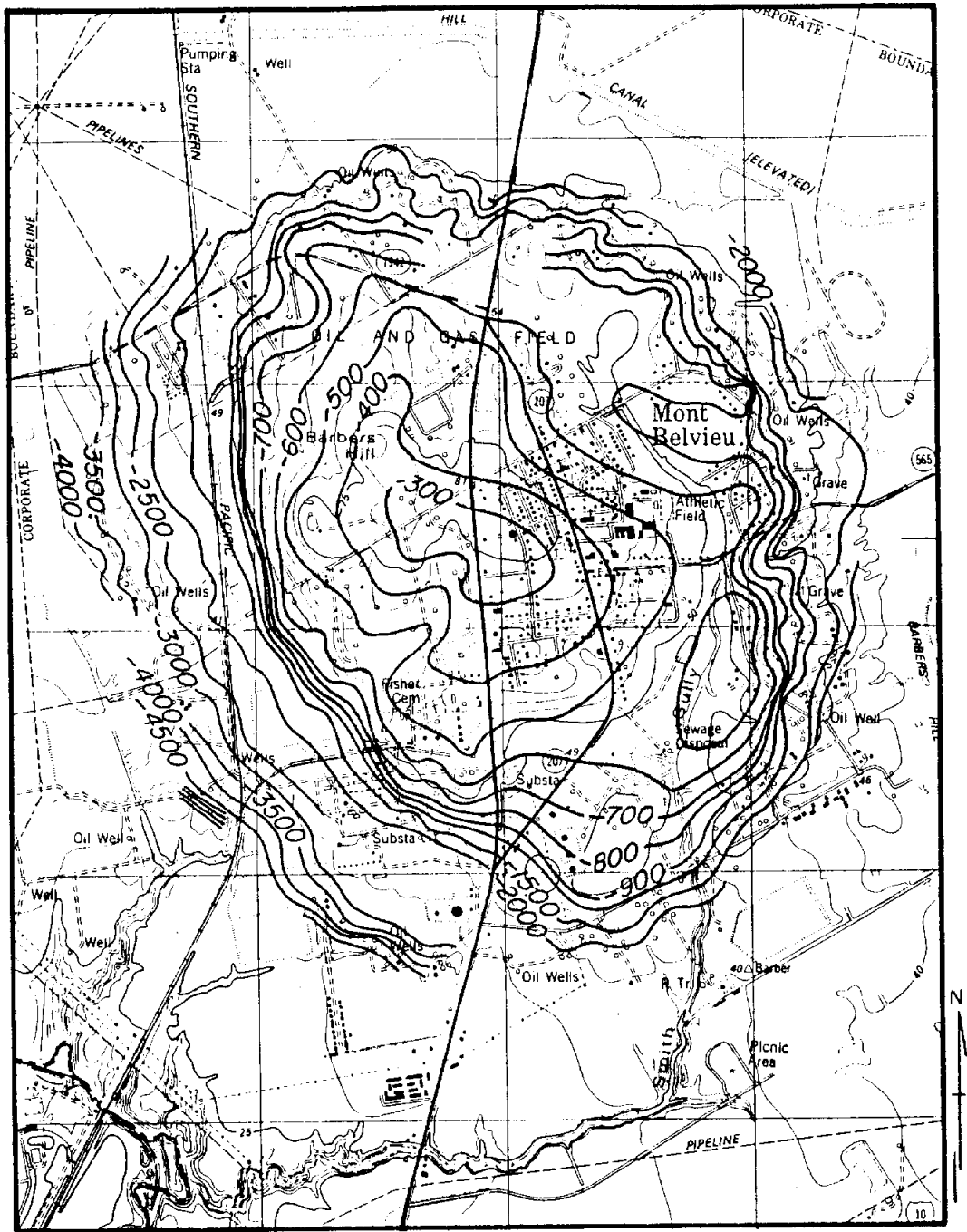


Figure 2. Structure-contour map of Barbers Hill Dome (Behrman, 1967) constructed on a topographic base, also showing cultural features.

storage caverns. Saltwater disposal in Barbers Hill cap rock began in 1956. An estimated 1.5 billion bbl of salt water have been injected into porous zones in the cap rock (Underground Resource Management, Inc., 1982). Currently, about 19 disposal wells inject 1 to 5 million bbl/mo (Railroad Commission, Underground Injection Control). Most of the brine disposed in cap rock is produced during storage-cavern construction and product storage.

Large amounts of ground water are produced relatively close to Barbers Hill Dome. Over 500 million g/d are withdrawn from shallow aquifers in the Houston area (Gabrysch, 1980). Although the Mont Belvieu area is one of the main ground-water production centers in Chambers County, only about 4 million g/d are produced in the entire county (Wesselman, 1971). However, ground-water development is extensive along the Harris/Chambers county line (Mont Belvieu/Baytown area).

Problems and potential problems are associated with high-density use of surface and subsurface resources around Barbers Hill. Salt caverns have failed, resulting in loss of product and endangering Mont Belvieu residents (Underground Resource Management, Inc., 1982). The dense array of surface pipelines on and around Barbers Hill makes gas leakage, fires, and explosions potential problems. Ground-water contamination is an important potential problem. Shallow, fresh ground waters may be naturally contaminated through the dissolution of salt or cap rock, or contamination may be man-induced. Brines disposed in the cap rock may be flowing into the fresh-water aquifers that enclose it.

The objectives of this study were to examine the available geologic and hydrologic data from the Barbers Hill area, and from this data, to describe the local geology, hydrogeology, and ground-water hydrochemistry. Because salt domes of the Texas Gulf Coast are geologically similar, general conclusions may be extrapolated from this study and applied to other coastal domes for which less data are available. A clear understanding of the architecture of the salt dome, cap rock, surrounding sediments and the hydrologic system, including three-dimensional permeability distribution, water-rock chemical

reactions, and ground-water flow patterns (Smith, this volume), could be invaluable in making important decisions affecting future industrial (including waste disposal), agricultural, and municipal activities around salt domes. The geology of the salt stock, cap rock, and surrounding strata needs to be understood in order to assess the stability of a salt dome for long- and short-term safe containment of toxic chemical wastes.

Major Findings

1. The cap rock at Barbers Hill is characterized by areas of high porosity and permeability called lost-circulation zones. The presence of gypsum and calcite in these zones indicates that ground-water circulation is occurring there.

2. The planar configuration of the salt/cap-rock contact and the presence of a layer of loose anhydrite grains overlying this contact indicate that ground-water flux and salt dissolution are occurring there.

3. Shallow sediments (less than 2,000 ft or 610 m) close around Barbers Hill cap rock are generally 30 to 75 percent sand, decreasing to 20 percent or less over the dome crest. Both shale and sand bodies are relatively locally continuous around the dome.

4. The large area of contact between cap rock and shallow aquifer sands indicates that permeable interconnections are likely at a number of different levels and locations.

5. The Burkeville aquitard is not a barrier to ground-water flow between the cap rock and the fresh-water aquifers, because these units contact each other above the level of the Burkeville.

6. Stratigraphic and structural data indicate that dome growth has slowed since the Eocene, but is still continuing today at a rate of about 40 to 60 ft (12 to 18 m) of uplift per million years. This low rate of diapirism would not be a significant factor affecting long-term stability of a toxic waste repository.

7. Ground-water salinities in individual aquifer sands increase with proximity to the dome.

8. A comparatively high degree of well-to-well variability in salinity and composition characterizes ground waters around the dome, including small areas of very poor water quality.

9. Compositionally, lower Chicot aquifer ground waters have, on average, greater proportions of dissolved sodium and chloride around Barbers Hill than they do outside this area.

10. A large and growing area of saline water in the lower Chicot aquifer extends several miles west and southwest of the dome and recently began to appear in public supply water wells northwest of the dome.

GENERAL GEOLOGY

Dome Geometry

Barbers Hill Dome is slightly elliptical in map view (fig. 2). The major axis is oriented northwest-southeast. Maximum cross-sectional area occurs 2,000 ft (610 m) below sea level. At this level the major axis is 11,600 ft (3,540 m) long, the minor axis is 9,000 ft (2,740 m) long, and the cross-sectional area is 2.7 mi² (7.0 km²). Between 6,000 ft (1,830 m) and 2,000 ft (610 m) below sea level, the north and south dome flanks diverge upward, but the eastern and western flanks are roughly parallel. The diapir axis, a line joining centers of successive horizontal cross sections through the salt stock (Jackson and Seni, 1984), plunges westward about 70°. This gives the dome an eastward tilt (fig. 3). The shape of Barbers Hill Dome below 6,000 ft (1,830 m) is relatively unknown.

Barbers Hill Dome has well-developed overhangs on all sides except possibly on the southwest, where overhang, if present, is deeper than 6,000 ft (1,830 m) below sea level. On the northern dome flank and continuing clockwise around to the southeastern flank, the overhang is 2,000 ft (610 m) below sea level and extends 400 to 1,640 ft (120 to 500 m) beyond the limits of the dome 6,000 ft (1,830 m) below sea level. From there the level of

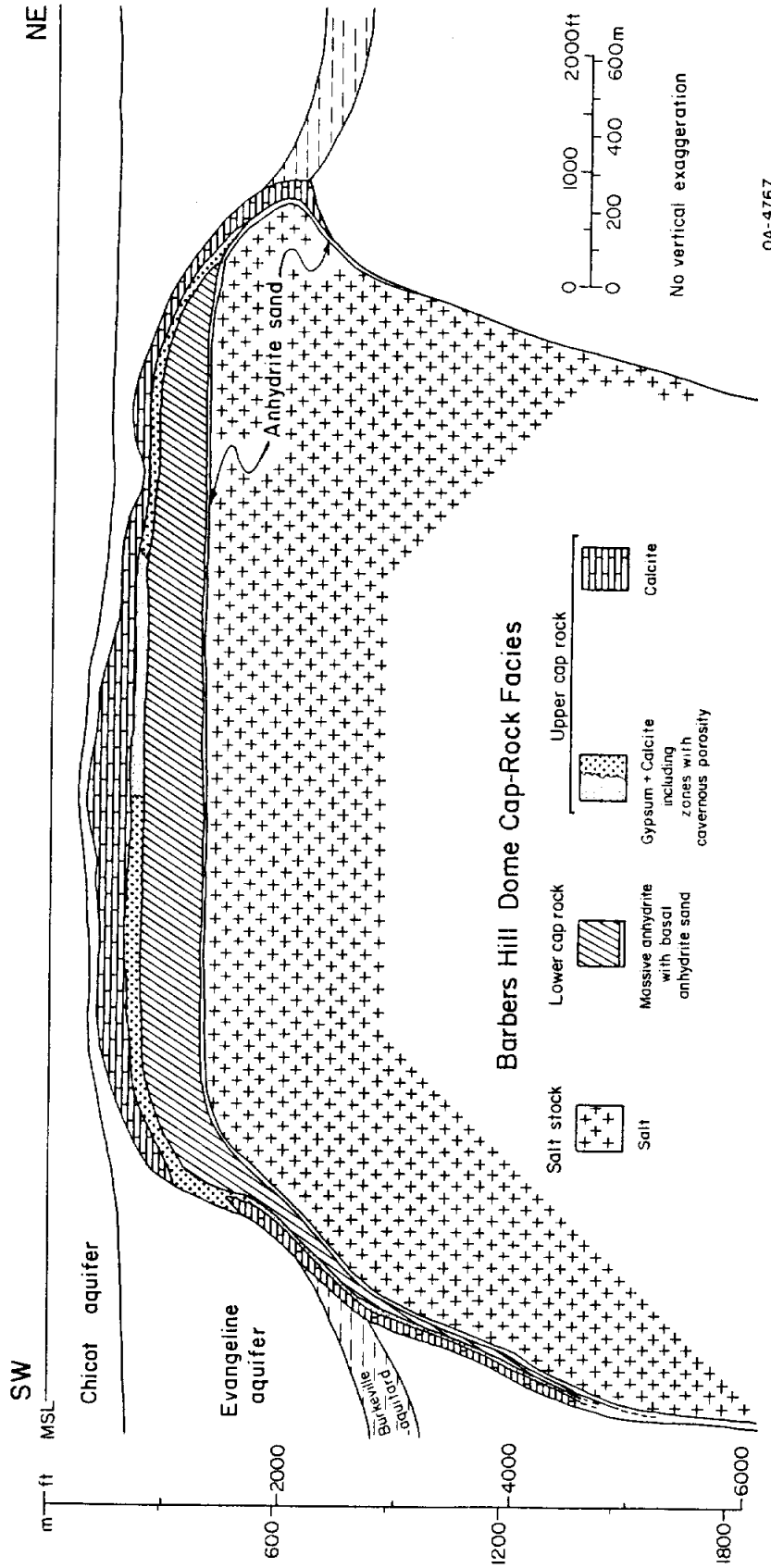


Figure 3. Generalized distribution of cap-rock facies and porous zones, Barbers Hill Dome. Line of section shown on figure 4. Data compiled from Railroad Commission Hearings files.

overhang descends the dome flanks in both directions around the dome toward the southwest.

From dome center to perimeter, top of salt at Barbers Hill is a nearly horizontal planar surface slightly greater than 1,300 ft (396 m) below sea level. The sides of the salt stock are more irregular, with dips ranging from about 40° to greater than 90° beneath overhangs. Several wells penetrated multiple, thick salt sections when drilling was close to the deeper dome flanks. If these holes are reasonably straight, then the dome flanks have salt projections and embayments with dimensions on the order of hundreds of feet or meters.

The shape of Barbers Hill Dome is a function of the interplay between upward salt flow and the dissolving powers of ground water. The planar top of salt delineates a horizontal zone above which active ground-water flow dissolves and removes salt. The uneven configuration of the dome flanks suggests a more irregular distribution of dissolution that may correspond to permeability heterogeneities in enclosing sediments.

Cap Rock

Cap rock at Barbers Hill is between 500 and 900 ft (150 and 275 m) thick over the dome crest, rising to less than 350 ft (107 m) below sea level (figs. 2 and 3). It thins irregularly toward the periphery of the dome, but maintains a vertical thickness of several hundred feet down the flanks to the levels of overhang. Examination of driller's (lithologic) logs reveals that the cap-rock/sediment contact is gradational and irregular. Masses of secondary calcite occur above and lateral to this contact and "false cap" carbonate cementation is common, especially adjacent to the dome flanks. Secondary mineralization locally extends outward from the cap rock concordant with bedding in surrounding sediments. In a few places on the western dome flank cap rock is missing entirely and sediments directly contact underlying salt. Thin cap rock below overhanging salt is also unevenly distributed. The cap-rock/salt contact is planar on the dome crest and relatively

smooth along the flanks. The cap-rock/sediment contact has a pattern of structural relief that is similar to and roughly concordant with the topography of the overlying land surface (fig. 2).

The cap rock is composed mainly of anhydrite, gypsum, and calcite arranged in irregular layers or zones (Bevier, 1925). A thick zone of anhydrite occurs closest to salt (fig. 3). It ranges from about 500 ft (150 m) thick on the crest to 25 ft (8 m) thick or less down the flanks and under overhanging salt. The anhydrite occurs in two forms: a lower, thin (25 ft or 8 m) layer of loose sand-sized anhydrite crystals overlain by a much thicker section of massive crystalline anhydrite (Judson and others, 1932). Anhydrite is overlain by a 40- to 200-ft (12- to 60-m) thick transition zone of mostly gypsum, but with variable amounts of anhydrite and secondary calcite and minor amounts of native sulfur and sulfides (Bevier, 1925). The transition zone separates the lower anhydritic and the upper calcitic cap rock (fig. 3).

The upper part of the cap rock is dominantly calcite. Its thickness and distribution are more irregular than the other cap-rock zones. This calcite is hard, dense, frequently fractured or brecciated, and apparently formed mainly by secondary alteration of calcium sulfate to calcium carbonate (Bodenlos, 1970).

These cap-rock zones or facies are, in detail, more heterogeneous and complexly distributed than outlined here. Bevier's (1925) statement about "no two sections [through the cap rock] being alike" is probably accurate. Several gypsum transition zones or none may be present locally. The lower cap-rock anhydrite zone is the most consistent and homogeneous, but even there variations are common.

Porosity and permeability in the cap rock at Barbers Hill Dome are also highly variable. Massive anhydrite and dense calcite typically have very low permeabilities. However, they are relatively soluble and have been subjected to the stresses of active diapirism. Therefore, the distribution and orientation of porosity and permeability in the cap rock depend on fracturing, brecciation, and dissolution. These processes have created

a vuggy to cavernous aquifer in the cap rock that is somewhat similar to a karstic limestone aquifer like the Cretaceous Edwards Formation of Central Texas. Zones of very high porosity and permeability control the overall hydrodynamic properties of the Barbers Hill cap rock.

The high-permeability pathways in Barbers Hill cap rock are called lost-circulation zones (Seni and others, 1984b). These zones are often so porous and permeable that it is difficult to get drilling mud to circulate back to the surface after a well penetrates one. The lost-circulation zones are probably distributed more or less irregularly throughout the cap rock. Several larger, more continuous lost-circulation zones have long been recognized and mapped (figs. 3 and 4).

The basal cap-rock anhydrite sand is unconsolidated, porous, permeable, and continuous across the cap-rock/salt contact. It extends under overhanging salt where it forms part of a "gouge zone" (Judson and others, 1932). This anhydrite sand is a residue of salt dissolution, has intergranular porosity, and therefore must have hydrologic properties similar to those of a sand or sandstone aquifer.

The second major lost-circulation zone is the gypsum/calcite transition zone that is in the upper cap rock, but which probably extends irregularly into the other cap-rock facies (figs. 3 and 4). High permeability is the result of a network of fractures and breccia zones that have been enlarged by dissolution. Porosity is vuggy to cavernous. The lateral continuity of this lost-circulation zone is problematic. It has been mapped as discontinuous, but it behaves hydraulically as a single integrated aquifer (Smith, this volume). The mapped extent (fig. 4) may represent the most cavernous areas in an extensive and continuous network of fracture-generated permeability.

The degree of interconnection of the lost-circulation zones and the extent of their communication with the enclosing sedimentary aquifers are not well understood. The basal anhydrite sand may be a conduit for ground-water flux, connecting the deeper dome flanks with the truncated top of salt (fig. 3). The presence of loose anhydrite grains at the

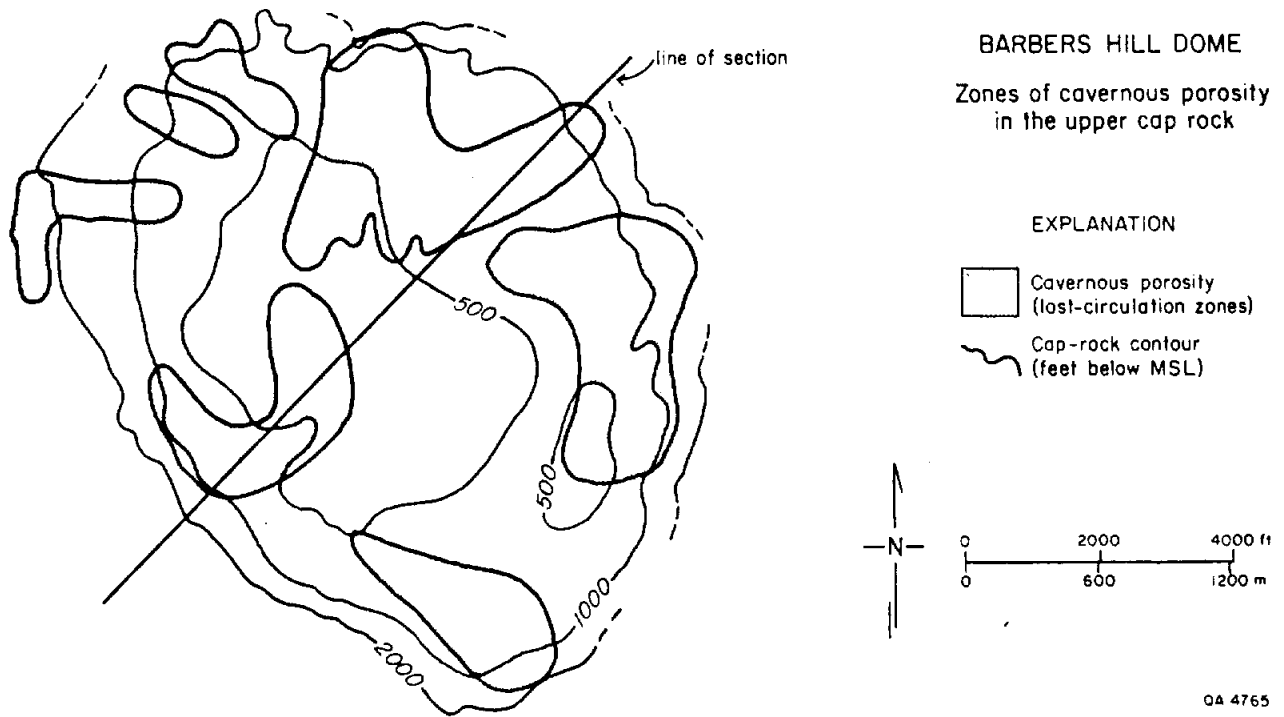


Figure 4. Distribution of lost-circulation zones in the upper part of Barbers Hill cap rock. Mapped by R. G. Behrman (1967).

salt/cap-rock interface indicates that fluid flux and salt dissolution are occurring there. In terms of permeability interconnections in the upper cap rock, two general situations are possible: (1) lost-circulation zones intersect the cap-rock/sediment contact above the level of top of salt by extending through the upper cap-rock calcite zone (fig. 3, left side); or (2) lost-circulation zones intersect the basal anhydrite sand which may extend down the dome flank without intersecting the cap-rock/sediment contact above the level of overhang (fig. 3, right side). Both of these possibilities are likely to exist somewhere in the heterogeneous body of Barbers Hill cap rock.

Stratigraphy

Barbers Hill Dome is surrounded by about 50,000 ft (15,000 m) of Mesozoic and Cenozoic sediments (McGookey, 1975), but the practical limit of well control is 12,000 ft (3,660 m) below sea level. This interval consists of terrigenous clastics of Eocene to Recent age (table 1). Stratigraphic and structural patterns were delineated and analyzed around Barbers Hill Dome in order to estimate the growth history and tectonic stability of the dome, and to characterize the aquifer/reservoir properties of the surrounding sedimentary strata.

The Yegua Formation (Eocene) was deposited by prograding deltas whose main sand depocenters never reached downdip quite as far as Barbers Hill Dome (Fisher, 1969). Distal delta front sands, each a few tens of feet or meters thick, make up from 0 to 15 percent of the Yegua around Barbers Hill (fig. 5). The rest of the formation consists of prodelta shales deposited seaward of the main deltaic depocenters. Thickness variations in the Yegua at Barbers Hill could not be determined because its base is below the limit of well control. Deep Yegua oil production at Barbers Hill, discovered in 1974, has totaled only a few thousand barrels.

The Vicksburg and Jackson Groups (Eocene to Oligocene) are nearly 100 percent prodelta and marine shales around Barbers Hill Dome (fig. 5). Age-equivalent deltaic sand

Table 1. Stratigraphic column, Barbers Hill area.

System	Series	Stratigraphic unit	Depositional systems	Top contact dome ft(m)	Isopach range ft(m)	Regional isopach ft(m)	Percentage thickening	Percentage thinning
Quaternary	Holocene	Undifferentiated	Fluviodeltaic	--	300-600 (90-180)	500 (150)	20	40*
	Pleistocene							
	Pliocene							
Miocene		Goliad Formation	Fluvial	--	30-1,800 (9-550)	1,700 (520)	6	98*
		Lagarto Formation	Coastal plain	2,000 (610)	1,400-1,700 (430-520)	1,600 (490)	6	12
		Oakville Formation	Coastal plain shoreline	3,400 (1,040)	1,400-2,000 (430-610)	1,700 (520)	18	18
Tertiary		Anahuac Formation	Marine	4,300 (1,310)	300-500 (90-150)	400 (120)	25	25
	Oligocene	Frio Formation	Deltaic	4,600 (1,400)	1,000-2,200 (300-670)	1,800 (550)	22	44
		Vicksburg Group Jackson Group	Prodeltaic marine	5,600 (1,710)	1,600-2,600 (490-790)	2,000 (610)	30	20
		Yegua Formation	Deltaic prodeltaic	7,600 (2,320)	?	>2,000 (>610)	?	?

*super domal thinning

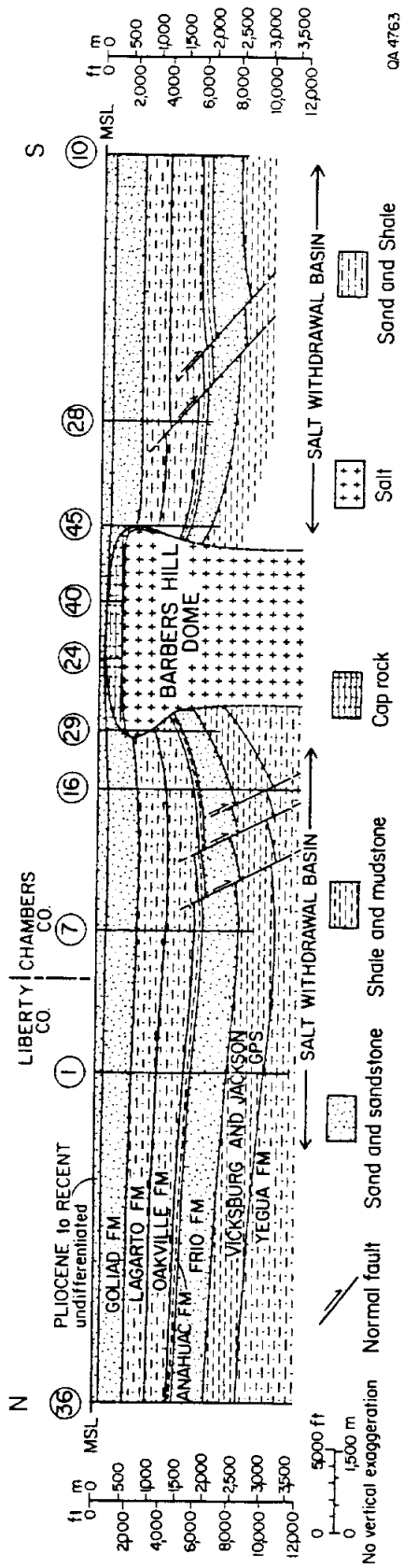


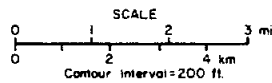
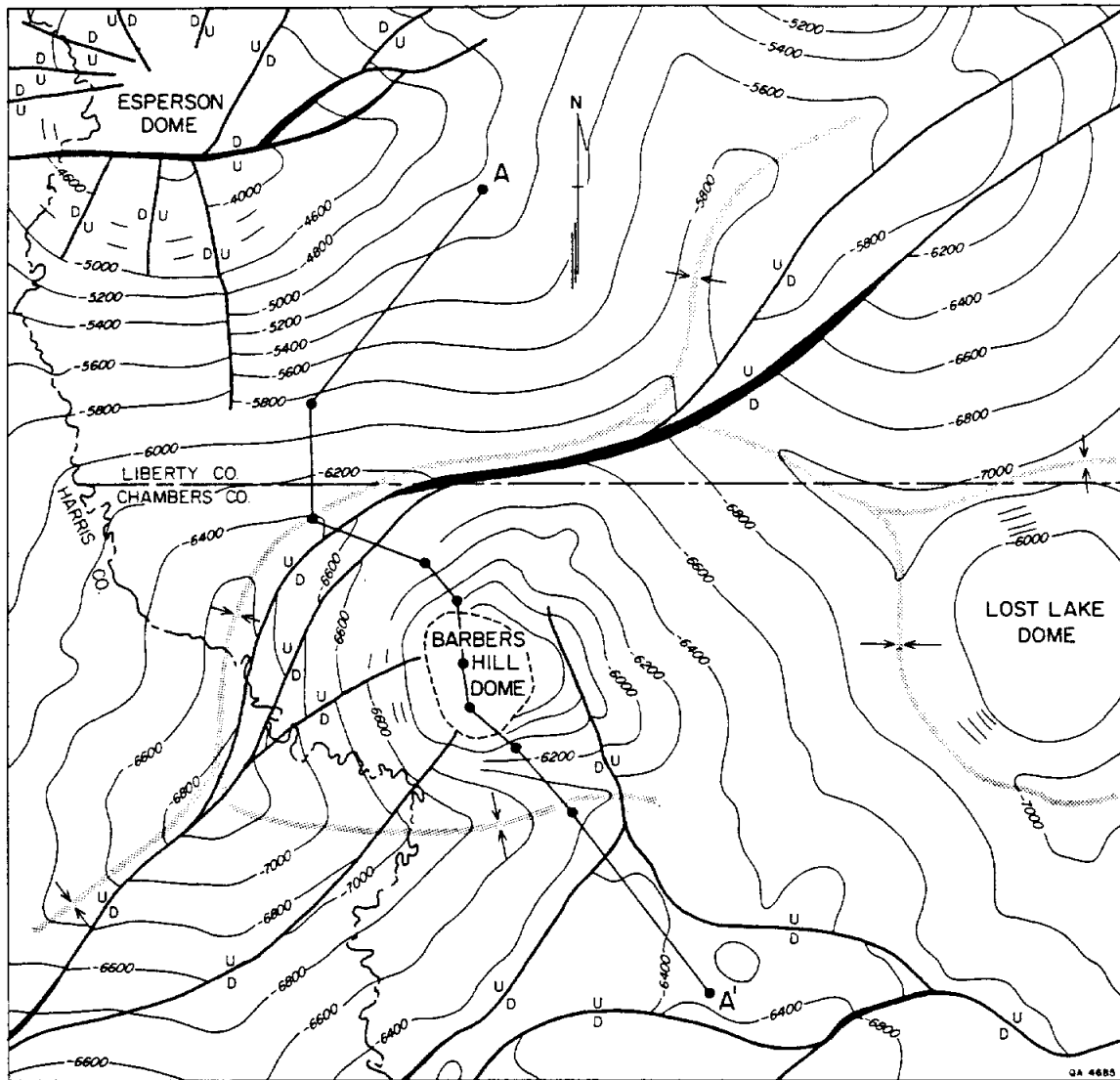
Figure 5. Dip-oriented structural cross section, Barbers Hill area. Line of section shown on figure 6.

depocenters occur updip in San Jacinto and northern Liberty Counties (Fisher and others, 1970). Near the top of this interval (Vicksburg Formation) a few isolated sands, 5 to 20 ft (2 to 6 m) thick, are present, signaling the beginning of the succeeding Frio deltaic progradation. Vicksburg/Jackson shales could be source rocks for oil trapped against the flanks of the dome in overlying Oligocene and Miocene sand reservoirs.

Barbers Hill Dome is located in the middle of a large Frio Formation (Oligocene) deltaic depocenter, named the Houston delta system by Galloway and others (1982). The Frio is 40 to 70 percent sand around Barbers Hill (fig. 5). Stacked delta-front and shoreline sand bodies dominate the lower part of the interval, whereas the upper part is a mixture of delta-front and delta-plain sands and shales. During Frio deposition the shoreline regressed seaward many miles, starting northwest of Barbers Hill and advancing southeast to the position of the present shoreline (Galloway and others, 1982). This was probably the first time since its formation that Barbers Hill Dome had significant amounts of nonmarine sediments deposited around it. Frio sands are the most prolific reservoir rocks in the Barbers Hill field. Dome growth-related thickness variations (table 1) and rim synclines due to salt withdrawal (fig. 6) are readily apparent in the Frio Formation.

The Anahuac Formation (Oligocene) was deposited during the extensive marine transgression that followed Frio progradation. The Anahuac is a wedge of shale that thickens downdip from 300 to 600 ft (90 to 180 m) in the Barbers Hill area (fig. 5), but also exhibits dome growth-related thinning and thickening close to the dome (table 1). During the Anahuac transgression Heterostegina sp. reef and related limestones accumulated around several domes in the Houston Embayment, including Barbers Hill (Collins, this volume). The "Het lime" is 0 to 80 ft (0 to 24 m) thick around Barbers Hill Dome. Reef-core communities probably colonized on dome-related bathymetric highs and shed debris into surrounding lows overlying salt-withdrawal basins.

In the Barbers Hill area, the Oakville Formation (Miocene) consists of sands and shales deposited along and landward of a rapidly advancing shoreline (Rainwater, 1964;



EXPLANATION

- | | | | |
|--|--------------------------------------|--|-----------------------------------|
| | Normal fault | | Cross section |
| | Axial trace of salt withdrawal basin | | Salt dome piercing Frio Formation |

Figure 6. Structure contour map, top of Frio Formation, showing deep faulting and salt-withdrawal basins around Barbers Hill, Lost Lake, Esperson, and South Liberty (off map top right) domes.

Galloway, 1985). The lower third of the formation is about one-half stacked shoreline sands and one-half nearshore shales. The upper two-thirds of the Oakville consists of coastal-plain fluvial sands (25 to 50 percent) and shales (fig. 5). A minor marine transgressive phase, the Amphistegina zone, occurs at the top of the Oakville and consists of a few hundred feet or meters of calcareous shales and sands.

The Lagarto Formation (Miocene) largely consists of nonmarine shales and sands in the Barbers Hill area (Murphy and Judson, 1930; Rainwater, 1964). This interval also contains significant amounts of calcareous sediments reworked from Cretaceous source rocks. The Lagarto is 15 to 35 percent sand and was deposited on a mud-rich coastal plain very similar to that which overlies Barbers Hill Dome today. This unit, as well as the alluvial part of the underlying Oakville, appears to be slightly sandier than average in the salt-withdrawal basins that surround Barbers Hill. The uppermost 300 to 500 ft (90 to 150 m) of the Lagarto Formation is the hydrogeologic unit known as the Burkeville aquitard (Wesselman, 1971; Baker, 1979).

The Goliad Formation (Miocene to ?Pliocene) is dominated by fluvial channel-fill sand bodies in the Barbers Hill area. The Goliad Formation is partly or entirely equivalent to the Willis Formation, which outcrops about 40 mi (64 km) north-northwest of Barbers Hill (Solis, 1981; Barnes, 1968). This unit is 50 to 80 percent sand around Barbers Hill. Percent sand generally increases upward through this formation, as does the freshness of the ground water it contains. Both the bases of brackish water and of fresh water generally occur within the Goliad in this area. This Goliad-Willis interval is equivalent to the hydrogeologic unit known as the Evangeline aquifer (Wesselman, 1971; Baker, 1979).

Goliad thickening into salt-withdrawal basins is subtle and largely masked by more obvious regional thickening to the south and southwest (fig. 5). Maximum withdrawal-basin thickening is only a few tens of feet or meters, but superdomal thinning is extreme (table 1). The top of the Goliad is the first stratigraphic horizon yet discussed that extends over Barbers Hill Dome (fig. 5). All underlying correlation horizons have been "pierced."

In the Barbers Hill area, the uppermost 500 to 600 ft (150 to 180 m) of sediments (Pliocene to Recent undifferentiated) were deposited in fluvial, deltaic, and marginal marine environments (Guevara-Sanchez, 1974). Glacially induced, rapid sea-level/shoreline fluctuations resulted in a complex but compressed stratigraphic record followed by an equally complex history of geologic study and nomenclatorial evolution (Guevara-Sanchez, 1974). However, around Barbers Hill, the general stratigraphy of this unit is relatively simple. The lower part of the interval, known hydrogeologically as the lower Chicot aquifer (Wesselman, 1971; Baker, 1979), is a single sand body, 30 to 300 ft (9 to 90 m) thick, with a few thin shale interbeds locally. The upper part of the interval, known as the upper Chicot aquifer, consists of 200 to 300 ft (60 to 90 m) of laterally discontinuous sands and shales.

The undifferentiated Pliocene to Recent unit is the only complete stratigraphic interval that overlies cap rock at Barbers Hill (fig. 5). Percent sand ranges from 30 to 75 percent around the dome, but decreases to less than 20 percent over the crest. Well-developed dome-related patterns of thickening and thinning occur in this interval (table 1). Salt-withdrawal basins around Barbers Hill Dome were favored locations for sandy fluvial and deltaic-distributary channels. The uplifted dome crest received mainly overbank (floodplain), fine-grained sediments.

Barbers Hill Dome is located along a Plio-Pleistocene fluvial axis (Fisher and others, 1972; Kreitler and others, 1977), a dip-oriented belt of coalesced and superimposed channel-fill sands delineating an area frequently reoccupied by rivers or delta distributaries. The dome appears as a "hole" (closed net-sand low) on the east side of a mapped lower Chicot channel-sand belt (fig. 7). The rivers that deposited this sand body frequently passed by the west dome flank, occasionally flowed around the east flank, but generally stayed close, following topographic lows that overlie salt-withdrawal basins. A shallow (Beaumont Formation) upper Chicot deltaic-distributary channel-sand belt wraps around the eastern flank of the dome and was mapped on aerial photographs (Fisher and others,

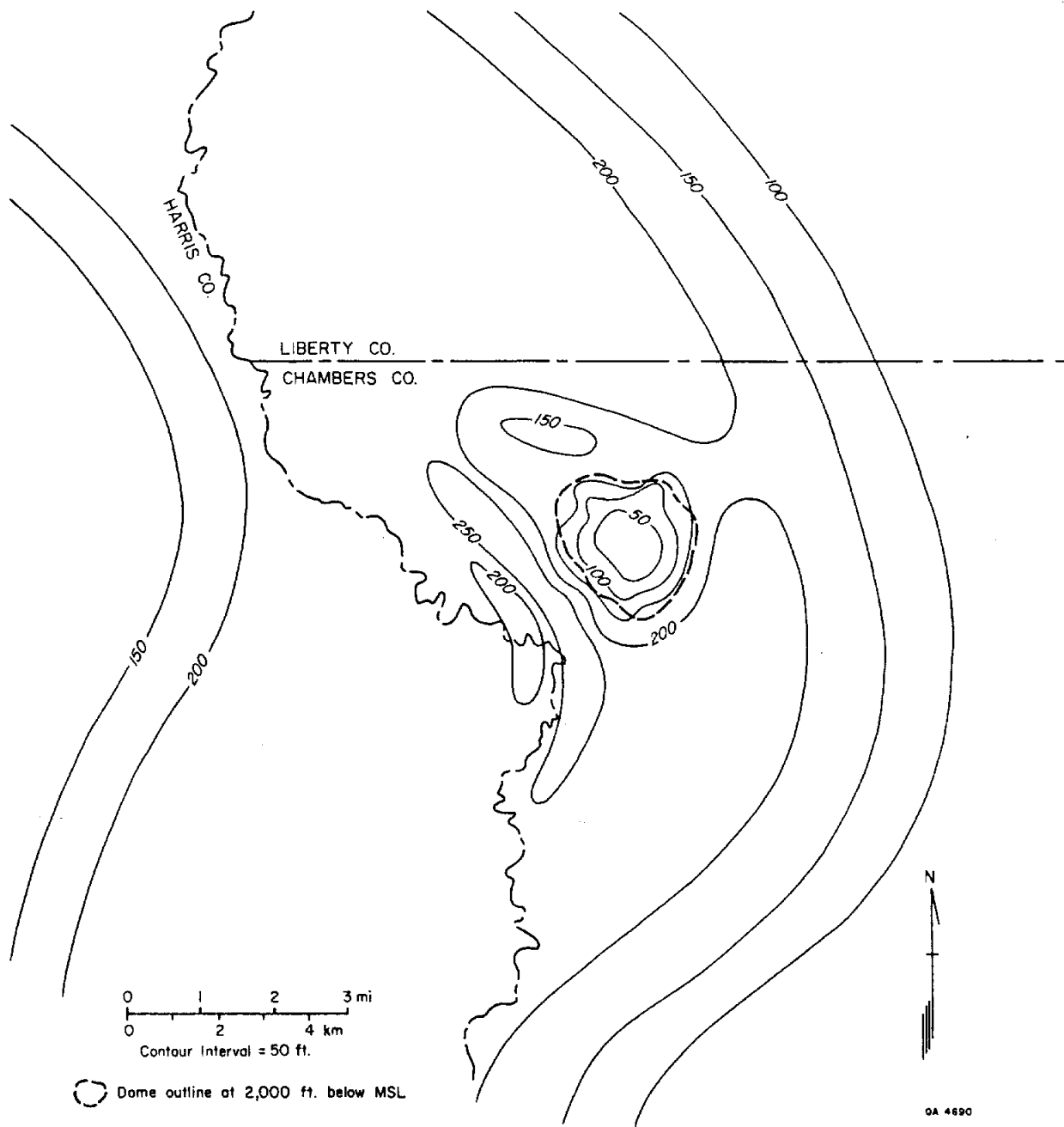


Figure 7. Generalized net sand map, lower Chicot aquifer. Dense well control used around dome, but sparse control used elsewhere.

1972). Despite this long period of channel deposition, the crest of the dome remained an area of channel bypass or erosion.

Structure

Salt diapirs are major structural features on the Texas Gulf Coast. The history of resource production at Barbers Hill Dome has provided evidence documenting the relationship between the salt dome and the structure of the surrounding strata. Barbers Hill Dome has clearly disrupted enclosing strata (figs. 5 and 6). Shallow intervals have been uplifted over the dome crest and all deeper strata are uplifted against the dome flanks. Subsidence or downwarping of strata appears to occur only in salt-withdrawal basins located 1 to 5 mi (1.6 to 8 km) away from the dome. Geometries and locations of salt-withdrawal basins around Barbers Hill are a function of the close spacing of the group of domes in this area (fig. 6). Withdrawal basins around individual domes have coalesced and are distorted owing to interference among several growing salt structures.

Most of the faulting identified around Barbers Hill Dome is related to salt tectonics. Radial faults intersect the dome on its southwest side, and concentric faults follow the axes of salt-withdrawal basins (fig. 6). Strata tend to dip toward these concentric faults from both sides, indicating collapse and breakage of overburden as deep-lying salt is withdrawn into growing diapirs (Seni and others, 1984b). Minor growth faulting, which may be related to deep salt structures, occurs about 5 mi (8 km) southeast of Barbers Hill Dome (fig. 6). Regionally extensive growth-fault zones are located 10 to 20 mi (16 to 32 km) coastward of Barbers Hill (Bebout and others, 1976).

Extensive faulting was not detected at shallower horizons, even though well-control was dense (fig. 8). Stresses in younger, unconsolidated intervals may be accommodated by arching, downwarping, or slumping, rather than by breakage and displacement.

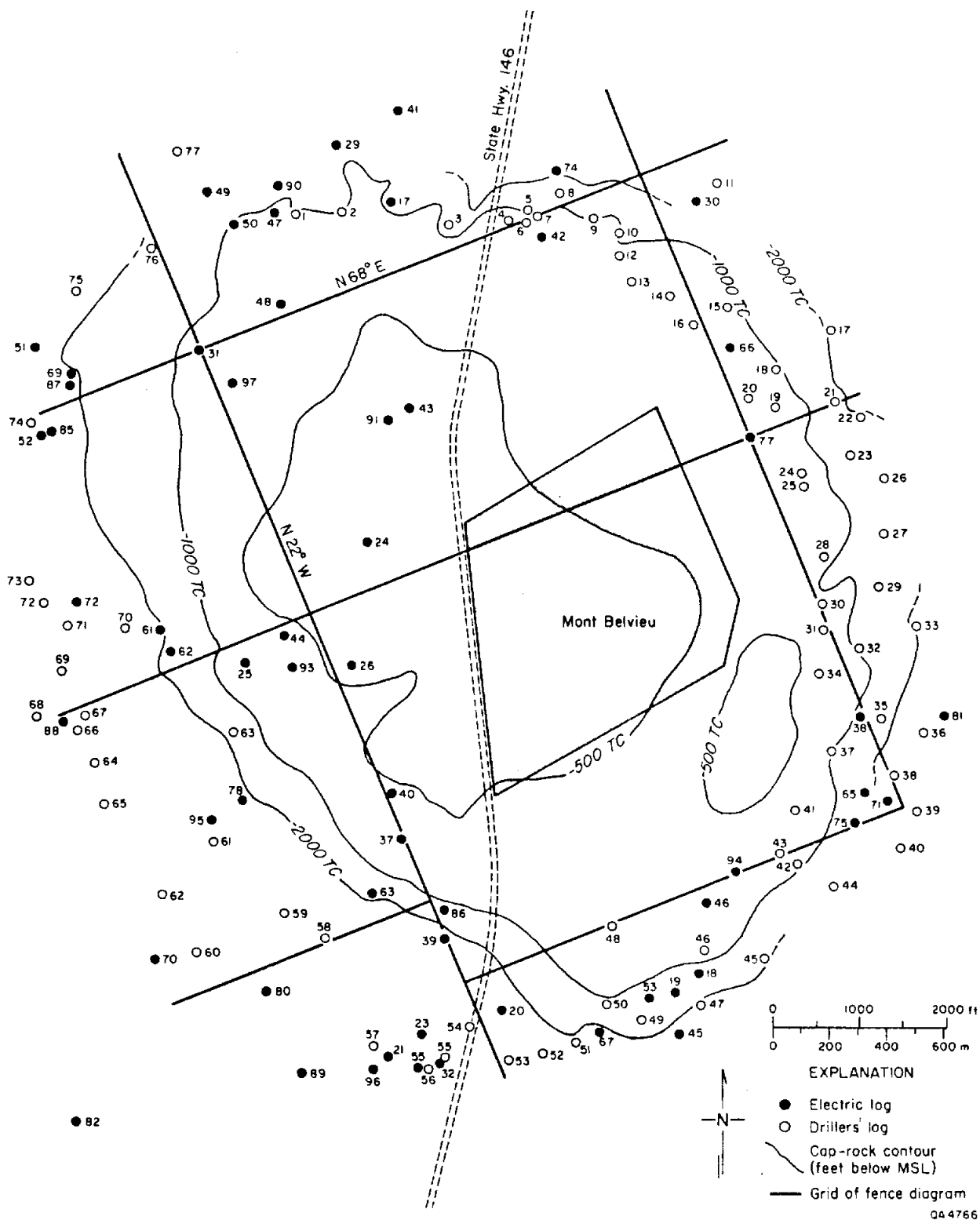


Figure 8. Well-control index map, Barbers Hill Dome, showing grid of fence diagram on figure 9. Well logs are identified in appendices 1 and 2.

Growth History

The growth history and tectonic stability of a salt dome can be revealed by analyzing lithofacies, thickness, and structural variations in surrounding strata (Giles and Wood, 1983; Seni and Jackson, 1983a, 1983b). Structural and stratigraphic data indicate continued growth of Barbers Hill Dome during the last 40 million yr (since late Eocene) at least.

Large-scale variations in sedimentation rates and lithofacies distributions caused by regionally shifting depositional patterns affect salt-dome growth (Seni and Jackson, 1983a). Salt ridges and pillows can be initiated by uneven loading of bedded salt due to rapid shoreline and shelf-margin sedimentation associated with prograding (advancing) deltas. Diapirs form when salt flows up out of a pillow into a vertical column. The pillow flanks collapse as salt is withdrawn, and rapid but localized sedimentation fills the resulting depressions (salt-withdrawal basins). The degree of syndepositional thickening into withdrawal basins and thinning against an actively growing salt diapir can provide a measurement of the rate of salt flow (Seni and Jackson, 1983a, 1983b).

In the Houston Embayment diapir province, major Paleocene to Oligocene depositional episodes (Wilcox Group, Yegua Formation, and Frio Formation) were characterized by rapid progradational sedimentation (Fisher, 1969; Galloway and others, 1982). Barbers Hill Dome probably formed from a salt pillow pushed up ahead of these advancing sediment wedges. During this period dome growth had to be rapid enough to keep pace with sedimentation. Syndepositional thickness variations in pre-Miocene intervals around Barbers Hill Dome are generally greater than those in younger strata (table 1).

Less rapid, more evenly distributed, aggradational deposition characterizes coastal plain sedimentation. In the Barbers Hill area, Miocene to Recent depositional episodes have been dominantly aggradational, syndepositional thickness variations are less pronounced, and coeval dome growth was probably less rapid than it was during earlier episodes.

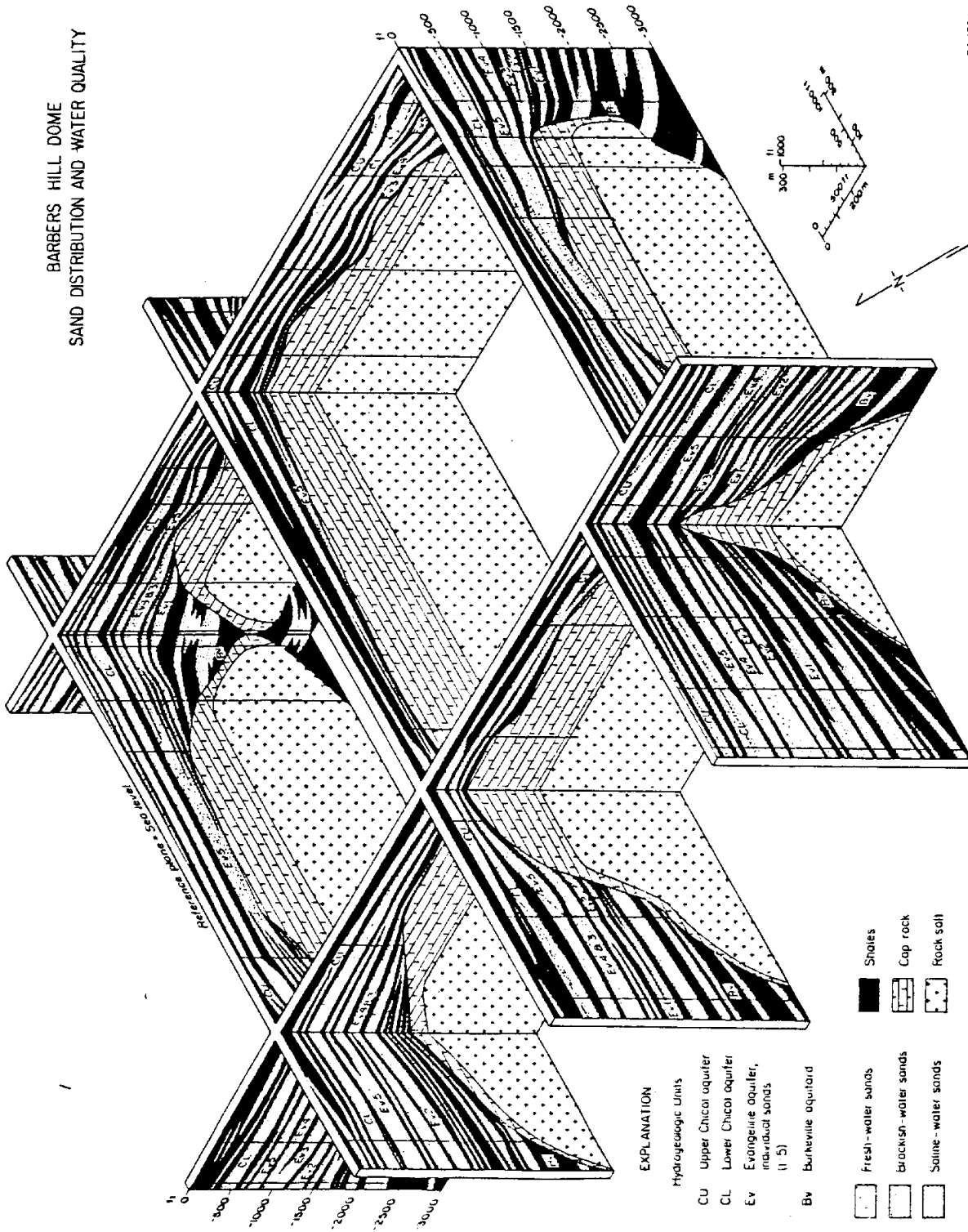
Structural disruption is another indication of active diapirism (Seni and others, 1984b). Faulting around Barbers Hill is concentrated in Oligocene-age and older strata. Faults shown in figure 6 tend to "die out" upward (fig. 5). Structural dip angles also decrease up section. This upward decrease in structural deformation of strata around Barbers Hill suggests a corresponding slowing of dome growth.

Thinning of superdomal strata, whether attributable to nondeposition or erosion, is indicative of dome growth (Seni and Jackson, 1983a, 1983b). The Goliad Formation thins radically over the crest of Barbers Hill Dome, whereas the Pliocene to Recent interval thins more modestly (table 1).

In coastal plain depositional environments, sandy sediments are generally associated with fluvial or distributary channels and tend to be concentrated along topographic lows. In the shallow nonmarine sediments around Barbers Hill, percent sand and thickness of individual sand bodies decrease over the dome crest but increase toward salt-withdrawal basins (fig. 9). Major Plio-Pleistocene dip-oriented channel-fill sand bodies wrap close around the dome flanks but avoid the crest (fig. 7).

Although dome growth at Barbers Hill may have slowed since the late Oligocene, there is evidence for continuing diapiric activity through the Recent. Because the Pliocene to Recent stratigraphic interval overlies the dome crest, it may be used to estimate dome growth during the last 5 million yr (beginning of Pliocene). Assuming the base of the Pliocene was originally horizontal, then the 200 to 300 ft (60 to 90 m) of structural relief seen on this surface today resulted from domal uplift (Seni and Jackson, 1983b). This is 40 to 60 ft (12 to 18 m) of uplift per million yr. This growth rate is similar to rates calculated for mature (post-diapir stage) salt domes in East Texas, northern Louisiana, and Germany (Seni and Jackson, 1983b). The hill overlying the dome today has about 40 ft (12 m) of topographic relief (fig. 2). The land surface is another uplifted surface that was once horizontal. Therefore, dome growth at Barbers Hill has been slow but relatively steady during the last 5 million yr.

BARBERS HILL DOME
SAND DISTRIBUTION AND WATER QUALITY



GA-4764

Figure 9. Fence diagram over Barbers Hill Dome showing distribution of sands, shales, and ground-water salinities.

HYDROGEOLOGY

Ground-water flow around a salt dome and its cap rock can endanger the integrity of a waste disposal facility. In order to determine possible pathways for shallow ground-water flow in those sediments most closely associated with Barbers Hill Dome, the distribution of high-permeability units (sands) and low-permeability units (shales) in the Chicot and Evangeline aquifers and in the underlying Burkeville aquitard was delineated in detail during this study. Electric and driller's logs were the data base for this delineation (fig. 8, apps. 1 and 2).

Electric logs were also used to estimate the salinities of ground waters contained in the various aquifer sands. Ground-water salinity patterns can be used to detect and trace salt dissolution or migration of cap-rock brines. An empirical, semiquantitative relationship was established between the salinity (total dissolved solids) of a ground water as determined by chemical analysis and the long-normal resistivity of the associated saturated sand as recorded on electric logs.

Only a few water wells were found in the Barbers Hill area for which both chemical analyses and electric logs were available, so data from other studies in the southeast Texas to southwest Louisiana area (Jones and Buford, 1951; Alger 1966) were also considered. The ground-water salinity/resistivity classification established is as follows:

Resistivity (ohm-meters)	TDS (mg/L)
>20	<1000 (fresh)
5-20	1000-3000 (brackish)
<5	>3000 (saline)

The estimated ground-water salinities based on this method are probably accurate to ± 500 mg/L. Methods used here are based on techniques developed and more fully described by Jones and Buford (1951), Turcan (1962), and Alger (1966).

Certain precautions were taken in order to decrease the inherent inaccuracies in this method that are due to uncontrolled variables. Drilling mud salinities affect measured down-hole resistivities, so only logs from wells drilled with natural muds were used, and mud resistivities recorded on log headers were monitored. Sands with numerous thin shale interbeds were avoided because shales reduce apparent resistivities. Lithologic, grain-size, grain-sorting, and temperature variations all affect measured resistivities, but in the relatively small area of this study all these parameters are fairly homogeneous.

Resistivity-derived salinities and detailed stratigraphic correlations were used to construct a hydrogeologic fence diagram (fig. 9) of Barbers Hill Dome and surrounding sediments down to 3,000 ft (915 m) below sea level.

Hydrogeologic Units

Burkeville Aquitard

The Burkeville aquitard is a shale-dominated interval, 300 to 500 ft (90 to 150 m) thick, occurring below the Evangeline aquifer and contacting cap rock at about 1,800 to 2,600 ft (550 to 790 m) below sea level (table 2, fig. 9). Regionally, the Burkeville is not a correlative time-stratigraphic unit, but is generally picked as the first low-sand interval below fresh to brackish water in the Evangeline (Baker, 1979). The Burkeville discussed here was delineated by Wesselman (1971) and is stratigraphically correlative in the vicinity of Barbers Hill. The Burkeville aquitard generally includes several sands, from 10 to 150 ft (3 to 30 m) thick, that are more laterally discontinuous than overlying aquifer sands. These sands usually pinch out before contacting the dome (fig. 9). Individual Burkeville shales range from 50 to 500 ft (15 to 150 m) thick.

At Barbers Hill Dome the Burkeville aquitard occurs 500 to 900 ft (150 to 270 m) below the base of brackish water. The Burkeville contacts the relatively thin cap rock on the dome flanks below the planar top of salt. It contacts thin cap rock and salt below

Table 2. Hydrogeologic units, Barbers Hill area.

System	Series	Stratigraphic units	Hydrogeologic units	Isopach ft (m)	Net sand ft (m)
Quaternary	Holocene	Alluvium	Upper Chicot aquifer	200-400 (60-120)	30-200 (9-60)
	Pleistocene	Beaumont Formation			
		?			
Tertiary	Pliocene	Lissie Formation	Lower Chicot aquifer	30-300 (9-90)	30-300 (9-90)
		?			
			Willis Formation Goliad Formation	Evangelina aquifer	30-1,800 (9-550)
			Burkeville aquitard	300-500 (90-150)	0-150 (0-46)
	Miocene	Lagarto Formation			

overhangs on the eastern side of the dome. Total area of cap-rock contact with the Burkeville is much less than it is with the Evangeline (fig. 9).

Evangeline Aquifer

The Evangeline aquifer includes 5 major sand bodies plus a number of thinner sands and shales (fig. 9). All the major sands contact the thick part of the cap rock above the level of top of salt. The major sands, numbered 1 to 5, contain all the fresh to brackish ground water that exists in the Evangeline around Barbers Hill Dome. These sands are separated from the underlying Burkeville aquitard by 2 to 4 saline-water sands and interbedded shales. The Evangeline is separated from the overlying Chicot aquifer by a continuous shale 30 to 200 ft (9 to 60 m) thick.

Aquifer tests were conducted in the Evangeline in two large industrial wells located about 1 mi (1.6 km) southwest of Barbers Hill Dome. Calculated permeabilities (hydraulic conductivities) were 244 and 327 g/d/ft² (0.00012 and 0.00015 m/s) (Wesselman, 1971). These are typical permeabilities for unconsolidated clean sands (Freeze and Cherry, 1979).

The major Evangeline sands range in thickness from 50 to 350 ft (15 to 107 m) and are interbedded with shales 0 to 100 ft (0 to 30 m) thick (fig. 9). Each major sand body extends farther up onto the cap rock than does the one below it. Toward the dome the sands generally thin, while the shales thicken. A few sands pinch out locally before contacting cap rock, but most do not. On the northern and southern dome flanks, shales tend to pinch out and sands 5, 4, and locally 3, coalesce, contacting cap rock over a broad area (fig. 9). Dips range from 0 to 20° on the Evangeline sands, increasing toward the dome and down section.

Ground-water salinity in the Evangeline aquifer increases eastward regionally and also locally around Barbers Hill. Sands 2 through 5 contain fresh to brackish water adjacent to the west and southwest dome flanks, but only sands 4 and 5 do so to the east (fig. 9). Ground-water salinities in individual sands tend to increase with proximity to cap rock and also with depth.

Chicot Aquifer

In the Barbers Hill area, the Chicot aquifer includes one continuous sand body, the lower Chicot, overlain by one to four laterally discontinuous sands, the upper Chicot (table 2, fig. 9). Chicot sands do not contact cap rock directly. Even over the shallowest part of the dome crest, the lower Chicot sand is separated from cap rock by 30 ft (9 m) of shale. The lower Chicot sand is separated from the upper Chicot sands by a continuous shale 20 to 150 ft (6 to 46 m) thick.

The lower Chicot sand is the most permeable fresh-water aquifer in the Barbers Hill area. Pump tests were made in two closely spaced wells tapping the lower Chicot. These wells supply the city of Mont Belvieu and are located less than 2,000 ft (610 m) northwest of the dome. Calculated permeabilities (Wesselman, 1971) are 821 and 762 g/d/ft² (0.00039 and 0.00036 m/s), slightly higher than Evangeline permeabilities, but still in the unconsolidated clean-sand range.

Salinity patterns in the lower Chicot sand are complex. Lower Chicot ground waters are fresh on the northeastern, northern, and northwestern sides of Barbers Hill Dome, but are brackish to saline around the rest of the dome and over the crest (fig. 9). A distinct high-salinity zone exists in the lower Chicot on the southwestern and southern dome flanks and apparently extends 6 mi (10 km) farther southwest toward Baytown (Wesselman, 1971). This saline plume is most likely due to natural dissolution of salt and/or to migration of cap-rock brines.

Aquifer lithology or original depositional salinities cannot account for this rather localized high-salinity zone in the lower Chicot. It occurs within the mapped channel-fill high-sand belt discussed earlier (fig. 7), where the lower Chicot characteristically contains fresh water. Lower Chicot ground water does become more saline regionally eastward (Wesselman, 1971) where the sand thins, it becomes finer grained, and is associated with shales of possible marine origin. But within the channel belt, electric and driller's logs indicate that the lower Chicot sand is thick, relatively coarse grained, and contains few shale interbeds.

Why the high-salinity zone is restricted to the lower Chicot is unknown. The continuity of shales separating the aquifer sands might help contain a salinity plume in a single sand body. These shales could inhibit the equilibration of an unstable density inversion (saline water above fresh water) by restricting vertical ground-water circulation. If some permeability conduit, possibly a fault zone, intersected only the lower Chicot and connected it to the dome, then the observed salinity pattern could form. This is a good example of the complexity of meteoric ground-water circulation around shallow salt domes.

The upper Chicot sands are each typically less than 100 ft (30 m) thick, although they coalesce locally, forming thicker sand bodies (fig. 9). These shallow sands have the greatest thickness variability and the least lateral continuity of all the fresh-water aquifer sands around Barbers Hill. Upper Chicot sands are thickest on the eastern and northeastern dome flanks, relatively thinner on the other flanks, and thinnest over the crest (fig. 9). A pump test reported for the upper Chicot from a well 10 mi (16 km) east of Barbers Hill obtained a permeability of 375 g/d/ft^2 (0.00018 m/s) (Wesselman, 1971).

Upper Chicot sands generally contain fresh water, even over the dome crest. Brackish to saline water does occur in the lowermost upper Chicot sand where it closely overlies the high-salinity zone in the lower Chicot sand (fig. 9).

Hydrochemistry

Chemical analyses of ground waters from 42 Chicot and Evangeline water wells in the Barbers Hill area were examined in order to detect possible dome-related hydrochemical patterns and to supplement resistivity-derived salinity data. Analyses were collected from Texas Department of Water Resources files and published reports for this area (Wesselman, 1971; Gabrysch and others, 1974), Texas Department of Health Resources, and a report by Underground Resource Management, Inc. (1982).

Ground-Water Salinity

Total dissolved solids (TDS) in ground waters from shallow wells (21 to 1,480 ft or 6 to 451 m) around Barbers Hill are in the fresh to brackish range (73 to 2,310 mg/L TDS) (fig. 10). Chloride concentrations range from very low (12 mg/L) to high (980 mg/L). Ground waters with chloride concentrations exceeding the 250 mg/L recommended limit for drinking (U.S. Public Health Service, 1962) are common (fig. 11).

Evangeline waters are more homogeneous and, on average, fresher than Chicot waters (table 3), but it is not uncommon to see greater compositional variability, and even higher TDS or chlorinity, in shallower wells (Kreitler and others, 1977; Henry and others, 1979; Fogg and Kreitler, 1982). The shallow meteoric zone (<500 ft or 150 m) is typically characterized by short-distance flow paths with numerous local discharge points, while deeper flow paths are longer and more regionally integrated. Shallow muddy sediments are compacting and dewatering, discharging saline formation waters into sandy aquifer systems that are too young to have yet been thoroughly flushed. In the Barbers Hill area the Chicot aquifer (especially the upper part) appears to be more lithologically heterogeneous than is the underlying Evangeline aquifer. Finally, shallower flow systems are more easily and quickly contaminated by land-surface features, such as brine pits and polluted streams.

Wells pumping from the Evangeline are concentrated on the western side of the dome (fig. 10). Resistivity data indicate that 500 to 600 ft (150 to 180 m) of fresh-water sands occur in the Evangeline in this same area (fig. 9).

Lower Chicot waters have the highest analyzed salinities and the greatest range of values. Average TDS approaches the upper limit for fresh water, and average chloride concentration is even closer to exceeding its recommended limit (table 3). The analytical results mapped in figures 10 and 11 do not tell the whole story; many lower Chicot wells have been abandoned or plugged back to shallower (upper Chicot) sands because of failure to produce adequate quality water (Wesselman, 1971; Underground Resource Management, Inc., 1982). Several abandoned lower Chicot wells overlie Barbers Hill Dome, including

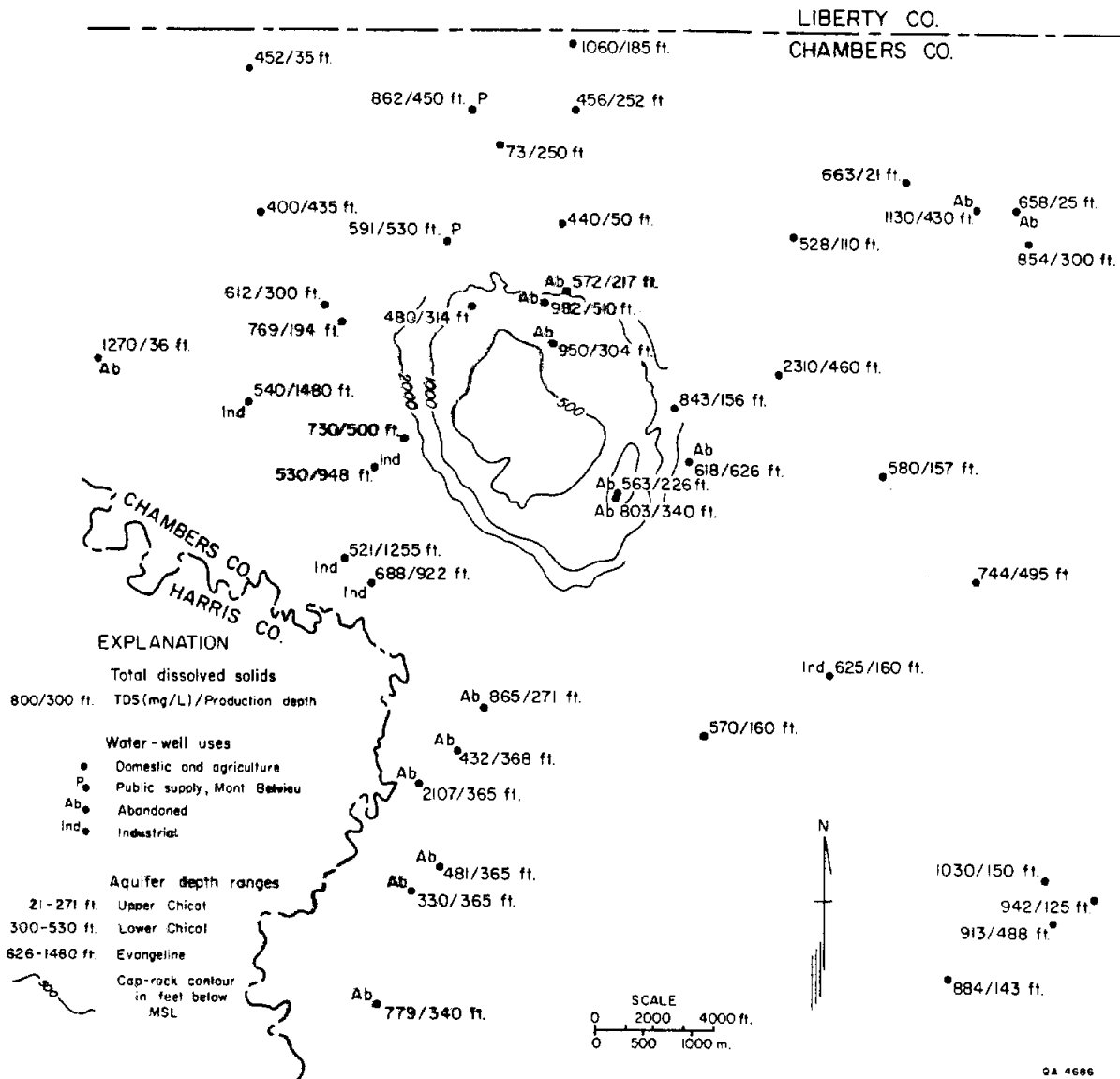


Figure 10. Distribution of total dissolved solids in well water around Barbers Hill.

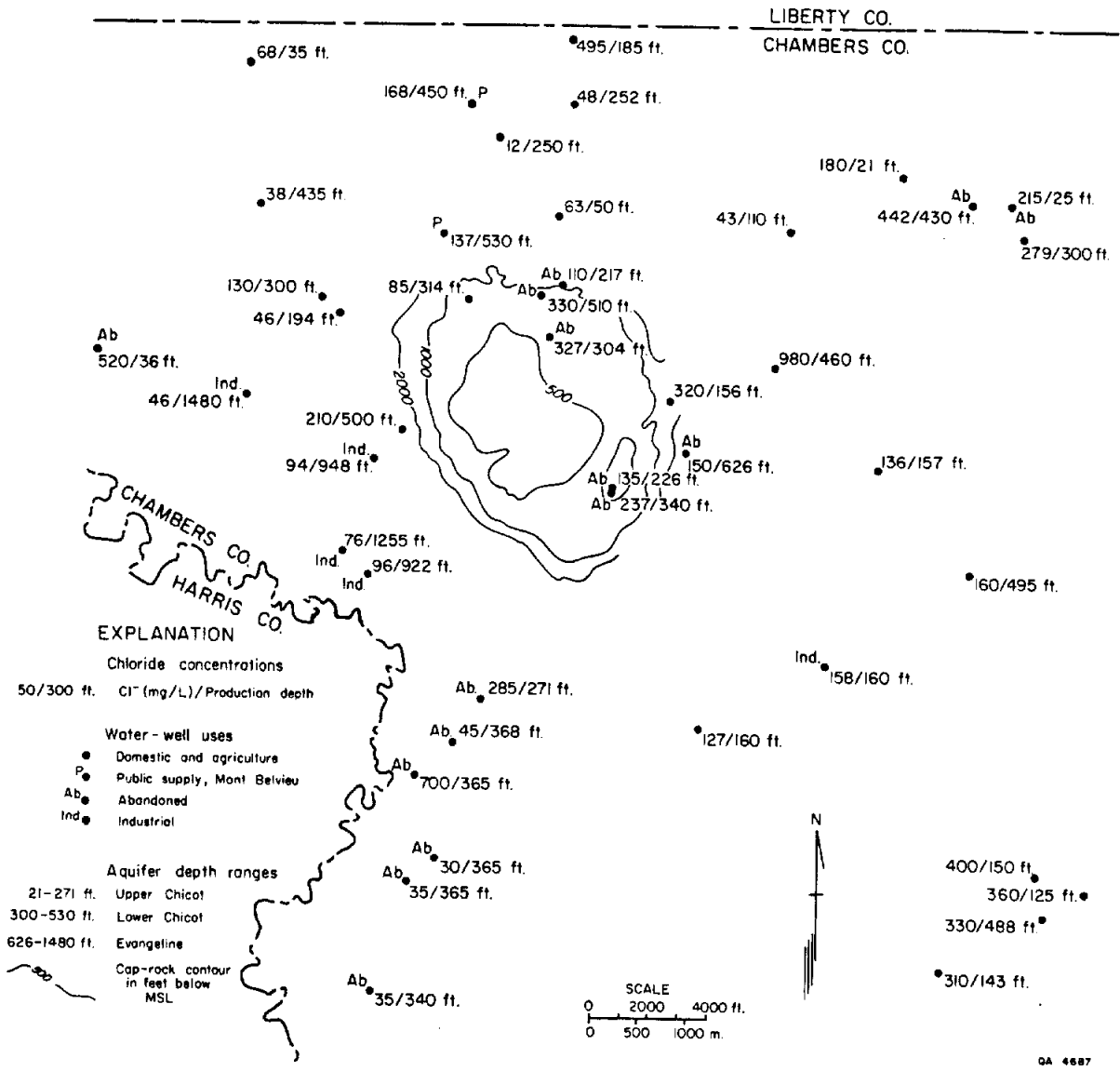


Figure 11. Distribution of chloride concentrations in well water around Barbers Hill.

Table 3. Total dissolved solids and chloride concentrations in water wells,
Barbers Hill area.

<u>Aquifer</u>	<u>No. Wells</u>	<u>TDS (mg/L)</u>		<u>Cl (mg/L)</u>	
		<u>Avg.</u>	<u>Range</u>	<u>Avg.</u>	<u>Range</u>
Upper Chicot	19	684	73-1270	195	12-250
Lower Chicot	18	853	330-2310	236	30-980
Evangeline	5	579	521-688	92	46-150

former Mont Belvieu public supply wells. The city now gets its water from several newer, lower Chicot wells north and northwest of the dome (fig. 10). The resistivity-derived high-salinity zone seen in the lower Chicot (fig. 9) is not well delineated here because few wells produce from this aquifer in the area closely adjacent to the southern and southwestern flanks of the dome. However, the line of lower Chicot wells located from 1 to 3 mi (1.6 to 4.8 km) south of the dome were abandoned due to salinity problems (Wesselman 1971; Underground Resource Management, Inc., 1982). Regional ground-water flow is to the southwest (Smith, this volume), so that these wells are down flow from the dome.

Most lower Chicot wells to the east of the dome produce brackish or near-brackish waters (fig. 10). This may be due to the thinning of this channel sand and increasing shale content as the eastern margin of the high-sand fluvial axis is approached (fig. 7). Better quality lower Chicot waters occur to the west and northwest, in the direction of increasing net sand.

Upper Chicot waters have the greatest well-to-well salinity variability, as might be expected for this shallow aquifer composed of laterally discontinuous sands and shales. The freshest individual analyses around Barbers Hill are from upper Chicot wells (table 3). General TDS and chlorinity patterns roughly coincide with those in the lower Chicot, suggesting a degree of hydrologic communication (figs. 10 and 11).

The quality of shallow ground waters around Barbers Hill is poorer than it is to the west, but better than it is to the east. Effects attributable to the presence of a salt dome are subtle and are largely masked by regional salinity patterns. In Chambers County, Chicot and Evangeline ground waters are generally brackish to saline everywhere except in the northwestern corner of the county, the Barbers Hill area (Wesselman, 1971). In a 20 to 30 mi² (50 to 80 km²) area around Barbers Hill Dome, shallow ground waters are fresh to brackish, but well-to-well variations are great. In a similar size area, 10 to 15 mi² (16 to 24 km²) west in Harris County, Chicot/Evangeline waters are generally quite fresh (<500 mg/L TDS), and well-to-well variations are much less (Gabrysch and others, 1974). The

regional trend in eastern Harris and western Chambers Counties is an east-to-west decreasing salinity in shallow ground waters that coincides with an increasing sandiness of the aquifers (Wesselman, 1971; Baker, 1979). At this scale of observation, only the distributional heterogeneity of ground-water quality causes the Barbers Hill area to stand out.

In order to check for chlorinity anomalies around Barbers Hill, Evangeline and lower Chicot water-well analyses from the similarly sized area in Harris County were compared with the Barbers Hill data. The Harris County data (Gabrysch and others, 1974) is as follows (compare with table 3):

No. Wells	TDS (mg/L)		Cl (mg/L)	
	avg.	range	avg.	range
20	636	310-1190	137	33-560

Although the selected Harris County wells have TDS concentrations similar to those in Barbers Hill wells, average chlorinity is lower. However, no significant differences were revealed with these small sample sizes.

Two possible dome-related salinity patterns exist in the local area around Barbers Hill. (1) A high-salinity plume in lower Chicot waters extends from the southwestern dome flank several miles down flow. (2) Because of poor water quality, most of the water wells directly overlying cap rock have been abandoned.

Hydrochemical Facies

Distribution patterns in the major dissolved ions found in most meteoric ground waters (sodium, calcium, magnesium, bicarbonate, chloride, and sulfate) can be traced and compared using the concept of hydrochemical facies. Hydrochemical facies are areally distinct ground-water solutions having diagnostic major-ion compositions (Back, 1966). They can often be used to trace sources of recharge, ground-water/aquifer-matrix reactions, and mixing of two or more ground waters. A Piper diagram (Hem, 1959) was

prepared to delineate the hydrochemical facies found in shallow ground waters around Barbers Hill (fig. 12). Hydrochemical facies are generally classified according to the relative abundances of the major dissolved cations and anions. Hydrochemical facies in ground waters around Barbers Hill are listed below.

Aquifer	Dominant Cation(s)	Dominant Anion(s)
Upper Chicot	Na, Ca	HCO ₃ , Cl
Lower Chicot	Na	Cl, HCO ₃
Evangeline	Na	HCO ₃

The Piper diagram reveals that these ground waters have very low sulfate concentrations--generally less than 10 mg/L and commonly less than 2 percent of total dissolved anions. The abundance of soluble sulfate minerals in the cap rock does not appear to be affecting surrounding meteoric ground-water composition. Kreitler and others (1977) note that Harris County ground waters are also low in sulfate. Lack of dissolved sulfate indicates reducing conditions.

A more general comparison between ground waters around Barbers Hill Dome and regional compositional trends in the same aquifers indicates that Barbers Hill waters are not significantly "abnormal," with the possible exception of lower Chicot waters. Regional down-flow hydrochemical trends for Gulf Coast shallow meteoric aquifers are increasing ratios of sodium/calcium, bicarbonate/depth, and depth/chloride (Foster, 1950; Kreitler and others, 1977; Henry and others, 1979). Sodium increases at the expense of calcium owing to cation exchange on clay minerals. Dissolution of carbonate minerals causes bicarbonate concentrations to increase with depth. Chloride tends to be variable to slightly decreasing in the shallow subsurface for the reasons discussed earlier, but does increase with depth at deeper levels when mixing of deep and shallow waters occurs and when soluble chloride minerals are present. Upper Chicot waters are the only ones in sandy aquifers around Barbers Hill that contain appreciable dissolved calcium. Cation exchange has effectively removed most calcium from lower Chicot and Evangeline waters (fig. 12). Bicarbonate

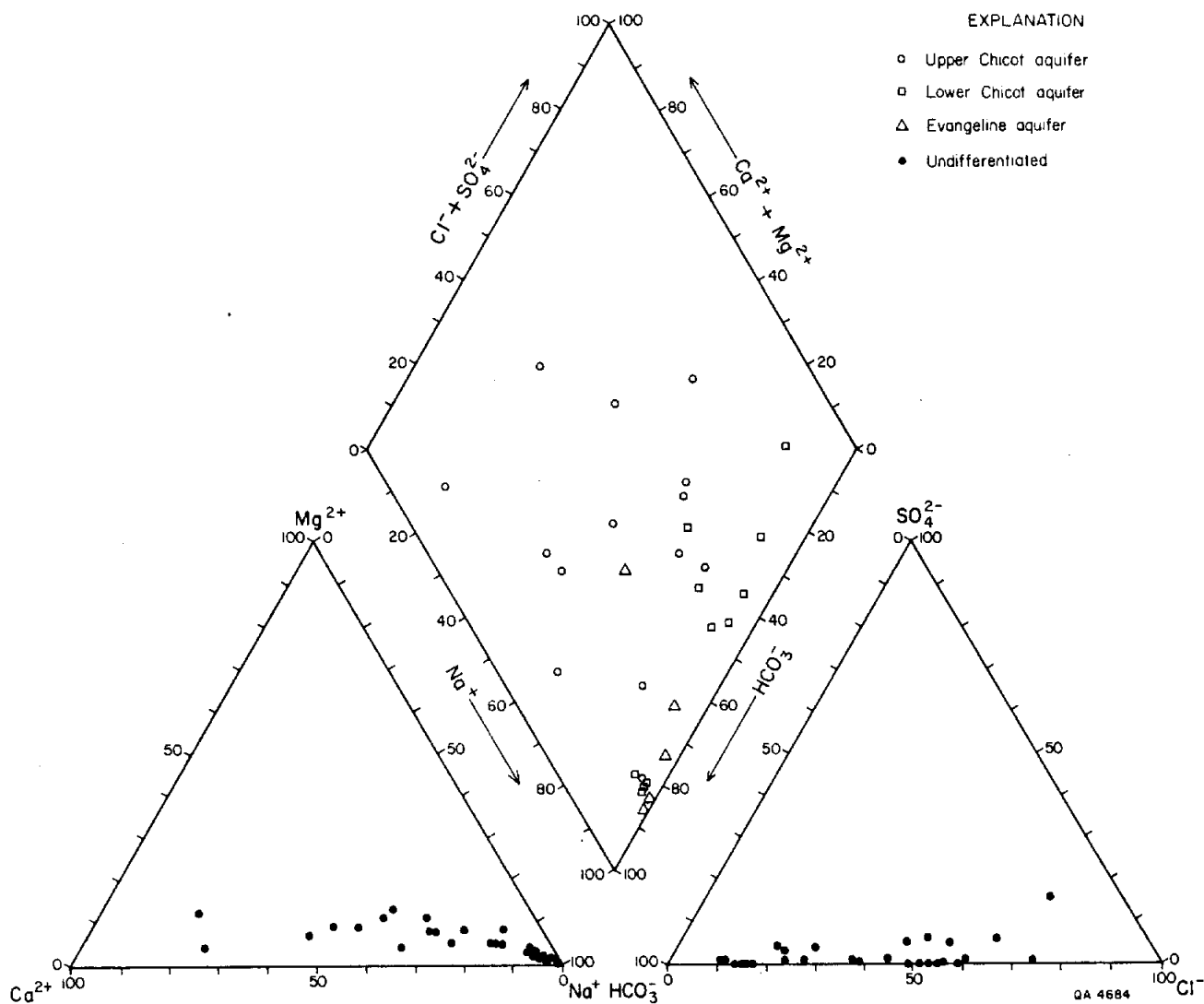


Figure 12. Piper diagram of water-well chemical analyses, Barbers Hill area.

concentration follows no obvious pattern in the Chicot aquifers, but is relatively more abundant in the Evangeline aquifer. Relative chloride concentrations are highest in the lower Chicot, most variable in the upper Chicot, and lowest in the Evangeline (fig. 12). Harris County ground waters are generally comparable to upper Chicot and Evangeline waters, while lower Chicot waters are more similar to Galveston County ground waters (Kreitler and others, 1977). Kreitler and others (1977) concluded that Galveston County ground waters are a mixture of Harris County ground waters and high-salinity sea water or formation water. Lower Chicot waters may be a mixture of "normal" Harris-type ground waters and waters that have been in contact with the Barbers Hill salt stock or that have migrated up the flanks of the dome from deep high-salinity zones.

Temporal Changes in Composition and Salinity

Available pertinent data were examined to see if ground-water quality around Barbers Hill has been changing through time, but because of the relatively slow rates of ground-water flow, long periods of time elapse between cause and effect. In the case of Barbers Hill, ground-water chemical analyses from individual wells are not consistently available for sufficiently long time spans.

A Piper diagram was constructed for well waters analyzed between 1941 and 1951, and another was made for well waters analyzed between 1966 and 1985. No significant difference was revealed. Hydrochemical facies had not changed during this period.

The electric well logs used in the resistivity-based salinity analysis range in vintage from 1948 to 1975, but no significant change in minimum observed lower Chicot resistivity was found.

It has already been noted that certain water wells around Barbers Hill either failed to consistently produced good quality water or produced water that deteriorated in quality through time. Systematic analyses of these waters over extended time periods were not made, so quality deterioration cannot be quantitatively traced.

Waters from two lower Chicot wells have been systematically analyzed annually since the late 1950's. These are closely spaced (<500 ft or 150 m apart) Mont Belvieu public supply wells that both produce from 530 ft (160 m) below land surface. They are located less than 2,000 ft (610 m) northwest of the dome outline at 2,000 ft (610 m) below sea level. On figures 10, 11, and 12 they are represented as a single well because analytical results have been essentially identical. Annual chemical analyses for these wells are on file at the Texas Department of Health Resources and have been graphed in figure 13.

The composition and salinity of water from the Mont Belvieu wells remained remarkably constant from 1958 to 1976. Total dissolved solids ranged between 400 and 425 mg/L (excluding 1964, when it was 450 mg/L). Chloride concentration was 45 to 50 mg/L. Sodium concentration was 160 to 180 mg/L. Then, between 1976 and 1985, TDS, chloride, and sodium all increased relatively constantly (fig. 13). In early 1985, TDS was 591 mg/L, chloride was 137 mg/L, and sodium was 227 mg/L. Concentrations of other major dissolved ions remained stable (fig. 13).

The absolute increase in sodium and chloride in these wells is the clearest evidence available for possible dome-related contamination of ground water around Barbers Hill. Systematic increases over a relatively short time period at a single point source strongly suggest some type of contamination, although these wells still produce fairly fresh water and the changes are within the normal range of variability for a Gulf Coast aquifer. Wesselman (1971), who noted the lower Chicot high-salinity plume discussed earlier, predicted that it would eventually extend to these wells.

REFERENCES

- Alger, R. P., 1966, Interpretation of electric logs in fresh water wells in unconsolidated formations: Seventh Annual Symposium, Society of Professional Well-log Analysts, Transactions, p. 1-25.

- Back, W., 1966, Hydrochemical facies and ground-water flow patterns in northern part of Atlantic coastal plain: U.S. Geological Survey Professional Paper 498-A, 42 p.
- Baker, E. T., Jr., 1979, Stratigraphic and hydrogeologic framework of part of the coastal plain of Texas: Texas Department of Water Resources Report 236, 43 p.
- Barnes, V. E., 1968, Beaumont sheet: The University of Texas at Austin, Bureau of Economic Geology, Geologic Atlas of Texas, scale 1:250,000.
- Bebout, D. G., Loucks, R. G., Bosch, S. C., and Dorfman, M. H., 1976, Geothermal resources--Frio Formation, upper Texas Gulf Coast: The University of Texas at Austin, Bureau of Economic Geology Geological Circular 76-3, 47 p.
- Behrman, R. G., 1967, Structure map Barbers Hill dome, Chambers County, Texas, contours on top of first domal material: Railroad Commission of Texas Hearings files, included in several dockets.
- Bevier, G. M., 1925, The Barbers Hill oil field, Chambers County, Texas: American Association of Petroleum Geologists Bulletin, v. 9, no. 6, p. 958-973.
- Bodenlos, A. J., 1970, Cap-rock development and salt-stock movement, in Kupfer, D. H., ed., Geology and technology of Gulf Coast salt domes: School of Geosciences, Louisiana State University, Baton Rouge, Louisiana, p. 73-86.
- Fisher, W. L., 1969, Facies characterization of Gulf Coast basin delta systems, with some Holocene analogs: Gulf Coast Association of Geological Societies Transactions, v. 19, p. 239-261.
- Fisher, W. L., McGowen, J. H., Brown, L. F., and Groat, C. G., 1972, Environmental geologic atlas of the Texas coastal zone--Galveston-Houston area: The University of Texas at Austin, Bureau of Economic Geology, 91 p.
- Fisher, W. L., Proctor, C. V., Jr., Galloway, W. E., and Nagle, J. S., 1970, Depositional systems in the Jackson Group of Texas--their relationship to oil, gas, and uranium: Gulf Coast Association of Geological Societies Transactions, v. 20, 234-261.

- Fogg, G. E., and Kreitler, C. W., 1982, Ground-water hydraulics and hydrochemical facies in Eocene aquifers of the East Texas Basin: The University of Texas at Austin, Bureau of Economic Geology Report of Investigations No. 127, 75 p.
- Foster, M. D., 1950, The origin of high sodium bicarbonate waters in the Atlantic and Gulf Coastal Plains: *Geochimica et Cosmochimica Acta*, v.1, p. 33-48.
- Freeze, R. A., and Cherry, J. A., 1979, *Groundwater*: New Jersey, Prentice-Hall, 604 p.
- Gabrysch, R. K., 1980, Development of ground-water in the Houston district, Texas, 1970-1974: Texas Department of Water Resources Report 241, 49 p.
- Gabrysch, R. K., Naftel, W. L., and McAdoo, G. D., 1974, Ground-water data for Harris County, Texas, chemical analyses of water from wells, 1922-1971: Texas Water Development Board Report 178, v. 3, 87 p.
- Galloway, W. E., 1985, Depositional framework of the lower Miocene (Fleming) episode; northwest Gulf Coast Basin: Gulf Coast Association of Geological Societies Transactions, v. 35, p. 67-74.
- Galloway, W. E., Hobday, D. K., and Magara, K., 1982, Frio Formation of Texas Gulf Coastal Plain: depositional systems, structural framework, and hydrocarbon distribution: American Association of Petroleum Geologists Bulletin, v. 66, no. 6, p. 649-688.
- Giles, A. B., and Wood, D. H., 1983, Oakwood salt dome, East Texas: geologic framework, growth history, and hydrocarbon production: The University of Texas at Austin, Bureau of Economic Geology Geological Circular 83-1, 55 p.
- Guevara-Sanchez, E. H., 1974, Pleistocene facies in the subsurface of the southeast Texas Coastal Plain: The University of Texas at Austin, Ph.D. dissertation, 133 p.
- Hem, J. D., 1959, Study and interpretation of the chemical characteristics of natural water: U.S. Geological Survey Water-Supply Paper 1473, 269 p.
- Henry, C. D., Basciano, J. M., and Duex, T. W., 1979, Hydrology and water quality of the Eocene Wilcox Group: significance for lignite development in East Texas: Gulf Coast Association of Geological Societies Transactions, v. 29, p. 127-135.

- Jackson, M. P. A., and Seni, S. J., 1984, Atlas of salt domes in the East Texas Basin: The University of Texas at Austin, Bureau of Economic Geology Report of Investigations No. 140, 102 p.
- Jones, P. H., and Buford, T. B., 1951, Electric logging applied to ground-water exploration: Geophysics, v. 16, no. 1, p. 115-139.
- Judson, S. A., Murphy, P. C., and Stamey, R. A., 1932, Overhanging cap rock and salt at Barbers Hill, Chambers County, Texas: American Association of Petroleum Geologists Bulletin, v. 16, no. 5, p. 469-482.
- Kreitler, C. W., Guevara, E., Granata, G., and McKalips, D., 1977, Hydrogeology of Gulf Coast aquifers, Houston-Galveston area, Texas: Gulf Coast Association of Geological Societies Transactions, v. 27, p. 72-89.
- McGookey, D. P., 1975, Gulf Coast Cenozoic sediments and structure: an excellent example of extra-continental sedimentation: Gulf Coast Association of Geological Societies Transactions, v. 25, p. 104-120.
- Murphy, P. C., and Judson, S. A., 1930, Deep sand development at Barbers Hill, Chambers County, Texas: American Association of Petroleum Geologists Bulletin, v. 11, no. 6, p. 719-741.
- Rainwater, E. H., 1964, Regional stratigraphy of the Gulf Coast Miocene: Gulf Coast Association of Geological Societies Transactions, v. 14, p. 81-124.
- Seni, S. J., and Jackson, M. P. A., 1983a, Evolution of salt structures, East Texas diapir province, part 1: sedimentary record of halokinesis: American Association of Petroleum Geologists Bulletin, v. 67, no. 8, p. 1219-1244.
- _____ 1983b, Evolution of salt structures, East Texas diapir province, part 2: patterns and rates of halokinesis: American Association of Petroleum Geologists Bulletin, v. 67, no. 8, p. 1245-1274.
- Seni, S. J., Mullican, W. F., III, and Hamlin, H. S., 1984a, Texas salt domes: natural resources, storage caverns, and extraction technology: The University of Texas at

Austin, Bureau of Economic Geology, report prepared for the Texas Department of Water Resources under interagency contract no. IAC (84-85)-1019, 161 p.

_____ 1984b, Texas salt domes: aspects affecting disposal of toxic-chemical waste in solution-mined caverns: The University of Texas at Austin, Bureau of Economic Geology, report prepared for the Texas Department of Water Resources under interagency contract no. IAC (84-85)-1019, 94 p.

Solis, R. F., 1981, Upper Tertiary and Quaternary depositional systems, central coastal plain, Texas--regional geology of the coastal aquifer and potential liquid-waste repositories: The University of Texas at Austin, Bureau of Economic Geology Report of Investigations No. 108, 89 p.

Turcan, A. N., Jr., 1962, Estimating water quality from electrical logs: U.S. Geological Survey Professional Paper 450-C, Article 116, p. C135-C136.

Underground Resource Management, Inc., 1982, Hydrogeologic investigation in the vicinity of Barbers Hill salt dome: report prepared for the City of Mont Belvieu, Texas, 108 p.

U.S. Public Health Service, 1962, Public Health Service drinking water standards: Public Health Service Publication 956, 61 p.

Wesselman, J. B., 1971, Ground-water resources of Chambers and Jefferson Counties, Texas: Texas Water Development Board Report 133, 173 p.

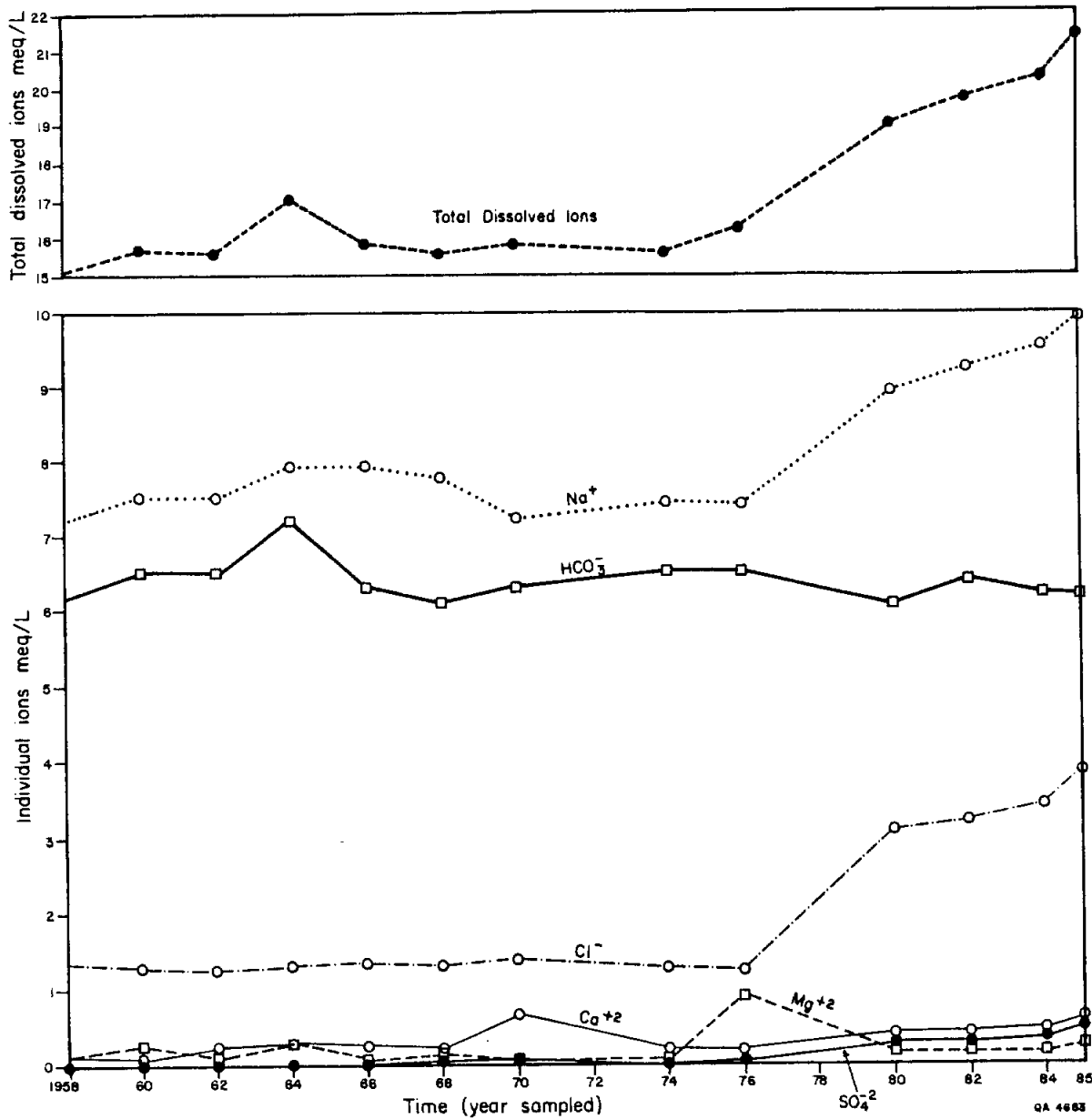


Figure 13. Graph of dissolved-ions concentrations in Mont Belvieu public supply water well no. 4, from 1958 to 1985. Chemical analyses from nearby water well no. 5 show identical trends.

Appendix 1. Barbers Hill Driller's Logs

County	Cross Section Well Number	Well Name
Chambers	1	Humble Oil Co. #B-1 Kirby Petroleum Co.
	2	Otis Russell #1-A E. W. Barber
	3	Humphreys Corp. #1-A E. W. Barber
	4	Texas Gulf Prod. Co. #B-3 E. W. Barber "B"
	5	Humphreys Corp. #2 E. W. Barber "B"
	6	Mills Bennett Prod. Co. et al. #1 Gulf Monongahela Fee
	7	Humphreys Corp. #1 Fitzgerald-Meadows lease
	8	Humphreys Corp. #1 D. N. Scott
	9	Humphreys Corp. #2 T. S. Fitzgerald
	10	Humphreys Corp. #1 Anna Davis
	11	Otis Russell #1 Mary O. Scott
	12	Texas Gulf Prod. Co. #2-D L. E. Fitzgerald Unit #1
	13	Texas Gulf Prod. Co. #3-E L. E. Fitzgerald Unit #1
	14	Texas Gulf Prod. Co. #1 Morgan-Fitzgerald lease
	15	Texas Gulf Prod. Co. #3 J. M. Fitzgerald
	16	Texas Gulf Prod. Co. #B-9 Kirby Petroleum Co. lease
	17	Mills Bennett Prod. Co. et al. #B-3 Kirby Petroleum Co.
	18	Texas Gulf Prod. Co. #B-28 Kirby Petroleum Co. "B"
	19	Texas Gulf Prod. Co. #2 Alma A. Eberspacher
	20	Texas Gulf Prod. Co. #B-27 Kirby Petroleum Co. "B"
	21	Texas Gulf Prod. Co. #C-2 Kirby Petroleum Co. "C"
	22	Mills Bennett Prod. Co. et al. #1 W. C. Smith et al.
	23	Mills Bennett Prod. Co. et al. & Republic Prod. Co. #2 J. B. Means et al.

Appendix I (cont.)

County	Cross Section Well Number	Well Name
Chambers	24	Texas Gulf Prod. Co. #2 McLean
	25	Mills Bennett Prod. Co. et al. #5 J. B. Means et al.
	26	Mills Bennett Prod. Co. et al. & Moody Corp. #2 Hamman-Armstrong
	27	The Texas Co. #4 J. F. Wilburn
	28	The Texas Co. #9 J. F. Wilburn
	29	Gulf Prod. Co. #4 J. F. Wilburn "A"
	30	Mills Bennett Prod. Co. et al. #B-9 J. F. Wilburn
	31	Sinclair Oil & Gas Co. #17-A Jerry Wilburn
	32	Sinclair Oil & Gas Co. #9 Jerry Wilburn
	33	Sun Oil Co. #1 J. Wilburn
	34	Sinclair Oil & Gas Co. #15 Jerry Wilburn
	35	Sun Oil Co. #10 Wilburn Fee
	36	Sun Oil Co. #1 Wilburn Fee
	37	Sun Oil Co. #16 Wilburn (Fee deed #182)
	38	McAlbert Oil Co. #5 E. F. Woodward
	39	Humphreys Corp. #A-6 Kirby Petroleum Co.
	40	Mills Bennett Prod. Co. et al. #1 Geo. W. Collier
	41	Texas Gulf Prod. Co. #9 J. F. Wilburn
	42	McAlbert Oil Co. #B-2 Higgins
	43	Sun Oil Co. #7 Annie Higgins
	44	Mills Bennett Prod. Co. et al. #3 Geo. W. Collier
	45	Mills Bennett Prod. Co. et al. #7 Gulf-Fisher
	46	Mills Bennett Prod. Co. et al. #3 Gulf Monongahela Fee "B"
	47	Sun Oil Co. #4 Chambers Co. Agricultural Assn.
	48	Mills Bennett Prod. Co. et al. #2 Gulf Monongahela Fee "B"
	49	Stanolind Oil & Gas Co. #31 Chambers Co. Agricultural Assn.
	50	Mills Bennett Prod. Co. et al. #1 Gulf Monongahela Fee "B"

Appendix 1 (cont.)

County	Cross Section Well Number	Well Name
Chambers	51	Mills Bennett Prod. Co. et al. #2 E. H. Fisher
	52	Mills Bennett Prod. Co. et al. #3 E. H. Fisher
	53	Mills Bennett Prod. Co. et al. #7 Gulf Fee "C" (E. H. Fisher Fee)
	54	Mills Bennett Prod. Co. et al. #7 D. J. Japhet
	55	Mills Bennett Prod. Co. et al. #1 Farrish-Blaffer Estate
	56	Mills Bennett Prod. Co. et al. #2 Farrish-Blaffer Estate
	57	Humble Oil Co. #4 Myers Fee
	58	T. J. Haberle #1 W. C. Richardson
	59	T. J. Haberle #1 E. W. Collier et al.
	60	Humble Oil Co. #6 Myers Fee
	61	Sun Oil Co. #2 Zadie Fisher
	62	Sun Oil Co. #1 Zadie Fisher
	63	T. J. Haberle #1 R. S. Hodges et al.
	64	Humphreys Corp. #1 E. H. Winfree
	65	Texas Gulf Prod. Co. #2 Lula Barber
	66	The Texas Co. #3 Elizabeth Winfree
	67	Humphreys Corp. #4 E. H. Winfree
	68	Sun Oil Co. #2 Winfree "B"
	69	Sun Oil Co. #3 J. H. Smith
	70	Texas Gulf Prod. Co. #13 E. H. Winfree
	71	Sun Oil Co. #2 O. K. Winfree & Wife
	72	Sinclair Oil & Gas Co. #1 J. H. Smith
	73	Mills Bennett Prod. Co. et al. #1 Gulf-J. H. Smith
	74	Texas Gulf Prod. Co. #A-8 A. E. Barber "A" lease
	75	Humphreys Corp. #A-10 Kirby Petroleum Co.
	76	Texas Gulf Prod. Co. #A-12 Kirby Petroleum Co. "A"
	77	Humble Oil Co. #1 Kirby

Appendix 2. Barbers Hill Electric Logs

County	Cross Section Well Number	Well Name
Liberty	1	M. T. Halbouty #E-1 Kirby Petroleum Co.
Chambers	2	M. T. Halbouty #1 Gilbert
	3	Cole & Harrell Drilling Co. #1 K. Williams
	4	The Texas Co. #3 Kirby Oil & Gas Co.
	5	The Texas Co. #1 Whaley
	6	General Crude Oil Co. #1 Nash Fee
	7	British Texan Oil Co. #1 Barber
	8	Gas Producers Enterprises, Inc. #1 Peter C. Ulrich
	9	Superior Oil Co. #1 O. Z. Smith
	10	Humble Oil & Refining Co. #B-1 Ben Dutton
	11	The Texas Co. #1 A. A. Davis
	12	The Texas Co. #1 Kirby Petroleum Co.
	13	M. T. Halbouty #1 Wilburn
	14	Kirby Petroleum #1 Fee Tract 8
	15	The Texas Co. #1 K. Fitzgerald
	16	The Texas Co. #2 Kirby Oil & Gas
	17	Sunray Oil Co. #C-2 E. W. Barber
	18	Stanolind Oil & Gas Co. #33 Chambers County Agric. Co.
	19	Stanolind Oil & Gas Co. #19 Chambers County Agric. Co.
	20	Marine Contractors Supply Inc. #1 Collier Heirs
	21	Mills Bennett #17 E. E. Barrows
	22	C. L. Chambers #1 Schilling-Lillie
	23	Gulf Coast Operators #3 E. C. Japhet
	24	Texas Eastern Transmission Corp. #S-8 Mont Belvieu Storage
	25	Humble Oil & Refining Co. #5 LPG Storage
	26	Texas Eastern Transmission Corp. #S-10 Mont Belvieu Storage
	27	The Texas Co. #1 Kirby Oil & Gas Co.

Appendix 2 (cont.)

County	Cross Section Well Number	Well Name
Chambers	28	Sierra Co. #1 Trichel
	29	Sunray-Mid Continent Oil Co. #A-8 Barber
	30	The Texas Co. #1 J. M. Fitzgerald Estate
	31	Harrison & Gilger #2 A. E. Barber
	32	Otis Russell #1 Blaffer-Farrish
Liberty	33	General Crude Oil Co. #B-3 Colby
Harris	34	The Texas Co. #1 Mrs. Emma K. Busch Estate
Chambers	35	Kirby Petroleum Co. #1 A. M. Wilburn
Liberty	36	General Crude Oil Co. #D-1 Moore's Bluff
Chambers	37	Warren Petroleum Co. #13 Mont Belvieu Storage
	38	Sun Oil Co. #23 J. Wilburn
	39	Warren Petroleum Co. #3 Caprock Disposal Well
	40	Warren Petroleum Co. #11 Mont Belvieu Storage
	41	Sunray DX Oil Co. #D-5 E. W. Barber
	42	Texas Gulf Prod. Co. #3-S L. E. Fitzgerald
	43	Texas Butadiene Co. #1 Fee
	44	Humble Oil & Ref. Co. #1 Mont Belvieu Storage
	45	Houston Oil & Minerals Corp. #12 Chambers County Agric. Co.
	46	Sun Oil Co. #1 Higgins "A"
	47	Humble Oil & Ref. Co. #B-9 Kirby Pet. Co. Fee
	48	Texas Eastern Transmission Corp. #11 N. T.
	49	Humble Oil & Ref. Co. #11 Kirby Pet. Co. Fee
	50	Humble Oil & Ref. Co. #B-14 Kirby Pet. Co. Fee
	51	Texas Gulf Prod. Co. #15 Kirby "A"
	52	Texas Gulf Prod. Co. #A-11 A. E. Barber
	53	Pan American Petroleum Corp. #37 Chambers County Agric. Co.
	54	R. A. Welch #2 Barrow Fee
	55	Mills Bennett #16 E. E. Barrow

Appendix 2 (cont.)

County	Cross Section Well Number	Well Name
Chambers	56	M. T. Halbouty & Hunt Oil Co. #1 Kirby Oil & Gas Co.
	57	Lloyd H. Smith, Inc. #1 Claude Williams
	58	Admiral Drilling Co., Inc. #1 Williams
	59	J. W. Mecom #3-B Mayes
Harris	60	Pan American Petroleum Corp. #1 Annie Schoeps Oil Unit #1
Chambers	61	E. Adams #A-2 O. K. Winfree
	62	E. Adams #A-1 O. K. Winfree
	63	McDaniel Bros. #1 G. W. Collier
	64	D. J. Harrison, Jr., et al. #1 Annie Donnelly Heirs
	65	McAlbert Oil Co. #6 Woodward
	66	Atlantic Richfield Co. #41 Kirby "B"
	67	Amoco Production Co. #40 Chambers Co. Agric. Co.
	68	The Texas Co. #4 A. B. Lawrence
	69	W. F. Newton and Nordix #1 A. E. Barber
	70	Kraftex Enterprises, Ltd. #1 Williams
	71	Sinclair Oil & Gas Co. #6 McKinney
	72	Sun Oil Co. #7 O. K. Winfree
	73	Sparta Oil Co. #1 Kirby Pet. Co. Fee
	74	The Texas Co. #1 Morgan
	75	H. L. Chavanne Trustee, et al. #1 Gulf Monongahela Fee
	76	Cole & Harrell Drilling Co. #1 C. F. Smith
	77	W. R. Johnson Trustee #C-1 Kirby
	78	T. J. Haberle #1 Traverso, et al.
	79	Glenn McCarthy #1 Kirby
	80	Humble Oil & Ref. Co. #B-1 W. D. Meyer Fee
	81	R. & S. Oil Co. #1 Wilburn
	82	Trice Production Co. #1 C. O. Williams

Appendix 2 (cont.)

County	Cross Section Well Number	Well Name
Chambers	83	Merit-Ingot Oil Cos. #1 Wright
	84	The Texas Co. #1 Richardson
	85	Harrison & Gilger, et al. #1 A. E. Barber
	86	The Texas Co. #1 Van Zandt
	87	S. E. Pyndus #1-B A. E. Barber
	88	The Dallas Group #1 O. K. Winfree
	89	Sun Exploration & Prod. Co. #1 Mary E. Bennett Trust
	90	Houston Oil & Minerals Corp. #8 Kirby Pet. Co. "B"
	91	Texas Butadiene & Chem. Co. #3 Barbers Hill Storage
	92	Diamond Alkali Co. #4 Fresh Water Well
	93	Humble Oil & Ref. Co. #4 LPG Storage
	94	Sun Oil Co. #3-A Higgins
	95	Anderson & Fullilove Pet., Inc. #2 SH Oil and Royalty
	96	Mills Bennett Prod. Co. #11 F. E. Barrow
	97	S. E. Pyndus #2 A. E. Barber

HYDRAULICS OF CAP ROCK, BARBERS HILL SALT DOME, TEXAS

by

D. A. Smith

CONTENTS

INTRODUCTION	239
HYDROGEOLOGY NEAR BARBERS HILL SALT DOME	242
Chicot and Evangeline Aquifer Distribution and Quality	245
Chicot and Evangeline Aquifer Hydraulics	247
CAP-ROCK HYDROLOGIC SYSTEM, BARBERS HILL SALT DOME	252
Distribution of Cap Rock and Lost-Circulation Zones	252
Water Levels in the Cap Rock	252
CAP-ROCK HYDRAULICS	255
Witherspoon Model	259
Evaluation of Brine Disposal Into Barbers Hill Cap Rock	260
Conclusions	268
IMPLICATIONS OF LOST-CIRCULATION ZONES	269
REFERENCES	271
APPENDIX. Calculation of the area of cap-rock/sand interface	273

Figures

1. Fence diagram, Barbers Hill Dome	240
2. Water levels, upper Chicot aquifer	241
3. Water levels, lower Chicot aquifer	249
4. Water levels, Evangeline aquifer	250
5. Cap-rock facies, Barbers Hill Dome	253
6. Static brine water levels, Barbers Hill Dome	254
7. Cap-rock brine pressure, Barbers Hill Dome	257
8. Water levels in cap rock during brine injection	258
9. Log-log plot, Warren SWD-4 well	263

10.	Log-log plot, Enterprise SWD-2 well264
11.	Log-log plot, Enterprise SWD-2 well265
12.	Graph of dissolved ion in public water well266
13.	Graph of brine disposal and oil production267
14.	Hydrologic profile270
15.	Hydraulic model of cap rock272

Tables

1.	Hydrologic units243
2.	Water quality terminology.244
3.	Transmissivity of Chicot and Evangeline aquifers251
4.	Cap-rock hydraulic head data.256

Appendix Figure

1A.	Method of estimating the surface area of the cap-rock/sand interface, Barbers Hill Dome274
-----	---	------

INTRODUCTION

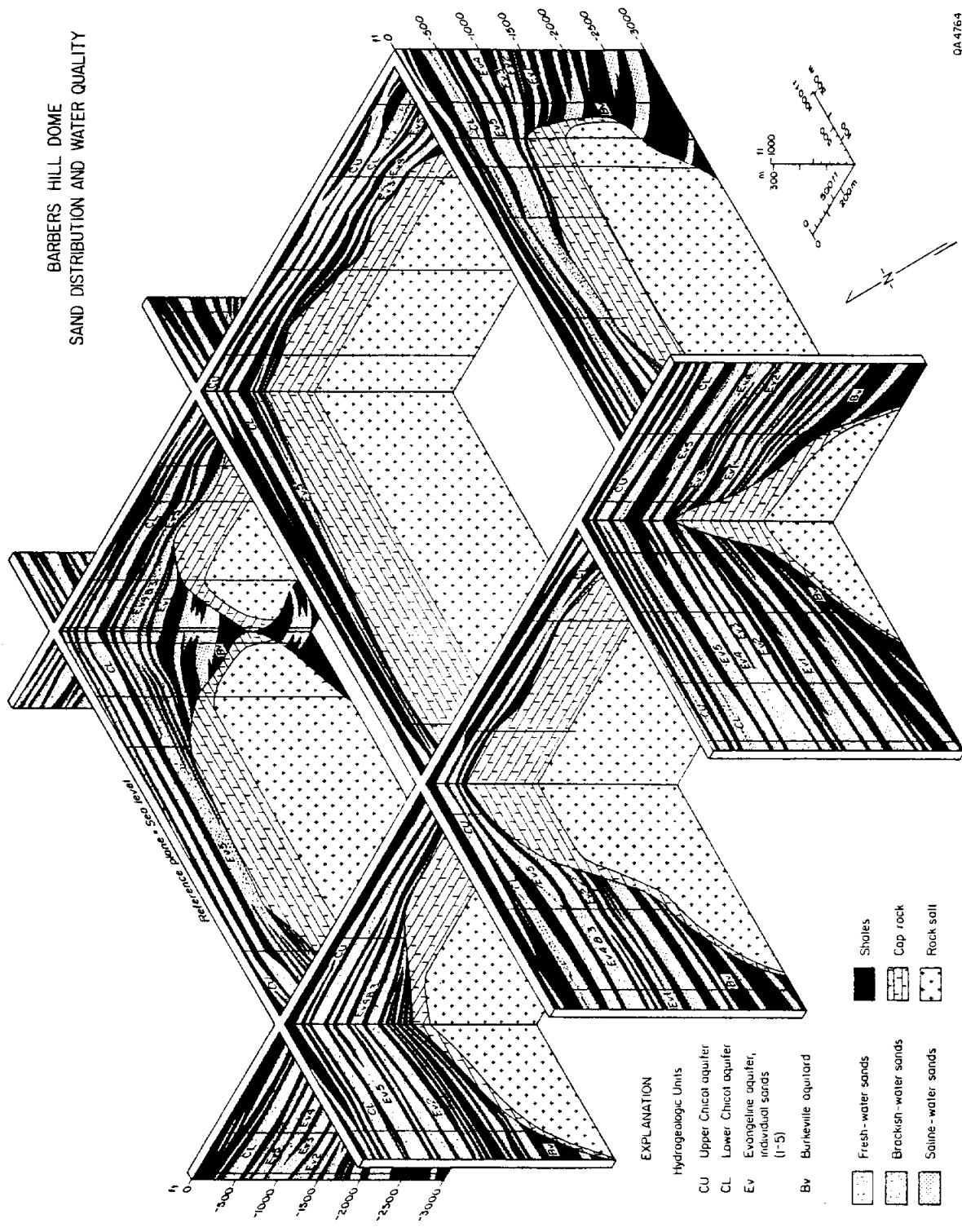
Barbers Hill salt dome underlies Mont Belvieu, Texas in Chambers County (Hamlin, this report, figs. 1 and 2). The dome is used extensively for storage of hydrocarbons in solution-mined caverns in the salt. Cap rock of the dome is also used for brine disposal. Storage caverns are mined by circulating fresh water, which dissolves the salt. Large volumes of brine are created during cavern construction. This excess brine is injected into disposal wells completed in the highly permeable cap rock overlying the dome.

Brine is used in the storage industry to control the pressure of the hydrocarbon product in the cavern and to displace product from the cavern. When product is being stored, brine is displaced from the caverns and must be injected into the cap rock. The fate of brines after injection has not been adequately studied. Possible environmental hazards could result if the brines migrate from the cap rock into aquifers that supply potable water. Salinity increases have been noted in water from public supply wells near the dome. The increase may be a result of natural dome dissolution or a result of brine-disposal activity. If contamination is from natural dome dissolution, however, this indicates that the fresh-water aquifers are in probable communication with the domal material.

Salt dome caverns have been proposed as sites for permanent disposal of toxic wastes much like hydrocarbon storage caverns. The toxic waste would be emplaced through tubing into the cavern in a liquid or slurry. Solidification by injecting a waste slurry with cement or a polymer has been proposed.

Hydrologic characterization of cap rock is an important element in the evaluation of salt domes for toxic waste storage, because cap rocks commonly have cavernous lost-circulation zones. It is difficult to complete a well in these zones, and when drilled, cementing the casing in zones of lost circulation is also difficult. The hydrology of Barbers Hill salt dome cap rock can be studied in detail because there are many wells completed in

BARBERS HILL DOME
SAND DISTRIBUTION AND WATER QUALITY



EXPLANATION

- Hydrogeologic Units
- CU Upper Chicot aquifer
 - CL Lower Chicot aquifer
 - Ev Evangeline aquifer, individual sands (1-5)
 - Bv Barneville aquifer

- Shales
- Cap rock
- Rock salt
- Fresh-water sands
- Brackish-water sands
- Saline-water sands

Figure 1. Fence diagram showing distribution and thickness of upper and lower Chicot aquifer and Evangeline aquifer sands and clays and the thickness and distribution of cap rock at the Barbers Hill salt dome, Chambers County, Texas (Hamlin, this volume). The relative quality of the waters in the aquifer sands as determined by electric logs is also shown.

QA 4764

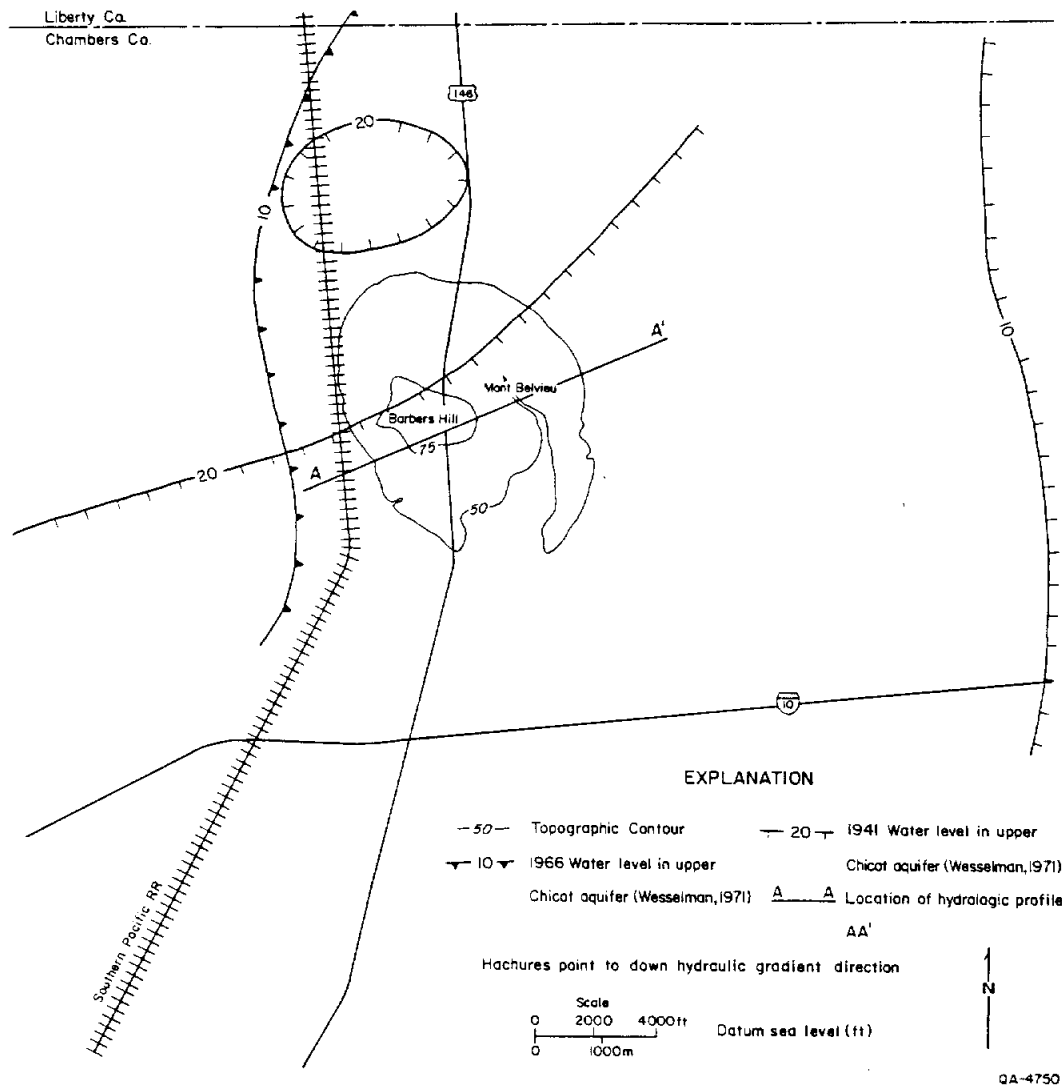


Figure 2. Water levels in the upper Chicot aquifer, northwestern Chambers County, (modified from Wesselman, 1971).

the cap rock for saltwater disposal. Information gained from the study of Barbers Hill will be useful in evaluating the proposed toxic waste disposal plans for other domes. No plans have been proposed to use Barbers Hill for toxic waste disposal.

HYDROGEOLOGY NEAR BARBERS HILL SALT DOME

The hydrologic framework in the region of the Barbers Hill salt dome, Mont Belvieu, Texas, consists of a series of sands, silts, and clays of Holocene to Miocene age and lost-circulation zones in the cap rock. The sands contain fresh to saline water. The distribution of fresh water is very limited and variable. According to Wesselman (1971), dome dissolution has affected water quality. Domal uplift has also truncated and thinned fresh-water-bearing sandstones. The base of fresh water is shallower than 1,000 ft below sea level in the Barbers Hill region. Directly overlying Barbers Hill salt dome the base of fresh water is shallower than 350 ft below sea level. In some areas, fresh-water-bearing sands are overlain by sands with higher salinity waters. The cap rock originally contained saline water and is currently the site of disposal of saline water. To understand the relationship between the cap rock and surrounding aquifers, we will first describe the general hydrogeologic conditions in the fresh-water aquifers around the dome, including the Chicot and Evangeline aquifers.

The terminology of Wesselman (1971) was modified for naming aquifers and confining beds of the Barbers Hill region (table 1) and for describing the quality of water (table 2). The uppermost Holocene and Pleistocene sands are called the Chicot aquifer, locally differentiated into the upper and lower unit of the Chicot. Underlying the Chicot aquifer is the Miocene Evangeline aquifer and the Miocene Burkeville aquitard. Below the Burkeville aquitard are saltwater-bearing sands of Miocene age. The Beaumont Formation is the shallowest upper Chicot in Chambers County. Little ground water recharges the aquifers through the Beaumont. Most fresh water in the Chicot and Evangeline aquifers in the

Table 1. Geologic and hydrologic units used in this report*.

SYSTEM	SERIES	Hydrologic unit	
Quaternary	Holocene	Upper Chicot	Chicot aquifer
	Pleistocene	Lower Chicot	
Tertiary	Pliocene	Evangeline aquifer	
	Miocene	Burkeville aquiclude	

*Also used in Wesselman (1971).

Table 2. Quality of water terminology.

<u>Description</u>	<u>Dissolved-solids content (mg/l)</u>
Fresh	less than 1,000
Slightly saline	1,000 to 3,000
Moderately saline	3,000 to 10,000
Very saline	10,000 to 35,000
Brine	more than 35,000

county is recharged in the outcrop areas of the aquifer formations in adjoining counties to the northeast (Underground Resource Management, 1982).

The Chicot aquifer contains fresh to moderately saline water. The upper Chicot contains small amounts of fresh water suitable for domestic use in nearly all of Chambers County, and in a few areas contains larger amounts suitable for public supply. Large quantities of slightly to moderately saline water are adjacent to the fresh waters, and pumpage of the fresh water causes saline water to move toward the discharging wells (Wesselman, 1971). In the Barbers Hill area the upper Chicot contains fresh and slightly saline water. In Chambers County the shallowest upper Chicot sands are recharged by rainfall, but little rainfall can move through the clayey Beaumont Formation into the lower unit of the Chicot and Evangeline aquifers.

The lower unit of the Chicot aquifer in Chambers County contains little fresh water. In the vicinity of the Barbers Hill salt dome poor quality water can be traced for miles from the dome along the ground-water flow path to the south (Wesselman, 1971). Northwest of the domes, however, there are usable quantities of fresh water (Wesselman, 1971). Wesselman (1971) also noted that the City of Mont Belvieu lower Chicot public supply wells were near the saline water and that water from these wells would probably become more saline with continued pumping. Waters from these wells have begun to show increased salinity (Underground Resource Management, 1982; Hamlin, this volume).

The Evangeline aquifer contains fresh water in part of Chambers County southwest of Barbers Hill salt dome. The line of saline water (Wesselman, 1971) cuts across the dome. Southeast of the dome the Evangeline aquifer contains saline water.

Chicot and Evangeline Aquifer Distribution and Quality

Figure 1 is a fence diagram showing the Barbers Hill salt dome cap rock, the sands and clays of the upper and lower units of the Chicot and Evangeline aquifers, and the

Burkeville aquitard (Hamlin, this volume). Electric-log resistivity (long normal log) was used to correlate sands and to estimate the quality of water in the sands. Two sections of the fence are approximately north-south and three sections of the fence are approximately east-west.

The north-south sections show general decrease in water quality from the north to the south along the ground-water flow path. In the upper Chicot, local zones of fresh water are present in the upper part of the aquifer. The east flank north-south section shows the upper Chicot completely fresh at the north end, but slightly saline in the deeper parts to the south. Both north-south sections show fresh water in the lower unit of the Chicot in the north and slightly saline to moderately saline water to the south. The Evangeline is everywhere more saline than 3,000 mg/L dissolved solids close to the dome, but contains slightly saline water in the shallower sands closer to the lower unit of the Chicot. South of the dome a sand contains fresh water.

The three east-west sections also show a general decrease of water quality from north to south. The north flank east-west section shows the upper Chicot nearly all fresh. The crestal section shows some slightly saline water and the south section shows a thin sand containing moderately saline water on the west. The north flank section also shows fresh water in the lower unit of the Chicot with more saline water to the south. The crestal section shows some moderately saline water in the lower unit of the Chicot and the south section shows that the lower unit of the Chicot contains slightly saline and moderately saline water.

The east-west sections of the fence show fresh water in parts of the Evangeline aquifer. The south flank east-west section shows that Evangeline sands 2, 3, 4, and 5 all contain fresh water west of the dome and Evangeline 5 contains fresh water completely across the dome. The north and south sections show fresh water in the Evangeline aquifer to the west and more saline water to the east.

Chicot and Evangeline Aquifer Hydraulics

Water levels in Evangeline and Chicot aquifers have fallen significantly owing to ground-water pumpage. The lower unit of the Chicot aquifer and the Evangeline aquifer are the principal sources of ground water for the Houston area. Immediately west of Chambers County, in Harris County, the lower unit of the Chicot aquifer is the primary source of ground water, and farther west in Harris County the Evangeline aquifer is the primary source of ground water (Gabrysch, 1980). In Chambers County, pre-development water levels probably increased with depth (that is, the Evangeline aquifer water levels were higher than the lower unit of the Chicot water levels, which were higher than the upper Chicot) and each of these levels probably decreased toward the Gulf of Mexico (that is, ground-water flow was downdip toward the coast) (Wesselman, 1971). Many years of ground-water development west of Chambers County have changed the water-level relationships, so that water levels in the upper Chicot aquifer are higher than those in the lower unit of the Chicot and Evangeline. Ground-water development in the Houston area has also changed the ground-water flow direction in the lower unit of the Chicot and Evangeline aquifers, such that flow in Chambers County is now to the southwest toward the large cone of depression in Harris County.

Water levels in the upper Chicot aquifer have declined owing to ground-water development in the lower unit of the Chicot. Cross-formational flow from the upper to the lower Chicot (Jorgensen, 1975) is inferred to be greater than flow because of local ground-water development in the upper Chicot. The decline in the upper Chicot is much smaller than in the underlying units. Water levels in the upper Chicot aquifer near Barbers Hill were 5 to 10 ft above sea level in 1966. This represents a decline of about 10 ft from 1941 (fig. 2). Flow direction in the upper Chicot near the dome was to the southeast in 1941. The hydraulic gradient level in 1966 was much flatter than in 1941. A small cone of depression was in eastern Chambers County and a very widespread flat area of water levels

5 ft above sea level extended from Barbers Hill across the Trinity river to the east. The ground-water flow direction in 1966 was slightly eastward, but the hydraulic gradient was so low that the flow rates in the upper Chicot were very low. Water levels in the upper Chicot have probably declined further since 1966.

Water levels in the lower unit of the Chicot have declined more than 100 ft in Chambers County near the Barbers Hill Dome since 1941. Even as early as 1941, the regional water-level surface in Chambers County was being lowered by ground-water development in the Houston area. Pre-development water levels were probably higher than land surface, and levels declined downdip toward the Gulf (Wesselman, 1971). The regional water-level surface shows a steep dip toward deep zones of depression in the Houston area (fig. 3). The hydraulic gradient is approximately 20 ft/mi or 0.004. Flow direction is from the Barbers Hill region to the south-southwest. Water level in the lower unit of the Chicot aquifer across the Barbers Hill salt dome in 1975 was approximately 100 ft below sea level and has probably lowered since that time.

Water levels in the Evangeline aquifer (fig. 4) display a pattern of decline similar to that in the lower unit of the Chicot. This decline in the Evangeline aquifer is also due to extensive ground-water development in the Houston area. The 1975 water-level contour for the Evangeline aquifer was estimated from Gabrysch (1980) by extrapolation and by comparing the result with mapped water levels from 1955 through 1967. Water levels in the Evangeline have probably declined as much as water levels in the lower unit of the Chicot aquifer (about 100 ft) and are currently near the same level as the lower Chicot (Wesselman, 1971). Based on these estimations, water levels in the Evangeline aquifer in the vicinity of Barbers Hill salt dome in 1975 were also near 100 ft below sea level and have probably lowered since that time. The transmissivity of the upper and lower Chicot and Evangeline aquifers is listed in table 3.

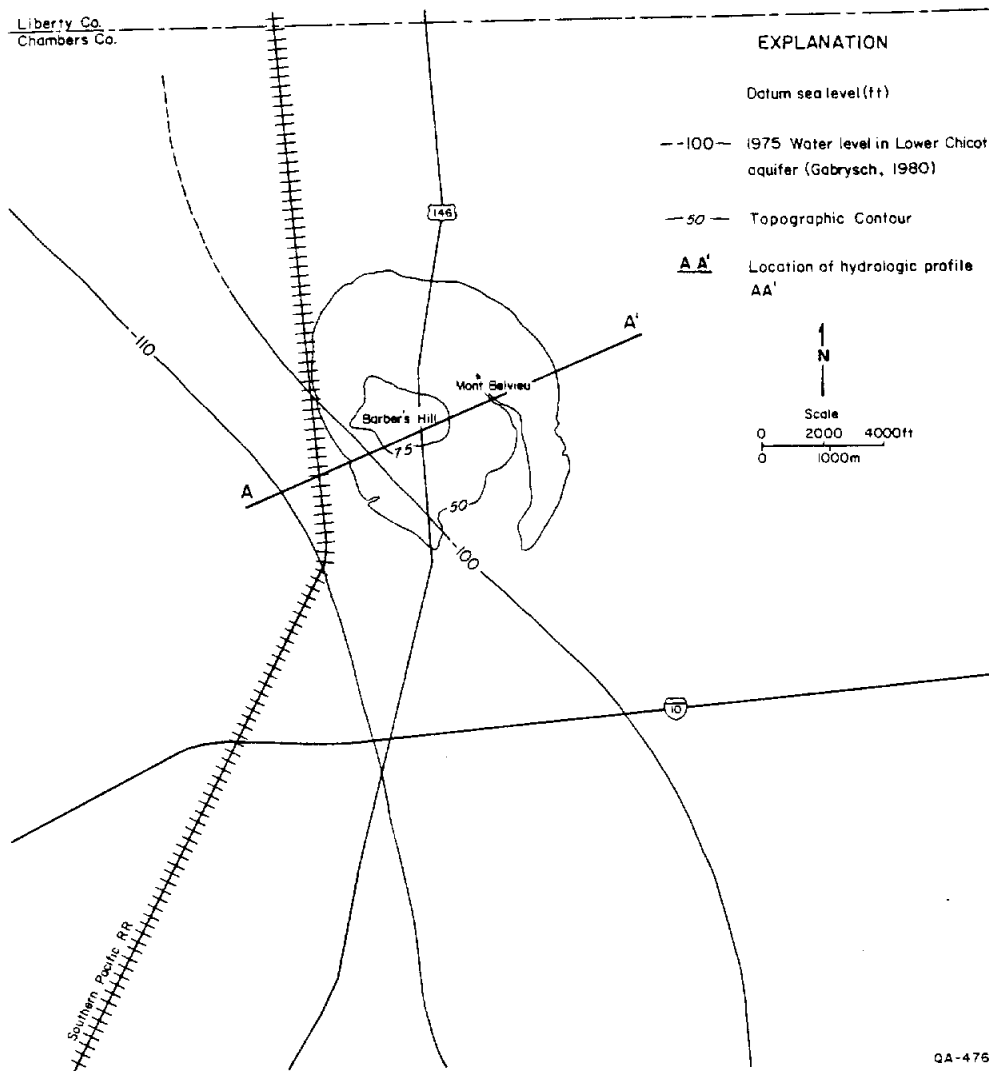


Figure 3. Water levels in the lower unit of the Chicot aquifer, northwestern Chambers County, (modified from Wesselman, 1971, and Gabrysch, 1980).

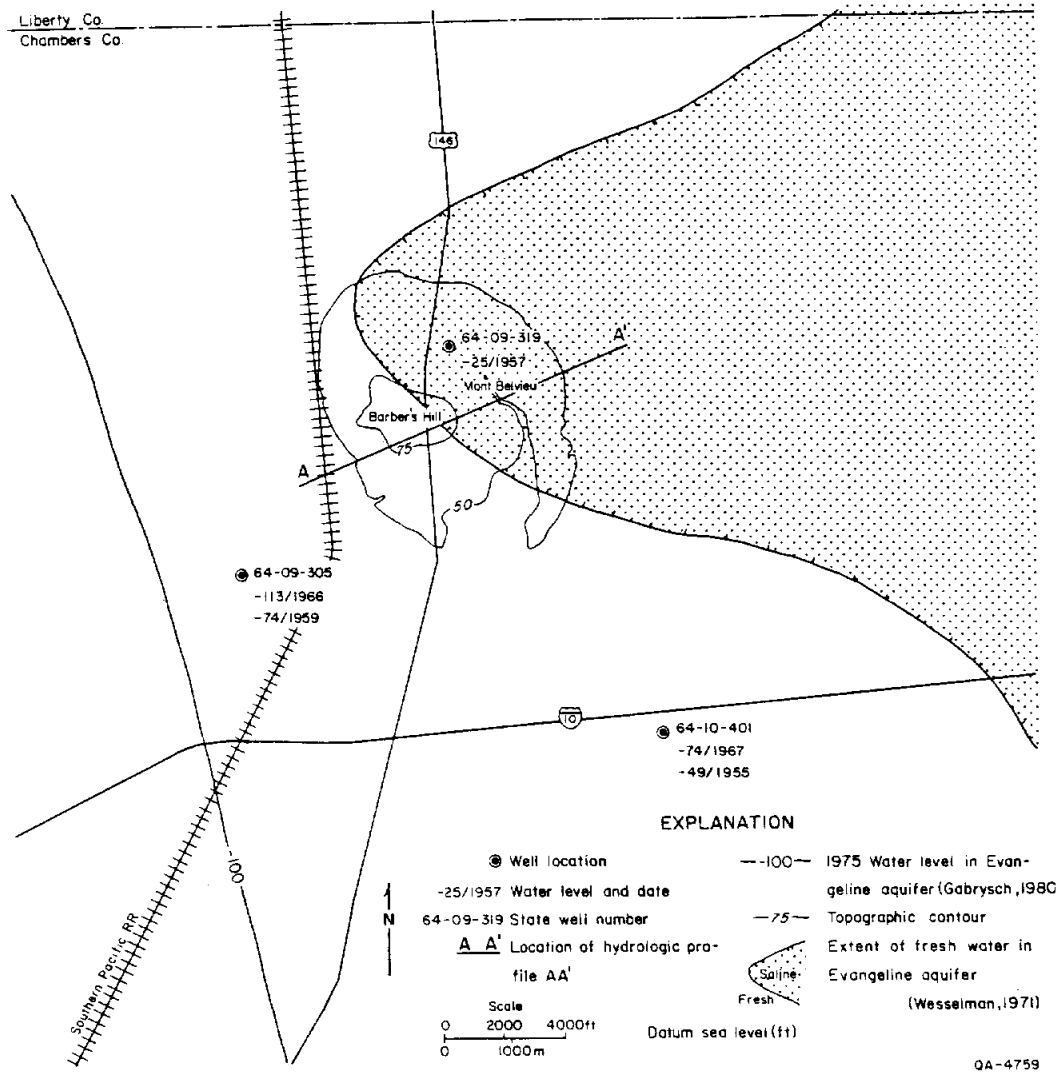


Figure 4. Water levels in the Evangeline aquifer, northwestern Chambers County, (modified from Gabrysch, 1980).

Table 3. Transmissivity of Evangeline and Chicot aquifers.

<u>Aquifer</u>	<u>Transmissivity (g/d/ft)</u>		<u>Number of tests</u>	<u>Source</u>
	<u>range</u>	<u>estimate</u>		
upper Chicot	10,800 - 29,800		9	Wesselman (1971)
lower Chicot	5,200 - 401,000	56,000	10	Wesselman (1971)
lower Chicot		56,000		Jorgensen (1975)
Evangeline	32,000 - 36,000		2	Wesselman (1971)
Evangeline		56,000		Jorgensen (1975)

CAP-ROCK HYDROLOGIC SYSTEM, BARBERS HILL SALT DOME

The hydrologic system of cap rock overlying the Barbers Hill salt dome is complex and can be best described in terms of the size of the cap rock, its lithology, the distribution of the highly porous lost-circulation zones in the cap rock, and the elevation of water levels in the cap rock (both static and during brine injection).

Distribution of Cap Rock and Lost-Circulation Zones

Figure 1 shows the thickness of cap rock over the crest and sides of the dome. Top of salt underlying the central part of the cap rock is very flat at 1,325 ft below sea level. Cap rock includes three facies (fig. 5): (1) massive anhydrite cap rock, which overlies the salt, (2) a transition zone of calcite, gypsum, and anhydrite between the anhydrite and calcite cap rock, and (3) calcite cap rock, which is the uppermost cap-rock layer. The lost-circulation zones mainly occur in two areas--in the transition zone and in a thin layer at the contact between the salt stock and the anhydrite cap rock. The lost-circulation zone at the salt contact consists of loose anhydrite--the insoluble residue left behind after salt is dissolved. The lost-circulation zone in the transition facies is related to the processes that alter the anhydrite to gypsum and calcite (Seni, this volume).

Brine is disposed of in lost-circulation zones in cap rock at Barbers Hill in the transition zone and in the basal anhydrite zone. Cap-rock disposal wells are commonly constructed with casing set at the top of cap rock and open hole through both lost-circulation zones (Underground Resource Management, 1982). The entire cap rock is now hydrologically connected owing to open-hole completion between lost-circulation zones.

Water Levels in the Cap Rock

Static brine water levels in the cap rock (fig. 6) vary depending upon the density of the brine (Witherspoon, 1984). Brine water levels from the three sets of pumping tests

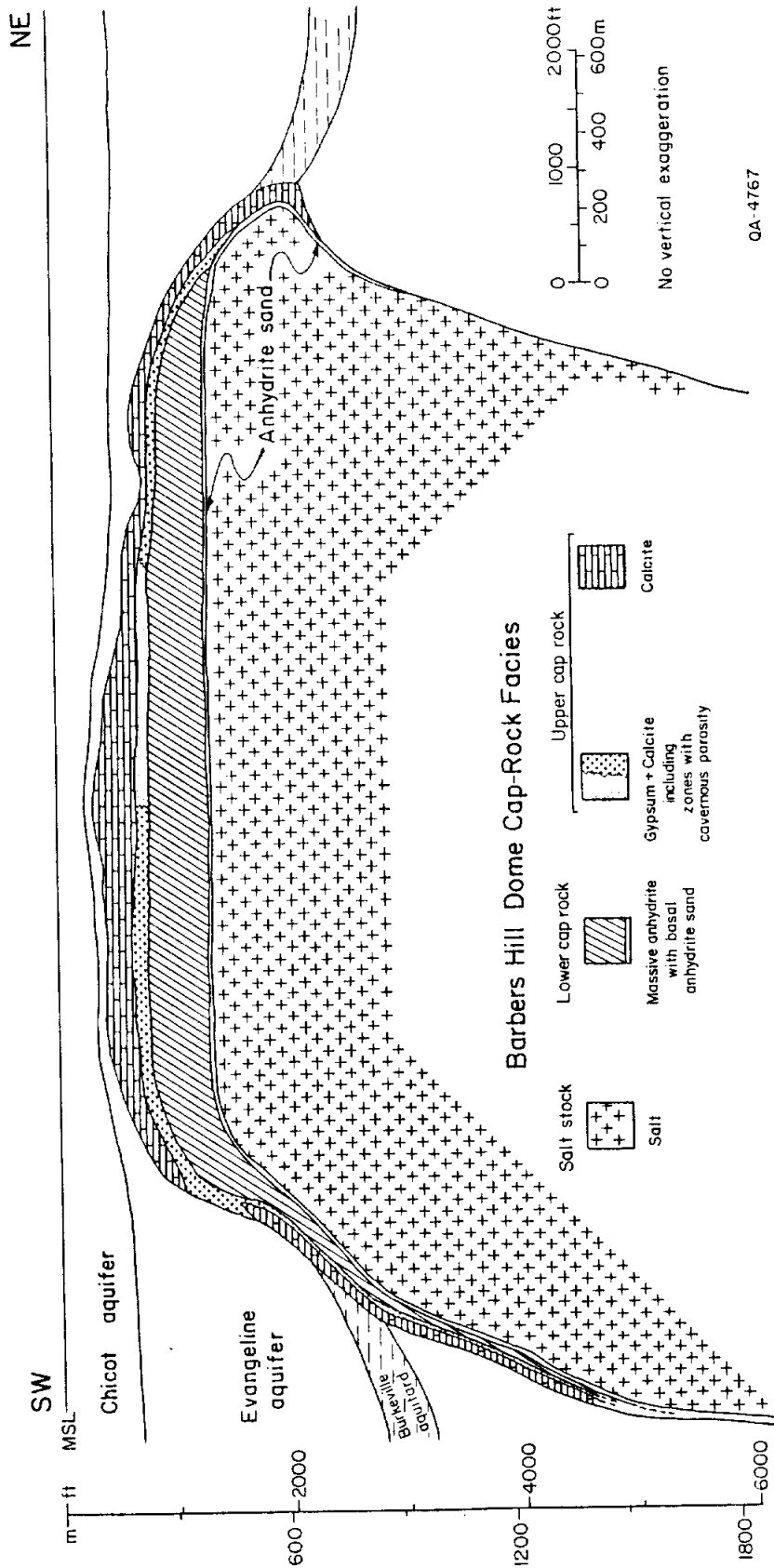


Figure 5. Facies of cap rock, Barbers Hill salt dome, Chambers County, Texas.

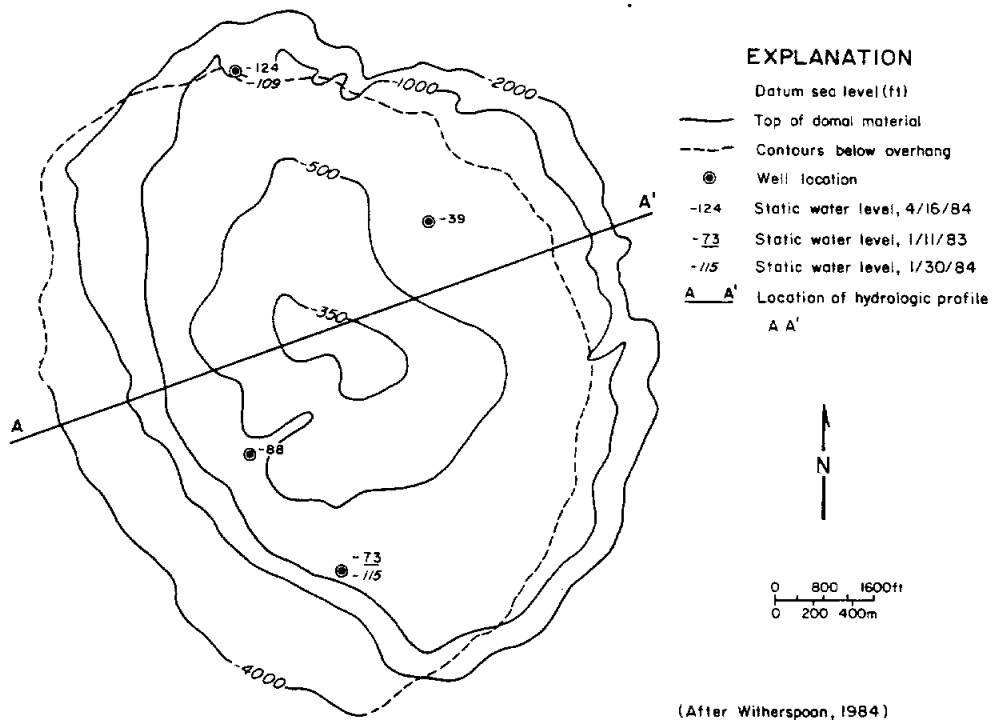


Figure 6. Static brine water levels in cap rock, Barbers Hill salt dome, Chambers County, Texas.

reported in Witherspoon (1984) were converted to pressure at a reference datum of 735 ft below sea level within the cap rock and using pressure gradients reported for each well (table 4, fig. 7). Pressures measured at the beginning of the three sets of pumping tests may not be completely static. The pressures at the beginning of tests on January 30, 1984 and April 16, 1984 are lower than the test of January 11, 1983 and are assumed to be closer to static pressure. Based upon these values, static water pressure in the cap rock is estimated to be approximately 310 psi everywhere in the cap rock at reference datum of 735 ft below sea level. Using an average brine pressure gradient of 0.50 psi/ft and a reference datum of 735 ft below sea level, 310 psi is equal to a water level of 115 ft below sea level.

Water levels during brine injection are dependent upon the rate of injection in each of the injection wells. During three sets of pumping tests (Witherspoon, 1984), brine water levels were measured in wells while known constant injection rate of 7,000 bbl/hr into two wells was maintained. In April and May of 1984, brine water levels in the cap rock (fig. 8) rose to higher than 50 ft below sea level and varied depending upon the density of the brine in the well (Witherspoon, 1984). These water levels were also converted to pressures at a reference datum based on density of brine reported in each well (table 4, fig. 7). Cap-rock brine pressure at 735 ft below sea level during brine disposal of 7,000 bbl/hr into two wells rose to higher than 350 psi in the well closest to the two injection wells. Using an average brine pressure gradient of 0.50 psi/ft, 350 psi at 735 ft subsea reference datum is equal to a water level of 35 ft below sea level.

CAP-ROCK HYDRAULICS

Witherspoon (1984), in a consulting study conducted for the Mont Belvieu Industry Association, investigated the hydraulic behavior of the cap rock of the Barbers Hill field and determined the amount of fluid level rise resulting from disposal of brine into cap rock.

Table 4. Cap-rock hydraulic head data.

<u>Well</u>	<u>Date</u>	<u>Land elevation (ft)</u>	<u>ALTITUDE OF WATER LEVEL</u>		<u>PRESSURE AT -735 FEET DATUM</u>	
			<u>Static brine</u>	<u>Pumping brine</u>	<u>Static pressure</u>	<u>Pumping pressure</u>
Warren 3a	1/11/83	45	-72.7	-71.4	343.1	343.8
Warren 3a	1/30/84	45	-114.9	-102.5	321.2	327.6
Enterprise 2	1/30/84	56	-108.8	-97.8	321.3	326.9
Enterprise 2	4/6/84	56	-124.1	-54.1	313.4	349.3
Warren 4	4/6/84	59	-87.6	-20.6	319.8	352.9
Tenneco 1	4/6/84	53	-39.2	+9.8	311.0	332.9

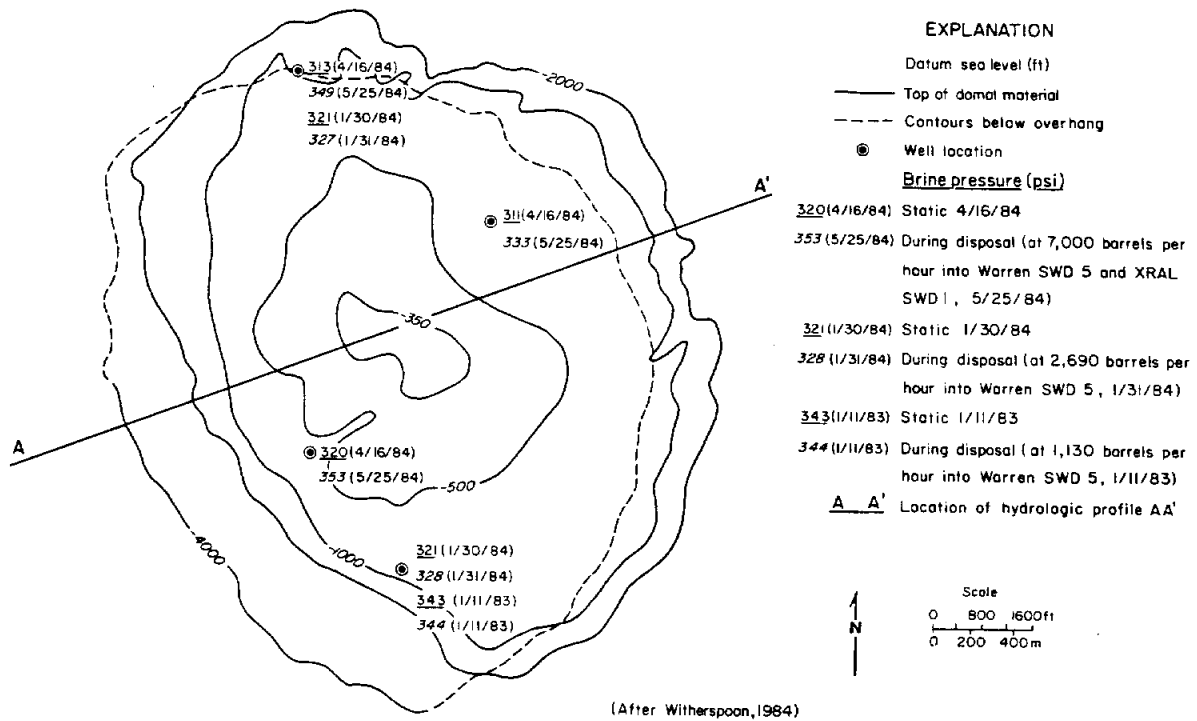


Figure 7. Cap-rock brine pressure, Barbers Hill salt dome, Chambers County, Texas.

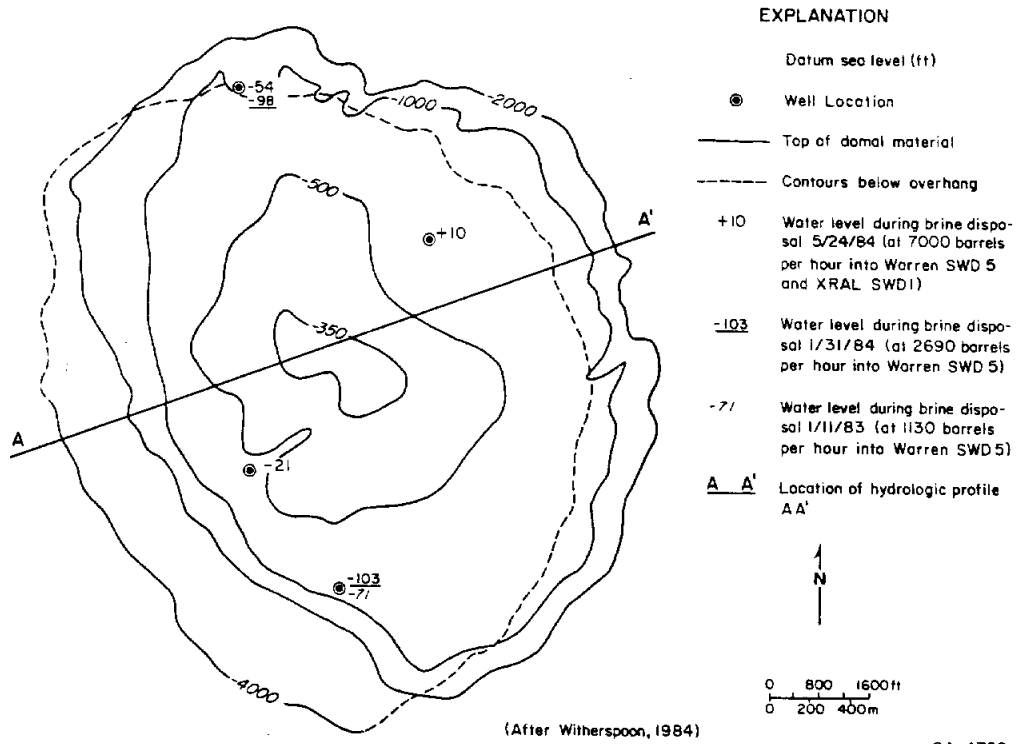


Figure 8. Water levels in cap rock, Barbers Hill salt dome, during brine injection.

Witherspoon (1984) reviewed geophysical logs, geologic cross sections, pumping test results and analyses, and literature of previous studies, and concluded that brine injected into the cap rock at Barbers Hill salt dome flows down the flanks of the cap rock and then migrates laterally into sands that are below the Burkeville aquitard.

The Bureau of Economic Geology has also studied the hydrogeologic system at Barbers Hill salt dome and has reviewed the evidence presented in Witherspoon (1984). This study indicates that the cap-rock hydrologic system is more leaky than Witherspoon's model. Fluid levels in the cap rock measured during long-term injection tests come to an equilibrium state where fluid level does not change with time. If Witherspoon's model as described in testimony were accurate, the fluid levels would not equilibrate, but would continue to build up throughout the injection period as illustrated in the type curves presented in Witherspoon (1984). The equilibration of fluid levels in the cap rock indicates that the boundary or interface between the cap rock and the surrounding sands is more leaky than the Witherspoon (1984) model predicts.

Witherspoon Model

Witherspoon's model depicts the cap rock as a very permeable bounded system with a leaky boundary at a radius of 8,000 ft. Leakage is down the flanks of the dome into saline formations beneath the Burkeville aquitard. Radial distance from the center to the edge of the cap rock is only 4,000 ft, but the linear distance within the cap from the center of the cap rock to the deepest edge of the cap rock down the flanks of the dome ranged from 6,000 to 9,000 ft. The boundary at 8,000 ft in Witherspoon's model is the ends of the cap rock, at depth, down the flanks of the dome.

Witherspoon (1984) analyzed brine-injection interference tests in cap rock to support the Witherspoon model. He developed type curves specifically for a circular aquifer with a boundary at 8,000 ft. Different type curves were used for each different arrangement of wells. The first type curve was for an aquifer with an impermeable boundary. Data from a

brine-injection test conducted January 11, 1983 were matched to this type curve to show that the data initially fit the Theis (infinite aquifer) type curve and then departed from the Theis curve at a time (2.5 minutes), indicating that a boundary had been reached at a distance of 8,000 ft.

Type curves were also developed for cases where the boundary at 8,000 ft was permeable, but less permeable than the cap rock. Data from a brine-injection interference test conducted January 30 and 31, 1984 were matched to these curves to show that the transmissivity of the sands outside the 8,000-ft boundary was one-tenth the transmissivity of the cap rock. From analysis of the January 11, 1983 and January 30 and 31, 1984 brine-injection interference tests, it was concluded that the transmissivity of the cap rock is 564,000 g/d/ft, and the transmissivity of the sands outside the cap rock, 8,000 ft from the point of injection and beyond the leaky boundary, is 56,400 g/d/ft.

A long-term brine-injection interference test was conducted from April 16 to June 4, 1984. This test included constant-rate injection into one well at 3,000 bbl/hr and then into a second well at 4,000 bbl/hr, for a combined injection rate of 7,000 bbl/hr. Brine water levels were measured in three observation wells in the cap rock. Data from the three observation wells were matched to predicted water levels based on the leaky boundary model, with the boundary at a radius of 8,000 ft and the transmissivity outside the boundary one-tenth that inside the boundary.

Evaluation of Brine Disposal Into Barbers Hill Cap Rock

Two elements of the hydrologic system at Barbers Hill are not compatible with the Witherspoon model; (1) the surface area of sands in contact with the cap rock is larger than the Witherspoon model requires and (2) water levels measured in brine-injection tests come to equilibrium in contrast with the Witherspoon model type curves. Several elements of the hydrologic system at Barbers Hill indicate that the injected brines are migrating into Evangeline sands. (1) Static water levels in the Evangeline and lower Chicot aquifer are

strikingly similar to static water levels in the cap rock; (2) water levels in the cap rock during injection are much higher than water levels in the Evangeline and lower Chicot aquifers; and (3) water from a public supply well in the lower Chicot aquifer near the dome is getting more saline. Oil production data from the Barbers Hill field can be correlated with brine-disposal data into the cap rock, indicating that part of the injected brine is moving into the deep sands below the Burkeville aquitard.

To assess a hydraulic model for cap rock, detailed data on the hydrogeologic framework was developed. The three-dimensional distribution of sands surrounding the cap rock were mapped (Hamlin, this volume). Hamlin's set of detailed cross sections across the dome shows that there are hundreds of feet of Evangeline aquifer sands that are in contact with the cap rock. Witherspoon (1984) indicates that all brine injected into the cap rock moves into sands below the Burkeville aquitard and none moves into sands above the Burkeville. The surface area of the cap-rock/sand interface above the Burkeville aquitard (Evangeline aquifer sands) is approximately equal to the surface area of the cap-rock/sand interface below the Burkeville aquitard (Miocene-age saltwater sands) (appendix). The surface area of the total cap-rock/sand interface is much larger than the surface area that is defined by the leaky aquifer model. The fact that there is more sand in contact with the cap rock than indicated in Witherspoon's model explains why the brine water levels came to equilibrium in the long-term injection interference tests.

The Theis type curve for an infinite aquifer shows a continual fluid level rise at a decreasing rate for as long as injection continues. The leaky boundary type curves depart from the Theis curve upward, indicating that fluid level rise in the cap rock in the leaky boundary model should be at a higher rate than in an infinite aquifer, and should also continue to rise as long as injection continues. During the long-term injection tests described in the Witherspoon (1984) testimony, water levels in the observation wells came to equilibrium at the first pumping rate after 10 to 20 days. Water levels in these wells did not continue to rise. Plots of the water level rise with time for the three observation wells

in the April 16, 1984 through May 25, 1984 test (figs. 9, 10, and 11); each falls below the Theis curve. These curves indicate that the system is more leaky than Witherspoon's model. The excess leakage is probably into Evangeline aquifer sands, which are interconnected with the cap rock above the Burkeville aquitard.

Static water levels in the Evangeline aquifer and lower Chicot aquifer are approximately equal and were at 100 ft below sea level when mapped by Gabrysch (1975). Water levels in these aquifers are probably 10 to 20 ft lower at this time owing to continued pumping of these aquifers in the Houston area. Static water levels in the cap rock are also approximately 115 ft below sea level; they fall to this level quickly when injection is stopped (Witherspoon, 1984).

Water levels in the cap rock before disposal practices began were probably near land surface (Witherspoon, 1984). Water levels in the lower Chicot and Evangeline aquifers were also near or above land surface before large-scale ground-water development began in the Houston area (Wesselman, 1971). Under current operating rules at the Barbers Hill field, water levels in the cap rock during brine injection are routinely allowed to rise to 70 ft below land surface (approximately sea level). If water levels continue to rise to 30 ft below land surface (approximately 40 ft above sea level or 155 ft above the water level in the adjacent Evangeline aquifer) injection is halted.

Chemical analyses of waters from the Chambers County Water District No. 1, Well No. 4 (completed into the lower unit of the Chicot aquifer) show an increase in sodium and chloride beginning with analyses in 1980 (fig. 12). The water was a sodium bicarbonate water with nearly constant levels of sodium, bicarbonate, chloride, calcium, magnesium, and sulfate from 1958 to 1980. From 1980 to 1985 the concentration of sodium and chloride increased, but the other constituents remained constant. The water is a sodium-bicarbonate-chloride water.

Oil-production levels from the Barbers Hill field from February 1983 to January 1984 can be correlated with brine-disposal levels from the same time period (fig. 13). The peak

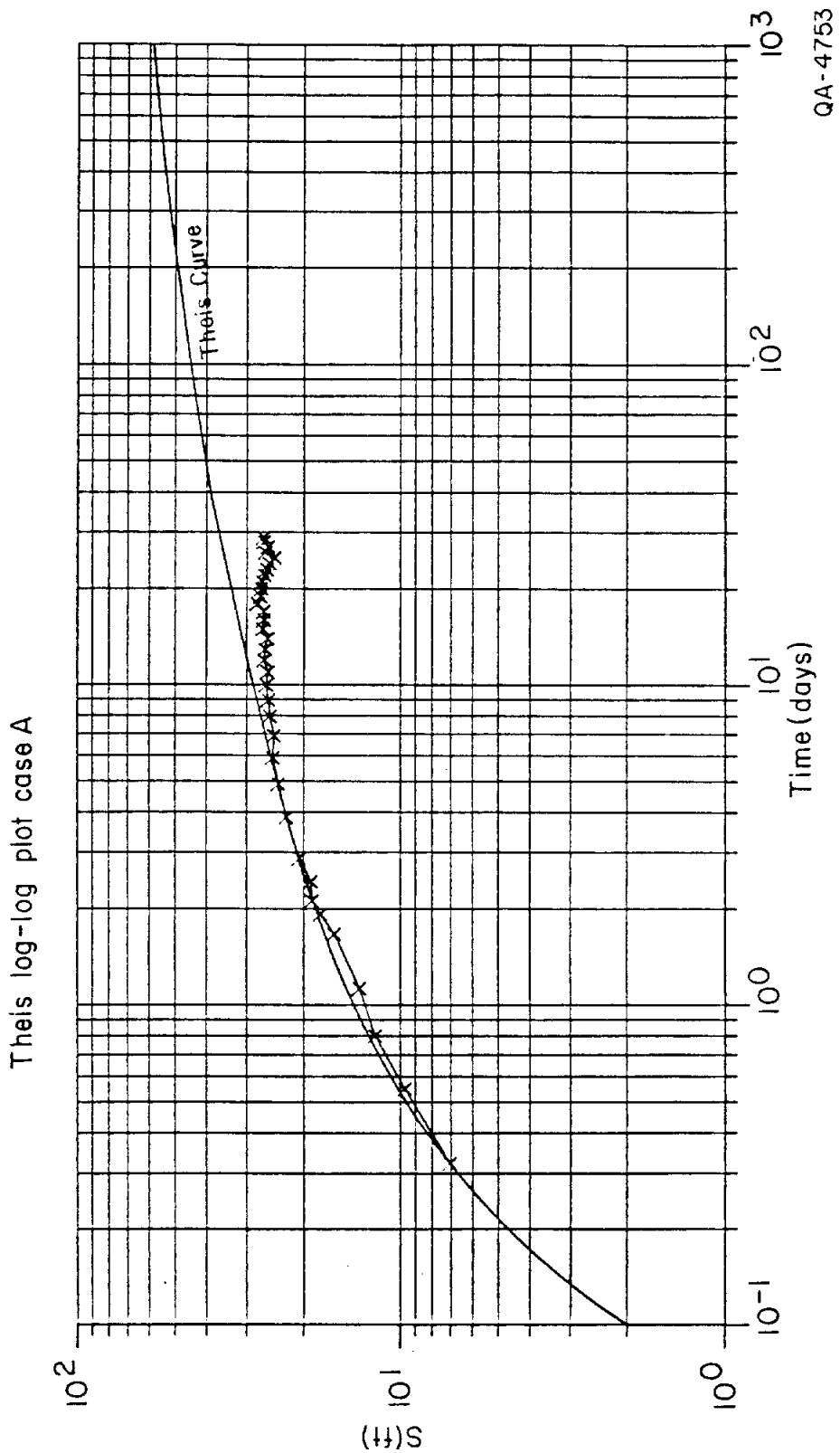


Figure 9. Log-log plot of fluid level rise with time measured in the Warren SWD 4 well during injection of 3000 barrels per hour of brine into the Warren SWD 5 well from April 16, 1984 to May 25, 1984 (from Witherspoon, 1984 Case A).

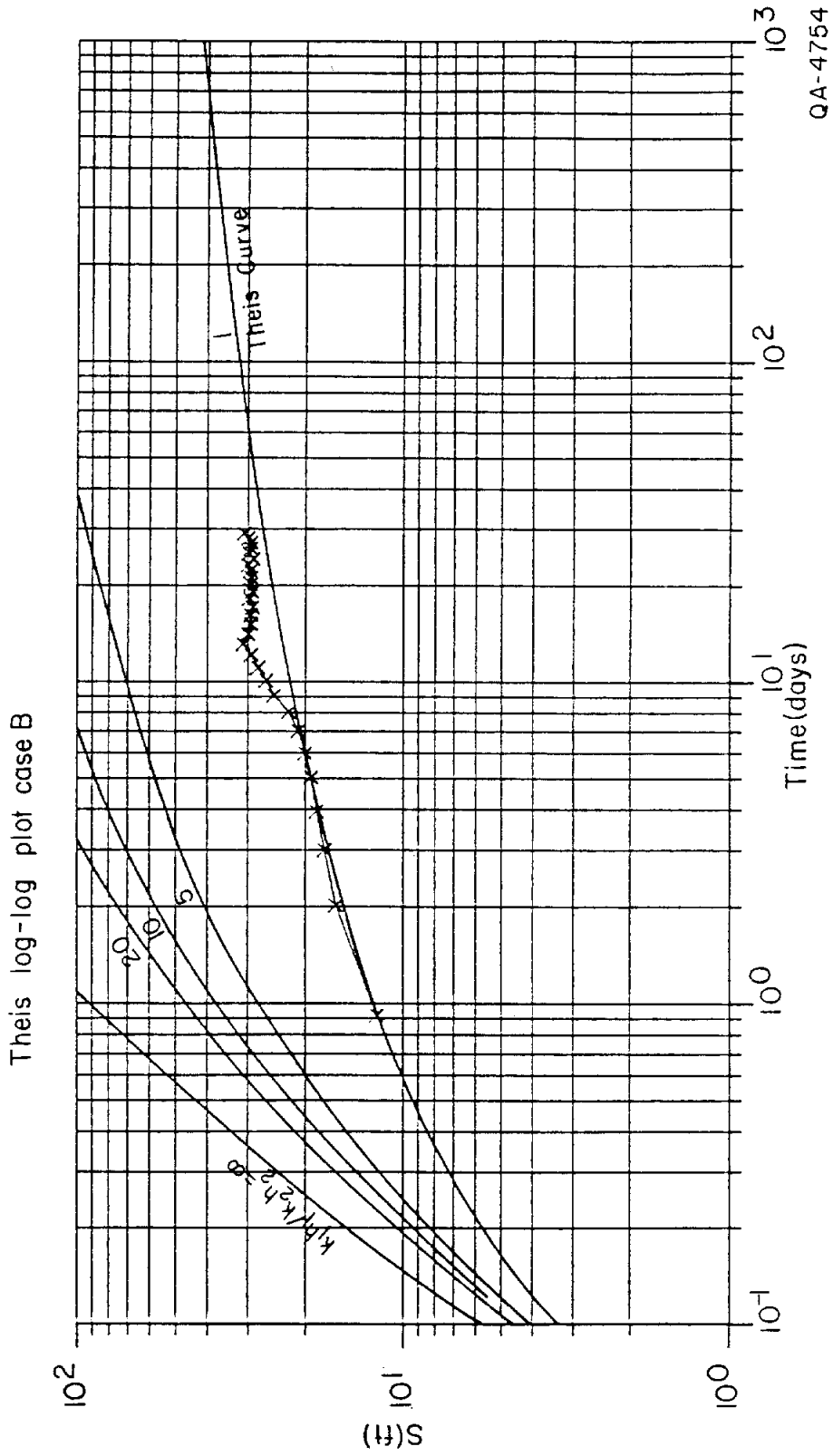
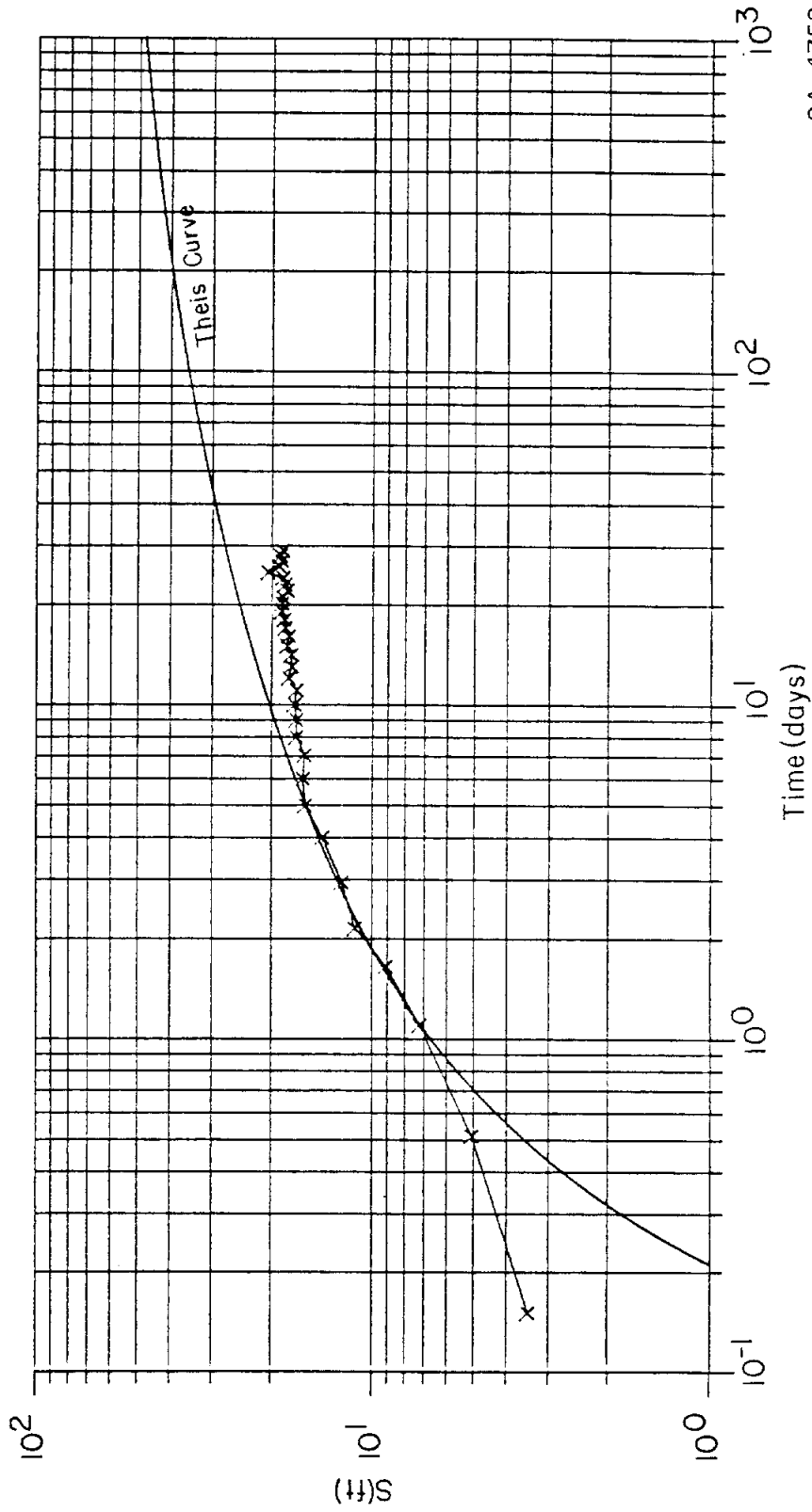


Figure 10. Log-log plot of fluid level rise with time measured in the Enterprise SWD 2 well during injection of 3000 barrels per hour of brine into the Warren SWD 5 well from April 16, 1984 to May 25, 1984 (from Witherspoon, 1984 Case B).

Thisis log-log plot caseC



QA-4752

Figure 11. Log-log plot of fluid level rise with time measured in the Tenneco SWD 1 well during injection of 3000 barrels per hour of brine into the Warren SWD 5 well from April 16, 1984 to May 25, 1984 (from Witherspoon, 1984 Case C).

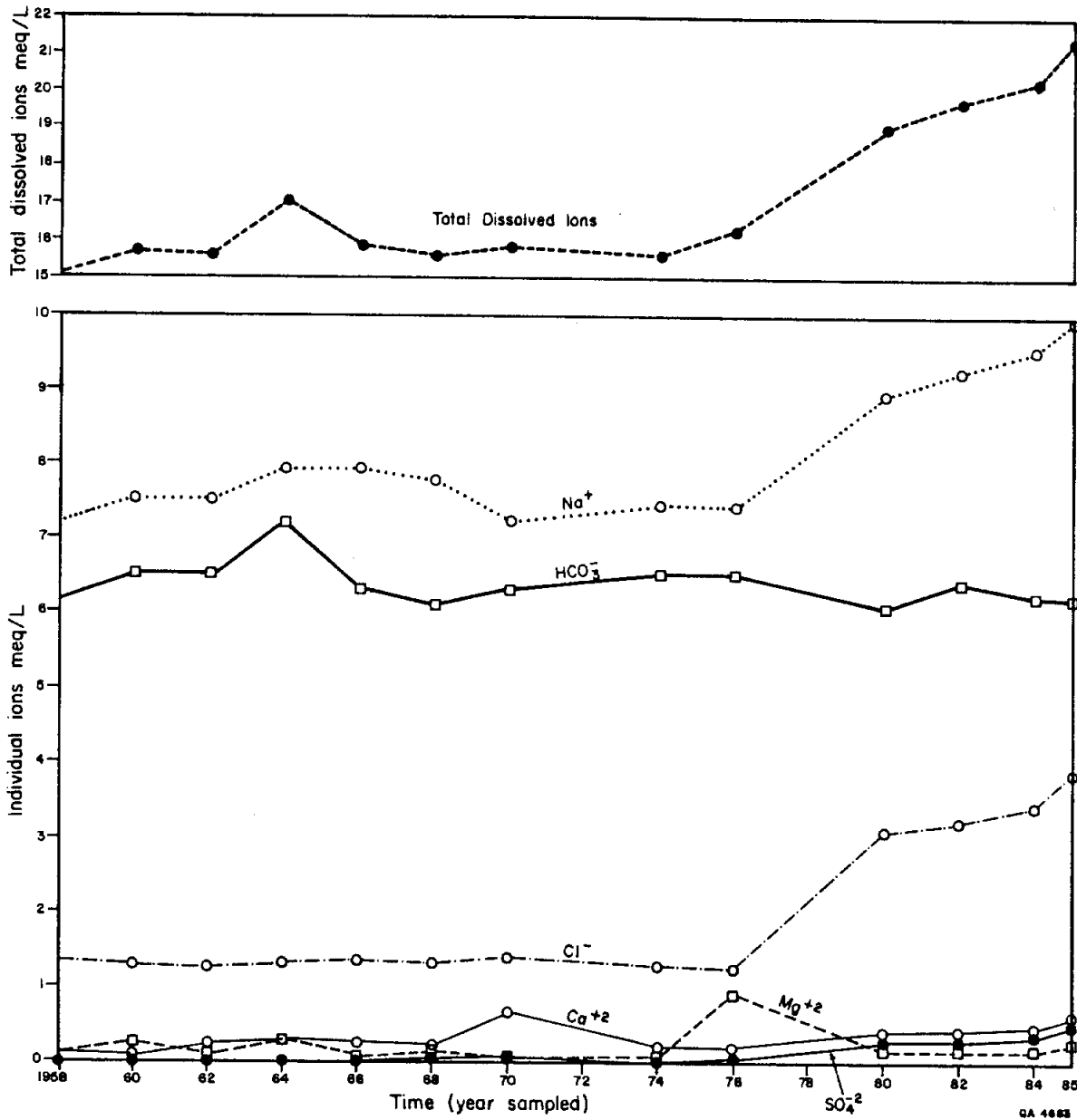


Figure 12. Dissolved ion concentration in water from the Chambers County Water Control & Improvement District No. 1 Water Well No. 4, from 1958 to 1985.

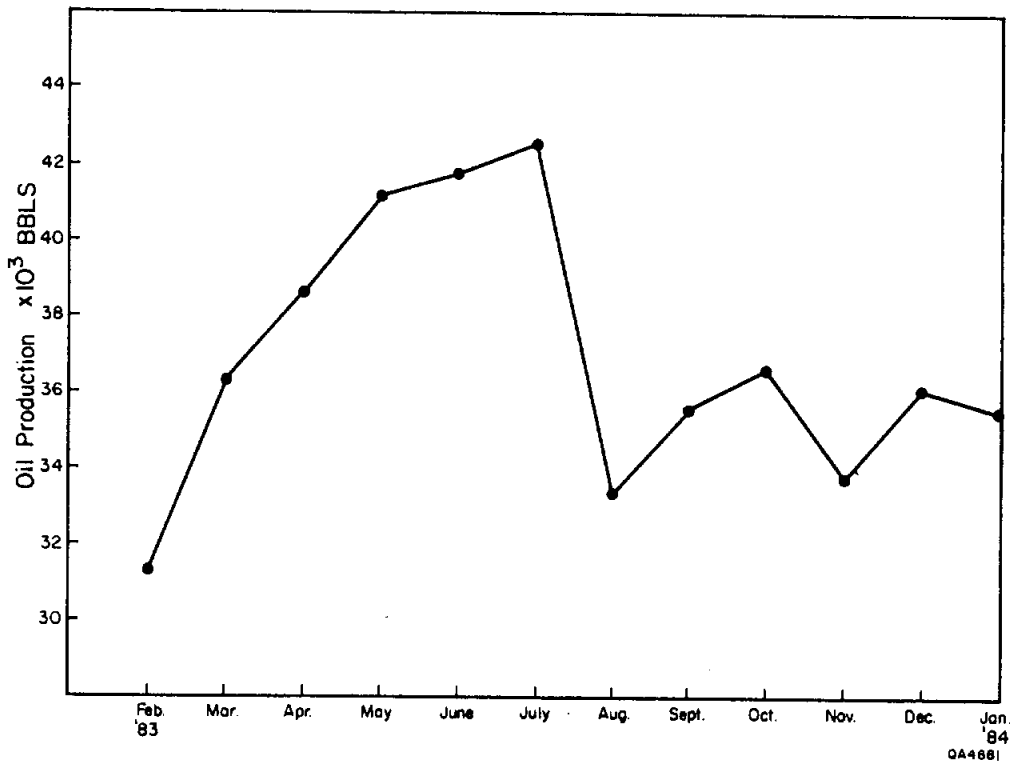
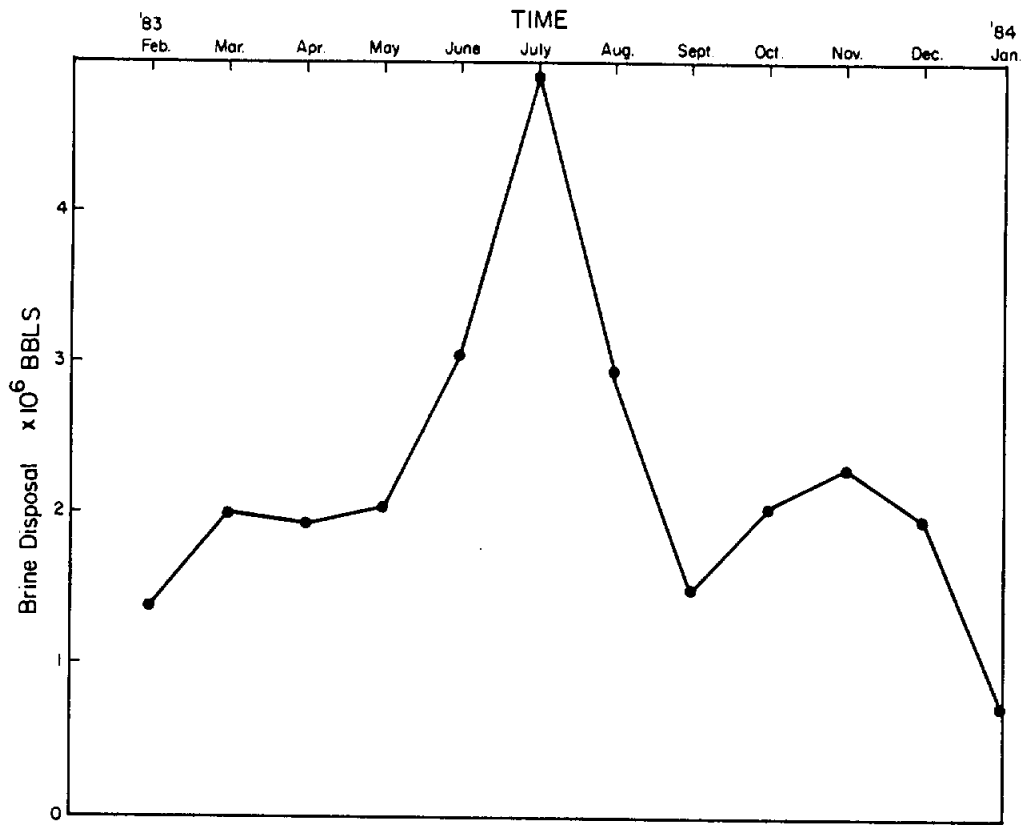


Figure 13. Total monthly brine disposal amounts into Barbers Hill disposal field correlated with monthly oil production from the Barbers Hill oil fields, from Texas Railroad Commission files.

disposal period in July of 1983 corresponds with peak oil production in the same month. The general trends of production for the 12-month period correspond with the general trends of disposal.

Conclusions

There is little doubt that brines disposed into the Barbers Hill cap rock are leaving the cap rock, because the volume of brine injected into the cap is larger than the cap-rock pore volume (Witherspoon, 1984). The following evidence indicates that brine injected into the cap rock at Barbers Hill is leaking into the fresh-water system above the Burkeville aquitard: (1) chemical analyses from a public water supply well, (2) results of brine-injection interference tests, and (3) comparisons of water levels in the aquifers and in the cap rock. Additional evidence indicates that the brines are leaking into the deep saltwater sands as well as into the fresh-water aquifers; (1) geologic cross sections from Hamlin (this volume) and (2) oil production data from the Barbers Hill field are correlatable with brine-disposal rates.

The chemical analyses from the Chambers County Water District Well No. 4 show that the water is becoming increasingly salty with time. It is likely that the origin of the salt in the water is the Barbers Hill salt dome. It does not matter whether it can be proved that the salt is from the brine-disposal activity or not, because if the salt is from the dome it had to come through the cap rock to get into the fresh-water aquifer. If the salt did come through the cap rock, the brines disposed into the cap rock are also moving into the fresh-water aquifer.

The results of brine-injection interference tests show that water levels in the cap rock reach an equilibrium state during injection at 3,000 bbl/hr. Water levels in the three observation wells come to equilibrium within 10 to 20 days. Equilibrium conditions indicate that the injected brine moves out of the cap rock past a leaky boundary at a rate equal to the injection rate. This requires a large surface area through which the injected brine can

pass. The system is more leaky than Witherspoon's model indicates. An additional major area of leakage is inferred to be through the cap-rock/sand interface above the Burkeville aquitard.

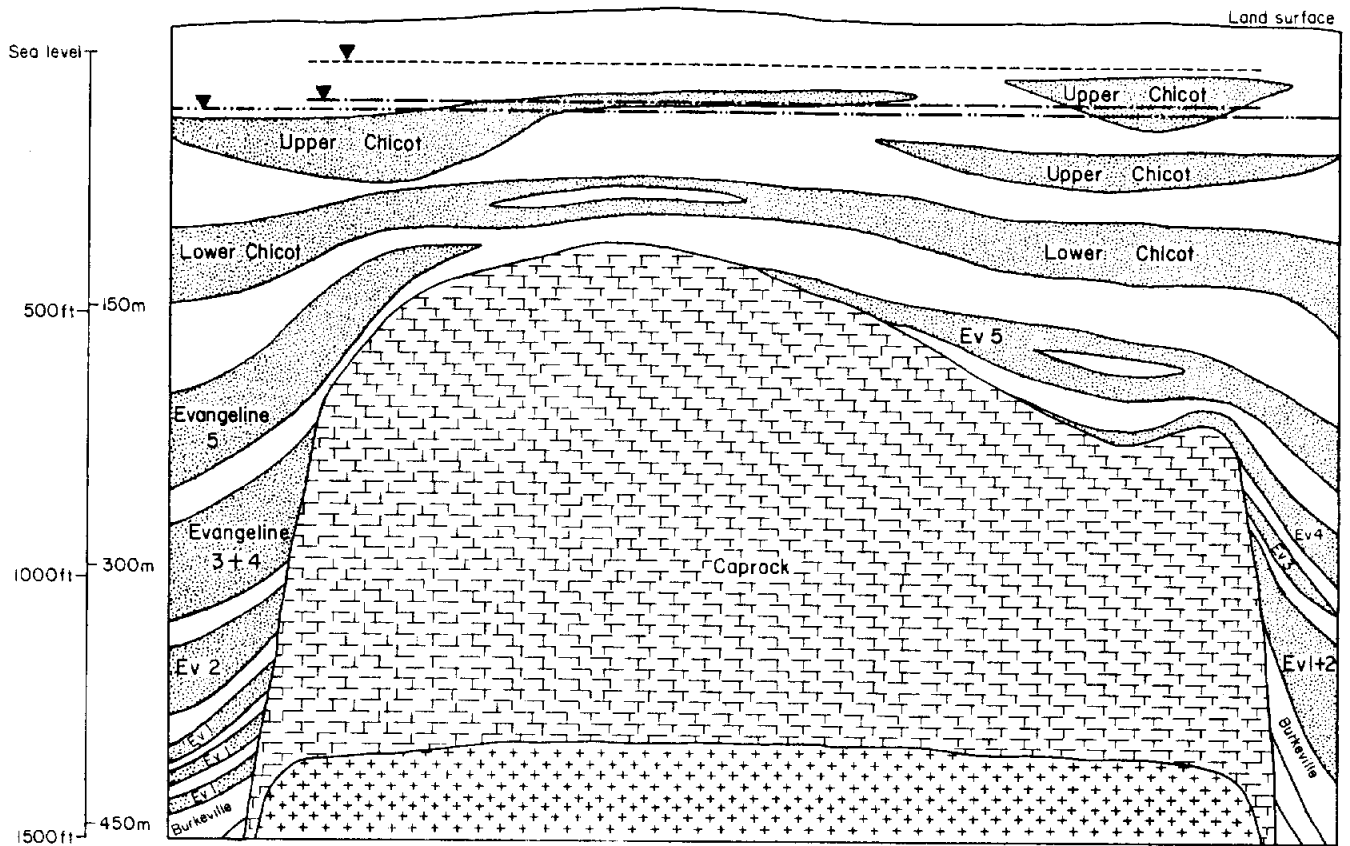
The hydraulic gradient between the dome and the Chambers County Well No. 4 has been reversed by man's activity. Before ground-water development, the hydraulic gradient was from the well toward the coast and thus toward the dome. Since ground-water development, the water level in the well has been lowered at least 100 ft. During brine injection into the cap rock, the water level in the cap rock is raised at least 100 to 150 ft. If the Chambers County well were pumping and the disposal operations at the cap rock were underway at the same time, it is probable that the water level in the cap rock would be 150 ft higher than in the lower Chicot near Well No. 4 (fig. 14) (20 ft above sea level in the cap rock and 130 ft below sea level in the water well).

Geologic cross sections (Hamlin, this volume) show that there are hundreds of feet of Evangeline aquifer sands that are in contact with the cap rock above the Burkeville aquitard. The surface area of the cap-rock/sand interface above the Burkeville is approximately equal to the surface area of the cap-rock/sand interface below the Burkeville, and the total cap-rock/sand area is larger than the leaky boundary model below the Burkeville.

The correlation between oil production and saltwater disposal indicates a probable connection between the cap-rock disposal zones and deeper saline aquifers that are adjacent to the oil sands. Injection into the cap rock acts as a water drive on the oil sand reservoirs.

IMPLICATIONS OF LOST-CIRCULATION ZONES

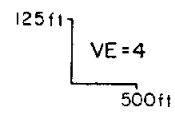
We have studied the cap-rock hydraulic system at the Barbers Hill Dome where lost-circulation zones are so extensive that they are used as a brine-disposal zone. Cap rock



EXPLANATION

- ▽--- Water level in cap rock during brine injection rate of 7,000 barrels per hour into XRAL SWD 1 and Warren SWD 2 (Witherspoon, 1984)
- ▽— Static water level in cap rock (Witherspoon, 1984)
- ▽··· Water level in lower Chicot aquifer (Gabrysch, 1980)

Geologic cross section after Hamlin, this volume



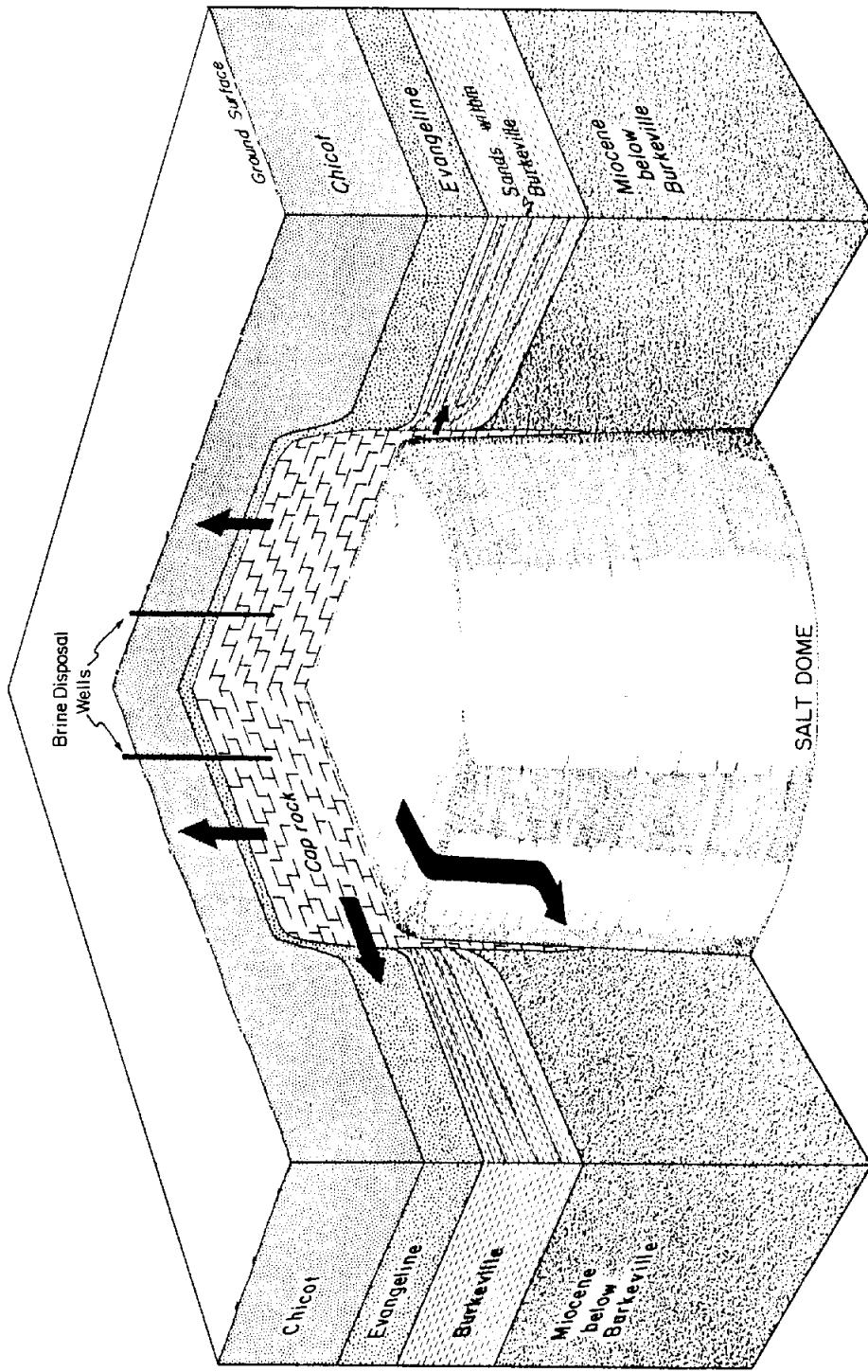
QA-4758

Figure 14. Hydrologic profile A-A'.

with extensive lost-circulation zones appears to have substantial hydraulic connection with adjacent sands. Cap rock at Barbers Hill acts as a single unit. Stress in one injection interval at one well is immediately felt throughout the cap rock. Lost-circulation zones are very permeable. Lost-circulation zones in cap rock penetrated by wells are capable of readily transmitting fluids to both fresh- and saline-water aquifers outside the dome (fig. 15). If toxic waste were lost from a breached cavern or casing into the cap-rock lost-circulation zones, the waste would migrate throughout the cap rock and would likely migrate into adjacent aquifers. Adjacent fresh-water as well as saline-water aquifers could be contaminated. Wherever extensive cap-rock lost-circulation zones are present, it is prudent to completely isolate the lost-circulation zones from well bores, which can transmit toxic materials.

REFERENCES

- Gabrysch, R. K., 1980, Development of ground water in the Houston District, Texas, 1970-1974: Texas Department of Water Resources Report 241, 49 p.
- Jorgensen, D. G., 1975, Analog-model studies of ground-water hydrology in the Houston District, Texas: Texas Water Development Board Report 190, 84 p.
- Underground Resource Management, Inc., 1982, Hydrogeologic investigation in the vicinity of Barbers Hill salt dome: consulting report for the City of Mont Belvieu, Texas, 108 p.
- Wesselman, J. B., 1971, Ground-water resources of Chambers and Jefferson Counties, Texas: Texas Water Development Board Report 133, 183 p.
- Witherspoon, P. A., 1984, Testimony to Texas Railroad Commission, December 13, 1984, concerning Barbers Hill salt dome: Docket 3-83,742, 25 Exhibits.



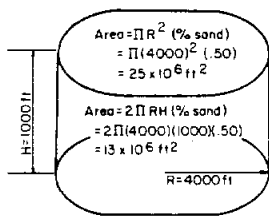
QA-4757

Figure 15. Schematic diagram illustrating hydraulic model of cap rock.

Appendix. Calculation of the Area of Cap-Rock/Sand Interface

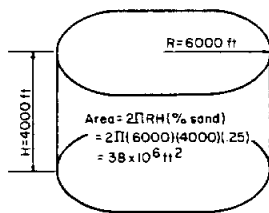
Figure A1 illustrates the method used to estimate the surface area of the cap-rock system, which is in connection with the Evangeline sands and the surface area of the cap rock, which is in connection with the Miocene sands below the Burkeville aquitard. Above the Burkeville aquitard the surface area of the cap rock was approximated by the top and sides of a cylinder with radius 4,000 ft and height 1,000 ft. The percent of the Evangeline aquifer that is sand in the vicinity of the dome was estimated by examination of geophysical logs to be 50%. The effective surface area of the cap-rock/sand interface is then the product of the fraction of the Evangeline, which is sand times the calculated surface area of the cylinder. From figure A1, the total cap-rock/sand interface above the Burkeville is estimated to be 38 million ft².

Below the Burkeville aquitard the area of the cap-rock/sand interface was approximated by the area of the sides of a cylinder with radius 6,000 ft and height 4,000 ft (fig. A1). The percent sand in the Miocene sand intervals close to the dome and below the Burkeville aquitard was estimated to be 25% by examination of geophysical logs. The effective surface area of the cap-rock interface with the Miocene sands below the Burkeville is also 38 million ft².



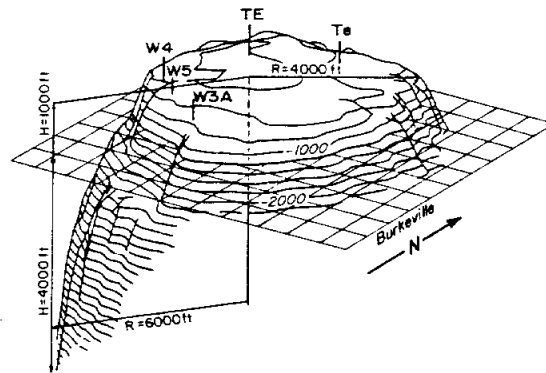
Area of cap rock-sand interface above the Burkeville approximated by the area of the top and the sides of a cylinder

$$\text{Total area} = 38 \times 10^6 \text{ ft}^2$$



Area of cap rock-sand interface below the Burkeville approximated the area of the sides of a cylinder

$$\text{Total area} = 38 \times 10^6 \text{ ft}^2$$



Cap rock viewed from southeast
Contour interval = 200 ft
(Witherspoon, 1984)

QA-4755

Figure A1. Method of estimating the surface area of the cap-rock/sand interface, Barbers Hill salt dome, Chambers County, Texas.

REVIEW OF THE GEOLOGY AND PLIO-PLEISTOCENE
TO POST-PLEISTOCENE DEFORMATION
AT DAMON MOUND SALT DOME, TEXAS

by

E. W. Collins

CONTENTS

INTRODUCTION	278
PREVIOUS STUDIES	278
STRATIGRAPHY	279
Oligocene	283
Miocene	283
Pliocene and Pleistocene	284
DAMON QUARRY	284
Cap Rock	285
Cap-Rock - Bedrock Contact	292
Oligocene-Miocene Strata	292
Pliocene-Pleistocene Strata	295
PLIO-PLEISTOCENE TO POST-PLESTOCENE DEFORMATION	297
SUMMARY	302
REFERENCES	303
APPENDIX. List of Wells.	306

Figures

1. Cross section A-A", southern part of Damon Mound diapir	280
2. Cross section B-B', northern part of Damon Mound diapir	281
3. Cross section A-A', southwest flank of Damon Mound diapir.	282
4. Geologic map and measured sections of strata, Damon Quarry	286
5. Cross section of the northeast wall, Damon Quarry	287
6. Cross section of the southeast wall, Damon Quarry	288
7. Lithologic log	289

8.	Photograph showing breccia texture of cap rock	290
9.	Photograph of fractures and calcite veins in cap rock	291
10.	Photograph of shale - cap rock contact	294
11.	Topographic profile and map of measured sections, Damon Quarry	296
12.	Cross section C-C', Boling, Damon Mound, and Nash Domes	298

Table

1.	Drape compaction estimates for the Damon Mound area	299
----	---	-----

INTRODUCTION

Damon Mound salt dome is located within the Texas Coastal Plain in Brazoria County. Damon Mound Quarry offers the unique opportunity to study the shallow stratigraphy over a coastal dome in outcrop and the subsurface, to view cap rock in outcrop, and to evaluate the most recent phase of deformation associated with diapir uplift.

Damon Mound Dome has salt less than 600 ft (180 m) from the surface. Depths to the cap rock vary because ground elevations above sea level range from about 65 ft (19.5 m) to more than 145 ft (42 m) and because the top of the cap rock is an irregular surface. Over the crest of the dome, cap-rock depths are usually estimated to be less than 100 ft (30 m) below the surface. At the dome margins the cap rock is deeper. Calcite cap rock crops out at the surface on the southeast part of the dome, and the quarry at the northwest side of the mound exposes cap rock and overlying strata. The surface expression over the dome exhibits about 80 ft (25 m) of relief, thus the mound is a significant topographic feature along the relatively flat Texas Coastal Plain. The mound displays radial drainage.

PREVIOUS STUDIES

A number of authors have reported on different aspects of the geology of Damon Mound. Hydrocarbons have been produced along the dome's flanks since 1915 and the early hydrocarbon production was reported by Bevier (1925). A later review of the hydrocarbon production history was done by Porter and Seren (1953). Production at Damon Mound has been from upper Frio sands (Oligocene), Heterostegina limestone (Oligocene-Miocene), and Catahoula sands (lower Miocene).

Hurlburt (1943) noted calcite cap rock exposed at the surface in the town of Damon (southeast side of the mound) and discussed its potential use as road metal. A small abandoned pit occurs in Damon. On the northwest side of the dome the Damon Quarry

operations produce "crushed limestone" (calcite cap rock). Cap rock is 75 to 125 ft (22 to 38 m) below the ground surface in the Damon Quarry.

Sulfur within the cap rock at Damon Mound was mined between 1953 and 1957. Approximately 140,000 long tons of sulfur have been removed by the Frasch process (Ellison, 1971, p. 16-18). Other minerals associated with the cap rock have been discussed by Smith (1979).

A variety of stratigraphic studies have also been conducted at Damon Mound. Cantrell and others (1959) and Ballard (1961) described subsurface characteristics of the Oligocene-Miocene Heterostegina limestone around the salt dome, and Frost and Schafersman (1978, 1979) studied the coralline limestone in outcrop and core. The cap rock and overlying Oligocene to Pleistocene strata exposed in the Damon Quarry have been discussed by Baker (1979); Jenkins (1979) has reported on the Late Pleistocene deposits exposed in the quarry.

This report reviews the subsurface and surface geology at Damon Mound salt dome and evaluates the latest phases of deformation associated with the dome's growth. The structural history of this diapir is important because information derived from these studies may be applied to other coastal diapirs. Salt domes are currently being considered as possible storage and disposal sites for chemical wastes. Knowledge about the geology and structural history of coastal salt domes is a critical aspect in developing an environmentally safe waste repository.

STRATIGRAPHY

Cross sections A-A" and B-B' show the general stratigraphy at four flanks of the dome (figs. 1 and 2). Figure 3 is a detail segment of section A-A" and exhibits the electric log patterns. The cross sections show the lithologies of Oligocene to Pleistocene strata at the dome.

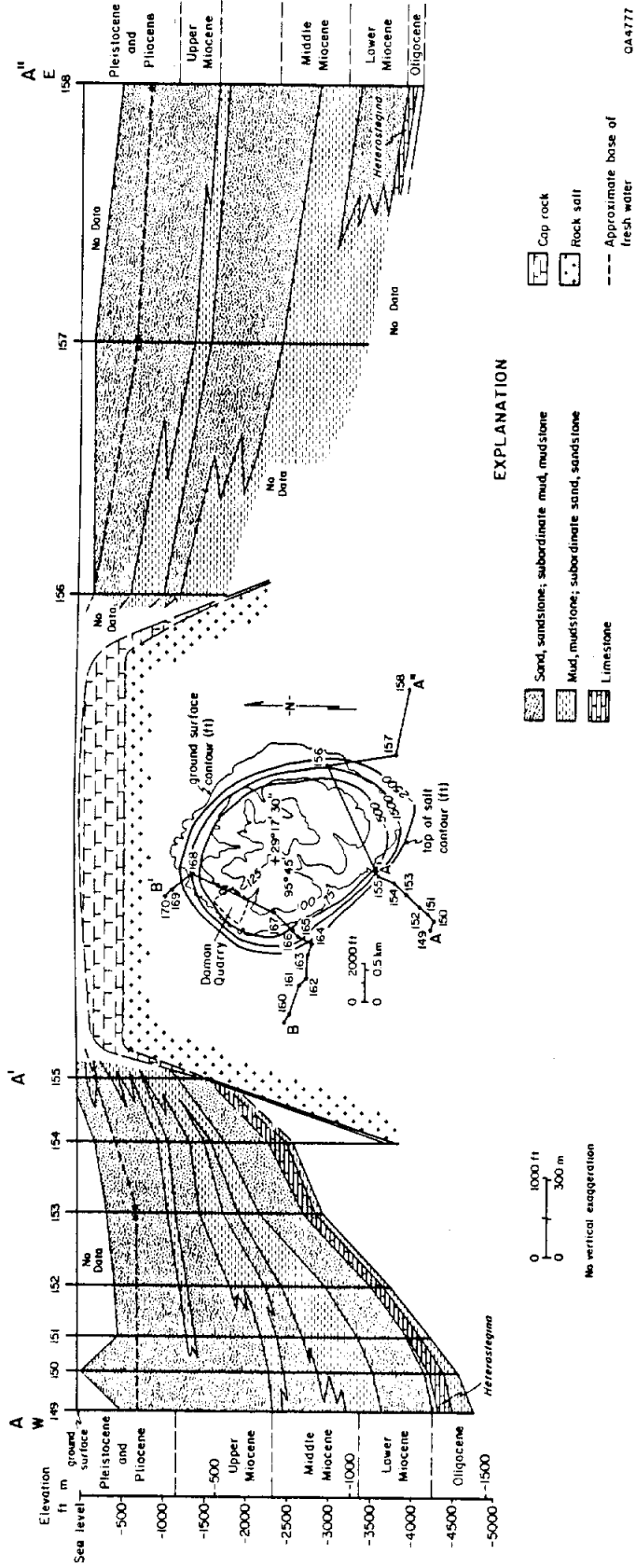
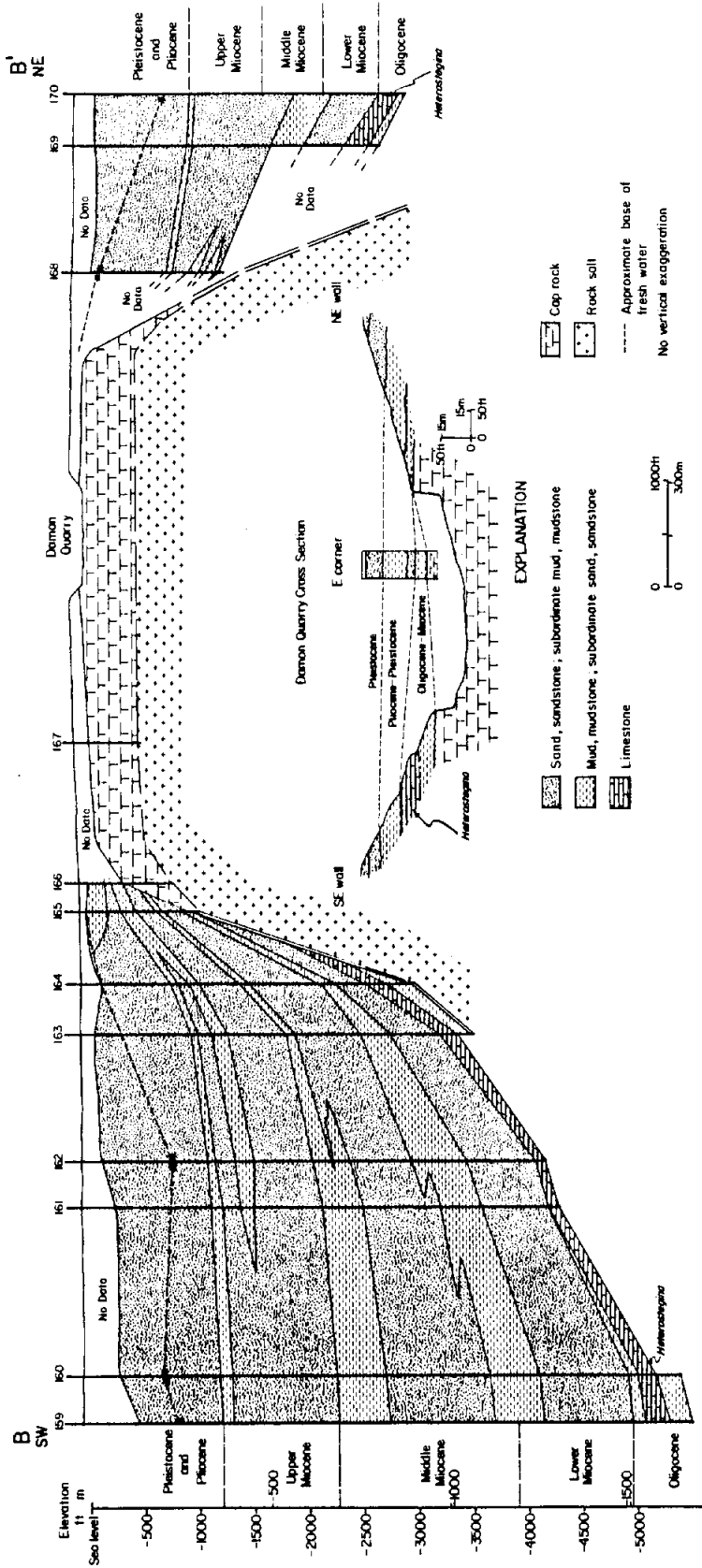


Figure 1. Cross section A-A' showing the general lithologies across southern part of Damon Mound diapir. Well names are listed in Appendix. The approximate base of fresh water was determined from electric logs (*) and Sandeen and Wesselman (1973).



QA-4778

Figure 2. Cross section B-B' showing the general lithologies across northern part of Damon Mound diapir. The location is shown in figure 1. Well names are listed in Appendix. The approximate base of fresh water was determined from electric logs (*) and Sandeen and Wesselman (1973).

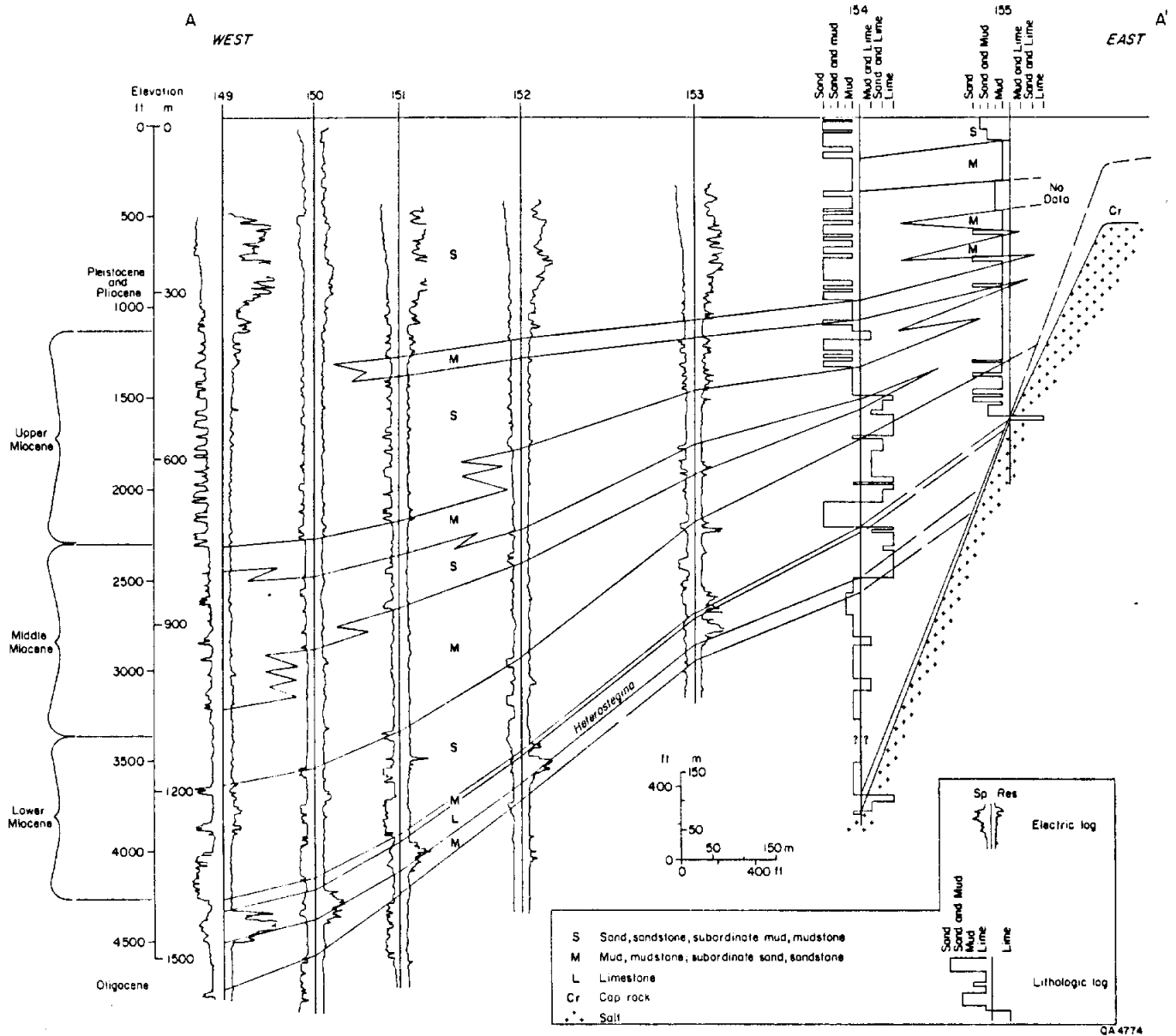


Figure 3. Cross section A-A' showing electric log patterns and general lithologies across southwest flank of Damon Mound diapir.

Oligocene

The Oligocene Heterostegina limestone ("Het" lime) is one of the better subsurface markers around the dome. A preserved block of "Het" limestone is also exposed in Damon Quarry, suggesting that the unit once covered the domal area. The Heterostegina limestone is a coralline limestone facies of the Heterostegina zone, a paleontological unit of the Oligocene Anahuac Formation (Ballard, 1961; Frost and Schafersman, 1978, 1979). The Heterostegina zone is defined by the presence of Heterostegina foraminifera in the faunal assemblage. The Discorbus and Marginulina zones, also of the Anahuac Formation, occur above and below the Heterostegina zone, respectively.

The limestone represents a reef facies that developed in a nearshore, shallow water environment. This reef facies occurs over several of the Gulf Coast domes (Boling, Nash, West Columbia, Barbers Hill, Stratton Ridge, and Damon Mound), indicating that seafloor relief over the diapirs may have influenced reef growth. Reef growth may have continued into early Miocene (Cantrell and others, 1959).

"Het" limestone at Damon Mound generally thickens away from the dome and then pinches out laterally into Heterostegina calcareous muds. The limestone is continuous eastward to Nash Dome, however it pinches out westward before it reaches Boling Dome (Cantrell and others, 1959; Ballard, 1961). It exhibits a structural relief of about 6,000 ft (1,700 m) off of Damon Mound. At the diapir margins, angular unconformities have been reported to separate the Anahuac Formation from the underlying Oligocene Frio Formation and the overlying lower Miocene sands (equivalent to the Oakville Formation updip at the surface).

Miocene

Miocene strata are divided into lower, middle, and upper sequences based on regional correlations with formations mapped at the surface and with paleontological data (figs. 1,

2, and 3). These boundaries are approximate. Early Miocene sands and muds represent shore-zone and marine deposits, whereas the later Miocene sands and muds are alluvial deposits (S. Hamlin, personal communication, 1985). Cross sections A-A", B-B', and A-A' show that Miocene strata thin toward the dome. Some sand sequences pinch out toward the dome, suggesting deposition probably was influenced by dome growth and associated positive relief. Miocene strata are exposed in the Damon Quarry on top of the dome. Structural relief on top of the upper Miocene is approximately 1,300 ft (400 m).

Pliocene and Pleistocene

Pliocene and Pleistocene (Plio-Pleistocene) sediments along the Texas Gulf Coast have been described by Bernard and LeBlanc (1965), Guevara-Sanchez (1974), and Winkler (1979). This stratigraphic sequence is predominantly composed of fluvial and deltaic deposits. The base of the Plio-Pleistocene indicated in figures 1, 2, and 3 is an approximate correlation based on regional correlations with formations mapped at the surface and with paleontologic data (S. Hamlin, personal communication, 1985). The mapped unit thickens away from Damon Mound. Guevara-Sanchez (1974) interpreted the Pleistocene strata in the vicinity of the diapir to be 40 to 60 percent sand. Pleistocene sands make up the Chicot aquifer and part of the Evangeline aquifer. The Evangeline aquifer also includes upper Miocene sands.

Structural relief at the base of the Plio-Pleistocene is 1300 ft (400 m). Late Pleistocene Beaumont Formation sediments cropping out at the surface have been warped about 80 ft (25 m).

DAMON QUARRY

Preserved strata over the dome crest exhibit lateral variations in lithology, erosional boundaries, and complex structural relationships. Together, these data provide evidence

for characterizing the timing of diapir uplift and environmental conditions over the dome crest.

The quarry at the northwest part of the mound exposes calcite cap rock, as well as Oligocene, Miocene, and Plio-Pleistocene strata (Baker, 1979) (fig. 4). This is currently one of the best exposures of sediments overlying a coastal salt dome in Texas. Three general chronostratigraphic units have been mapped above the cap rock in the quarry (fig. 4). They are units composed of Oligocene-Miocene, Pliocene-Pleistocene, and Pleistocene strata. Cross sections of the northeast and southeast quarry walls are shown in figures 5 and 6. Vegetation and slumping currently cover a large portion of the northwest and southwest walls.

Cap Rock

Cap-rock thickness at Damon Mound varies from 375 to 575 ft (110 to 260 m) (Bevier, 1925). Core of the cap rock described by Bevier (1925) indicates three zones: (1) a calcite upper zone, (2) a middle zone composed of anhydrite and gypsum with abundant sulfur, and (3) a gypsum lower zone containing some sulfur (fig. 7). The Damon Quarry has cut into approximately 60 ft (18 m) of the upper calcite zone.

Cap rock exposed in the quarry is predominantly fine- to medium-grained crystalline calcite. It also contains varying amounts of quartz sand and locally, near the upper contact, the rock is a calcareous sandstone rather than a "limestone." The cap rock is commonly a breccia of dark- and light-colored calcite (fig.8). The color variations may indicate different generations of calcite precipitation and variations in purity. Baker (1979) observed large lenses of green mudstone in the cap rock, although recent quarry operations may have dug out these lenses. Fractures are common throughout the calcite rock and are usually filled with brown or light, coarse crystalline calcite, although cavities also exist (fig. 9). Pyrite is common and traces of sulfur also occur.

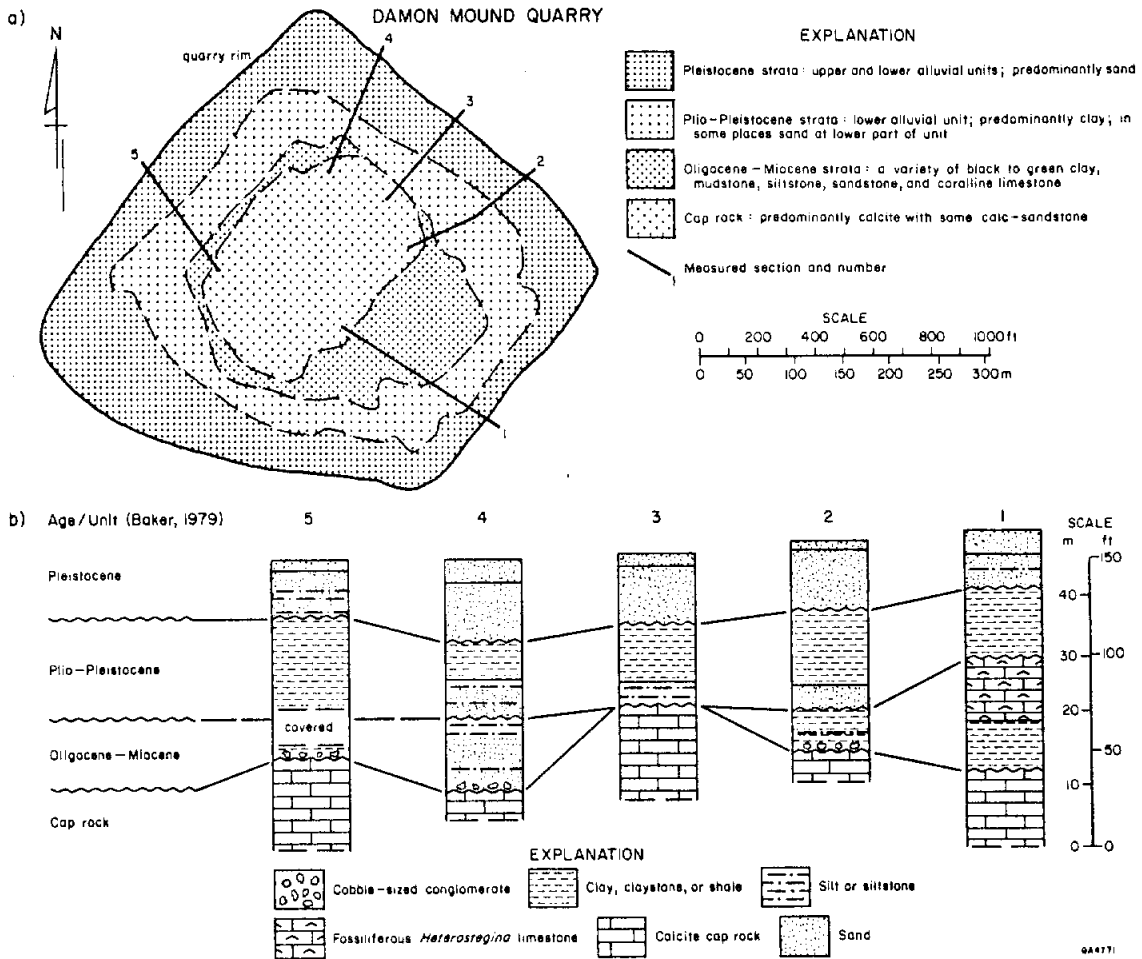
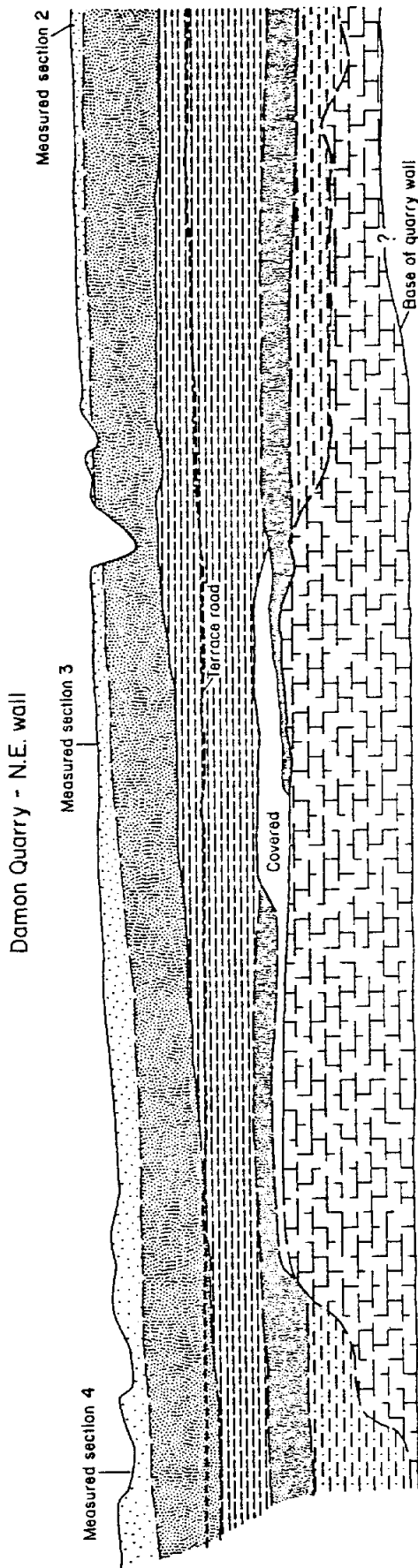








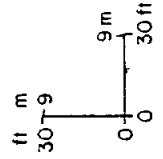
Figure 4. a) Geologic map of Damon Quarry (modified from Baker, 1979) and locations of measured sections. b) Measured sections of strata in Damon Quarry.



Damon Quarry - N.E. wall

EXPLANATION

-  Sand, tan to red; upper alluvial unit
 -  Sand, white; middle alluvial unit
 -  Claystone to mudstone, green to gray; lower alluvial unit
 -  Sand, fine-grained, and siltstone; lower alluvial unit
 -  Claystone to siltstone, some sandstone, green to black
 -  Cap rock
- Pleistocene**
- Pliocene - Pleistocene**
- Oligocene - Miocene**



044776

Figure 5. Cross section of the northeast wall at Damon Quarry. The section was constructed using measured sections and photographs. The general topography at the quarry is shown in figure 2.

Damon Quarry - Part of S.E. wall

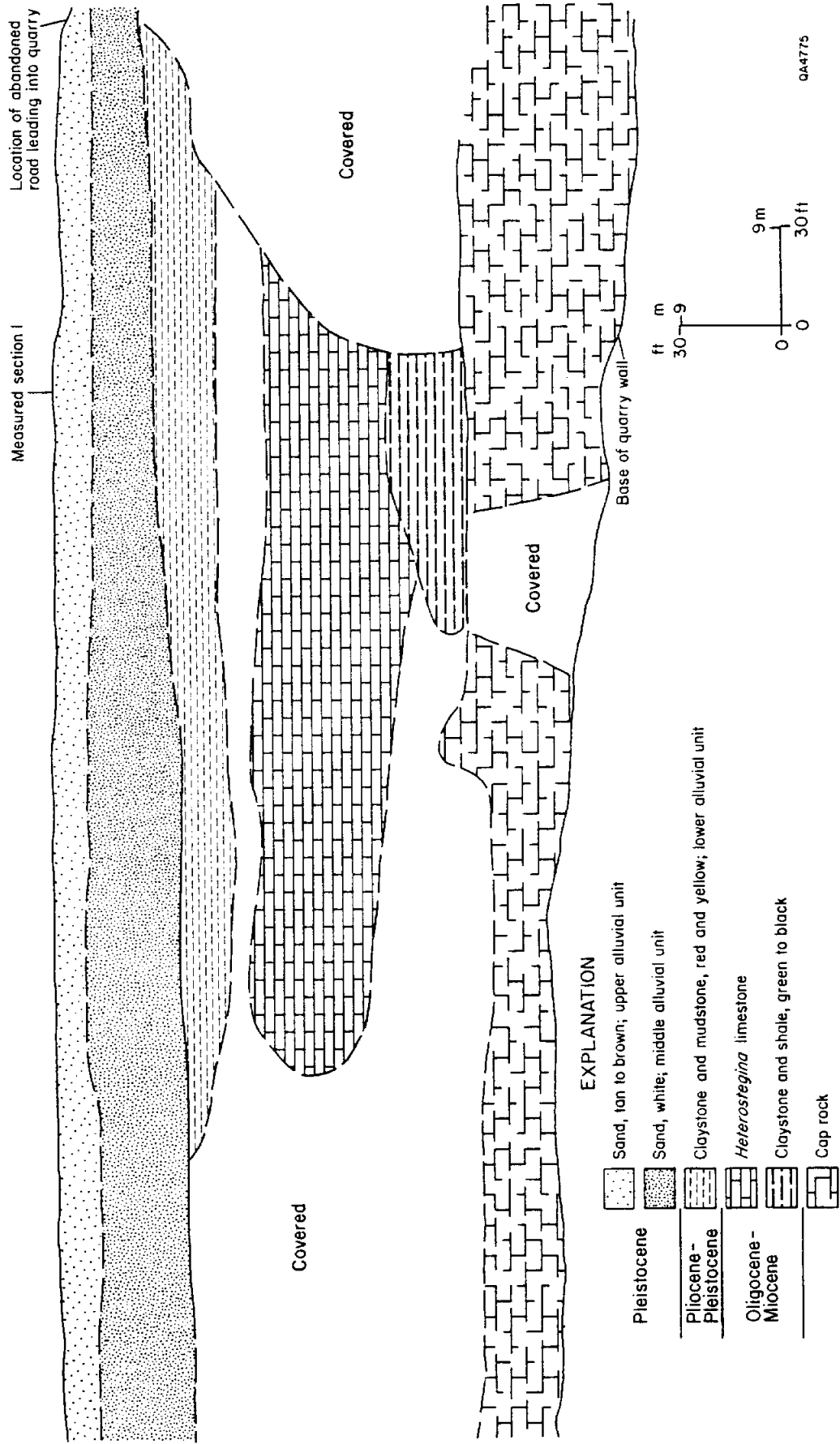
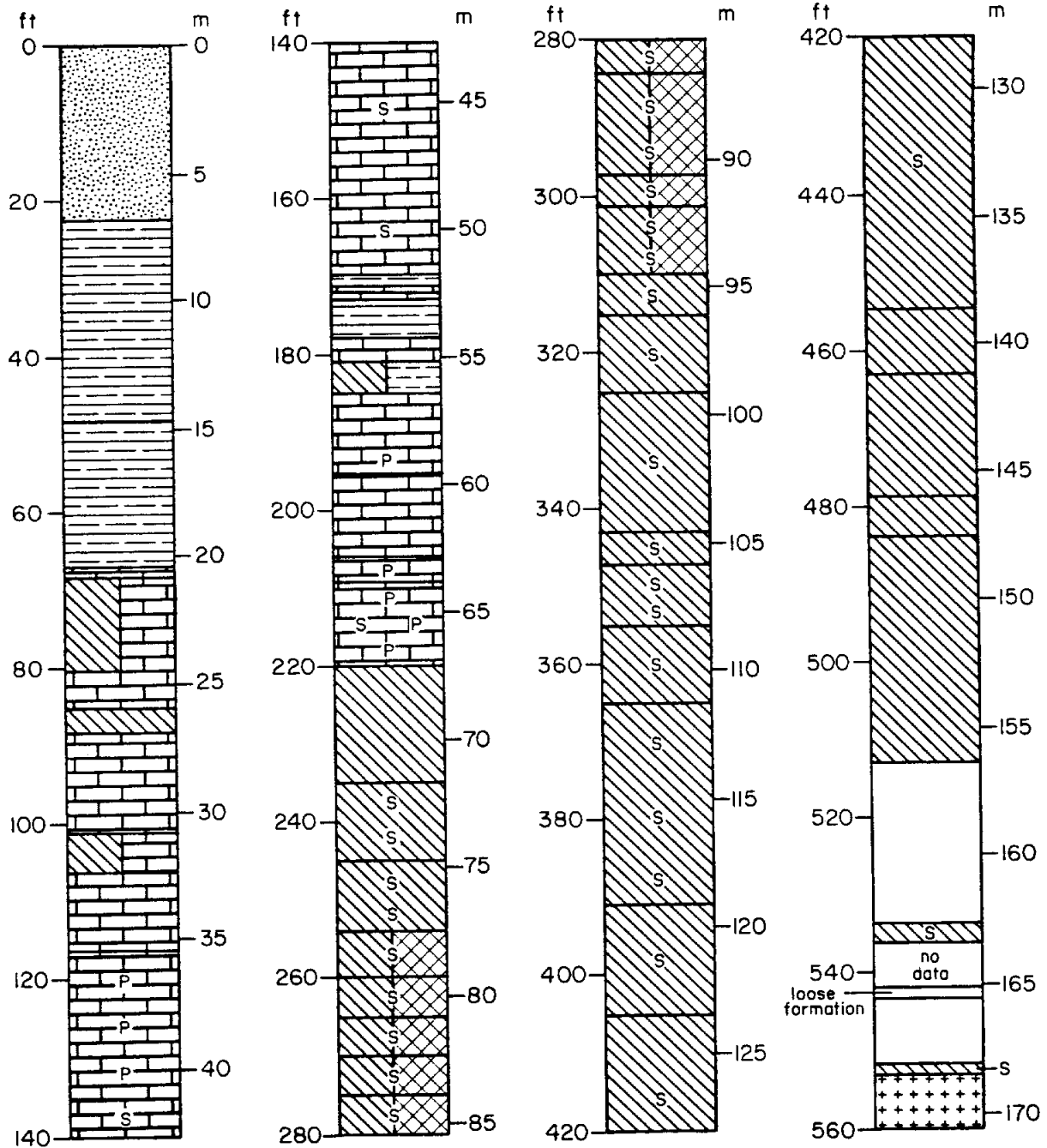
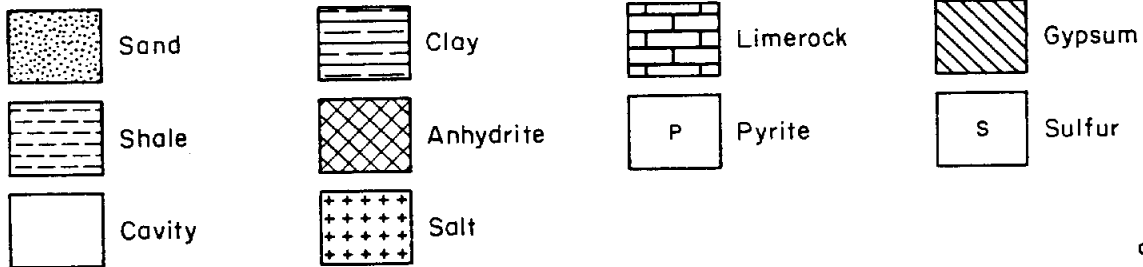


Figure 6. Cross section of the southeast wall at Damon Quarry. The cross section was constructed using measured sections and photographs. The general topography at the quarry is shown in figure 2.

Texas Exploration Co.
#R-24 b



EXPLANATION



QA4770

Figure 7. Lithologic log of the Texas Exploration Company R-24-b well located over the northwest part of Damon Mound diapir (data from Bevier, 1925).



Figure 8. Photograph showing breccia texture of cap rock exposed in Damon Quarry. The camera lens cover shown for scale is 2.0 inches (50 mm) in diameter.



Figure 9. Photograph of fractures and calcite veins in cap rock exposed in Damon Quarry. The staff is 5 feet (1.5 m) long.

Cap-Rock - Bedrock Contact

The cap-rock contact with overlying strata is relatively sharp and both Oligocene-Miocene and Pliocene-Pleistocene strata lie directly on cap rock. In some places the contact is marked by a breccia zone with clasts that are pebble to cobble size. Clast lithologies include calcite cap rock, calcareous sandstone, and mudstone-siltstone. Calcite veins sometimes cut overlying strata above the cap-rock - bedrock contact. Clay fills some fractures in the upper part of the cap rock, but it could not be determined if clay was squeezed into the fractures during deposition and diapir growth, or if fractures were filled during slumping or recent deposition while the quarry was filled with water.

Oligocene-Miocene Strata

Oligocene and Miocene strata have been mapped together in the quarry (fig. 4). Different pulses of dome growth and erosion have made the stratigraphy of the pre-Pliocene strata difficult to differentiate. An example of the stratigraphic complexities exhibited in the Oligocene-Miocene unit has been demonstrated in the detailed studies by Baker (1979). Using paleontologic evidence, he interpreted a black clay immediately below the Oligocene-Miocene "Het" lime to be part of the Vicksburg Group. Frio Formation sediments are missing. Several hundred feet nearby, a black oily shale interpreted to be Frio Formation is overlain by Miocene green clay. The "Het" limestone and possibly lower Miocene sands are missing at this location (Baker, 1979, pp. 17 and 23). It is likely that pulses of dome growth accompanied by erosion and faulting caused reworking of diagnostic fossils into strata of different age. Thus, some of the paleontologic data may be misleading.

Lateral variations in the lithology of the Oligocene-Miocene unit also exist across the quarry. Green-black claystone and siltstone are the most common rock types, although coralline limestone ("Het" limestone), medium- to coarse-grained calcareous sandstone, and

a green sand (possibly glauconitic) also exist. Shale overlies the cap rock along the southeast quarry wall. A green-black clay and the "Het" limestone also make up the Oligocene-Miocene strata along this wall (figs. 4 and 6). The "Het" limestone is overlain by Pliocene-Pleistocene claystone. In the east corner of the quarry, black-green claystone-siltstone overlies the cap rock. The cap-rock contact at this location contains breccia of calcareous sandstone and calcite cap rock. Pliocene-Pleistocene sand and claystone overlies the Oligocene-Miocene strata here (fig. 4). Along part of the northeast wall, the cap rock is in contact with Pliocene-Pleistocene siltstone and claystone (figs. 4 and 5). At the north corner of the quarry, the Oligocene-Miocene unit consists of a green, fine-grained quartz sand and siltstone, as well as medium- to coarse-grained, calcareous sandstone. Breccia of siltstone and calcareous sandstone is at the cap-rock contact and calcite veins are common in the Oligocene-Miocene strata. Near the west corner of the pit, cap rock is overlain by a fractured, green claystone. The cap-rock surface is irregular (fig. 10). Round cobbles (up to 8 inches long) of "Het" limestone occur within the green claystone.

The "Het" limestone is the only Oligocene-Miocene strata in the quarry that has been studied in detail (Frost and Schafersman, 1978, 1979; Baker, 1979). The reef fauna comprises 13 to 14 species; Antiguastrea cellulosa is the dominant frame builder. Other corals common in the reef core facies are Montastrea intermedia, Porites panamensis, and Goniopora micropica. Favites mexicana is less common in this facies (Frost and Schafersman, 1978, 1979). Black mudstone occurs below the "Het" limestone, and clay has been squeezed upward along fractures in the limestone. Frost and Schafersman (1978, 1979) also recognized breccia of reef rock within this black mudstone. Above the "Het" limestone they described a mantle up to 30 ft thick of weathered cap rock and reef rubble unconformably overlying the dipping limestone. The present weathered condition of the quarry wall prevents this mantle unit from being easily distinguished from recent rubble.

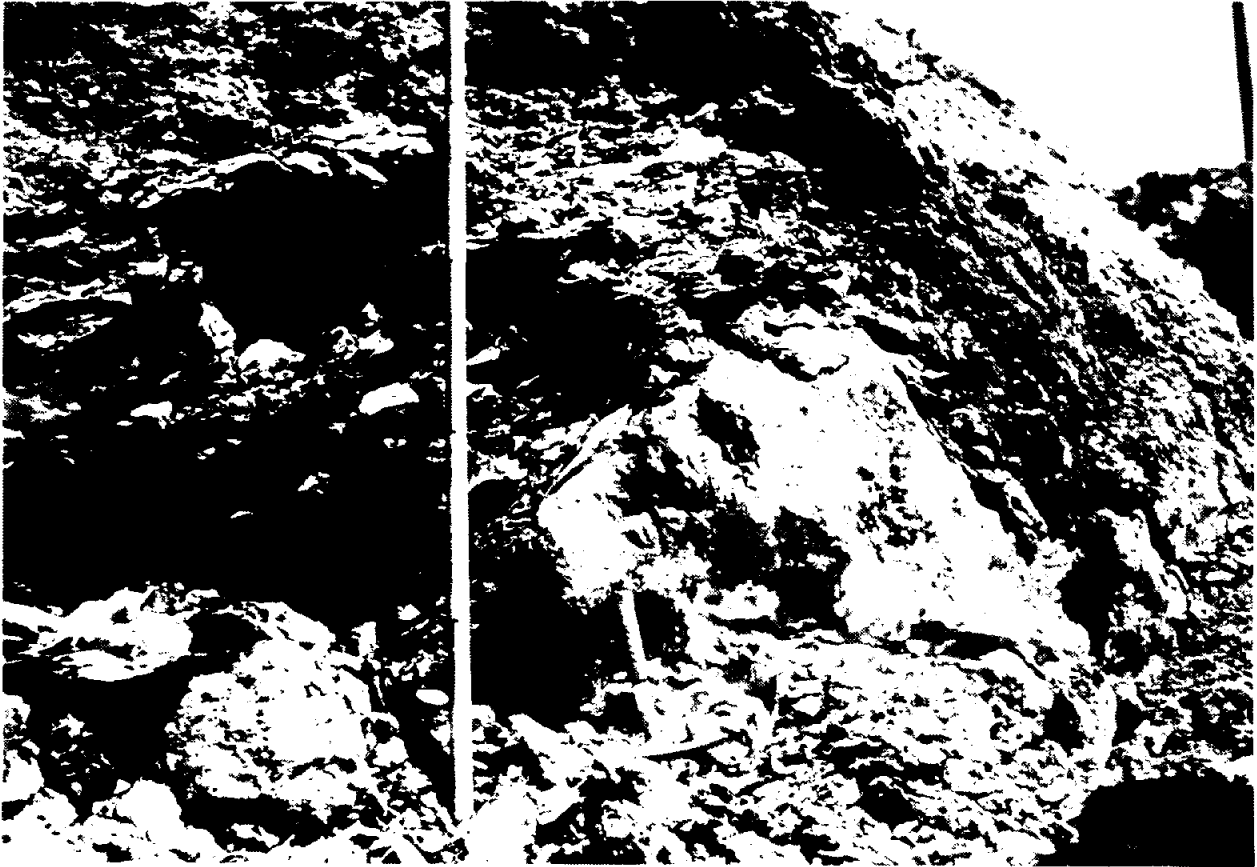


Figure 10. Photograph of shale - cap rock contact exposed in the west corner of Damon Quarry. The cap rock displays an irregular surface and the contact is relatively sharp at this location. The staff is 5 feet (1.5 m) long.

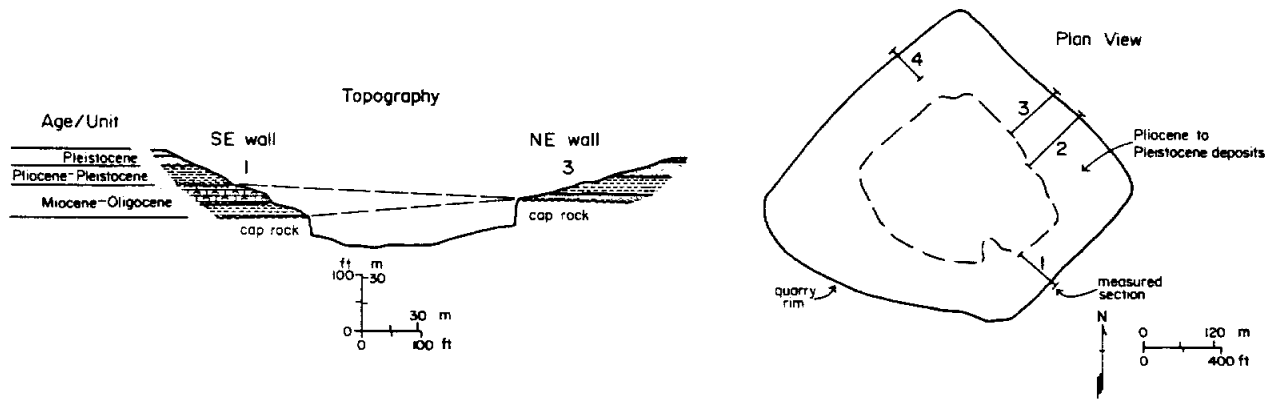
Pliocene-Pleistocene Strata

Pliocene and Pleistocene alluvial deposits (fig. 11) have been described in some detail by Baker (1979) and Jenkins (1979). Baker described a lower alluvial unit that is predominantly clay. At the east corner of the quarry he recognized fine sand and silt with root casts below the clay. Calcareous layers at the upper part of the clay have been interpreted to be caliche (Baker, 1979). The age of this lower alluvial unit is thought to be Pliocene-Pleistocene, however, no firm age date has been determined (Baker, 1979; Schafersman, 1979).

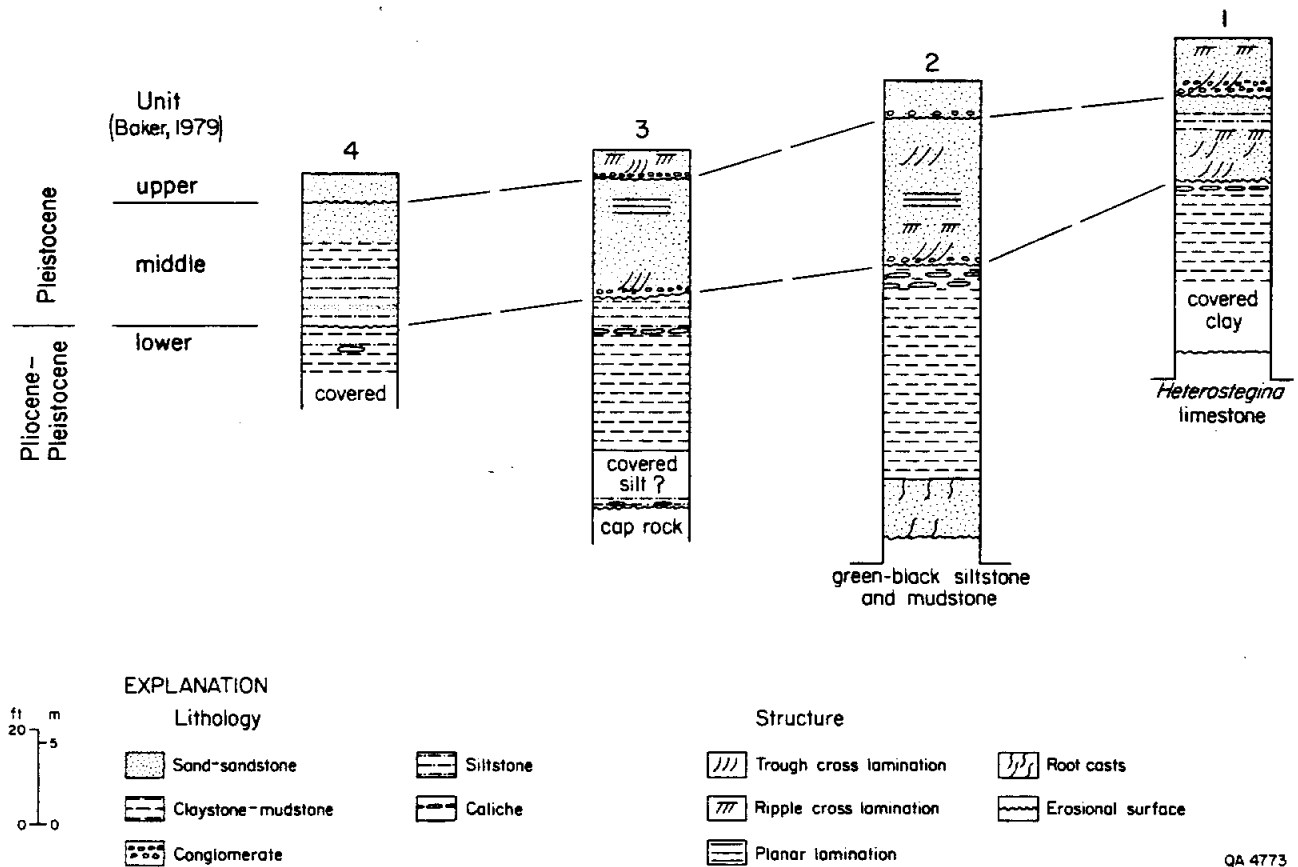
Above the clayey lower alluvial unit, Baker (1979) recognized sandier, middle and upper alluvial units. At the northeast quarry wall, the base of the middle alluvial unit is characterized by basal conglomerate consisting primarily of pebbles of vein quartz, chert, and sandstone, as well as clay clasts. Scouring of the lower alluvial clay unit is evident where the calcareous layers have been eroded away. At the northeast and southeast quarry walls, the middle alluvial unit is predominantly a fine to medium sand displaying large-scale trough cross-laminations with overlapping scour and fill features (Baker, 1979). Finer grained silts and clays exhibiting planar to flaser bedding (Jenkins, 1979) occur laterally to the coarse alluvial unit at the northwest quarry wall. Jenkins (1979) as well as Baker (1979) concluded that these sediments were deposited in a meandering stream system, and they recognized point bar, abandoned channel, levee, and floodbasin facies.

The upper alluvial unit discussed by Baker (1979) is an upward-fining sequence of sand and clay. At the northeast end of the quarry these sands appear to merge with middle alluvial unit sands, suggesting the two units could represent one depositional episode. A thin carbonaceous zone in the upper sands has been dated by pollen analysis as being late Miocene to late Pleistocene (Baker, 1979). Jenkins (1979) believes the middle and upper alluvial units represent a fluvial deposit that is correlative with the Late Pleistocene Beaumont Formation. The units are mapped as Pleistocene strata (figs. 4 and 11).

a)



b)



QA 4773

Figure 11. Topographic profile (a) of Damon Quarry and map of the Pliocene to Pleistocene strata showing locations of measured sections; measured section (b) illustrates alluvial deposits exposed at Damon Quarry.

PLIO-PLEISTOCENE TO POST-PLEISTOCENE DEFORMATION

Plio-Pleistocene deposits thicken in salt-withdrawal basins between Damon Mound, Boling and Nash diapirs, suggesting Plio-Pleistocene diapir growth (fig. 12). Damon Mound has approximately 80 ft (25 m) of topographic expression and Late Pleistocene Beaumont sediments are warped over the diapir. Two mechanisms that may have caused this last recorded episode of deformation are drape compaction and salt dome uplift.

Drape compaction is the equal percentage compaction of an interval, such that the structure of an underlying horizon is superimposed on an overlying layer (Billingsely, 1982). Compaction of strata is dependent on lithology, depth, and time. More than 80 ft (25 m) of compaction in Plio-Pleistocene strata unaffected by the dome is required for drape compaction to have caused the observed warping of strata and topographic relief at Damon Mound. Cross section C-C' (fig. 12) and calculations of compaction amounts and rates (table 1) indicate that drape compaction is not the major process accountable for the warping of strata and topographic relief exhibited at Damon Mound.

Cross section C-C' shows the topography and Plio-Pleistocene section across Boling, Damon Mound, and Nash diapirs (fig. 12). Damon Mound has about 80 ft (25 m) of relief, whereas Boling and Nash Domes display little to no topographic expression. The Plio-Pleistocene strata between the dome is approximately 1,300 ft (400 m) thick and the strata's composition is generally 50 percent sand (Guevera-Sanchez, 1974). About 60 ft (18 m) of Plio-Pleistocene sediments are exposed in the Damon Quarry on Damon Mound, and over Boling Dome about 360 ft (110 m) of Plio-Pleistocene strata has been inferred from detailed sections across the dome. The upper 340 ft (103 m) of strata at Boling Dome are relatively flat-lying over the dome and at the dome flanks. Strata below this depth dips and commonly thickens away from the diapir flanks. Compaction of sediment below about 340 ft (103 m) cannot account for the topography over Damon Mound if it has not

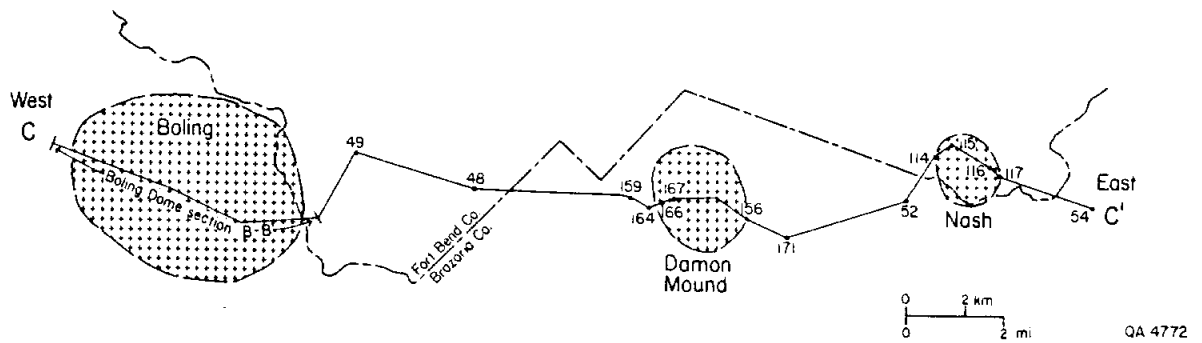
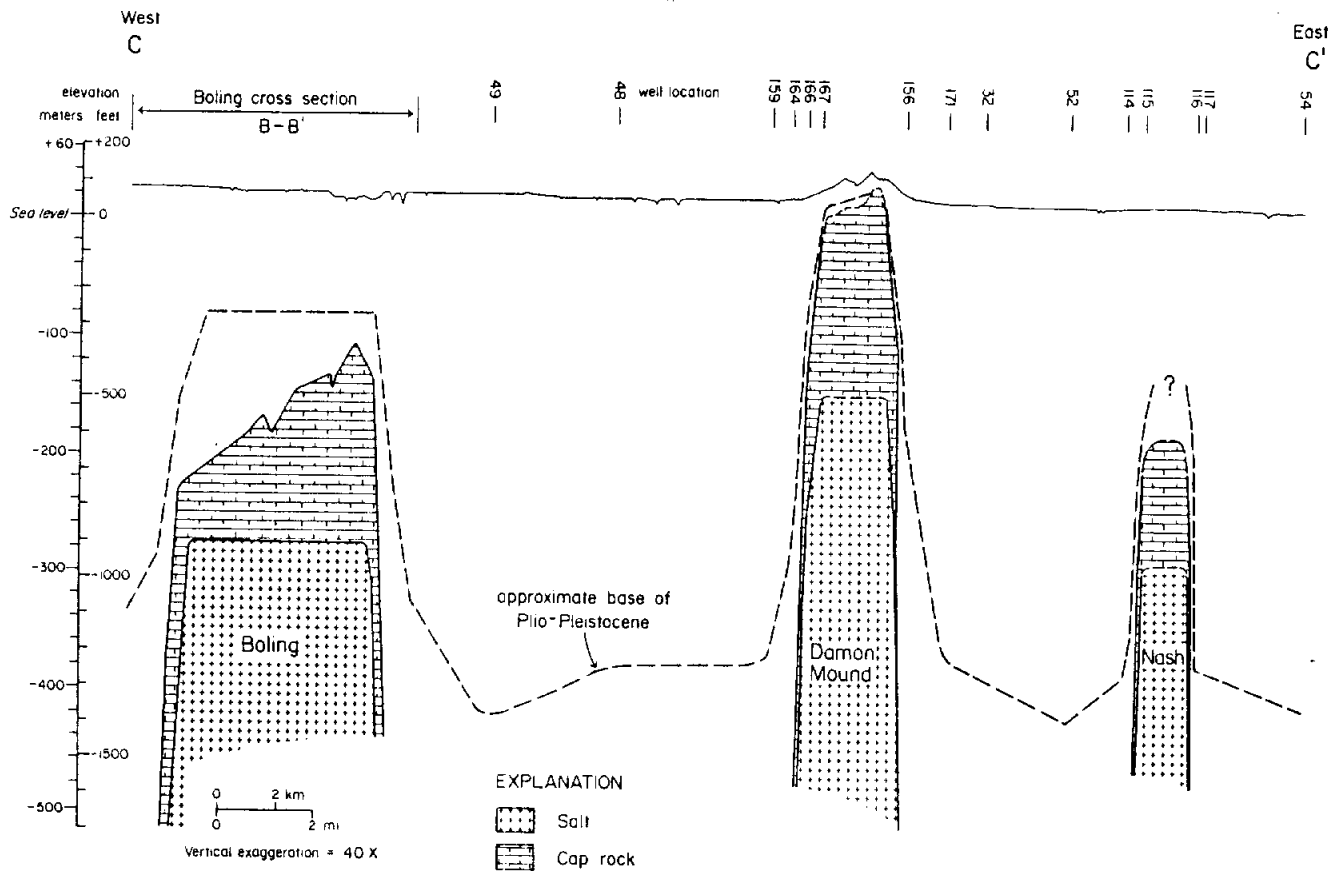


Figure 12. Cross section C-C' showing topography and thickness of Pliocene-Pleistocene strata at Boling, Damon Mound, and Nash Domes. Well names are listed in Appendix.

Table 1. Drape compaction estimates for the Damon Mound area.

1. Compaction equation (Billingsely, 1982)

$$T_{uc} = T_c \frac{1-\phi_c}{1-\phi_{uc}}$$

T_{uc} = uncompacted thickness

T_c = compacted thickness

ϕ_{uc} = uncompacted porosity

ϕ_c = compacted porosity

a. Assumption: The compacted thickness (T_c) away from Damon Mound used in these calculations is 340 ft because this is the approximate strata thickness over Boling Dome that shows no evidence of draping. Thus, compaction of sediment below this depth (340 ft) could not account for the topography over Damon Mound if it has not affected shallow strata at Boling.

b. Assumption: Porosity values used are as follows (Dickenson, 1953; Pryor, 1973):

ϕ uncompacted sand = 40%

ϕ compacted sand at shallow depth (<500 ft) = 30%-35%

ϕ uncompacted shale = 60%

ϕ compacted shale at shallow depth (<500 ft) = 45%

c. Possible uncompacted thickness of upper 340 ft of strata (T_{uc}) away from Damon Mound:

$$T_{uc \text{ sand}} = 170 \text{ ft} \cdot \frac{1-.30}{1-.40} = 198 \text{ ft}$$

$$T_{uc \text{ shale}} = 170 \text{ ft} \cdot \frac{1-.45}{1-.60} = 234 \text{ ft}$$

$$T_{uc \text{ sand} + \text{shale}} = 432 \text{ ft}$$

2. Possible thickness change due to compaction:

$T_{uc} - T_c$ = possible thickness change

$$432 \text{ ft} - 340 \text{ ft} = 92 \text{ ft}$$

Table 1. (cont.)

3. Rate of Compaction (modified from Barton, 1933)

$$\text{time necessary for amount of compaction} = \frac{\text{depth } T_c}{\text{depth base of Plio-Pleistocene}} \cdot \text{age of Plio-Pleistocene}$$

a. Assumption: Compaction is continuous with sediment burial.

b. Assumption: Away from Damon Mound salt diapir, the depth at the base of the Plio-Pleistocene is approximately 1300 ft.

$$\text{c. } \frac{340 \text{ ft}}{1300 \text{ ft}} \cdot 5,000,000 \text{ yr} = 1,300,000 \text{ yr (rounded)}$$

$$\text{d. Compaction rate} = 92 \text{ ft per } 1,300,000 \text{ yr} \\ = 7 \text{ ft per } 100,000 \text{ yr}$$

affected shallow strata and topography at Boling Dome. Thus, compaction of only the upper 340 ft (103 m) of strata would have to account for the 80 ft (25 m) of relief over Damon Mound.

The compaction calculations are presented in table 1. The actual figures in the calculations are only of value in indicating a probable magnitude of compaction. The calculations indicate that even though the probable amount of compaction may account for the topographic relief over Damon Mound, the compaction rates are much too slow to have warped Late Pleistocene strata. The rate of compaction at this shallow depth is estimated at about 7 ft (2.1 m) per 100,000 yr. The warped Late Pleistocene sediments at Damon Mound are thought to have accumulated during a Wisconsin interstadial that occurred approximately 34,000 yr B.P. (Jenkins, 1979). Jenkins (1979) correlated these deposits with the Beaumont Formation. Other Gulf Coast stratigraphers correlate Beaumont sediments with the Sangamon interstadial of about 115,000 to 130,000 yr B.P. (DuBar, personal communication, 1985). The calculations in this report are based on the 34,000 yr B.P. age for the uppermost Late Pleistocene deposits over this diapir (Jenkins, 1979). The compaction of this upper strata during the last 34,000 yr is about 2 ft (0.6m)--not enough to account for the topographic relief over Damon Mound.

Actual uplift of the salt dome has probably caused the warping of the Late Pleistocene strata at Damon Mound. Seafloor relief seems to have existed over Damon Mound, Boling, and Nash diapirs during the Oligocene as evidenced by the "Het" limestone reef facies that developed over these domes. If relief existed over these domes, it is inferred that these diapirs were at shallow depths and possibly at about the same elevation. Damon Mound is currently shallower than Boling or Nash Domes, suggesting that diapir growth at Damon Mound continued after uplift of the other domes ceased or that uplift rates at Damon Mound have been faster.

Structural relief of the "Het" limestone and "top of Miocene" has been used to crudely estimate uplift rates at Damon Mound. These estimates do not account for (1) strata subsidence at the diapir margin as salt is withdrawn from the salt-stock margins

during diapir uplift (Seni and Jackson, 1984), or (2) pulses of rapid diapir growth between periods of relatively slow to no diapir growth. This amount of structural relief suggests an uplift rate of about 0.25 ft (0.075 m) per 1,000 yr. Eighty feet of relief of Late Pleistocene Beaumont strata indicates an uplift rate of about 2 ft (0.6 m) per 1,000 yr. This rate is approximately one order of magnitude greater than the long-term estimates, suggesting that pulses of varying uplift rates probably do occur. The uplift rates during the Late Pliocene for Damon Mound are very rapid when compared to long-term uplift rates calculated by other researchers (Seni and Jackson, 1984).

SUMMARY

Geologic investigations at Damon Mound provide information that may be useful in characterizing coastal salt domes in Texas. Data indicate that diapir growth has influenced sediment deposition in the area. An Oligocene reef facies ("Het" limestone) over the diapir suggests seafloor relief and possibly a shallow depth to the salt dome during Oligocene time. Miocene strata thins toward the dome and some sandy units appear to pinch out. Although subsurface data of Plio-Pleistocene strata are sparse, this sequence also thins over the dome.

Cap rock, as well as Oligocene to Pleistocene sediments, is exposed on top of the mound in Damon Quarry. The top of the predominantly calcite cap rock is an irregular surface and cap-rock - bedrock contacts are relatively sharp. Zones of breccia/conglomerate occur in places at the contact between cap rock and bedrock. Oligocene and Miocene strata in the quarry consist of claystone, siltstone, coralline limestone, and a medium- to coarse-grained calcareous sandstone. The coralline limestone is a block of "Het" limestone that has been preserved at the top of the dome as well as along the flanks where it is recognized in the subsurface. Structural relief of the "Het" is about 6,000 ft (1,700 m).

About 60 to 90 ft (18 to 27 m) of Plio-Pleistocene strata is exposed at Damon Quarry. Baker (1979) recognized three alluvial units in this sequence. He described a lower, predominantly clay unit overlain by two sandier units. The two upper units are thought to represent Late Pleistocene fluvial deposits based on pollen and vertebrate fossils and have been tentatively correlated with the Beaumont Formation (Baker, 1979; Jenkins, 1979).

Late Pleistocene strata have been warped over the diapir, resulting in about 80 ft of topographic relief. Drape compaction cannot account for this amount of relief, thus actual salt diapir uplift has occurred. The uplift rate since Late Pleistocene time has been rapid; it is estimated to be 2 ft (0.6 m) per 1,000 yr. The average uplift rate since Oligocene time is about one order of magnitude less (0.25 ft [0.075 m] per 1,000 yr).

REFERENCES

- Baker, H. W., 1979, General geology of Damon Mound, in Damon Mound, Texas: Houston Geological Society Guidebook, p. 10-25.
- Ballard, E. O., 1961, Limestone in the Heterostegina Zone (Oligocene-Miocene) on Damon Mound salt dome, Brazoria County, Texas: Gulf Coast Association of Geological Societies, v. 11, p. 213-223.
- Barton, D. C., 1933, Mechanics of formation of salt dome with special reference to Gulf Coast salt domes of Texas and Louisiana: American Association of Petroleum Geologists Bulletin, v. 17, no. 9, p. 1025-1083.
- Bernard, H. A. and LeBlanc, R. J., 1965, Resume of the Quaternary geology of the northwestern Gulf of Mexico province, in Wright, H. E. and Frey, D. G., eds., The Quaternary of the United States: Princeton University Press, p. 137-185.
- Bevier, G. M., 1925, The Damon Mound oil field, Texas: American Association of Petroleum Geologists Bulletin, v. 9, no. 3, p. 505-526.

- Billingsely, L. T., 1982, Geometry and mechanisms of folding related to growth faulting in Nordheim field area (Wilcox), DeWitt County, Texas: Gulf Coast Association of Geological Societies, v. 32, p. 263-274.
- Cantrell, R. B., Montgomery, J. C., and Woodard, A. E., 1959, Heterostegina reef on Nash and other piercement salt domes in northwestern Brazoria County, Texas: Gulf Coast Association of Geological Societies Transactions, v. 9, p. 59-62.
- Dickenson, G., 1953, Geological aspects of abnormal reservoir pressures in Gulf Coast Louisiana: American Association of Petroleum Geologists, v. 37, no. 2, p. 410-432.
- Ellison, S. P., Jr., 1971, Sulfur in Texas: The University of Texas at Austin, Bureau of Economic Geology, Handbook No. 2, 48 p.
- Frost, S. H., and Schafersman, S. D., 1979, Upper Oligocene coral reef of the Anahuac formation, in Damon Mound, Texas: Houston Geological Society Guidebook, p. 26-44.
- _____ 1978, Oligocene reef community succession, Damon Mound, Texas: Gulf Coast Association of Geological Societies, v. 28, p. 143-160.
- Guevara-Sanchez, E. H., 1974, Pleistocene facies in the subsurface of the southeast Texas coastal plain: The University of Texas at Austin, Ph.D. dissertation, 133 p.
- Hurlburt, E. M., 1943, Limestone on Damon Mound, Brazoria County, Texas: University of Texas, Austin, Bureau of Economic Geology, Bulletin 4301, p. 265-269.
- Jenkins, J. T., Jr., 1979, Geology and paleontology of the upper clastic interval at Damon Mound, in Damon Mound, Texas: Houston Geological Society Guidebook, p. 45-62.
- Porter, R. L., and Seren, G. W., 1953, Damon Mound field, Brazoria County, Texas, in Guidebook of field trip routes, oil fields, geology: Houston Geological Society Guidebook, p. 107-114.
- Pryor, W. A., 1973, Permeability-porosity patterns and variations in some Holocene sand bodies: American Association of Petroleum Geologists Bulletin, v. 57, no. 1, p. 162-189.

- Sandeen, W. M., and Wesselman, J. B., 1973, Ground-water resources of Brazoria County, Texas: Texas Water Development Board, Report 163, 199 p.
- Schafersman, S. D., 1979, An introduction to the features and history of Damon Mound, in Damon Mound, Texas: Houston Geological Society Guidebook, p. 1-9.
- Seni, S. J., and Jackson, M. P. A., 1984, Sedimentary record of Cretaceous and Tertiary salt movement, East Texas Basin: times, rates, and volumes of salt flow and their implications for nuclear waste isolation and petroleum exploration: The University of Texas at Austin, Bureau of Economic Geology Report of Investigations No. 139, 89 p.
- Smith, A. E., 1979, Minerals from Damon Mound, in Damon Mound, Texas: Houston Geological Society Guidebook, p. 84-91.
- Winkler, C. D., 1979, Late Pleistocene fluvial-deltaic deposition, Texas coastal plain and shelf: The University of Texas at Austin, Master's thesis, 187 p.

Appendix. List of Wells

County	Location Number	Operator	Well No.-Lease	Field
Fort Bend	48	Mack Hank Petr. Co.	1-Moore	Wildcat
	49	Mack Hank Petr. Co.	1-Armstrong	Wildcat
	114	Humble Oil & Refining Co.	2-Paul Mier	Nash
	115	Rycade Oil Corp.	2-Julius Meier	Nash
	116	Halbouty & Casey	1-Groce	Nash
	117	Hollis Oil Co.	4-Kitty Nash Groce	Nash
	Brazoria	149	Progress Petr.	1-Wruck
150		Progress Petr.	1-Gulf Fee	Damon
151		Merrick	2-Gulf-Harrison	Damon
152		Merrick	1-Gulf-Harrison	Damon
153		Merrick	3-Bryan Estate	Damon
154		Sinclair Prairie Oil	31-Elmira Bryan	Damon
155		Dr. C. A. Slaughter	2-Thomas Res. Oil Co.	Damon
156		J. M. Flower	1-W. F. Thomas	Damon
157		McKenzie Drlg. Co.	1-Sinclair Fee	Damon
158		Baldrige and King	1-Continental Oil Co.	Damon
159		L. D. French	52-Belle Wisdom	Damon
160		A. Nelson McCarter	1-Kentucky Homes	Damon
161		General Crude Oil Co.	7-Belle Wisdom	Damon
162		General Crude Oil Co.	1-Wisdom	Damon
163		General Crude Oil Co.	9-Belle Wisdom	Damon
164		Union Oil Co. of California	2-Jackson Kelley	Damon
165		Brazo Oil Co.	1-Belle Wisdom	Damon
166		Brazo Oil Co.	2-Belle Wisdom	Damon
167		Oil Coast Corp.	"2-A"-Wisdom Estate	Damon

Appendix (cont.)

County	Location Number	Operator	Well No.-Lease	Field
Brazoria	168	Sinclair Oil & Gas Co.	2-May W. Wallace	Damon
	169	Hogg Oil Co.	8-Mike Hogg et al. "A"	Damon
	170	Hamby and McGuirt	1-Cansler	Damon
	171	William K. Davis	1-Hurley-Lockwood	Damon
	52	The Texas Co.	1-J. H. Mazac	Damon
	54	Brewster and Barrie	1-M. L. Mellon et al.	Damon
	33	Southern Minerals Corp.	1-Ramsey State Farm	Damon

APPENDIX A. LIST OF DOMES

Code	Dome Name	County
AL	Allen	Brazoria
AR	Arriola	Hardin
BB	Barbers Hill	Chambers
BA	Batson	Hardin
BE	Bethel	Anderson
BC	Big Creek	Fort Bend
BI	Big Hill	Jefferson
BL	Blue Ridge	Fort Bend
BG	Boggy Creek	Anderson/Cherokee
BO	Boling	Wharton/Fort Bend
BR	Brenham	Austin/Washington
BK	Brooks	Smith
BH	Brushy Creek	Anderson
BM	Bryan Mound	Brazoria
BU	Bullard	Smith
BT	Butler	Freestone
CP	Cedar Point	Chambers
CL	Clam Lake	Jefferson
CC	Clay Creek	Washington
CM	Clemens	Brazoria
CO	Concord	Anderson
DM	Damon Mound	Brazoria
DN	Danbury	Brazoria
DH	Davis Hill	Liberty
DA	Day	Madison
DR	Dilworth Ranch	McMullen
ET	East Tyler	Smith
EL	Elkhart	Anderson
ES	Esperson	Harris/Liberty
FN	Fannett	Jefferson
FC	Ferguson Crossing	Brazos/Grimes
GC	Girlie Caldwell	Smith

APPENDIX A. (cont.)

Code	Dome Name	County
GS	Grand Saline	Van Zandt
GU	Gulf	Matagorda
GP	Gyp Hill	Brooks
HA	Hainesville	Wood
HR	Hankamer	Chambers/Liberty
HK	Hawkinsville	Matagorda
HI	High Island	Galveston
HO	Hockley	Harris
HM	Hoskins Mound	Brazoria
HU	Hull	Liberty
HB	Humble	Harris
KE	Keechi	Anderson
KI	Kittrell	Houston/Walker
LR	La Rue	Henderson
LP	Long Point	Fort Bend
LL	Lost Lake	Chambers
MA	Manvel	Brazoria
MK	Markham	Matagorda
MQ	Marquez	Leon
MC	McFaddin Beach	State waters
MI	Millican	Brazos
MO	Moca	Webb
MB	Moss Bluff	Chambers/Liberty
MS	Mount Sylvan	Smith
MY	Mykawa	Harris
NA	Nash	Brazoria/Fort Bend
ND	North Dayton	Liberty
OK	Oakwood	Freestone/Leon
OR	Orange	Orange
OC	Orchard	Fort Bend
PA	Palangana	Duval
PL	Palestine	Anderson

APPENDIX A. (cont.)

Code	Dome Name	County
PE	Pescadito	Webb
PP	Piedras Pintas	Duval
PJ	Pierce Junction	Harris
PN	Port Neches	Orange
RB	Racoon Bend	Austin
RF	Red Fish Reef	State waters
SF	San Felipe	Austin
SN	San Luis Pass	State waters
SA	Saratoga	Hardin
SO	Sour Lake	Hardin
SH	South Houston	Harris
SL	South Liberty	Liberty
SP	Spindletop	Jefferson
ST	Steen	Smith
SR	Stratton Ridge	Brazoria
SU	Sugarland	Fort Bend
TH	Thompson	Fort Bend
WE	Webster	Harris
WC	West Columbia	Brazoria
WH	Whitehouse	Smith

